

1-1-1994

The relaxation behavior of highly entangled polybutadiene critical gels/

Michael E. DeRosa

University of Massachusetts Amherst

Follow this and additional works at: https://scholarworks.umass.edu/dissertations_1

Recommended Citation

DeRosa, Michael E., "The relaxation behavior of highly entangled polybutadiene critical gels/" (1994). *Doctoral Dissertations 1896 - February 2014*. 826.

https://scholarworks.umass.edu/dissertations_1/826

This Open Access Dissertation is brought to you for free and open access by ScholarWorks@UMass Amherst. It has been accepted for inclusion in Doctoral Dissertations 1896 - February 2014 by an authorized administrator of ScholarWorks@UMass Amherst. For more information, please contact scholarworks@library.umass.edu.



312066011003512

THE RELAXATION BEHAVIOR OF HIGHLY ENTANGLED
POLYBUTADIENE CRITICAL GELS

A Dissertation Presented

by

MICHAEL E. DEROSA

Submitted to the Graduate School of the
University of Massachusetts Amherst in partial fulfillment
of the requirements for the degree of

DOCTOR OF PHILOSOPHY

February 1994

Polymer Science and Engineering

Copyright © by Michael E. DeRosa

1994

All Rights Reserved

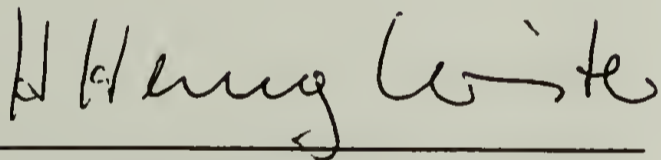
THE RELAXATION BEHAVIOR OF HIGHLY ENTANGLED
POLYBUTADIENE CRITICAL GELS

A Dissertation Presented

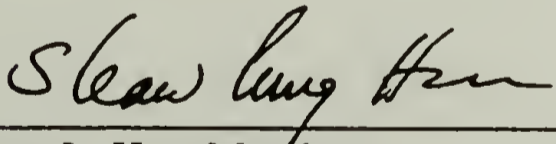
by

MICHAEL E. DEROSA

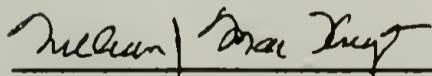
Approved as to style and content by:



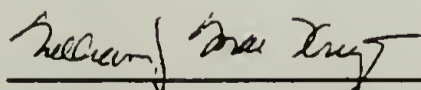
H. Henning Winter, Chair



Shaw L. Hsu, Member



William J. MacKnight, Member



William J. MacKnight, Department Head
Polymer Science and Engineering

To my Mom and Dad

ACKNOWLEDGMENTS

Over the past four years I have received help, in one way or another, from many individuals who have made it possible for me to complete this work. Special thanks go to my advisor Professor H. Henning Winter for providing me with his guidance. Throughout this project he gave me the freedom to explore new areas and supported my ideas in a way which has made my graduate school experience a challenging, positive and enjoyable one. I would also like to thank Professor Shaw Ling Hsu and Professor William J. MacKnight for their helpful discussions and for providing their input from a fresh perspective outside of my research group. I sincerely appreciate Professor Hsu's cooperation in allowing me to use his laboratory facilities.

I am extremely grateful to Michael Masse and Joe Machado at Shell Development Company for providing the polybutadiene samples and their helpful support and encouraging discussions throughout this study. Adi Shefer, Jim Scanlan and Akihiro Izuka also provided useful advice at the initial stages of this project.

I am indebted to several of my labmates for developing the software packages that I used extensively to perform analysis and modeling of the rheological data. Since my computer programming skills are practically nonexistent, I couldn't have gone too far without their contributions. I would like to acknowledge Michael Baumgaertel, who developed IRIS and IRIS Development Systems and Marian Mours, who developed the "Gelpro" software. I am thankful for their cooperation in teaching me how to use the programs and for their discussions. I am particularly grateful to Judy Jackson who upgraded the IRIS.DS software and worked closely with me on the rheological modeling. She provided plenty of in-depth discussions and constructive comments and criticisms which always kept me on my toes.

I would also like to thank the rest of my friends and current labmates Jörg, Ioannis, Paul, Mohan, Wolfgang, Sandeep, Carina, Maria, and past labmates, Sundar, Ye-Gang,

Suresh, and Heung-Woo for all of their help and encouragement in and out of the lab. I also greatly appreciate the cooperation of all of the secretarial staff in the Polymer Science and Chemical Engineering Department and those students in other laboratories who have helped make my work a little easier.

In the last three years I was fortunate enough to be involved in a successful local band with my close friends John Savage, Jeff Simpson, and Frank Rossitto. For me, the band was an invaluable extracurricular activity I needed as an outlet which helped keep my mind clear and provided balance to my life outside of the lab.

My deepest feelings of gratitude go out to my Mom, Dad, and brother Dave. Their love and support over the years have enabled me to make it this far.

This project was supported by the Center for the University of Massachusetts Industry Research in Polymers.

ABSTRACT

THE RELAXATION BEHAVIOR OF HIGHLY ENTANGLED POLYBUTADIENE CRITICAL GELS

FEBRUARY 1994

MICHAEL E. DEROSA, B.S. UNIVERSITY OF MASSACHUSETTS AMHERST

Ph.D. UNIVERSITY OF MASSACHUSETTS AMHERST

Directed by: Professor H. Henning Winter

The stress relaxation behavior of critical gels originating from six highly entangled polybutadienes of low polydispersity with molecular weights from 18,100 to 97,000 g/mole were investigated. The polymers were vulcanized by a hydrosilation reaction which takes place nearly exclusively at the pendant 1,2-vinyl sites which are distributed randomly along the polybutadiene chain. The empirical BSW-spectrum was found to describe the relaxation behavior of the uncrosslinked precursor state. A characteristic parameter of the BSW-spectrum is the longest relaxation time of the precursor. Crosslinking increases this longest relaxation time even further but had little effect on the relaxation behavior in the entanglement and transition zones. The relaxation time spectrum of the material at the gel point (critical gel) was found to be well represented by the superposition of the BSW-spectrum and CW-spectrum with minor modifications to the intermediate time regime. The long time behavior follows a power law as described by the Chambon-Winter equation, $G(t) = St^{-n}$. n was found to be constant with a value close to 0.5 over a stoichiometric ratio range of $0.25 < r < 3.0$. The gel strength (S) was found to scale with the precursor molecular weight as $S \sim M_w^{zn}$ where z is the exponent from the

zero shear viscosity molecular weight relationship $\eta_0 \sim M_w^z$, is commonly found to be $z=3.3-3.6$. A simple empirical model combining first order kinetic analysis with the Flory-Stockmayer branching theory was developed to predict the gel time as a function of stoichiometric ratio and precursor functionality. *in-situ* rheological measuring techniques of gelation allow for accurate determination of the gel point. The kinetic model was found to agree well with experimental data.

TABLE OF CONTENTS

ACKNOWLEDGMENTS	v
ABSTRACT.....	vii
LIST OF TABLES	xiii
LIST OF FIGURES.....	xv
LIST OF SYMBOLS	xxiv
Chapter	
1. INTRODUCTION.....	1
2. MATERIALS AND CHARACTERIZATION	9
2.1 Polybutadiene Prepolymer	10
2.2 Crosslinker	15
2.3 Catalyst and Crosslinking Reaction	18
2.4 Catalyst Poisoning.....	25
2.5 Sample Preparation.....	25
2.6 Experimental Error in Sample Preparation	27
3. EXPERIMENTAL METHODS	28
3.1 Rheological Techniques.....	28
3.1.1 Rheological Material Functions for Shear Flow	28
3.1.2 Linear Viscoelastic Functions.....	30
3.1.3 Apparatus	34
3.2 Evaluation of the Discrete Relaxation Time Spectrum.....	35
3.2.1 Conversion of the Discrete to Continuous Spectrum	38
3.3 Rheological Techniques to Study Critical Gels.....	40
3.3.1 "Stopped" Samples	40
3.3.2 Consecutive Frequency Sweep (CFS).....	40
3.4 Spectroscopic Techniques	43

4.	RELAXATION BEHAVIOR OF PRECURSOR MATERIALS.....	46
4.1	Rheological Characterization of Bulk Polybutadienes.....	46
4.1.1	Experimental Procedure	46
4.1.2	Dynamic Mechanical Data of Polybutadiene	47
4.2	Relaxation Time Spectrum of Bulk Polybutadienes (BSW-Spectrum) ..	54
4.2.1	BSW-Spectrum and Its Properties.....	55
4.2.2	Molecular Weight Dependence of BSW Parameters	58
4.2.3	Procedure for Evaluating the BSW Parameters.....	60
	4.2.3.1 Parameter Initialization.....	60
	4.2.3.2 Iteration Procedure for Improving the Fit	62
	4.2.3.3 Final Parameter Evaluation	62
4.2.4	Modeling Results	62
4.2.5	Discussion	67
4.3	Relaxation Behavior of Diluted Precursor	68
4.3.1	Diluent Effect of Crosslinker on the BSW-Spectrum	68
5	DYNAMIC MECHANICAL BEHAVIOR OF CROSSLINKING SAMPLES	77
5.1	Motivation.....	77
5.2	Experimental Procedure.....	79
5.3	Data Analysis	80
	5.3.1 Conversion of Raw Data Files to IRIS Format	80
	5.3.2 "Gelpro" Analysis of CFS Data	81
5.4	Results of CFS Measurements	90
5.5	Sources of Error.....	96
	5.5.1 Mutation Number (N_{mu}).....	96
	5.5.2 Sample Homogeneity	98
5.6	Discussion	100
	5.6.1 Effect of Physical Entanglements on Gel Point Detection	100
	5.6.2 Effect of Stoichiometry on the Gel Strength.....	105

5.6.3	Effect of Stoichiometry on the Critical Relaxation Exponent ..	106
5.6.4	Effect of Stoichiometric Window on Critical Gel Properties.....	108
6	EVOLUTION OF MECHANICAL PROPERTIES DURING GELATION ..	110
6.1	Experimental Procedure.....	110
6.1.1	Rheological Measurements.....	110
6.1.2	Spectroscopic Measurements	114
6.2	Rheological Results of Stopped Samples.....	119
6.3	Critical Extent of Reaction at the Gel Point.....	127
6.4	Relaxation Behavior at the Gel Point	134
6.4.1	Empirical Relaxation Time Spectrum for Highly Entangled Critical Gels.....	137
6.4.2	Precursor Molecular Weight Dependence of S	147
6.5	Mechanical Properties of Fully Cured Networks	150
6.5.1	Experimental Procedure	150
6.5.2	Fully Cured Networks at Balanced Stoichiometry ($r=1$).....	151
6.5.3	Fully Cured Networks at Imbalanced Stoichiometry ($r\neq 1$)	154
6.5.4	Bubble Formations in Fully Cured Samples	158
7	KINETIC STUDY OF GELATION.....	161
7.1	Experimental Procedure.....	161
7.1.1	Rheological Measurements.....	161
7.1.2	F.T.i.r. Measurements	162
7.2	Effect of Precursor Composition on the Gel Time	163
7.2.1	Effect of Stoichiometric Ratio on t_c	163
7.2.2	Effect of Functionality on t_c	165
7.2.3	Branching Theory Prediction.....	165
7.3	Simple Kinetic Model to Predict the Gel Time	167
7.3.1	Reaction Mechanism	168
7.3.2	Derivation of the Kinetic Model to Predict the Gel Time	169
7.3.3	Evaluation of Kinetic Model Parameters.....	173
7.3.4	Comparison of Predicted Gel Time to Experimental Results ...	180
7.3.5	Discussion	180

7.4	Frequency Dependence of the Complex Modulus During Cure	188
7.4.1	Effect of Precursor Molecular Weight on the Value of κ	194
8	CONCLUSIONS AND SUGGESTIONS FOR FUTURE RESEARCH	196
8.1	Conclusions.....	196
8.2	Suggestions for Future Research.....	198
	REFERENCES	200

LIST OF TABLES

Table		Page
2.1	Characterization summary of polybutadiene precursor polymers.....	11
4.1	Zero shear viscosity values for PBD samples diluted with stoichiometric amounts of crosslinker (12 wt%). η_0 was obtained from η^* in the low frequency limit.....	52
4.2	BSW parameters for polybutadiene precursor polymers.....	63
4.3	BSW parameters for polybutadiene precursor polymers diluted with a stoichiometric amount ($r=1$) of crosslinker.....	75
5.1	Summary of critical gel strength, S , and critical relaxation exponent, n , for PBD gel samples for five precursor molecular weights at various stoichiometric ratios, r . All data was taken at 28°C.....	95
5.2	Reported results found for the critical exponent, n , for different systems over a wide range of stoichiometric ratios. $r < 1$ denotes a crosslinker deficiency.	107
6.1	Parameters for the BSW-CW gel model.	144
6.2	Final network properties of fully cured samples with balanced stoichiometry ($r=1$). G_e is taken as $G^*(\omega)$ at 0.01 rad/s. $G^*(\omega)$ measurements were made at 28°C.	153
6.3	Equilibrium modulus (G_e) of fully cured PBD samples as a function of stoichiometric ratio (r). G_e is taken as $G^*(\omega)$ at 0.01 rad/s. Measurements were made at 28°C.....	155
7.1	Gel times measured by CFS ($t_{gel,CFS}$) for samples cured at 28°C.....	181
7.2	Gel times measured by CFS ($t_{gel,CFS}$) for samples cured at 34 °C.....	181
7.3	Gel times measured by CFS ($t_{gel,CFS}$) for samples cured at 40°C.....	182
7.4	Rate constants evaluated from kinetic data.	184
7.5	Parameters of the gel time kinetic model.....	184
7.6	Experimental CFS gel times compared to predicted gel times at three temperatures using the kinetic model with parameters in table 7.5.....	186

7.7 Values of the critical exponent κ for PBD samples cured at 28°C at various stoichiometric ratios (r).. 193

LIST OF FIGURES

Figure	Page
1.1	Schematic representation of the evolving equilibrium shear mechanical shear properties as a function of crosslinking reaction time. At the critical gel time (t_g) the zero shear viscosity (η_0) is infinite while the equilibrium shear modulus (G_e) is zero. 4
2.1	Polybutadiene system: (a) polybutadiene precursor prepolymer; (b) crosslinker molecule p-bis(dimethylsilyl)benzene; (c) catalyst cis-dichlorobis(diethylsulfide)-platinum II. The 1,4 internal backbone C=C bonds exist in cis and trans isomers..... 12
2.2	F.T. Raman spectrum of PBD20 C=C stretch region. The trans, cis, and vinyl peaks appear at 1666cm^{-1} , 1654cm^{-1} and 1641cm^{-1} respectively. Due to its low content, the vinyl peak at 1641cm^{-1} only appears as a shoulder. 13
2.3	F.T.i.r. spectrum of PBD18. The C=C stretch region from 1630cm^{-1} to 1670cm^{-1} appears as very weak absorption bands. More easily detectable unsaturation bands due to CH wagging occur at 968cm^{-1} for trans, 727cm^{-1} for cis, and 911cm^{-1} and 992cm^{-1} for vinyl. 14
2.4	Gas Chromatography (GC) data for crosslinker p-bis(dimethylsilyl)benzene as received from HULS America Inc. 16
2.5	(a) F.T. Raman and (b) F.T.i.r. spectrum of crosslinker p-bis(dimethylsilyl)benzene. In both spectra, the silane (Si-H) bond gives rise to a strong band near 2120cm^{-1} 17
2.6	Chemical crosslinking reaction. The reactivities of the olefin units on the polybutadiene are as follows: vinyl \gg cis \gg trans \cong 0. The stoichiometric ratio (r) is defined as [moles of SiH]/[moles of vinyl units]..... 19
2.7	F.T.i.r. kinetic data showing C=C stretch region of PBD18 during crosslinking with a stoichiometric amount of crosslinker (r=1). Absorptions occur at 1664cm^{-1} , 1651cm^{-1} , and 1637cm^{-1} for the trans, cis, and vinyl olefin units respectively. The reaction was monitored for 125 minutes at $25 \pm 1^\circ\text{C}$. Reaction of the vinyl site can be seen by the decrease of the intensity in the C=C vinyl stretch at 1637cm^{-1} 22

2.8	F.T.i.r. kinetics data of CH wagging region of PBD18 during crosslinking with a stoichiometric amount of crosslinker ($r=1$). The reaction was monitored for 125 min at $25\pm^{\circ}\text{C}$. Evidence of vinyl reactivity is seen by decreasing peaks at 992cm^{-1} and 911cm^{-1} . A possibility of cis reactivity is seen by the decreasing peak at 729cm^{-1} . A slight increase in the trans CH wag is seen at 966cm^{-1}	23
2.9	Master curves of the complex modulus of PBD18 showing the effectiveness of vacuum stripping in removing toluene from the sample introduced by the catalyst solution. PBD18 standard is data of bulk PBD18. G^* of PBD18 with 8 wt% of toluene is shifted down and to higher frequencies due to plasticization. After vacuum stripping at 60°C for 2h, G^* returns to the same behavior as the bulk material. $T_{\text{ref}} = 28^{\circ}\text{C}$	26
3.1	(a) Simple shear flow for two parallel plate and (b) parallel disk geometry.....	29
3.2	Sinusoidal strain and stress response for dynamic mechanical measurement.	32
3.3	Maxwell-Wiechert model with i Maxwell modes in parallel. The relaxation time of each mode is given by λ_i . The distribution of relaxation modes, g_i vs. λ_i , gives the discrete relaxation time spectrum.	37
3.4	Relaxation time spectra of PBD201 calculated with IRIS software. The Parsimonious Model is given by the discrete modes (g_i, λ_i) while the continuous spectrum is given by $H(\lambda)$. $T_{\text{ref}} = 28^{\circ}\text{C}$	39
3.5	Consecutive Frequency Sweep (CFS) experiment. $\tan \delta$ is plotted versus reaction time for at least two decades of frequency with "Gelpro" software. Intersection of the $\tan \delta$ curves at the critical gel time t_c indicates power law behavior of the dynamic mechanical properties over the frequencies scanned.	41
4.1	Dynamic moduli (G', G'') master curves of the bulk polybutadiene precursors. The open and filled symbols represent the storage modulus (G') and loss modulus (G'') respectively. All master curves are shifted with a reference temperature $T_{\text{ref}} = 28^{\circ}\text{C}$	48
4.2	$\tan \delta$ master curves of the dynamic data shown in figure 4.1. The reference temperature is 28°C	49

4.3	Time-temperature superposition horizontal shift factor (a_T) and vertical shift factor (b_T) of the dynamic data in figure 4.1. The WLF equation describes a_T as a function of temperature with the parameters given in figure 4.1.....	50
4.4	Complex viscosity (η^*) of the dynamic data in figure 4.1. The reference temperature is 28°C. The zero shear viscosity (η_0) is taken as the value of η^* in the long time region where η^* is independent of frequency.	51
4.5	Zero shear viscosity (η_0) of bulk polybutadiene precursors and polybutadiene precursors diluted with a stoichiometric ($r=1$) amount of crosslinker (~12wt%). η_0 is taken as η^* in the low frequency limit. η_0 scales with M_w to the 3.52 and 3.51 for the bulk and diluted precursors respectively.	53
4.6	Schematic of the BSW-spectrum with labeled parameter. λ_1 represents the intercept of the asymptotes of the power laws from the entanglement and transition zones. λ_1 is found to decrease with decreasing M_w while λ_c is constant for all M_w 's.	57
4.7	Loss moduli for sample PBD201. Power law fits through the entanglement zone and onset to glass transition zone give initial slope values of $n_e=0.18$ and $n_g=0.71$ respectively.....	61
4.8	BSW-spectra calculated for the molecular weights of the polybutadiene samples with parameters in table 4.2.	64
4.9	Comparison of the storage modulus (G') data of samples PBD18 through PBD97 with the storage modulus calculated from the BSW-spectra in figure 4.8.....	65
4.10	Comparison of the loss modulus (G'') data of samples PBD18 through PBD97 with the loss modulus calculated from the BSW-spectra in figure 4.8.....	66
4.11	Dynamic moduli of bulk PBD38 and PBD38 mixed with stoichiometrically balanced amount (12 wt%) of crosslinker. The plasticizing effect of the crosslinker shifts the data vertically down and horizontally to higher frequencies.....	69
4.12	Dynamic moduli of PBD samples PBD18 through PBD97 diluted with stoichiometrically balanced amounts of crosslinker.....	70

4.13	Schematic representation of the BSW-spectrum for bulk polymers compared to the BSW-spectrum of concentrated solution. Due to the dilution effect, the plateau modulus (G_N^0) and λ_{\max} of the bulk material is shifted down to $G_{N,d}^0$ and $\lambda_{\max,d}$ respectively.	74
4.14	(a) Storage and (b) loss modulus data of diluted PBD samples PBD18 through PBD97. The modified BSW model accounting for the diluent effect is given by the solid line.	76
5.1	Evolution of G' , G'' versus reaction time for PBD38 at stoichiometric conditions at 28°C. The data are sorted with "Gelpro" by frequency. The solid line represents the smoothed fit of the data. Symbols are actual data points.	82
5.2	CFS data showing the evolution of $\tan \delta$ during the reaction time for PBD38 at stoichiometric conditions at 28°C. The frequency range of the window is from 1 to 100 rad/s. t_c indicates the critical gel time. ...	83
5.3	CFS data for PBD18 at $r=0.25$ at 28°C. Slow reactions tend to smear out the intersection point of $\tan \delta$ making determination of t_c more difficult. Error bars in t_c are given by Δt_c . Δt_c becomes smaller as the rate of gelation increases.	85
5.4	"Gelpro" interpolated dynamic moduli at three times in the vicinity of the gel point from the smoothed curve data of PBD38 at stoichiometric conditions at 28°C. The symbols are interpolated data points. The solid line only serves to connect the points and is not a fit to the data.	86
5.5	Tan δ of interpolated data in figure 5.4. At the gel point, $\tan \delta$ is independent of frequency with a value close to 1. The solid line connects the interpolated data points and is not a fit.	87
5.6	Normalized phase ($2\delta/\pi$) of interpolated data in figure 5.4. At the gel point, $2\delta/\pi$ gives the exponent $n = 0.5$. The solid line connects the interpolated data points and is not a fit.	88
5.7	Comparison of interpolated G' , G'' data points calculated by Gelpro at t_c to G' , G'' of stopped sample. The stopped sample and CFS sample are both PBD18 at $r=1$ measured at 28°C.	89

5.8	CFS data showing $\tan \delta$ versus reaction time in the vicinity of the gel point for samples (a) PBD18 (b)PBD20 (c) PBD38. All measurements were carried out at balanced stoichiometry with a temperature of 28°C.....	91
5.9	CFS data showing $\tan \delta$ versus reaction time in the vicinity of the gel point for samples (a) PBD44 (b) PBD70 (c) PBD97. All measurements were carried out at balanced stoichiometry with a temperature of 28°C.....	92
5.10	Critical gel strength (S) versus stoichiometric ratio (r) for samples PBD18 through PBD70. All measurement were made at 28°C.....	93
5.11	Critical relaxation exponent (n) versus stoichiometric ratio (r) for samples PBD18 through PBD70.....	94
5.12	Rate of change the dynamic moduli at t_c versus frequency at 28°C for sample PBD38 at balanced stoichiometry.....	97
5.13	CFS data illustrating an example of the inhomogeneous cure of PBD18, $r=1$, at 28°C. The lowest two frequencies do not intersect with the other frequencies.....	99
5.14	Interpolated $\tan \delta$ data points at three times in the vicinity of t_c for the gelation of PBD97 at $r=1$ and 28°C. Solid lines connect the interpolated data points and are not fits to the data.	101
5.15	Interpolated dynamic moduli for the same conditions as in figure 5.13. Solid lines connect the interpolated data points and are not fits to the data.	102
5.16	Master curves of bulk PBD18, PBD44, PBD97, and PBD201 precursors at $T_{ref}=28^\circ\text{C}$. The dotted lines give the upper and lower values of the frequency window scanned with the CFS technique. As the precursor molecular weight increases, more of the entangle region enters into the CFS window thus making gel point detection more difficult.....	104
6.1	Schematic of the removable sample mold for used for stopped samples.....	111
6.2	CFS data showing G' , G'' of PBD18 at 28°C as a function of time for three frequencies after spraying on poisoning solution to stop the reaction.....	113

6.3	Dynamic data master curves of sample PBD38 mixed with stoichiometric amount of crosslinker. One of the samples has been sprayed with poison solution (<2wt%). Open symbols represent G' and filled symbols represent G'' . $T_{ref} = 28^{\circ}C$	115
6.4	F.T. Raman calibration curve showing the linear dependence of the normalized silane peak intensity as function of stoichiometric ratio (r).	117
6.5	F.T. Raman spectra of three stopped PBD20 samples compared to the initial uncrosslinked material. Conversion of silane is seen by the decreasing peak intensity at $2120cm^{-1}$	118
6.6	Evolution of master curves of (a) the storage modulus (G') and (b) the loss modulus (G'') of PBD18 stopped samples. The power law of the critical gel (CG) is given in the terminal zone. All samples are at balanced stoichiometry. $T_{ref} = 28^{\circ}C$	120
6.7	Horizontal shift factor (a_T) for the stopped PBD18 samples of figure 6.6. The WLF parameters are given in the figure.....	122
6.8	Tan δ master curves of dynamic data in figure 6.6.	123
6.9	Normalized phase angle ($2\delta/\pi$) of tan δ data given in figure 6.8.	124
6.10	Evolution of the relaxation time spectrum calculated by IRIS software for the dynamic data in figure 6.6.....	125
6.11	Dynamic data master curves showing the comparison of PBD44 critical gel to the precursor state of PBD44 mixed with $r=1$ amount of crosslinker. Open symbols represent G' and filled symbols represent G'' . $T_{ref} = 28^{\circ}C$	126
6.12	Dynamic data master curves of stopped samples near the critical gel point. Open symbols represent G' and filled symbols represent G'' . $T_{ref} = 28^{\circ}C$	128
6.13	Master curves of (a) tan δ and (b) normalized phase angle ($2\delta/\pi$) for dynamic data in figure 6.12.....	129
6.14	Relaxation time spectra of stopped critical gel samples calculated with IRIS software.	130
6.15	Horizontal shift factor (a_T) of stopped critical gel samples. a_T can be described by WLF behavior with the parameters in the figure.....	131

6.16	Evolution of $\tan \delta$ master curves of stopped PBD20 samples at balanced stoichiometry. $T_{\text{ref}} = 28^{\circ}\text{C}$. The extent of reaction (p), measured by F.T. Raman spectroscopy, of three of the samples are labeled.....	132
6.17	Schematic representation of the model spectra for entangled critical gels. Comparison is shown for the simple superposition of BSW-spectrum of the precursor and CW-spectrum, and the modified spectra with decreased slope in the entanglement region.....	138
6.18	Calculated dynamic moduli from the model gel spectra in equation 6.8 (simple BSW-CW-spectrum) and modified gel spectra model in equation 6.9 for a sample with precursor M_w of 97000 g/mole. The experimental dynamic data of stopped PBD97 critical gel is shown in comparison to the model. $T_{\text{ref}} = 28^{\circ}\text{C}$	141
6.19	Relaxation time spectra calculated with the gel model of equation 6.9 and parameters in table 6.1 for precursors PBD18 through PBD97.	142
6.20	Dynamic moduli calculated with the BSW-CW gel model spectra in figure 6.19 compared to experimental data of stopped samples near the critical gel point. $T_{\text{ref}}=28^{\circ}\text{C}$	143
6.21	The characteristic modulus G_0 marks the upper limit observed for critical gel power law behavior. G_0 is calculated to be $2.5 \text{ E}+5 \text{ Pa}$ with equation 6.13. The corresponding characteristic shortest relaxation times of the power law behavior are given by $\lambda_{0,1}$, $\lambda_{0,2}$, and $\lambda_{0,3}$ for samples PBD18, PBD38 and PBD97 respectively.....	146
6.22	Scaling relationship of gel strength (S) with the precursor M_w . The slopes are 1.76 and 1.80 for gel strengths calculated from CFS and stopped sample data respectively.	149
6.23	Complex modulus of fully cured samples PBD18, PBD38, PBD44, PBD70, and PBD97 at balanced stoichiometry. Measurements were made at 28°C	152
6.24	Complex modulus (G^*) of fully cured PBD18 samples at different values of stoichiometric ratio (r). Measurements were made at 28°C	156
6.25	Equilibrium modulus (G_e) of fully cured PBD18 as a function of stoichiometric ratio (r). G_e is taken as G^* at 0.01 rad/s.....	157

6.26	Complex modulus (G^*) for fully cured samples with and without tiny air bubbles. Measurements were made 28°C with balanced stoichiometry.....	159
7.1	Evolution of the dynamic moduli at 3.16 rad/s during gelation for sample PBD38 at 28°C for three values of stoichiometric ratio (r). Filled symbols represent G'' . The approximate gel times (t_g) are indicated by the dotted hash marks.	164
7.2	Evolution of the dynamic moduli at 3.16 rad/s during gelation at balanced stoichiometry for three precursor molecular weights. Filled symbols represent G'' . The approximate gel times (t_g) are indicated by the dotted hash marks.	166
7.3	Schematic of kinetic experiment showing the extent of reaction (p) versus reaction time (t_r). p and t_r are given initially as p_i and t_i at the beginning if the CFS measurement in the cure zone with temperature of the rheometer ($T_{\text{rheometer}}$).....	171
7.4	F.T.i.r. kinetic data at $25\pm 1^\circ\text{C}$ showing the conversion of silane at 2116cm^{-1} of PBD18 with stoichiometric amount of silane. The peak at 1436cm^{-1} was used as an internal reference peak.	174
7.5	F.T.i.r calibration curved showing the linear dependence of the normalized silane peak intensity versus stoichiometric ratio (r).....	175
7.6	F.T.i.r. kinetic data results. Extent of reaction of silane (p) is plotted versus reaction time for two initial compositions of PBD18 and crosslinker ($r=1$, and $r=0.5$). The values of the critical extents of reaction (p_c), calculated by branching theory, are given for the two initial compositions. The temperature is $25\pm 1^\circ\text{C}$	177
7.7	F.T.i.r. kinetic data plotted for determination of the reaction order. R is the normalized silane peak ratio which is directly proportional to silane concentration. Data is plotted for initial compositions of (a) $r=1$ and (b) $r=0.5$	178
7.8	Experimental gel times measure by CFS ($t_{\text{gel, CFS}}$) plotted vs. a function of p_c from equation 7.13. p_c is calculated from equation 7.1. Data is plotted for three temperature. The slope of the plot gives the rate constant - $1/\bar{k}$	183
7.9	Plot of the rate constant vs. the cure temperature. The slope gives the activation energy $-E_a / R$	185

7.10	G* vs. reaction time for PBD18 at $r=1$ at 28°C for three frequencies. The slope at time t gives the rate of gelation.	189
7.11	Plot of the rate of gelation at t_c time versus frequency for PBD18 at $r=1$ at 28°C . The slope gives the critical exponent $-\kappa$	191
7.12	Rate of gelation versus frequency at t_c for PBD44 at $r=1$ at 28°C . Deviation from the power law at higher frequencies is seen for higher molecular weights.	195

LIST OF SYMBOLS

Times Roman Symbols

A	A value in the range $0 < A < 1$ used in the BSW-CW gel spectrum model to adjust the slope in the entanglement regime
A	preexponential frequency factor calculated from Arrhenius kinetic analysis
a	prefactor of the molecular weight/zero shear viscosity relationship
a_i	local spacing of the discrete relaxation time spectrum
a_T	horizontal shift factor
b_T	vertical shift factor
f	functionality of the polybutadiene precursor
G	shear modulus of Hookean solid
G'	shear storage modulus (Pa)
G''	shear loss modulus (Pa)
G^*	complex shear modulus (Pa)
G_0	characteristic modulus for critical gels (Pa)
G_e	equilibrium modulus of a viscoelastic solid
G_N^0	plateau modulus (Pa)
$G_{N,d}^0$	plateau modulus of the precursor diluted with a stoichiometric amount of crosslinker
$G(t)$	shear stress relaxation modulus (Pa)
g_i	relaxation strength of the discrete relaxation time spectrum (Pa)
$H(\lambda)$	continuous relaxation time spectrum
M_0	monomer molecular weight
M_c	Crossover molecular weight which indicates the molecular weight just large enough to show entanglement behavior.
$M_{c,d}$	crossover molecular weight of the precursor diluted with a stoichiometric amount of crosslinker
M_n	number average molecular weight

M_w	weight average molecular weight
n	reaction order
n	critical relaxation exponent, slope of the CW-spectrum for critical gels
n_e	slope of the entanglement region in the BSW-spectrum
n_g	slope of the glass transition region in the BSW-spectrum
N_{mu}	mutation number
p	extent of reaction
p_c	critical extent of reaction at the gel point
p_i	initial extent of reaction at the beginning of kinetic CFS measurement
r	stoichiometric ratio
r_l	lower limiting stoichiometric ratio for a crosslinking sample to reach the critical
r_u	upper limiting stoichiometric ratio for a crosslinking sample to reach the critical gel point
t_c	critical gel time
T_g	glass transition temperature
$t_{gel,CFS}$	critical gel time measured by CFS technique, equal to $t_c - t_i$
t_i	initial time at the beginning of the kinetic CFS measurement
T_{ref}	reference temperature
v	volume fraction of polymer in concentrated solutions
$\overline{X_w}$	weight average degree of polymerization
$\overline{X_n}$	number average degree of polymerization gel point

Greek Symbols

α	branching coefficient
$\Gamma(n)$	Euler's gamma function
γ	shear strain

δ	phase angle between stress and strain (rad)
η_0	zero shear viscosity (Pa s)
κ	critical exponent used in gelation kinetic analysis
λ	relaxation time
λ_0	characteristic relaxation time of critical gel
λ_c	crossover relaxation time
$\lambda_{c,d}$	crossover relaxation time for diluted precursor
λ_{\max}	longest relaxation time
$\lambda_{\max,d}$	longest relaxation time of the diluted precursor
$\lambda_{p,d}$	longest relaxation time of the precursor in the critical gel, marks the shortest time observed for critical gel power law behavior
ξ	branching index
ξ_c	critical branching index at the critical gel point
ρ	density
σ	shear stress (Pa)
ω	frequency (rad/s)
ω_0	characteristic frequency of critical gel, upper limit of power law behavior

Script symbols

\mathcal{J}	torque
---------------	--------

CHAPTER 1

INTRODUCTION

During the chemical crosslinking reaction of a polymer, the material undergoes a phase transition from a viscous liquid to a rubbery solid when the temperature is above the glass transition temperature (T_g). At this liquid-solid transition, called the critical gel point, the material possesses mechanical properties intermediate of the two states and is called a critical gel, to distinguish it from other materials commonly called gels.

Engineers specializing in reactive polymer processing, such as in thermosetting resins, are interested in the evolution of the network mechanical properties and knowledge of critical gel properties can be a tremendous aid in modeling the processing behavior of thermosets.

Gelation of polymeric materials can also occur by phase separation processes. Such an example is a phase separated elastomer where the elasticity in the material arises from a soft rubbery phase physically crosslinked by phase separated hard domains. For example, these types of hard domains can be crystalline, such as in thermoplastic elastomers (te Nijenhuis and Winter, 1989; Lin et al., 1991; Richtering et al., 1992), or ionic aggregations, such as in ion-containing polymers called ionomers (Tant and Wilkes, 1988; Lantman et al. 1989). Another example occurs in solutions of polypeptide residues derived from animal collagen, or gelatin gels, where the physical crosslinks are comprised of ordered collagen-like triple helices (Clark and Ross-Murphy, 1987; Ross-Murphy, 1991). Materials of the types mentioned are said to undergo "physical" gelation and the process is often reversible. Gels of the physical type were not the focus of this project. The objective of this work was to study gelation where crosslinks were produced by creating bonds by means of an irreversible chemical reaction.

On a molecular level, chemical gelation can be depicted in the simplest way by either the step growth polymerization of multifunctional small molecules or by the

crosslinking of long polymer chains. Gelation by step growth polymerization can take place for the cases when 1) two species of molecules react in which the functionality of one of the species is two while the other species has a functionality greater than two 2) when two species of molecules react and the functionality of both of the species are greater than two 3) or when a molecule with a functionality greater than two reacts with its own species in a homopolymerization type reaction. Gelation can also occur by crosslinking a polymer at many random sites along the backbone of the chain (vulcanization) or by connecting the polymers at the chain ends (endlinking). As the reaction proceeds, clusters of molecules begin to grow in size until at the critical gel point, one cluster reaches infinite size ($M_w \rightarrow \infty$) and spans the entire spatial dimensions of the sample holder.

Statistical theories have been developed to predict the amount of functional sites that need to be converted in order to reach the critical gel point. The classical theory of gelation was presented by Flory (1941,1953) and Stockmayer (1943) who used a statistical method to derive an expression that predicts the critical extent of reaction needed for the weight average degree of polymerization, \overline{X}_w , to approach an infinite value. The theory assumes that 1) the reactivity of all the functional groups of the same type are equal and independent of molecular size and 2) that no intramolecular reactions between functional groups on the same molecule occur (no loop formations). A similar result was derived by the recursive approach of Macosko and Miller (1976). The predictions of these theories provide a simple expression for the critical extent of reaction (p_c) needed to reach the infinite cluster as a function of stoichiometric ratio and functionality of the precursor materials. Experimental results have been found to agree extremely well with these predictions (Flory, 1941; Valles and Macosko, 1979; Venkataraman et al. 1989; Muller et al. 1991).

Another important contribution to gelation theory has been made by using percolation theory. This theory describes statistical cluster growth on specific types of

lattices and for different spatial dimensions. Percolation theory has been used to describe other types of critical phenomena and the unique scaling relationships associated with properties of materials at critical transitions (Stauffer et al., 1982; Stauffer, 1985; Zallen, 1983).

Rheologically, gelation can be characterized by the evolution of the equilibrium shear properties shown in figure 1.1. As the reaction proceeds in the liquid state, clusters grow in size as a function of reaction time. The zero shear viscosity (η_0) increases steadily at first and later diverges ($\eta_0 \rightarrow \infty$) at the critical gel time (t_c). After the gel point, the material is a viscoelastic solid and can be characterized by an equilibrium modulus (G_e). G_e increases until it reaches a limiting, constant value as the extent of reaction (p) approaches completion ($p \rightarrow 1$). Therefore, at the gel point, the critical gel is characterized by an infinite zero shear viscosity and an equilibrium modulus equal to zero.

This relatively simple representation of the crosslinking process works to schematically describe the evolution of mechanical properties during the gelation of small multifunctional molecules as well as vulcanized polymers. Up until now, most of the rheological work accomplished in studying gelation has focused on the relaxation behavior of critical gels that have been made from precursors below their critical molecular weight for entanglement, M_c . The molecular mobility of linear flexible polymers is known to be reduced when the molecular weight exceeds this characteristic value. Above M_c , the molecules are long enough to form entanglements and at intermediate time scales the melt behaves like a rubber having a plateau modulus G_N^0 (Ferry, 1980). Chemical crosslinking of such high molecular weight polymers increases the molecular weight even further. It results in a rheological behavior which somehow combines the elasticity of the entangled molecular structure with the elasticity of the evolving chemical network during gelation. What is not well understood at this time is how the presence of physical entanglements effects the gelation process.

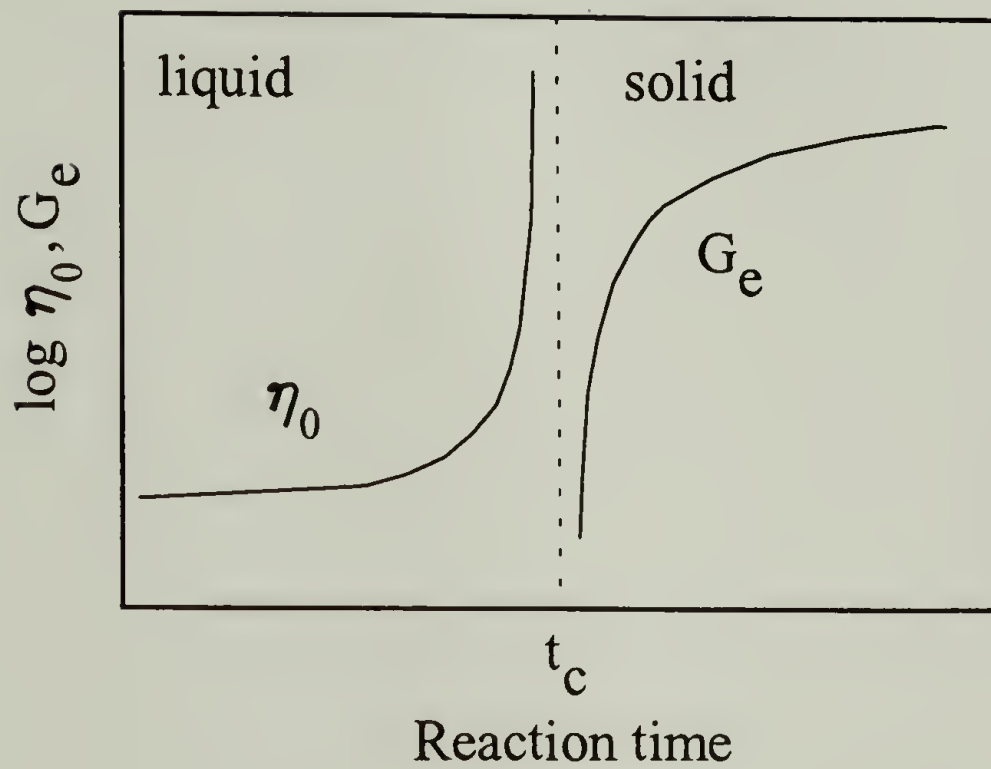


Figure 1.1 Schematic representation of the evolving equilibrium shear mechanical properties as a function of crosslinking reaction time. At the critical gel time (t_c) the zero shear viscosity (η_0) is infinite while the equilibrium shear modulus (G_e) is zero.

In past studies, precursors without entanglements were chosen so as to avoid their interference with the gelation process. While such restriction was appropriate in the beginning, the tools are available now for attacking the more complicated problem of gelation in the presence of physical entanglements. This study will focus on investigating the effects that physical entanglements have on the crosslinking process and on the rheological properties of the critical gel.

Before the relaxation of entangled gels is examined, the relaxation behavior of the uncrosslinked material needs to be understood. In general, the viscoelasticity of materials is defined by the relaxation time spectrum, $H(\lambda)$, for the transient part of the relaxation modulus (Ferry, 1980)

$$G(t) = \int_0^{\infty} H(\lambda) e^{-t/\lambda} \frac{d\lambda}{\lambda} + G_e \quad (1.1)$$

where G_e is the equilibrium modulus. G_e is finite for viscoelastic solids and is zero for the liquid and for the material at the gel point. The effect of entanglements on gelation can be investigated experimentally by mechanically probing molecularly well defined samples and by searching for characteristic patterns in the relaxation time spectrum, $H(\lambda)$, as a function of increased extent of crosslinking, p .

As a starting point for studying the gelation in the presence of entanglements, a precursor polymer was chosen with long linear flexible chains of nearly uniform length whose molecular weight is above M_c . For such a fluid, the effect of entanglements is well known (Ferry, 1980; Graessley, 1974; Doi and Edwards, 1986) and theories of the molecular dynamics have been developed to predict the spectrum from models for the molecular motion and the averaged forces on the molecules (Rouse, 1953; de Gennes, 1979; Doi and Edwards, 1986; Bird, 1987; des Cloizeaux, 1990).

Recently, the relaxation time spectrum of a linear flexible polymer above M_c and of low polydispersity has been shown to be well represented by an empirical model described by the superposition of two power laws (BSW-spectrum) (Baumgaertel et al., 1990, 1992)

$$H(\lambda) = \begin{cases} n_e G_N^0 [(\lambda/\lambda_c)^{-n_g} + (\lambda/\lambda_{\max})^{n_e}] & \text{for } 0 < \lambda < \lambda_{\max} \\ 0 & \text{for } \lambda > \lambda_{\max} \end{cases} \quad (1.2)$$

The characteristic material parameters are the plateau modulus G_N^0 , the power law exponents n_g and n_e for the glass transition and the entanglement region respectively, a crossover time λ_c for the onset of the glass transition and the longest relaxation time λ_{\max} . This model gives us a rheologically well defined starting point of the uncrosslinked precursors and will be discussed in greater detail in chapter 4.

Since it is impossible to measure the equilibrium shear properties of a critical gel directly, a new description of the relaxation behavior at the gel point is needed. It has been found by Chambon and Winter (1985, 1986, 1987) that polymers at the critical gel point have a terminal relaxation time spectrum which is self-similar (CW-spectrum). The empirical CW-spectrum has a power law distribution of relaxation times,

$$H(\lambda) = \frac{G_0}{\Gamma(n)} \left(\frac{\lambda}{\lambda_0} \right)^{-n}, \quad \lambda_0 < \lambda < \infty \quad (1.3)$$

where the critical relaxation exponent (n) may take on the values $0 < n < 1$ and Γ is Euler's gamma function. G_0 is a material characteristic modulus which, for endlinking systems, has been proposed to be a value near the plateau modulus (Scanlan and Winter, 1991) or near the modulus of the fully crosslinked material (Izuka et al., 1992). This issue will be discussed in greater detail in chapter 6. The lower limit, λ_0 , of the CW-spectrum depends on small scale details of the material. For the previously studied low

molecular weight precursor materials having molecular weights $\leq M_c$, it marked the crossover to the glass transition. For high molecular weight materials, it marks the transition to the entanglement region as will be shown in this study.

A consequence of the critical gel having such a self-similar spectrum is that the transient part of the relaxation modulus also exhibits power law behavior described by the gel equation as

$$G(t) = St^{-n}, \quad \lambda_0 < t < \infty \quad (1.4)$$

where $S = G_0 \lambda_0^n$ is the gel strength. n is the critical relaxation exponent of equation 1.3.

The complex modulus at the critical gel point is also a power law and is given by

$$G^*(\omega, p_c) = \Gamma(1-n)S(i\omega)^n, \quad \lambda_0 < \omega < \infty. \quad (1.5)$$

The storage modulus (G') and loss modulus (G'') are related by

$$G'(\omega) = \frac{G''(\omega)}{\tan \frac{n\pi}{2}} = S\omega^n \Gamma(1-n) \cos \frac{n\pi}{2}, \quad 1/\lambda_0 < \omega < \infty. \quad (1.6)$$

From equation 1.6 it follows that the phase angle (δ) between cyclic stress and strain is independent of frequency but proportional to n as

$$\delta = n\pi/2. \quad (1.7)$$

In this study several significant findings have been made which provide new information about the gelation of high molecular weight precursors. First, it was found that the precursor molecular weight, and the presence of entanglements, has a profound effect on the detection of the gel point by rheological methods. Second, the evolution of

the relaxation time spectrum during gelation of entangled polymers was explored and led to the development of an empirical model for the spectrum at the gel point for entangled critical gels which is discussed in chapter 6. This model has provided new insight to the relaxation behavior of entangled critical gels and has led to the finding of a new scaling relationship between the gel strength in equation 1.4 and the precursor molecular weight. Finally, a kinetic model was developed to predict the gel time as a function of the stoichiometric ratio and the functionalities of the precursor materials.

CHAPTER 2

MATERIALS AND CHARACTERIZATION

A system was chosen such that the precursor molecules were long enough to form entanglements, could be easily crosslinked, and could be synthesized with a narrow molecular weight distribution (i.e. $M_w/M_n < 1.1$). There was a choice of precursor polymers which could be crosslinked either at the chain ends or at sites along the chain. However, endlinking systems of very high molecular weight polymers prove to be problematic for such a study because the concentration of the reactive endgroups decreases as the molecular weight of the precursor is increased. As this occurs, it becomes difficult to control stoichiometry and to perform quantitative analysis accurately. Another complication which may arise is that the reaction rate may become so low that it would not be possible to reach the gel point in a finite experimental time. Therefore, in order for an endlinking system to have entanglements and overcome these drawbacks, it must have a very low M_c .

This inherent problem is overcome when crosslinking not only at the molecular chain ends but at sites along the backbone. For critical gels of this type, the molecular weight between crosslinks is random not only because the reactive sites are distributed randomly along the precursor chain but also because the probability that a chemical reaction will take place at these sites is random.

For this study, polybutadiene was chosen as the precursor polymer. The polymer chains will be crosslinked at specific sites along the backbone chain through a well defined chemical reaction. The details of the prepolymer and crosslinker characterization and crosslinking chemistry will be discussed in this chapter.

2.1 Polybutadiene Prepolymer

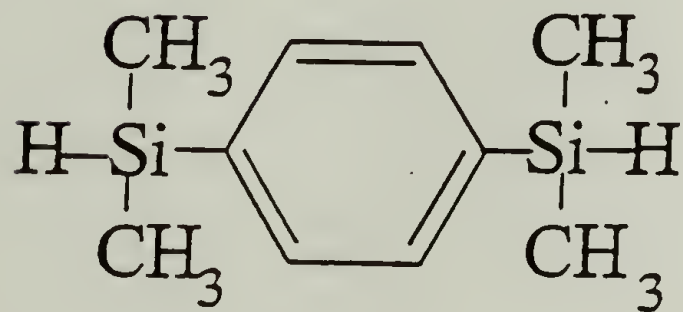
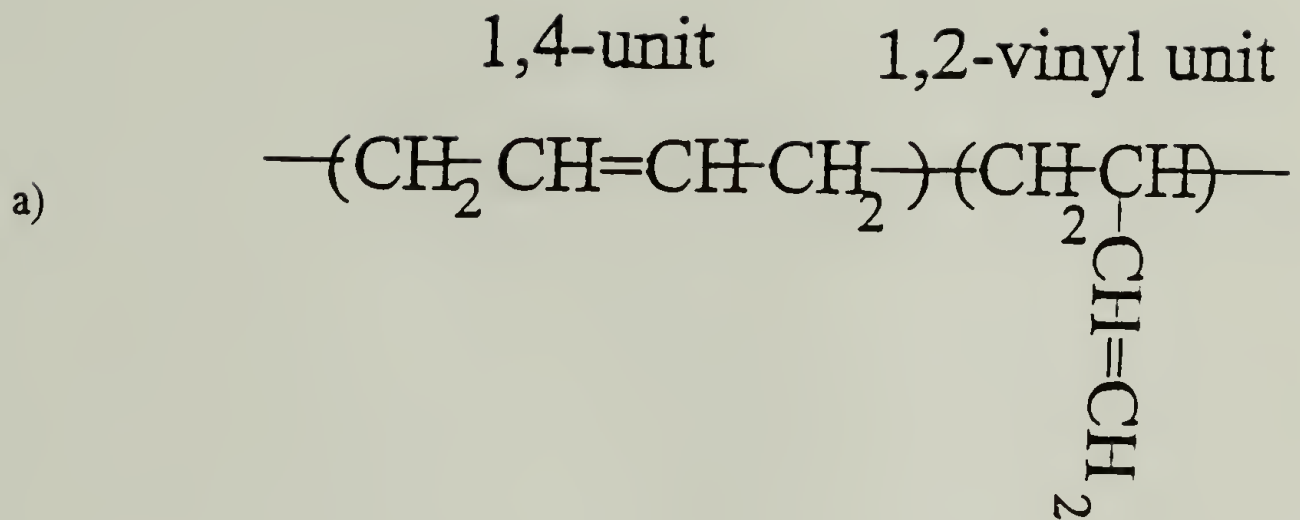
Seven polybutadiene (PBD) samples of different molecular weights and of low polydispersity were synthesized by Dr. Michael Masse (Shell Development Co.) using a standard anionic polymerization technique. Approximately 0.5% by weight of Ethanox was added to all samples to prevent oxidation. The samples were stored in the refrigerator to further prevent the chance of oxidation or polymerization of the unsaturated sites. Initial characterization was performed at Shell Development Co. by using Gel Permeation Chromatography (GPC) to determine the molecular weights and polydispersities, and proton Nuclear Magnetic Resonance (^1H NMR) analysis to measure the 1,2-vinyl content. Table 2.1 gives the summary of the characterization data.

The chemical structure of the polybutadienes (see figure 2.1) was analyzed by spectroscopic methods. The relative cis and trans content of the polybutadienes was measured by analyzing the olefinic C=C stretch region by F.T. (Fourier Transform) Raman spectroscopy. The quantitative analysis of the C=C cis and trans structures was done by using peak height ratios. This method was used by Cornell and Koenig (1969) who analyzed Raman spectra of polybutadienes. The F.T. Raman spectrum of polybutadiene is shown in figure 2.2. The Fourier Transform infrared (F.T.i.r.) spectrum of polybutadiene was also taken and is shown in figure 2.3. This data was taken because the curing kinetics, to be discussed in chapter 7, were to be monitored by F.T.i.r. The i.r. analysis of polybutadiene has been reported by Silas et al. (1959). A comprehensive analysis of general chemical structures and their respective Raman and i.r. bands is given by Colthup et al. (1990, 1991)

The glass transition temperatures were measured on a DuPont DSC instrument model 2910 at a heating rate of 20K/min. The T_g 's were taken as the inflection point of the temperature scans. The glass transition temperatures, given in Table 2.1, are independent of molecular weight. This behavior is expected for high molecular weight polymers as is seen for entangled polymers whose molecular weight is above M_c . The T_g

Table 2.1 Characterization summary of polybutadiene precursor polymers.

Sample	M_w	M_w/M_n	%cis	%trans	%vinyl	T_g ($^{\circ}\text{C}$)
PBD18	18100	1.03	41	52	7.30	-92
PBD20	20700	1.04	39	53	8.19	-91
PBD38	37900	1.05	41	51	7.70	-92
PBD44	44100	1.04	39	53	8.11	-90
PBD70	70200	1.02	43	50	7.30	-93
PBD97	97000	1.07	41	51	8.04	-90
PBD201	201000	1.27	44	48	7.88	-92



c)

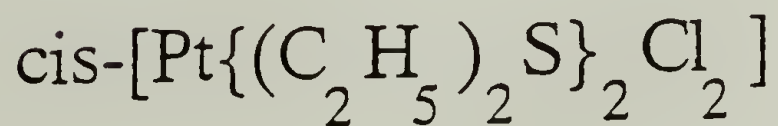


Figure 2.1 Polybutadiene system: (a) polybutadiene precursor prepolymer; (b) crosslinker molecule p-bis(dimethylsilyl)benzene; (c) catalyst cis-dichlorobis(diethylsulfide)-platinum II. The 1,4 internal backbone C=C bonds exist in cis and trans isomers.

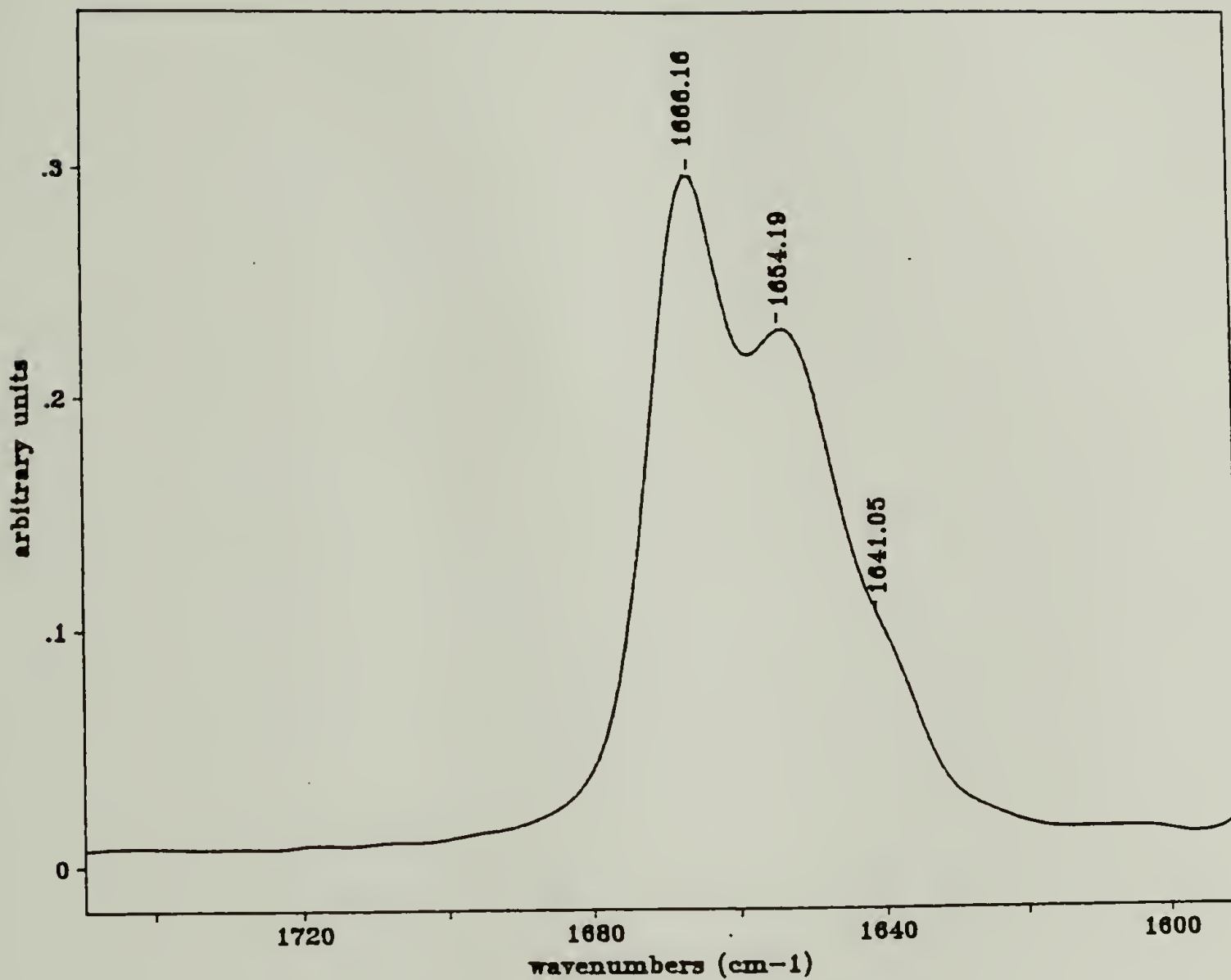


Figure 2.2 F.T. Raman spectrum of PBD20 C=C stretch region. The trans, cis, and vinyl peaks appear at 1666cm^{-1} , 1654cm^{-1} and 1641cm^{-1} respectively. Due to its low content, the vinyl peak at 1641cm^{-1} only appears as a shoulder.

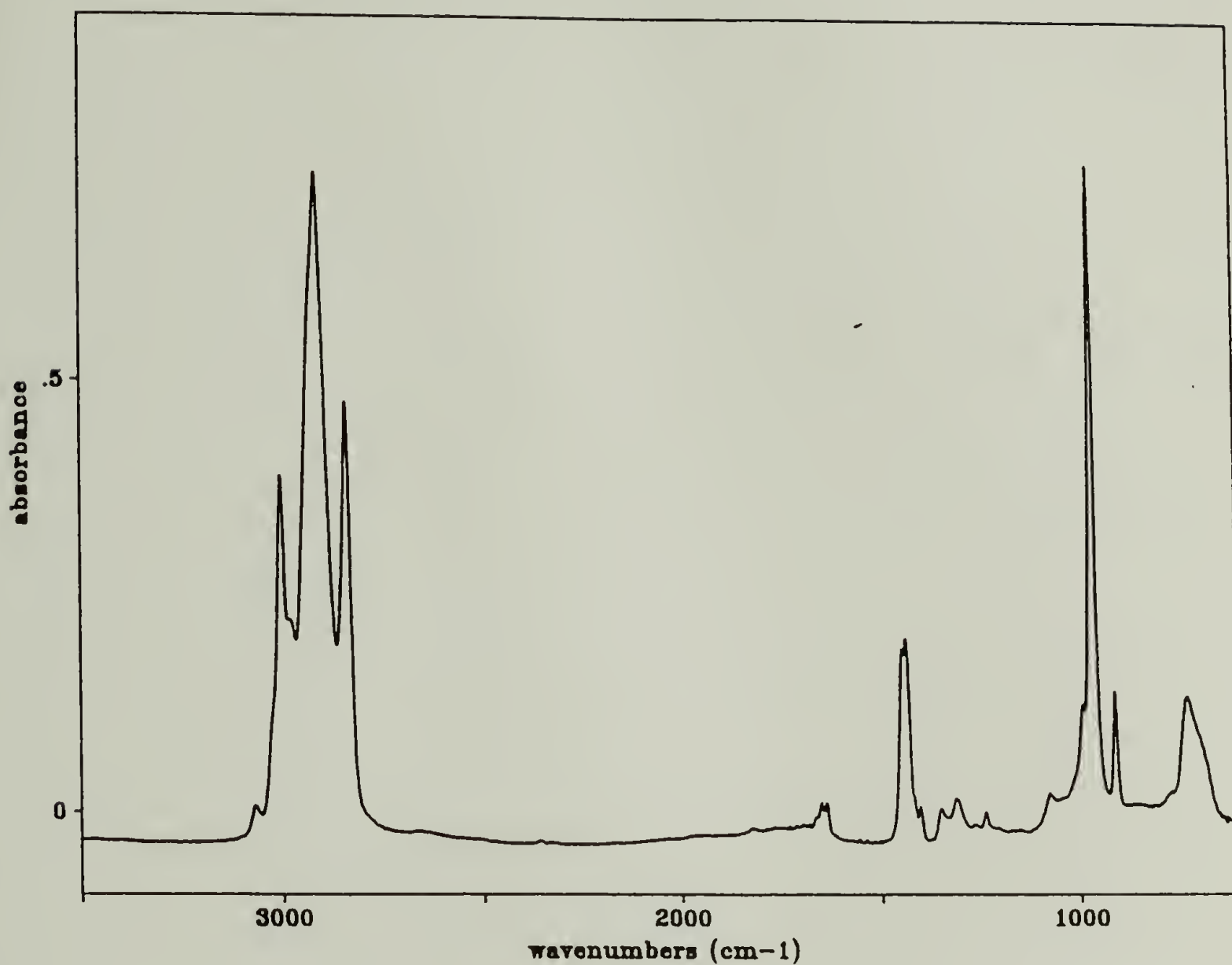


Figure 2.3 F.T.i.r. spectrum of PBD18. The C=C stretch region from 1630cm^{-1} to 1670cm^{-1} appears as very weak absorption bands. More easily detectable unsaturation bands due to CH wagging occur at 968cm^{-1} for trans, 727cm^{-1} for cis, and 911cm^{-1} and 992cm^{-1} for vinyl.

is expected to change for polymers with $M_w < M_c$. This relationship is given by the Fox-Flory equation (Ferry, 1980; Aklonis and MacKnight, 1983). The density of polybutadiene was taken to be 0.895 g/ml at 25°C from the literature (Valentine et al., 1968; Colby et al., 1991).

2.2 Crosslinker

The molecule chosen to crosslink the polybutadienes was *p*-bis(dimethylsilyl) benzene, an aromatic bifunctional silane whose chemical structure is shown in figure 2.1. This molecule has been used to crosslink polybutadienes by hydrosilation of the pendant 1,2 vinyl units (Friedmann and Brossas, 1984,1985; Aranguren and Macosko, 1988). By using an aromatic silane as a crosslinker, the reaction is virtually free of side reactions at the silane site (Aranguren and Macosko, 1988). Such undesired side reactions were always a concern when using siloxy silanes as crosslinkers at relatively high temperatures of 65°C to 110°C which could consume as high as 20-30% of the silane (Aranguren and Macosko, 1988; Chambon, 1986; Macosko and Saam, 1985). However, side reactions were essentially avoided when crosslinking was carried out at lower temperatures (Fischer and Gottlieb, 1986) (e.g. 28°C to 40°C) as was done in this work. The chemistry of the hydrosilation reaction will be discussed in the next section.

The crosslinker, as purchased from HULS America Inc., was found to be > 99.5% pure by Gas Chromatography (GC) analysis, shown in figure 2.4, and was used as received without any further purification. The density is 0.872 g/ml at 20°C and the formula weight is 194.2 g/mole.

For chemical structure determination, F.T. Raman and F.T.i.r. spectra were taken of the crosslinker molecule. The spectra are shown in figure 2.5.

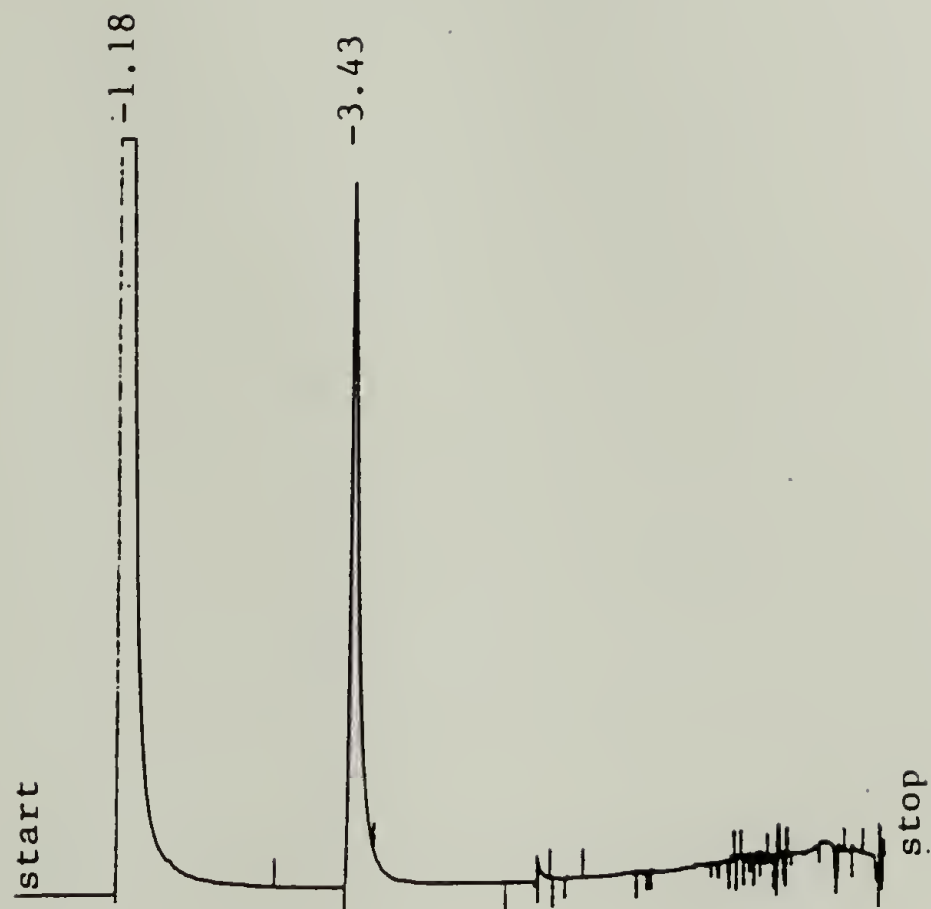


Figure 2.4 Gas Chromatography (GC) data for crosslinker p-bis(dimethylsilyl)benzene as received from HULS America Inc. The peak at 1.18 min is methylene chloride solvent. The crosslinker appears at 3.43 min.

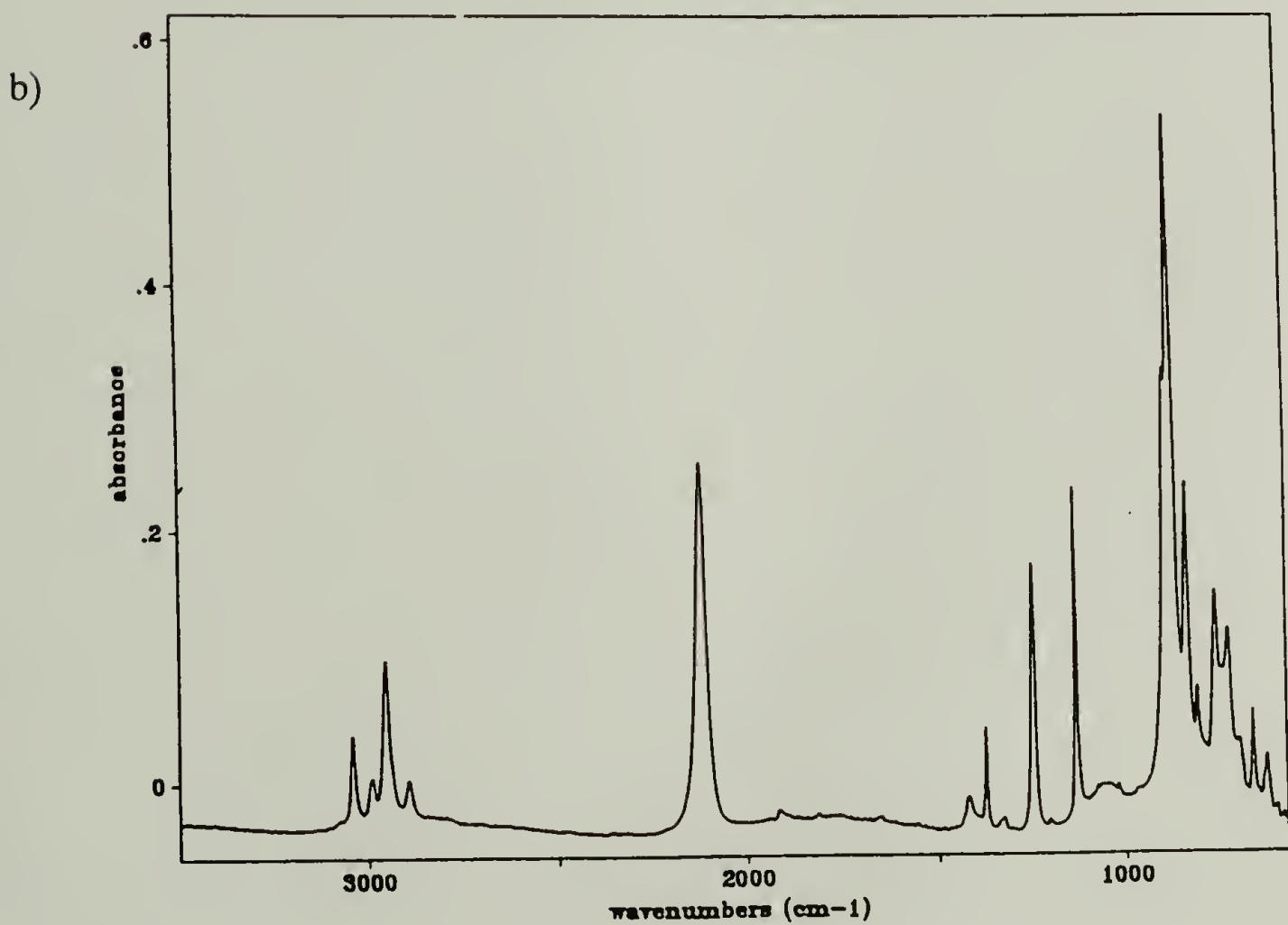
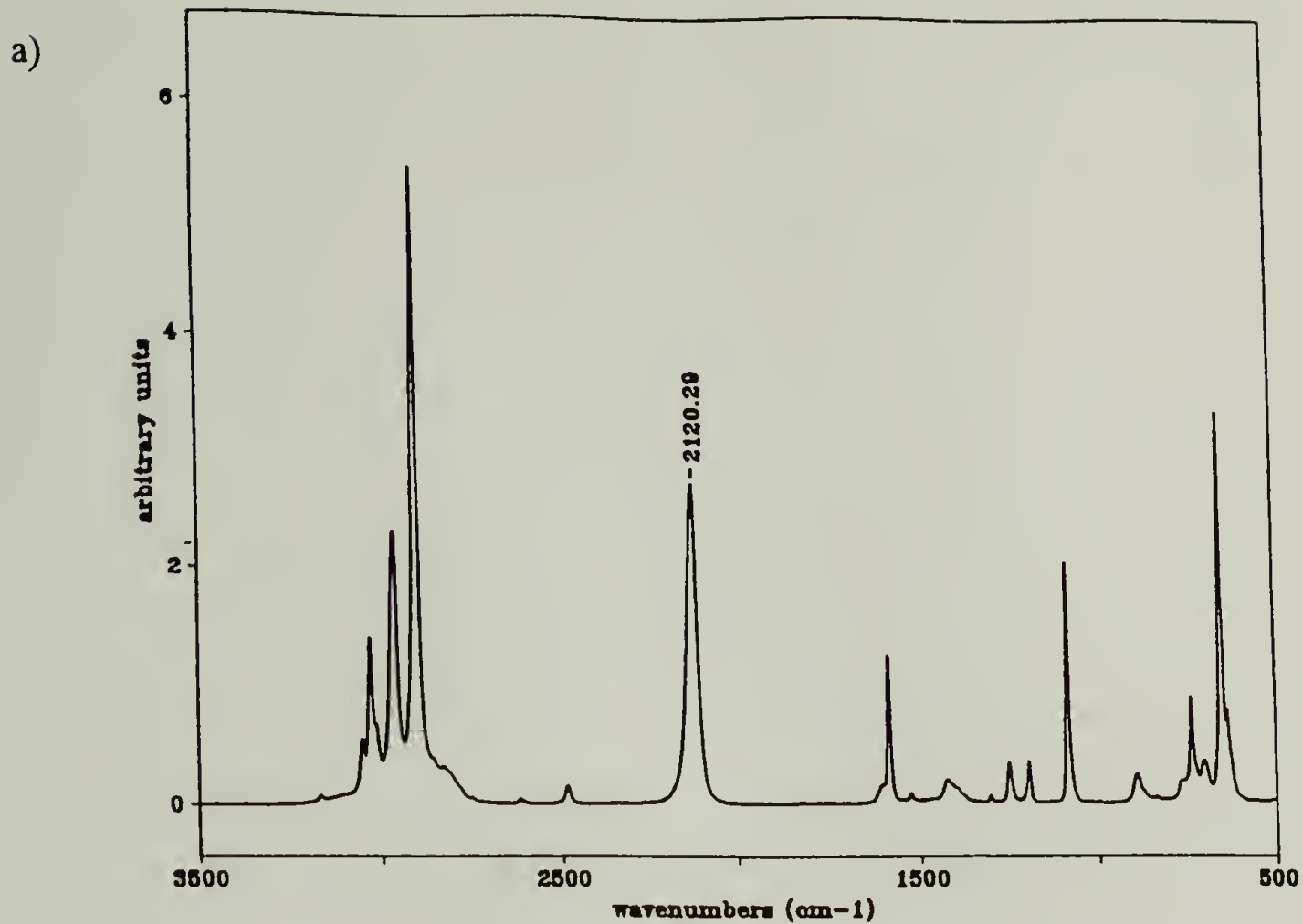


Figure 2.5 (a) F.T. Raman and (b) F.T.i.r. spectrum of crosslinker p-bis(dimethylsilyl)benzene. In both spectra, the silane (Si-H) bond gives rise to a strong band near 2120cm^{-1} .

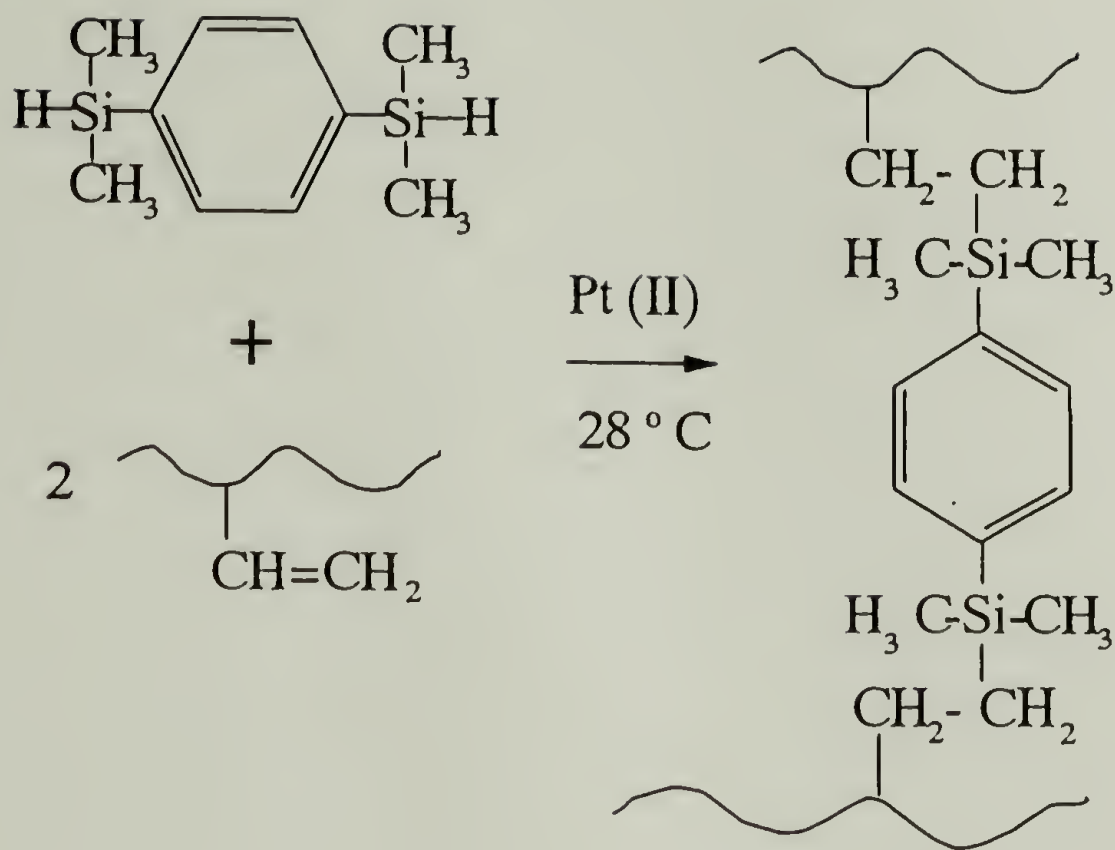
2.3 Catalyst and Crosslinking Reaction

A hydrosilation reaction is used to crosslink the polybutadiene chains at the pendant 1,2-vinyl sites along the backbone with p-bis(dimethylsilyl)benzene. A platinum compound, cis-dichlorobis(diethyl sulfide) platinum II shown in figure 2.1, catalyzed the reaction. A general schematic of the reaction is shown in figure 2.6. The detailed mechanism of hydrosilation has been proposed by Chalk and Harrod (1965) and is outlined in chapter 7.

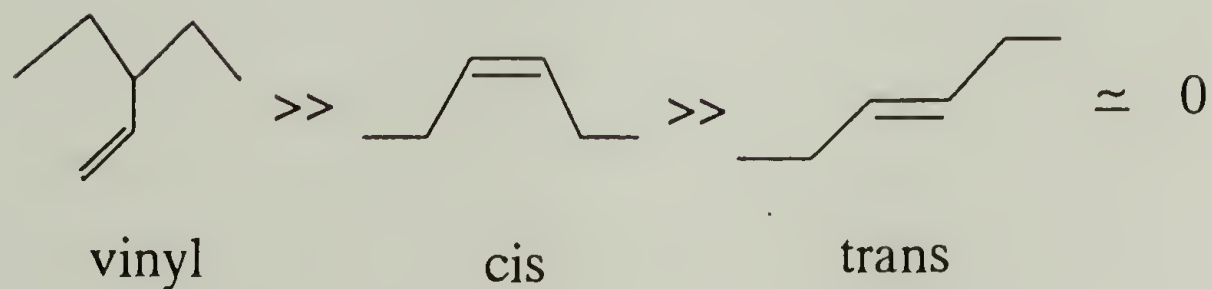
The catalyst was synthesized according to the method suggested by Kauffman and Cowan (1969). After drying the yellowish crystals of the cis isomer overnight, the catalyst was recrystallized four times. The melting point was found to be 104-105°C. The same melting point was observed by Chambon (1986) after synthesis. However, this was slightly lower than 107-108°C reported by Kauffman and Cowan (1969). The catalyst was made into a solution of concentration 8.0×10^{-3} moles/liter in dry toluene. The catalyst concentration was adjusted to this value so that a reasonable rate of gelation with a gel time of approximately 30 to 60 minutes would occur at room temperature ($\approx 25^\circ\text{C}$) with the amount used.

Crosslinking by hydrosilation has the advantage over other curing methods, such as peroxide or sulfur vulcanization, in that it takes place nearly exclusively at well defined sites on the chain, the 1,2-vinyl sites. The reactivity of the 1,2-vinyl sites has been found to be much higher than that of the 1,4-cis or trans units (Miron et al., 1973; Friedmann et al., 1982; Friedmann and Brossas, 1984,1985; Aranguren and Macosko, 1988). Knowing where the reaction takes place will make it possible to calculate the functionality of the chain and control the stoichiometric ratio of added crosslinker. This is not possible when vulcanizing with peroxide or sulfur. The functionality of the chain, f , was calculated as (Friedmann and Brossas, 1984)

$$f = p_{\text{vinyl}} \overline{X}_n \quad (2.1)$$



Reactivity of the butadiene units



$$r = [\text{SiH}] / [\text{vinyl}]$$

Figure 2.6 Chemical crosslinking reaction. The reactivities of the olefin units on the polybutadiene are as follows: vinyl \gg cis \gg trans ≈ 0 . The stoichiometric ratio (r) is defined as [moles of SiH]/[moles of vinyl units].

where p_{vinyl} is the percent of total butadiene monomer units in the chain that are vinyl units measured by ^1H NMR given in table 2.1. \overline{X}_n is the number average degree of polymerization and is calculated as (Odian, 1981)

$$\overline{X}_n = \frac{M_n}{M_0} \quad (2.2)$$

where M_0 is the molecular weight of the butadiene monomer (54 g/mole). The stoichiometric ratio in this study is defined as

$$r = \frac{[\text{moles of SiH}]}{[\text{moles of vinyl units}]} \quad (2.3)$$

where the moles of vinyl units equals f times the moles of PBD used.

M_w could be used to calculate f in equation 2.1. However, since in this study, the molecular weight distribution is so narrow either M_w or M_n could be used. In fact, for a specific value of r desired, the difference in the amount of silane calculated to be added by using M_w or M_n is smaller than the accuracy of silane that can be measured by the syringe. For samples with higher polydispersities, it may be better to use M_w since most polymer mechanical properties are affected more by the larger molecules and therefore the weighted value of M_w would be better to characterize the polymer than M_n (Odian, 1981).

By crosslinking polybutadiene at the randomly distributed pendant vinyl sites, the crosslinks will be distributed randomly along the chain, therefore, the molecular weight between crosslinks will also be random. Since crosslinking takes place along the chain and not at the chain ends, this is a type of vulcanization reaction and the terminology should not be confused with other types of crosslinking reactions commonly classified as vulcanizations that utilize sulfur, peroxides, or u.v. and ionizing radiation (Odian, 1981).

There are two types of side reactions that could occur. The first is that the internal 1,4-cis and trans units could possibly be involved in the hydrosilation reaction to form

crosslinks. Such a reaction would increase the functionality of the chain. Earlier studies with this system reported that hydrosilation takes place exclusively at the pendant 1,2-vinyl units (Miron et al., 1973; Friedmann and Brossas, 1982,1985). However, more recently, it was reported that when crosslinking at stoichiometrically balanced conditions or when excess crosslinker is used ($r \geq 1$) reaction of the internal double bonds was observed to occur (Aranguren and Macosko, 1988). Aranguren and Macosko (1988) did not observe this side reaction when a deficiency of crosslinker was used ($r < 1$).

In this study, F.T.i.r. was used to monitor the curing kinetics of curing PBD18 at stoichiometrically balanced conditions at $25 \pm 1^\circ\text{C}$ for 125 minutes. The details of the spectroscopic experimental technique will be given in chapter 7. Figure 2.7 shows clear evidence of the reaction of the vinyl unit by the disappearance of the peak at 1637cm^{-1} due to the vinyl C=C stretch. Figure 2.8 shows the disappearance of the vinyl CH wag at 911cm^{-1} and 992cm^{-1} . The decrease in the peak at 729cm^{-1} , representative of the CH wag for the cis unit, may suggest that the cis unit becomes involved in the hydrosilation reaction as observed by Aranguren and Macosko (1988). Though this side reaction may be occurring, it was apparent that the reactivity of the vinyl unit is much higher than that of the cis unit. No evidence at all was observed for the reaction of the trans unit with silane.

Another possible side reaction that could occur is that of a rearrangement reaction of the pendant vinyl unit to an internal double bond site (Gustavson et al., 1982; Macosko and Saam, 1987; Saam and Spier, 1961). This type of reaction was observed to occur for the hydrosilation cure of polyisobutene (Macosko and Saam, 1987). In figure 2.8, the peak at 964cm^{-1} due to the CH wag of the trans unit, was observed to increase moderately. This may suggest that such a rearrangement reaction is taking place. However, there was no increase in the C=C trans stretch peak observed. Therefore, it is uncertain from this data whether a rearrangement reaction has taken place.

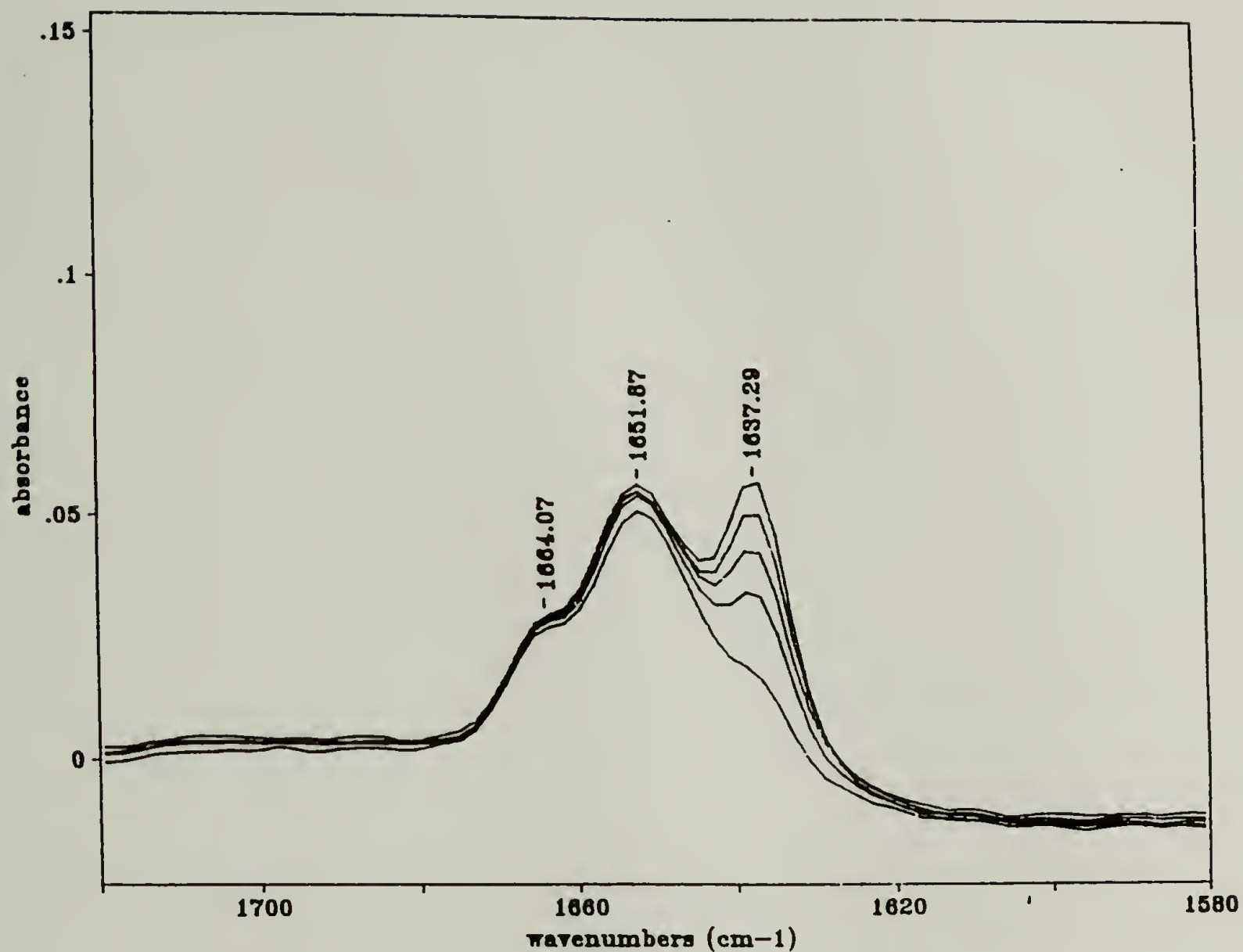


Figure 2.7 F.T.i.r. kinetic data showing C=C stretch region of PBD18 during crosslinking with a stoichiometric amount of crosslinker ($r=1$). Absorptions occur at 1664cm^{-1} , 1651cm^{-1} , and 1637cm^{-1} for the trans, cis, and vinyl olefin units respectively. The reaction was monitored for 125 minutes at $25\pm 1^\circ\text{C}$. Reaction of the vinyl site can be seen by the decrease of the intensity in the C=C vinyl stretch at 1637cm^{-1} .

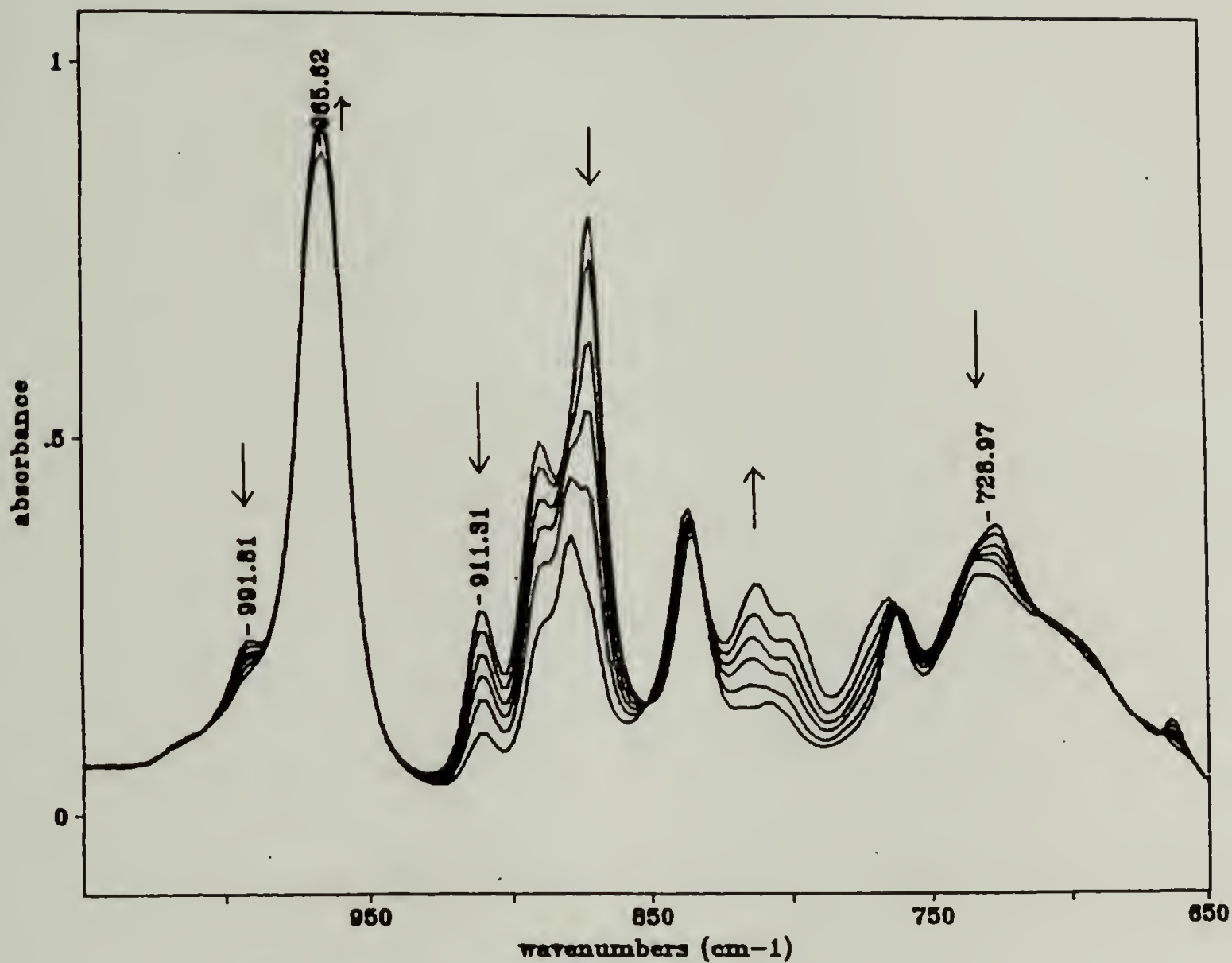


Figure 2.8 F.T.i.r. kinetics data of CH wagging region of PBD18 during crosslinking with a stoichiometric amount of crosslinker ($r=1$). The reaction was monitored for 125 min at $25\pm^{\circ}\text{C}$. Evidence of vinyl reactivity is seen by decreasing peaks at ns at 992cm^{-1} and 911cm^{-1} . A possibility of cis reactivity is seen by the decreasing peak at 729cm^{-1} . A slight increase in the trans CH wag is seen at 966cm^{-1} .

F.T.i.r. kinetic measurements were also done on samples starting with one half ($r=0.5$) the amount of crosslinker as was used for the data shown in figures 2.7 and 2.8. Similar trends were seen for the side reactions but were not as pronounced. This could suggest that these types of side reactions have finite probabilities of occurring even when a deficient amount of crosslinker (i.e. $r < 1$) is used. This is contrary to Aranguren and Macosko's (1988) findings. A possible explanation for this observation could be explained in the following manner. As less and less silane is made available for crosslinking by decreasing the initial stoichiometric ratio, while keeping the number of cis, trans and vinyl units constant, detection of side reactions would become more difficult to observe. This happens simply because the absolute number of side reactions has decreased due to the decrease in the absolute number of moles of silane present. However, the percentage of side reactions taking place would be the same irrespective of how much silane was present.

In conclusion, from the F.T.i.r. data it was observed that the pendant vinyl unit was much more reactive than the internal cis unit when crosslinking by hydrosilation. No evidence was seen of the internal trans unit reacting with silane. There also may be a marginal amount of a rearrangement reaction occurring at the vinyl units. However, there is no definitive proof of this. Though side reactions may be occurring, a majority of the reactions ($>85\%$) are taking place by hydrosilation at the pendant vinyl unit. If the assumption about the a constant percentage of side reactions taking place at all initial crosslinker concentrations is true, then the stoichiometric ratio, given by equation 2.3, can be used. However, it may be on the order of about 10% too low due to the fact reactive cis units increase the functionality of the chain. Therefore the total functionality of the chain would be calculated as the number of vinyl units plus the number of cis units involved in the hydrosilation reaction.

2.4 Catalyst Poisoning

In order to measure the dynamic mechanical properties of samples at one particular extent of reaction, it was necessary to somehow stop or "poison" the chemical reaction. This could be achieved by spraying <2wt% of an 80% tetramethylethylenediamine, TMEDA (Aldrich Chemical Co.), solution in toluene with an atomizer onto the surface of a reacting sample (Chambon, 1986; Venkataraman and Winter, 1990). Relative to work performed by Chambon (1986) and Venkataraman (1990), a much higher concentration of TMEDA solution was needed to effectively stop the reaction. This was due to the fact that more platinum per gram of PBD for crosslinking was needed than for PDMS due to the high vinyl content of PBD. Chambon (1986) suggested using a molar ratio of TMEDA to platinum of 1000.

Since TMEDA is a liquid at room temperature the poison solution rapidly diffuses into the sample, deactivates the Pt catalyst and stops the hydrosilation reaction at room temperature so that a discrete set of samples with different stages of crosslinking became available for detailed experiments. Other chemicals are also effective in stopping the hydrosilation reaction such as sulfur (Valles and Macosko, 1979; Chambon and Winter, 1985) and dimethylformamide (Chambon, 1986).

2.5 Sample Preparation

Samples for rheological measurements were prepared by mixing 0.6g of polybutadiene with 0.06ml (~350ppm, 8% by wt) of catalyst solution (8.0×10^{-3} mole/liter in toluene) for 10-12 min with a microspatula in a ceramic crucible. Since the toluene introduced with the catalyst solution has a plasticizing effect on the precursor, it must be removed. This is accomplished by vacuum stripping the mixture 60°C and 80°C for two hours (See figure 2.9).

After vacuum stripping, the sample was allowed to cool to room temperature. Stoichiometrically balanced or imbalanced amounts of the crosslinker were added using a

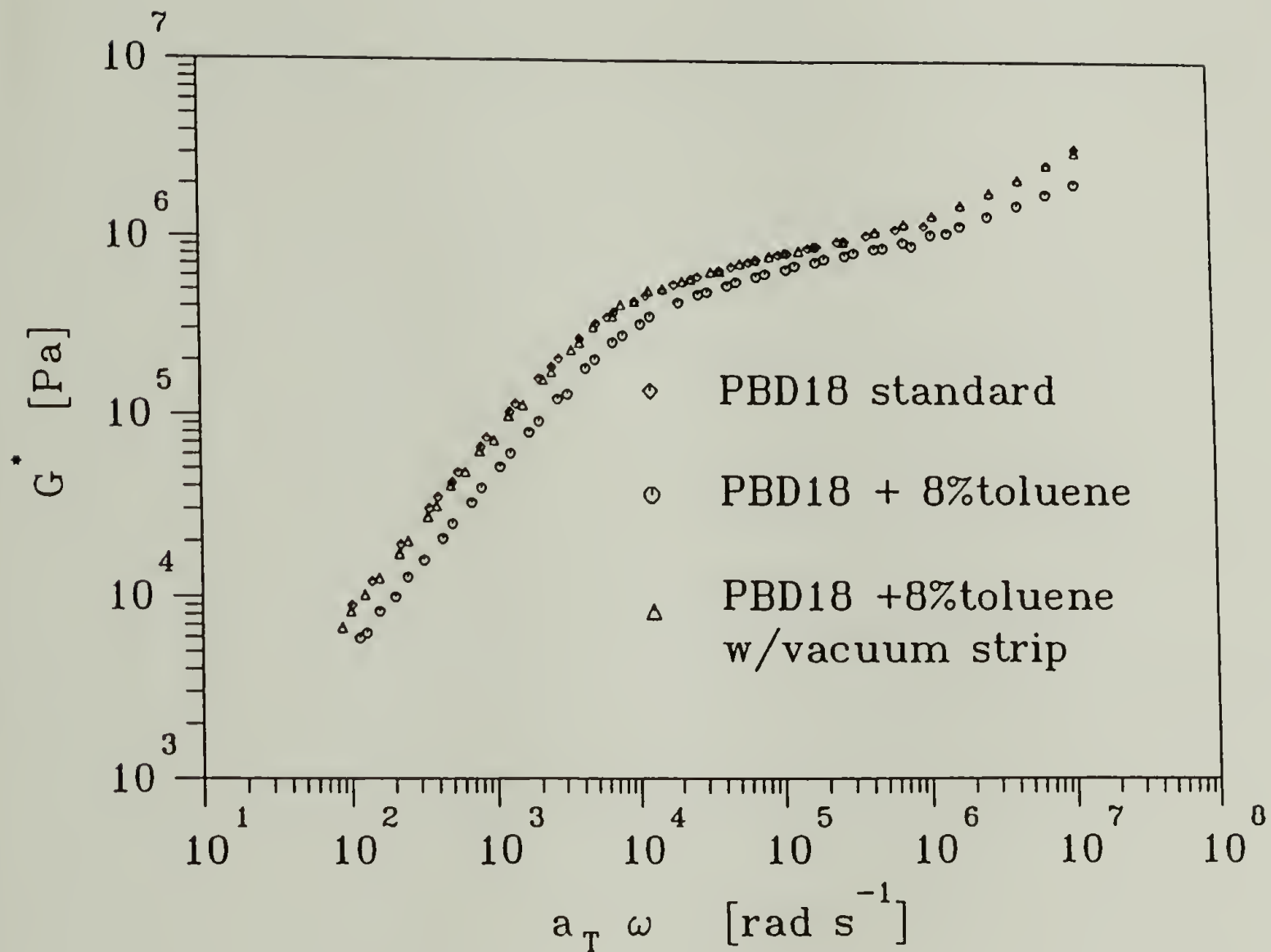


Figure 2.9 Master curves of the complex modulus of PBD18 showing the effectiveness of vacuum stripping in removing toluene from the sample introduced by the catalyst solution. PBD18 standard is data of bulk PBD18. G^* of PBD18 with 8 wt% of toluene is shifted down and to higher frequencies due to plasticization. After vacuum stripping at 60°C for 2h, G^* returns to the same behavior as the bulk material. $T_{ref} = 28^\circ\text{C}$.

0.1ml Hamilton syringe. Stoichiometric ratios ranged from 0.1 to 3.0. Immediately after adding the crosslinker, the crosslinking reaction began. The reacting mixture was stirred by hand for 6-7 min at ambient conditions to disperse the crosslinker. After this mixing time, the samples were then used either for in-situ rheological measurements by using the Consecutive Frequency Sweep (CFS) technique or for stopped sample measurements as will be described in the next chapter.

2.6 Experimental Error in Sample Preparation

To test the stability of PBD at vacuum oven temperatures, PBD201 was placed in the vacuum oven at 80°C for 34 h and then measured on the RDS7700. The dynamic data after vacuum stripping was observed to be almost the same as before stripping. Some light crosslinking may have been thermally initiated at the 1,2-vinyl sites due to the exposure at elevated temperatures. Evidence of slight crosslinking may be inferred from the minor discrepancy of G' data in the terminal zone. Since such little change in the data was observed after 34h at 80°C, it was assumed that changes due to vacuum stripping for other samples at 2h at 60°C to 80°C would be virtually negligible.

The stability of PBD mixed with catalyst was measured by monitoring the dynamic modulus at 30 rad/s at 28°C for 1.5 h and at 50 rad/s at 60°C for 2.5 h. No change in the dynamic modulus was observed at all during the measurements and was therefore assumed that no premature crosslinking reactions took place when catalyst was present with PBD at elevated temperatures.

The accuracy of the volume of crosslinker added is estimated to be ± 0.003 ml. Therefore, the accuracy of the amount of moles of SiH delivered to mix with PBD is limited. For $r=1$ conditions, the value of r has a relative experimental error of approximately $\pm 3\%$. This error becomes larger as the value of r needed for experiments decreases and smaller as the value of r needed for experiments increases.

CHAPTER 3
EXPERIMENTAL METHODS

3.1 Rheological Techniques

3.1.1 Rheological Material Functions for Shear Flow

For simple shear flow (figure 3.1) the shear stress is given by

$$\sigma = \frac{F}{xy} \quad (3.1)$$

where F is the applied force and xy is the area of the top plate over which the shear force is applied. The shear strain (γ) for this geometry is defined as

$$\gamma = \frac{\Delta x}{h} \quad (3.2)$$

where Δx is the displacement of the top plate and h is the distance between the two plates.

For simple shear flow with parallel disk geometry (figure 3.1) the shear stress is given by

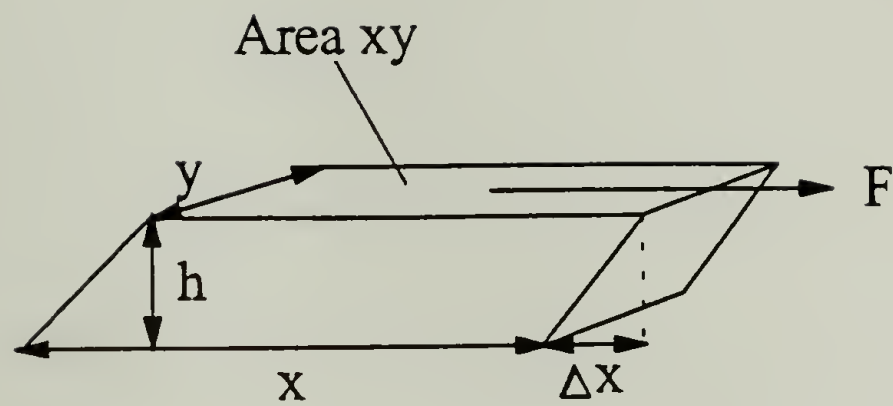
$$\sigma = \frac{2\mathcal{J}}{\pi r^3} \quad (3.3)$$

where \mathcal{J} is the torque and r is the radius of the plate. The shear strain in this geometry is defined as

$$\gamma = \frac{r\theta}{h} \quad (3.4)$$

where θ is the angular displacement and h is the width of the gap. $\omega = \frac{d\theta}{dt}$ is the angular velocity of the moving plate during steady shear when the deformation is a function of time.

(a)



(b)

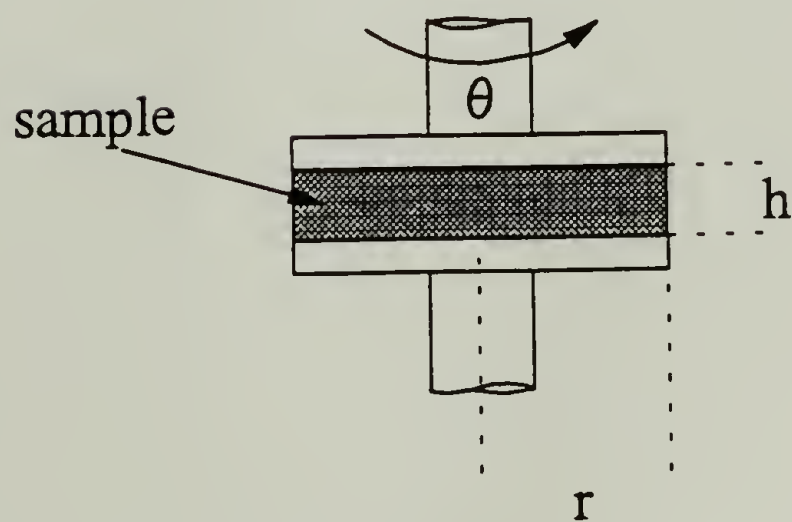


Figure 3.1 (a) Simple shear flow for two parallel plate and (b) parallel disk geometry.

Another geometry that is commonly used is cone and plate. It produces a uniform strain in the sample which is advantageous in large strain steady shear experiments.

Experimentally it is much easier to use parallel disks especially when small strain oscillatory experiments are performed on samples over a range of temperatures. In this study, only the parallel disk geometry was used.

3.1.2 Linear Viscoelastic Functions

The shear stress and strain are related by the shear modulus G and compliance J .

For a Hookean solid G and J are defined as

$$G = \frac{\sigma}{\gamma}; \quad J = \frac{\gamma}{\sigma} = \frac{1}{G} \quad (3.5)$$

For viscoelastic materials, the shear modulus and compliance become time dependent. In each case, either the stress or strain can be held constant in an experiment in order to measure the time dependent modulus $G(t)$ or compliance $J(t)$. For creep experiments, the shear stress is held constant (σ^0) and the strain is measured as a function of time ($\gamma(t)$).

Thus equation 3.5 becomes

$$J(t) = \frac{\gamma(t)}{\sigma^0}. \quad (3.6)$$

For stress relaxation experiments, the shear strain is held constant (γ^0) and the stress is measured as a function of time ($\sigma(t)$). Thus equation 3.5 becomes

$$G(t) = \frac{\sigma(t)}{\gamma^0}. \quad (3.7)$$

The constitutive equations of the three idealized states of crosslinking are given for the liquid, critical gel and solid. For a Newtonian liquid before crosslinking the shear stress is

$$\sigma = \eta \dot{\gamma} \quad (3.8)$$

where $\dot{\gamma}$ is the shear rate. The critical gel is described by the gel equation of Chambon and Winter (1985, 1986, 1987)

$$\sigma = S \int_{-\infty}^t (t - t') \dot{\gamma}(t') dt. \quad (3.9)$$

At full extent of reaction, the material is a Hookean solid

$$\sigma = G\gamma. \quad (3.10)$$

In dynamic mechanical measurements of viscoelastic materials, the sample is subjected to a sinusoidally oscillating deformation where $\gamma(t)$ has the form

$$\gamma(t) = \gamma^0 \sin(\omega t) \quad (3.11)$$

where γ^0 is the amplitude of the strain and ω is the frequency (figure 3.2). For viscoelastic liquids and solids, the stress response to the imposed strain is also sinusoidal but lags behind the strain by the phase angle δ

$$\sigma(t) = \sigma^0 \sin(\omega t + \delta) \quad (3.12)$$

where σ^0 is the stress amplitude. In principle, either the stress or the strain can be programmed for sinusoidal oscillation. However, the two instruments used in this study operate by programming a sinusoidal strain and measuring the stress response and phase angle δ .

By use of a trigonometric identity, equation 3.12 can be rewritten as

$$\sigma(t) = \sigma^0 \cos \delta \sin \omega t + \sigma^0 \sin \delta \cos \omega t. \quad (3.13)$$

The dynamic moduli, G' (storage modulus) and G'' (loss modulus), are given as

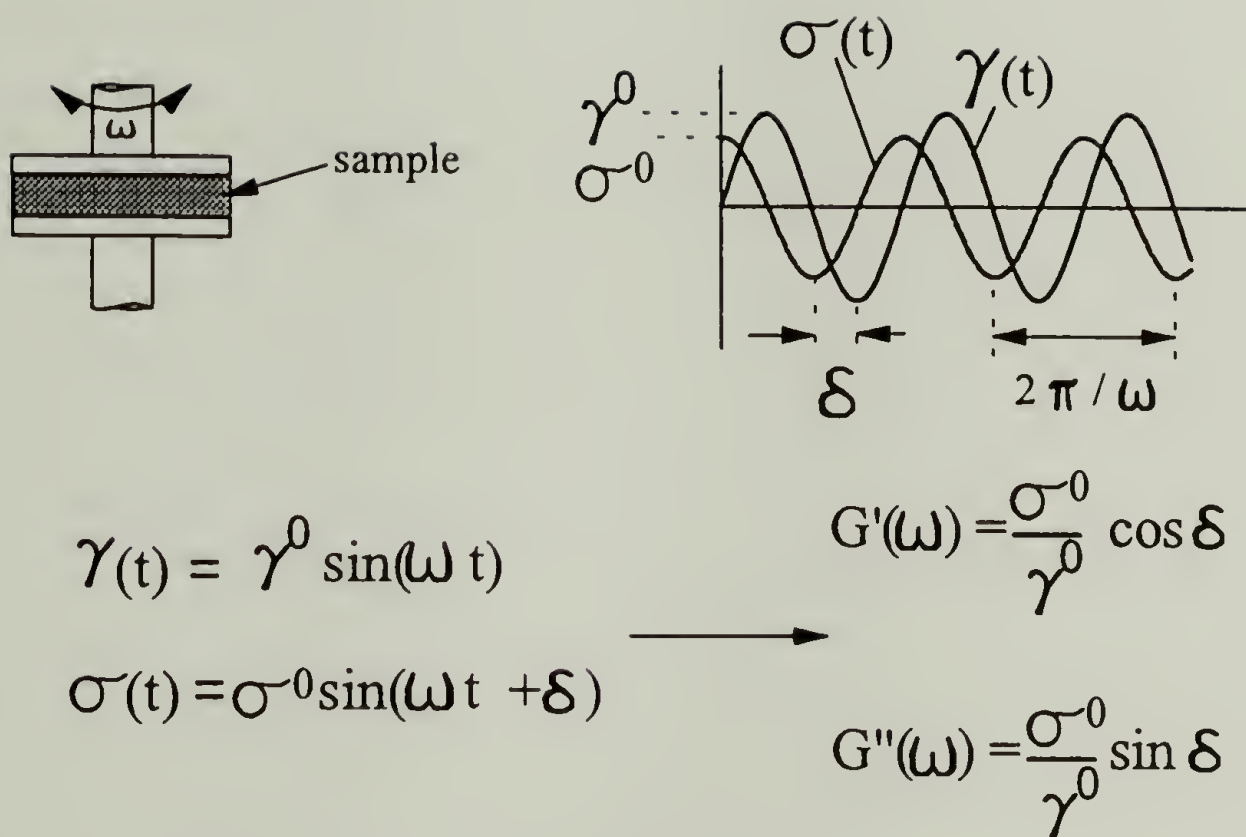


Figure 3.2 Sinusoidal strain and stress response for dynamic mechanical measurement.

$$G' = \left(\frac{\sigma^0}{\gamma^0} \right) \cos \delta \quad (3.14)$$

$$G'' = \left(\frac{\sigma^0}{\gamma^0} \right) \sin \delta \quad (3.15)$$

$$\frac{G''}{G'} = \tan \delta \quad (3.16)$$

The storage modulus is a measure of the amount of mechanical energy stored per cycle of deformation and the loss modulus is a measure of the amount of mechanical energy dissipated per cycle of deformation.

The dynamic moduli can also be given in complex form as

$$\frac{\sigma^*}{\gamma^*} = G^* = G' + iG'' \quad (3.17)$$

$$|G^*| = \frac{\sigma^0}{\gamma^0} = \sqrt{G'^2 + G''^2}. \quad (3.18)$$

For materials in the linear viscoelastic range, the complex modulus is independent of the strain amplitude. When the modulus begins to change as a function of strain amplitude, the material is said to be in the nonlinear range. Initial measurements should be made on materials to test the linear range so that strain levels in the linear range can be used.

The dynamic and complex moduli are commonly reported in the literature to describe the mechanical behavior of viscoelastic materials. However, other dynamic functions such as the dynamic and complex compliance (J^* , J' , J'') and viscosity (η^* , η' , η'') are also widely used. All of these viscoelastic functions are related to one another as shown by Ferry (1980).

Dynamic measurements can be performed over a particular frequency window at several temperatures. By doing this, master curves can be constructed which expand the

frequency window of the dynamic moduli. Data at different temperatures can be shifted horizontally along the frequency axis according to the time-temperature superposition principle. This principle works for polymers in which there is no change in the morphology as a function of temperature such as is the case with multiphase polymers (e.g. block copolymers and liquid crystalline polymers) and semicrystalline polymers.

The horizontal shift factor, denoted by a_T , for amorphous polymers can be represented as a function of temperature by the Williams, Landel, and Ferry (WLF) equation (Ferry, 1980)

$$\log a_T = -\frac{C_1(T - T_{ref})}{C_2 + T - T_{ref}} \quad (3.19)$$

where C_1 and C_2 are constants which have been found to be polymer dependent and T_{ref} is the reference temperature to which the data is shifted. The change in density (ρ) of the polymer as a function of temperature causes a vertical shift, b_T

$$b_T = T_{ref} \rho(T_{ref}) / T \rho(T). \quad (3.20)$$

The shifted dynamic moduli at the reference temperature can be represented as a function of the measured moduli at the measured temperatures with the applied shift factors as

$$G'(\omega, T_{ref}) = b_T G'(a_T \omega, T) \quad (3.21)$$

$$G''(\omega, T_{ref}) = b_T G''(a_T \omega, T). \quad (3.22)$$

3.1.3 Apparatus

For rheological measurements, two instruments were used: the Rheometrics Dynamic Mechanical Spectrometer, model RDS7700, and the Rheometrics Mechanical Spectrometer, model RMS800. Both instruments are fitted with torque transducers with a

2000g-cm limit. Before operation, the instruments were calibrated for torque by the procedure recommended by the manufacturer (Rheometrics, 1990). Viscosity standard fluids (Cannon Instruments Co.) were used to check the measured viscosity. Both instruments were found to agree with the standards within 5%. Data was acquired by using Rheometrics Rhios software. All rheological data was later analyzed by using standard IRIS (Innovative Rheological Interface Software) software designed by Paul Soskey and Michael Baumgaertel. Other rheological software that was used included "Gelpro", developed by Marian Mours, which analyzes rheological data evolving as a function of time. IRIS DS (IRIS Development Systems) developed by Michael Baumgaertel and Judy Jackson, was also used for modeling relaxation time spectra and dynamic data calculations.

3.2 Evaluation of the Discrete Relaxation Time Spectrum

In order to be able to describe the relaxation behavior of viscoelastic materials it is necessary to obtain an expression for the relaxation time spectrum $H(\lambda)$. The relaxation time spectrum can not be measured directly, but rather must be evaluated from observable material functions such as the storage modulus, $G'(\omega)$ and the loss modulus, $G''(\omega)$;

$$G'(\omega) = \int_0^{\lambda_{\max}} H(\lambda) \frac{\omega^2 \lambda^2}{1 + \omega^2 \lambda^2} \frac{d\lambda}{\lambda}, \quad (3.23)$$

$$G''(\omega) = \int_0^{\lambda_{\max}} H(\lambda) \frac{\omega \lambda}{1 + \omega^2 \lambda^2} \frac{d\lambda}{\lambda}. \quad (3.24)$$

With an appropriate representation of $H(\lambda)$, one can model the dynamic moduli as well as other material functions such as the relaxation modulus, $G(t)$, or the dynamic viscosity, $\eta^*(\omega)$ (Ferry, 1980). In this study IRIS software was used to analytically

compute the discrete relaxation time spectrum from experimentally measured dynamic data. The results of this type of analysis was extremely useful in ultimately formulating an expression for the relaxation time spectrum of entangled critical gels.

The relaxation behavior of a viscoelastic liquid can be approximated by the Maxwell-Wiechert model which consists of a number of Maxwell elements connected in parallel shown in figure 3.3 (Aklonis and MacKnight, 1983). Each Maxwell element consists of a spring and dashpot in series. The modulus of the spring of the i th element is characterized by g_i and the viscosity of the dashpot of the i th element is characterized by η_i . The relationship between g_i and η_i is given by

$$\eta_i = \lambda_i g_i \quad (3.25)$$

where λ_i is the relaxation time of the i th element.

The stress relaxation modulus for the Maxwell-Wiechert model with N modes is given by

$$G(t) = G_e + \sum_{i=1}^N g_i e^{-(t/\lambda_i)} \quad (3.26)$$

where G_e is finite for a solid and zero for a liquid and critical gel. The dynamic moduli are given by

$$G'(\omega) = G_e + \sum_{i=1}^N g_i \frac{(\omega\lambda_i)^2}{1 + (\omega\lambda_i)^2} \quad (3.27)$$

$$G''(\omega) = G_e + \sum_{i=1}^N g_i \frac{\omega\lambda_i}{1 + (\omega\lambda_i)^2} \quad (3.28)$$

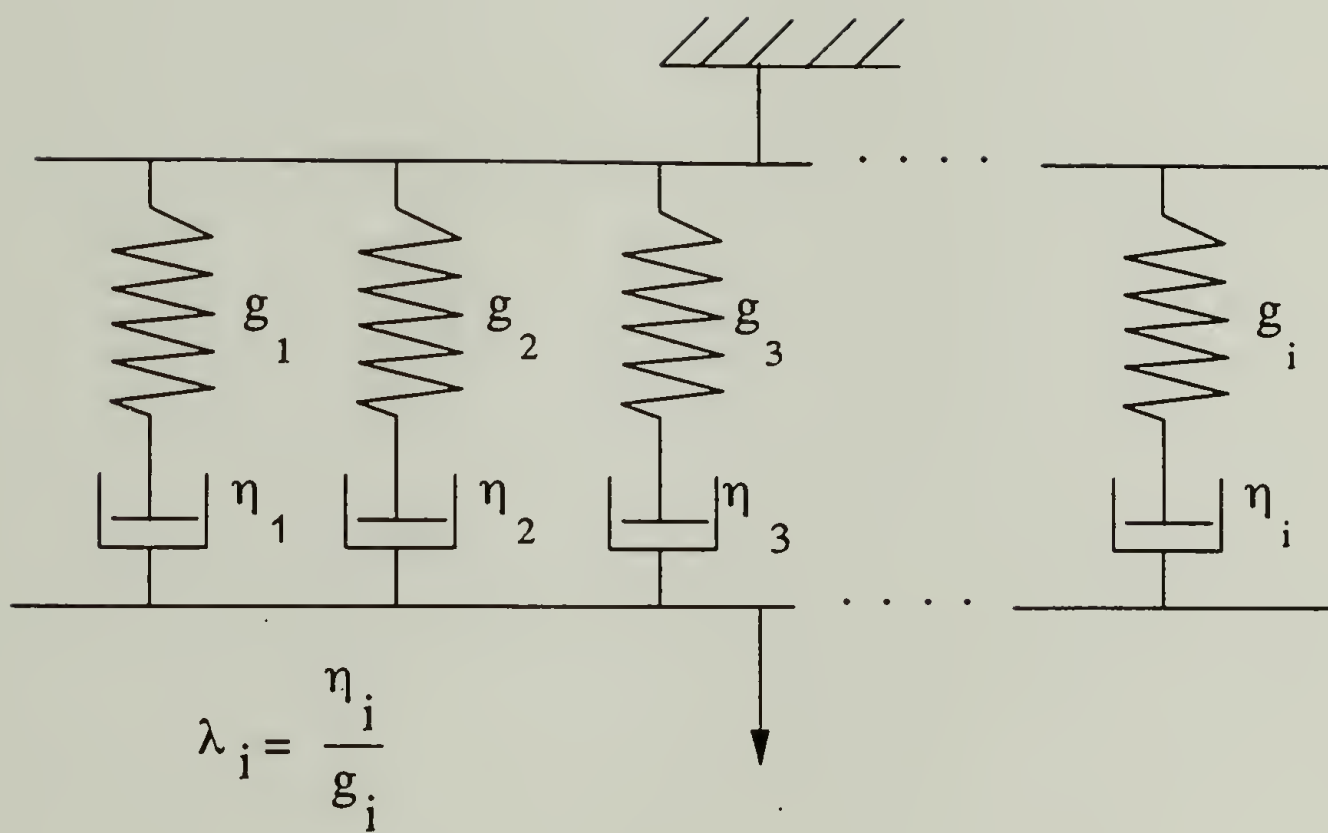


Figure 3.3 Maxwell-Wiechert model with i Maxwell modes in parallel. The relaxation time of each mode is given by λ_i . The distribution of relaxation modes, g_i vs. λ_i , gives the discrete relaxation time spectrum.

The discrete relaxation time spectrum is given by a plot of g_i versus λ_i . In the simplest manner, each mode of the spectrum represents relaxation behavior at a characteristic time given by λ_i . The time constant associated with each mode is proportional to the some length scale representative of a subsection of the entire chain length. Shorter times correspond to relaxation of small sections of the chain while longer times to correspond to larger subsections of the chain. The longest relaxation time, or λ_{\max} , represents the time scale that the entire chain is allowed to relax. At times longer than λ_{\max} , chains undergo viscous flow.

Baumgaertel and Winter (1989) have shown that the discrete relaxation time spectrum can be evaluated from dynamic data. This procedure is performed with the IRIS software. In essence, the spectrum is evaluated by taking a dynamic data set and using equations 3.27 and 3.28. The program adjusts parameters g_i , λ_i , and N to achieve the best fit of the dynamic data by nonlinear regression. The spectrum is represented with the fewest possible number of Maxwell modes while still remaining within the experimental scatter of the data. Such a spectrum has been termed the "parsimonious" model (PM-spectrum) (Baumgaertel and Winter, 1992; Winter and Baumgaertel, 1993). An example of the result of the calculated discrete spectrum is given in figure 3.4.

3.2.1 Conversion of the Discrete Spectrum to the Continuous Spectrum

Once the discrete spectrum has been evaluated, it is converted to a continuous spectrum. Baumgaertel and Winter (1992) have recently reported the interrelation between the continuous and discrete relaxation time spectrum. This is primarily achieved by taking g_i of each mode and dividing it by the local spacing, a_i , between adjacent modes. The continuous spectrum, given by $H(\lambda)$ is related to the discrete spectrum by

$$g_i = \ln a_i H(\lambda_i) \quad (3.29)$$

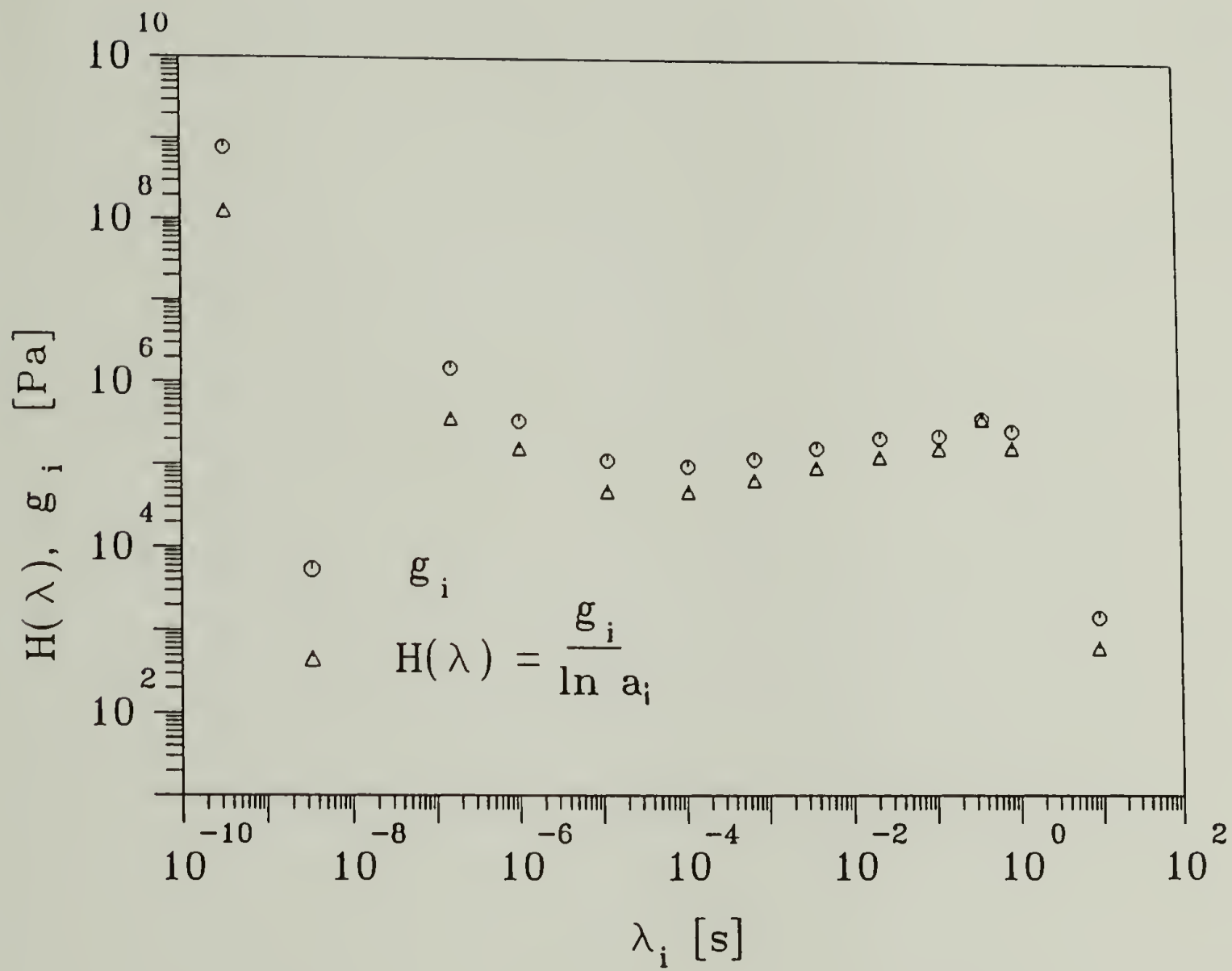


Figure 3.4 Relaxation time spectra of PBD201 calculated with IRIS software. The Parsimonious Model is given by the discrete modes (g_i, λ_i) while the continuous spectrum is given by $H(\lambda)$. $T_{\text{ref}} = 28^\circ\text{C}$.

where a_i is given by

$$a_i = \lambda_i / \lambda_{i+1}. \quad (3.30)$$

The result is given by discrete points on the continuous spectrum. Figure 3.4 shows the discrete and continuous spectrum.

3.3 Rheological Techniques to Study Critical Gels

3.3.1 "Stopped" Samples

There are two primary methods that have been used to study rheological behavior of critical gels. The first involves the investigation of "stopped" samples. Stopped samples are precursors that have been chemically crosslinked to some extent, and before the reaction can proceed further, the reaction is stopped by chemical means discussed in chapter 2. The result is that the reaction is "frozen". The sample is representative of a stable, homogeneous sample at one state of network development. Time-temperature superposition can then be used to expand the frequency window. Such methods were used by Chambon and Venkataraman with an endlinking PDMS system (Chambon and Winter, 1985, 1986, 1987; Venkataraman and Winter, 1990). The details of the sample preparation and measurements of stopped samples for this study will be discussed later.

3.3.2 Consecutive Frequency Sweeps (CFS)

The second method used to study critical gels involves utilizing the technique of Consecutive Frequency Sweeps (CFS). CFS is an *in-situ* technique which involves probing a sample dynamically in the rheometer over at least two decades of frequency while the sample is crosslinking. Each frequency is sampled data at a different time and the sweep is repeated again for many cycles in the vicinity of the gel point. Data analysis is performed with "Gelpro" software. The data are sorted by frequency and smoothed by a fitting spline. The result of the measurement is a plot of $\tan \delta$ for the frequencies probed versus reaction time. A schematic of the experiment is shown in figure 3.5. This

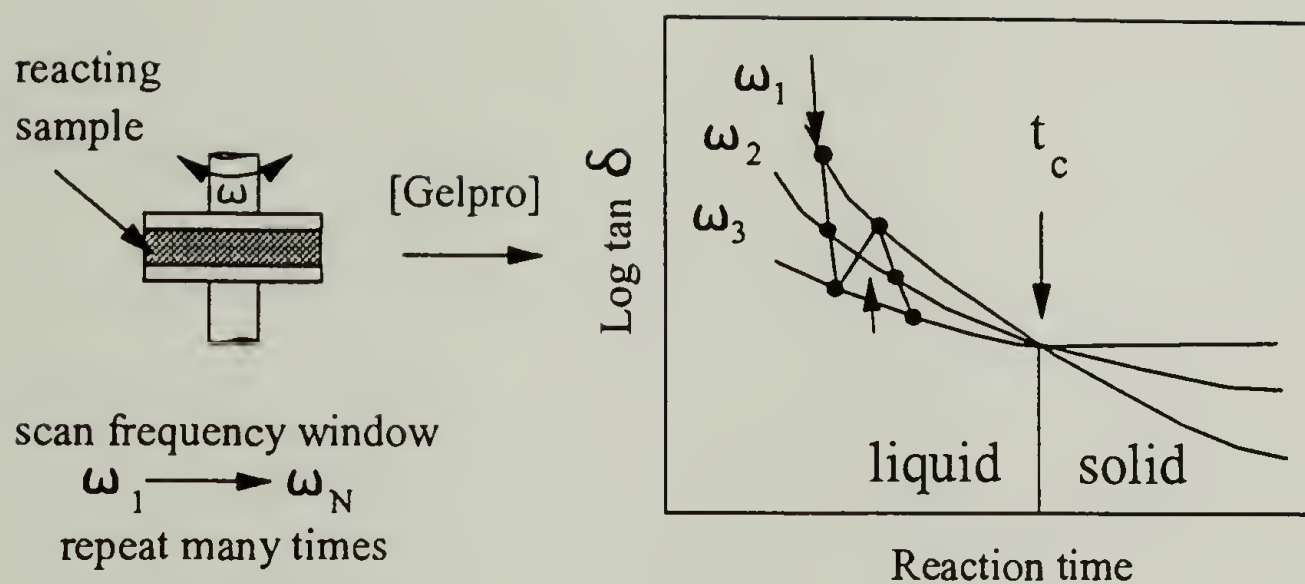


Figure 3.5 Consecutive Frequency Sweep (CFS) experiment. $\text{Tan } \delta$ is plotted versus reaction time for at least two decades of frequency with "Gelpro" software. Intersection of the $\text{tan } \delta$ curves at the critical gel time t_c indicates power law behavior of the dynamic mechanical properties over the frequencies scanned.

technique has been used by Scanlan and Winter (1991) to monitor the evolution of an endlinking PDMS and by Izuka et al. (1992) for an endlinking polycaprolactone. A similar technique utilizing Fourier Transform Mechanical Spectroscopy (FTMS) has also been used (Holly et al., 1988). In such an experiment, several frequencies are measured simultaneously resulting in a superimposed complex waveform instead of using consecutive sweeps.

Since the measurement at each frequency represents the dynamic mechanical properties at one particular stage of crosslinking, it is important that the rate of reaction is much slower than the time that it takes to perform one frequency measurement. A dimensionless parameter called the mutation number, N_{mu} , has been defined for specifying the limits of this technique (Winter et al., 1988; Scanlan and Winter, 1991) as

$$N_{\text{mu}} = \Delta t \frac{1}{G^*} \frac{\partial G^*}{\partial t} \quad (3.31)$$

where for low frequencies, $\Delta t \approx 2\pi/\omega$ indicates the time for a single measurement at one frequency. A low frequency measurement requires a larger Δt and thus results in a large N_{mu} . N_{mu} tells by what percent the dynamic mechanical properties have changed during the measurement time Δt . Data can be accepted for $N_{\text{mu}} \ll 1$. The mutation number should be calculated for the lowest frequency in a CFS measurement since the lowest frequency has the largest Δt . N_{mu} will become smaller as the frequency increases. N_{mu} can be reduced by slowing the reaction down by lowering the temperature or using less catalyst.

The gel point can be easily detected by monitoring the evolution of the $\tan \delta$ as a function of time for several frequencies. As the reaction proceeds, the curves begin to converge. At the gel point, all of the $\tan \delta$ curves will intersect at the critical time t_c (see figure 3.5). This intersection indicates that the ratio of G'' to G' is constant over the

frequency window probed. Thus this is the instant that power law relaxation is observed in this frequency range. As mentioned in chapter 1, it is this power law in the relaxation behavior that characterizes the critical gel state.

Data from CFS measurements provide several important pieces of information about the critical gel. First, it is possible to measure the rate of crosslinking and the gel time necessary for kinetics studies. Second, by using Gelpro, it is possible to interpolate the dynamic moduli at any point in time along the cure cycle from the smoothed data. This makes it possible to later calculate the gel strength and relaxation exponent discussed in chapter 1. The details of the experimental procedure, analysis, and results of CFS measurements will be discussed in chapters 5, 6, and 7.

3.4 Spectroscopic Techniques

It is of particular interest to obtain information about the evolving molecular structure during the crosslinking reaction and at the gel point. In reference to rheological techniques, the gel time (t_g) is most often used to determine the instant at which gelation occurs. Though rheological methods are successful in monitoring crosslinking processes and measuring mechanical shear properties at the gel point, they do not provide direct information about the molecular structure of the network. One common technique used to elucidate chemical structure during crosslinking is vibrational spectroscopy. In this study, two techniques of vibrational spectroscopy were used, Fourier Transform infrared (F.T.i.r.) spectroscopy and Fourier Transform Raman spectroscopy.

F.T.i.r. spectroscopy has been used to monitor the extent of reaction for crosslinking processes for a variety of materials (Friedmann and Brossas, 1985; Venkataraman et al., 1989; Adolf and Martin, 1990; Ishida and Smith, 1991; Muller et al., 1991). This technique is able to provide quantitative measurements of the amount of a particular chemical reactive site (chemical bond) that is present in the reacting material. This can be done by measuring either the peak heights or the peak areas that correspond

to the bond during the reaction. If Beer's law (Colthup et al., 1990) holds for the concentration of reactive sites present, then a direct relationship exists between the concentration of reactive sites and the percent absorbance measured by the peak height or area. The percent conversion of the site can be calculated from this type of analysis. Usually a calibration curve of known concentration in the range that will be used is constructed to test whether Beer's law will be valid.

Though rheology and F.T.i.r. can give kinetic information of crosslinking reactions, the gel time is greatly influenced by factors such as temperature, catalyst concentration, etc. These parameters that influence the rate of crosslinking make it experimentally more difficult to combine rheological and spectroscopic information on critical gel behavior. To avoid these interfering parameters, the extent of reaction and the rheological properties of a sample should be measured directly and not the gel time. To accomplish this objective F.T. Raman spectroscopy can be used in combination with the stopped sample technique of sample preparation.

Raman spectroscopy provides information complementary to F.T.i.r. data. Both techniques measure the characteristic bond vibrational frequencies. However, due to different selection rules, F.T.i.r. gives strong signals for polar bonds, which are weak in Raman, while Raman gives strong signals for non-polar bonds, which are weak in F.T.i.r. The two methods together give a more complete description of the molecular structure of compounds. A more detailed discussion of the theory of Raman spectroscopy is given in the literature (Schlotter, 1989; Colthup et al., 1990).

Conventional, or dispersive, Raman spectroscopy has been used in the past for quantitative analysis (Pasco and Waters, 1976; Covington et al., 1973) and for monitoring crosslinking reactions (Grasselli et al., 1979). However, it has several drawbacks that make it impractical to combine with rheological measurements by some *in-situ* means. Conventional Raman spectroscopy has been plagued by many experimental shortcomings

such as tedious sample alignment, fluorescence interference from sample impurities, and long measurement times ranging from several minutes to several hours.

Recently, the collection and processing of Raman data has been markedly improved by the incorporation of Fourier Transform technology (Cutler, 1990). This improvement has provided some new experimental advantages over dispersive Raman for gel studies. Data can now be obtained with dramatically increased signal-to-noise ratio and in shorter periods of time, usually only a few minutes. F.T. Raman is virtually free from fluorescence interference due to sample impurities. It can also be adapted for fiber optic capabilities, which make it an attractive prospect for *in-situ* rheological measurements. F.T. Raman is gaining increased exposure in industrial analysis (Williams and Mason, 1990), the analysis of polymers and elastomers (Jackson et al., 1990; Hendra and Jones, 1991) and has been used for monitoring the curing of an epoxy system (Walton and Williams, 1991).

F.T. Raman also has a few experimental advantages over using F.T.i.r. The presence of CO₂ or water vapor do not interfere in F.T. Raman data as is the case with F.T.i.r. In addition to this, a variety of sample shapes and sizes can be measured directly with usually little or no special sample preparation. This is not the case for F.T.i.r. where samples are usually restricted to very thin dimensions (~100µm) and require special sample preparation and the use of salt plates to hold the sample.

CHAPTER 4

RELAXATION BEHAVIOR OF PRECURSOR MATERIALS

4.1 Rheological Characterization of Bulk Polybutadienes

Before crosslinking the precursor polymers, it is important to measure their initial rheological behavior. As the samples are reacted to the gel point, it will be possible to analyze the evolution of the crosslinked material and compare it to this initial rheological state. This will ultimately provide new information on the relaxation behavior of entangled gels.

4.1.1 Experimental Procedure

Storage and loss moduli of the uncrosslinked polybutadiene melts were measured with a Rheometrics Dynamic Spectrometer, RDS 7700, with 25 mm parallel plate geometry. The frequency ranged from 0.1 rad/s to 500 rad/s. The gap setting was adjusted between 0.6 mm to 1.5 mm. Strain levels of 0.25 (25%) and less were used to achieve acceptable torque values. For the lower molecular weight precursors, insufficient torque values (<2 g-cm) cause scatter of the data at the lowest frequencies and these points were discarded. Cooled nitrogen was continuously circulated in the environmental chamber to obtain subambient temperatures. For every decrease in the temperature by 10K, the programmed gap input to the computer was increased by 0.01 mm to account for thermal expansion of the plates. Measurements at temperatures in the range of -75°C to 28°C extended the experimental frequency window through time-temperature superposition. Data was shifted to a reference temperature of 28°C .

Most difficult were the experiments at the lowest temperatures ($< -50^{\circ}\text{C}$) where it was found that dynamic data at the last few highest frequencies tended to decrease abruptly. This was attributed to sample slipping thus causing a decrease in the observed dynamic modulus. To reduce the effect of sample slip, several experimental techniques

were used. First, a low level of strain was applied (< 0.05) at these reduced temperatures. Second, the temperature was reduced in steps by 5K from -50°C down to the lowest temperature of about -75°C . Having many data sets at lower and lower temperatures improved the shifting into the master curve and provided a better representation of the trend of the dynamic data at the highest frequencies into the glass transition zone. It also proved to be important to measure at the absolute lowest rheometer temperature possible in order to measure as far into the glass transition region as possible.

4.1.2 Dynamic Mechanical Data of Polybutadiene

Dynamic moduli and $\tan \delta$ master curves of all seven polybutadienes are shown in figures 4.1 and 4.2 at a reference temperature of 28°C . Distinct regions denote flow at low frequencies (terminal zone), entanglements at intermediate frequencies characterized by a plateau modulus in G' , and the transition to the glass at high frequencies.

The dynamic data measured obeyed the time-temperature superposition principle. The temperature dependence of the horizontal shift factor shown in figure 4.3, can be described by the WLF equation. The shifting parameters do not depend on the molecular weight as expected. The vertical shift factors are also given in figure 4.3.

The dynamic viscosity (η^*) in the terminal zone, where it is independent of frequency, denotes the zero shear viscosity (η_0) (see figure 4.4). Values of η_0 are given in table 4.1. Figure 4.5 shows the zero shear viscosity for all of the PBD samples as a function of the weight average molecular weight. The slope of this curve on a log-log plot was found to be 3.52 for all seven PBD samples which is slightly higher than the value of 3.4 commonly reported in the literature (Colby et al., 1987; Ferry, 1980; Berry et al., 1968). The viscosities of the five highest molecular weights were found to scale with an exponent of 3.43. The two viscosities of the two samples with the lowest molecular weights, PBD18 and PBD20, were found to be slightly lower than the 3.43 scaling relationship would predict. This indicates that as the molecular weight begins to approach

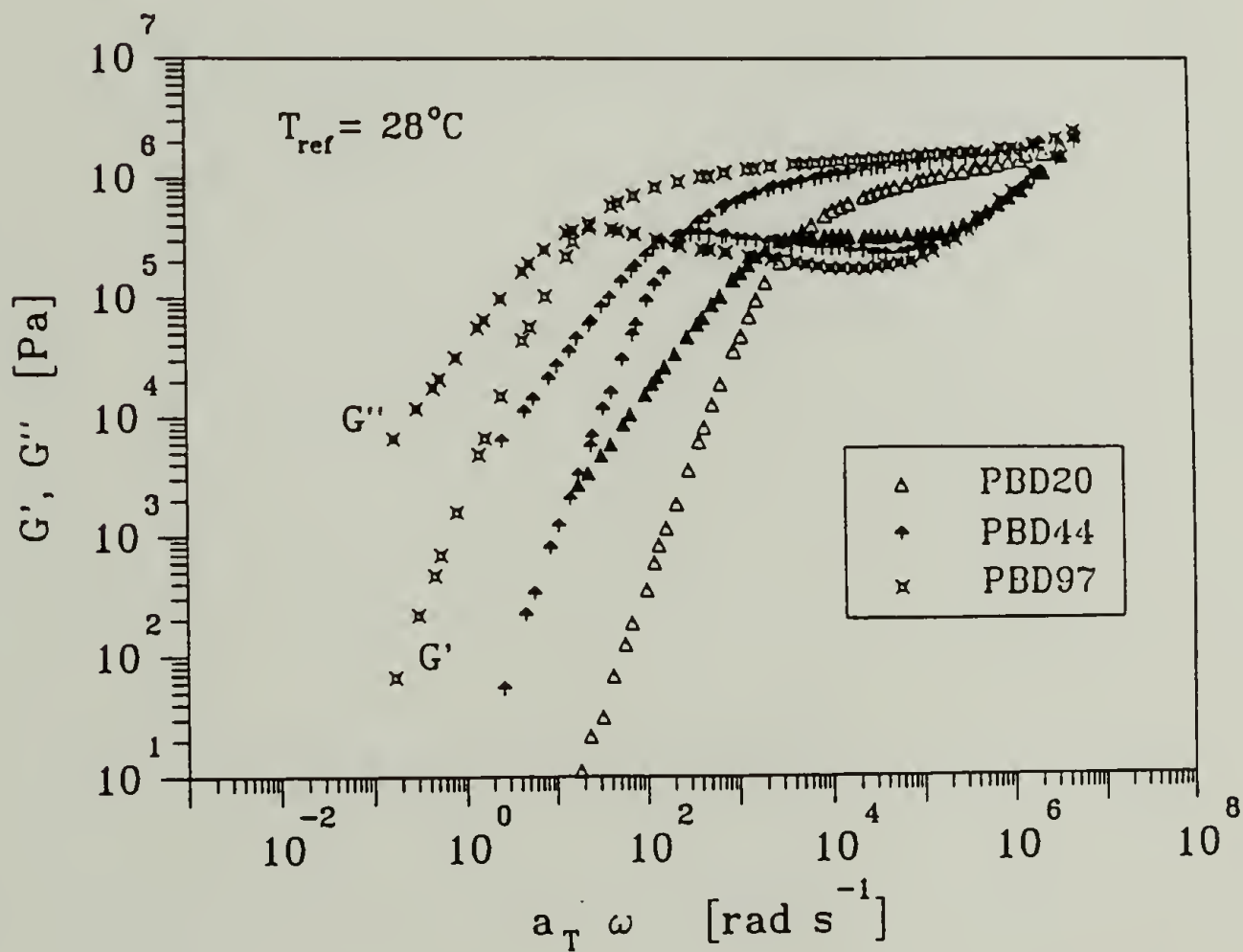
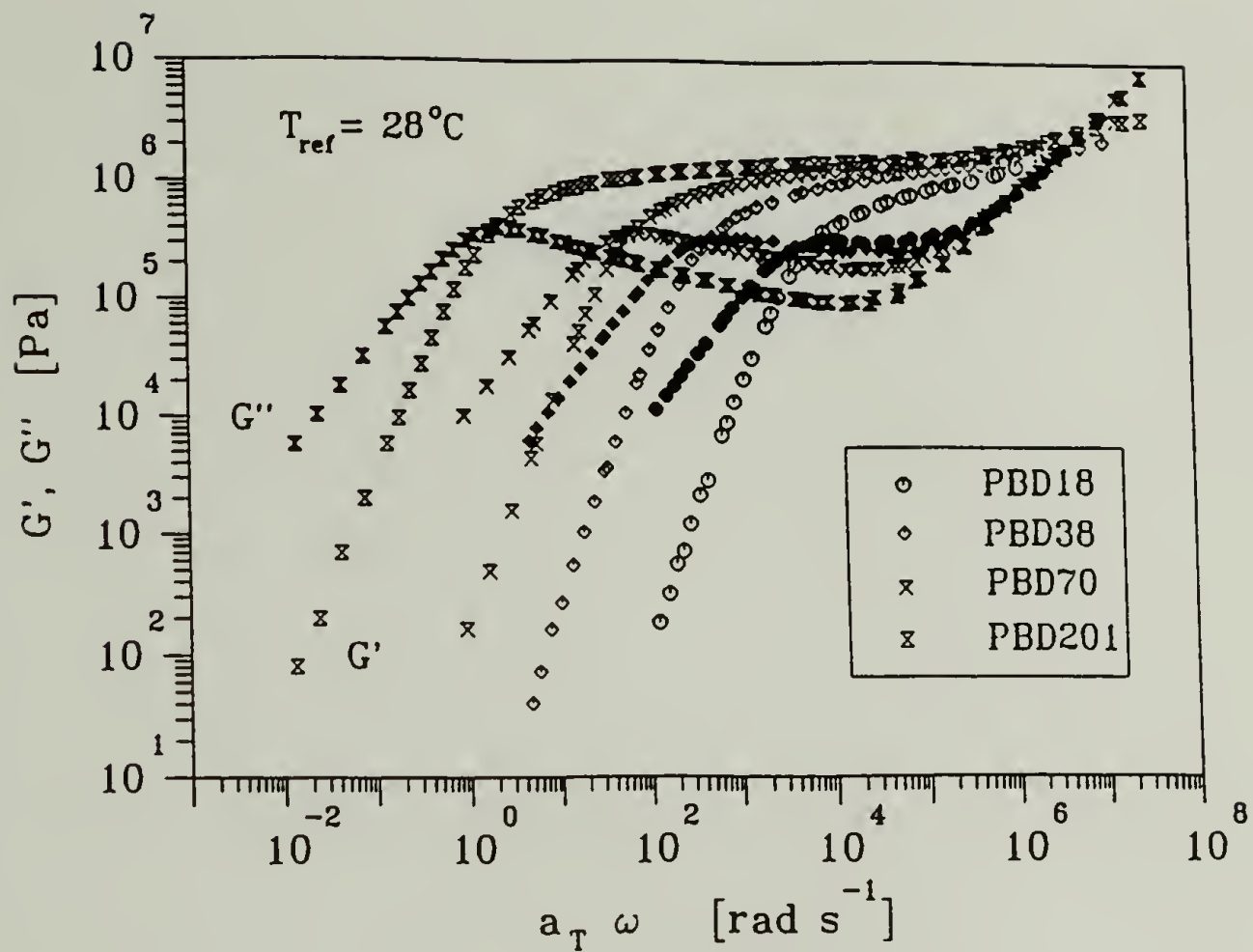


Figure 4.1 Dynamic moduli (G', G'') master curves of the bulk polybutadiene precursors. The open and filled symbols represent the storage modulus (G') and loss modulus (G'') respectively. All master curves are shifted with a reference temperature $T_{ref} = 28^{\circ}\text{C}$.

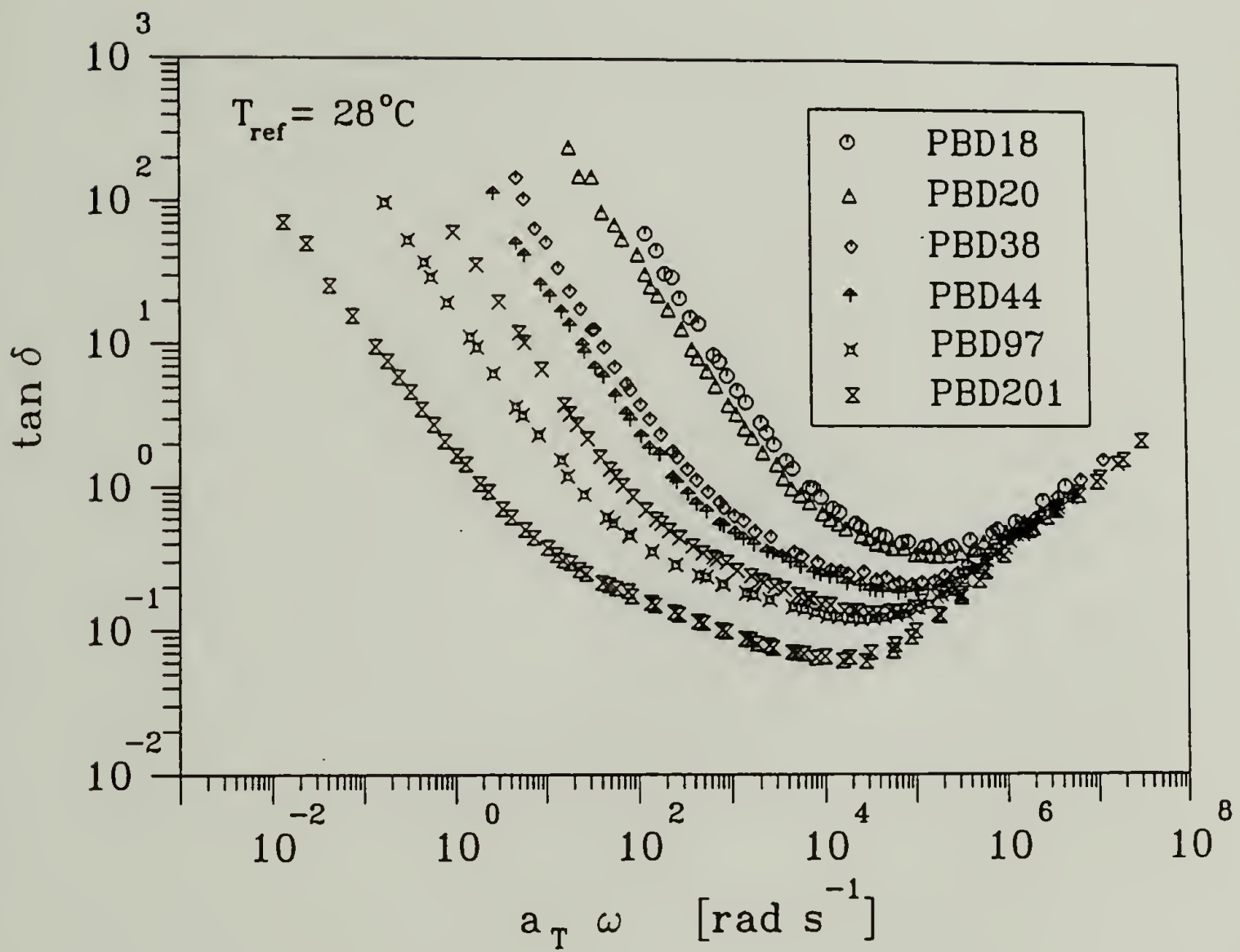


Figure 4.2 Tan δ master curves of the dynamic data shown in figure 4.1. The reference temperature is 28°C .

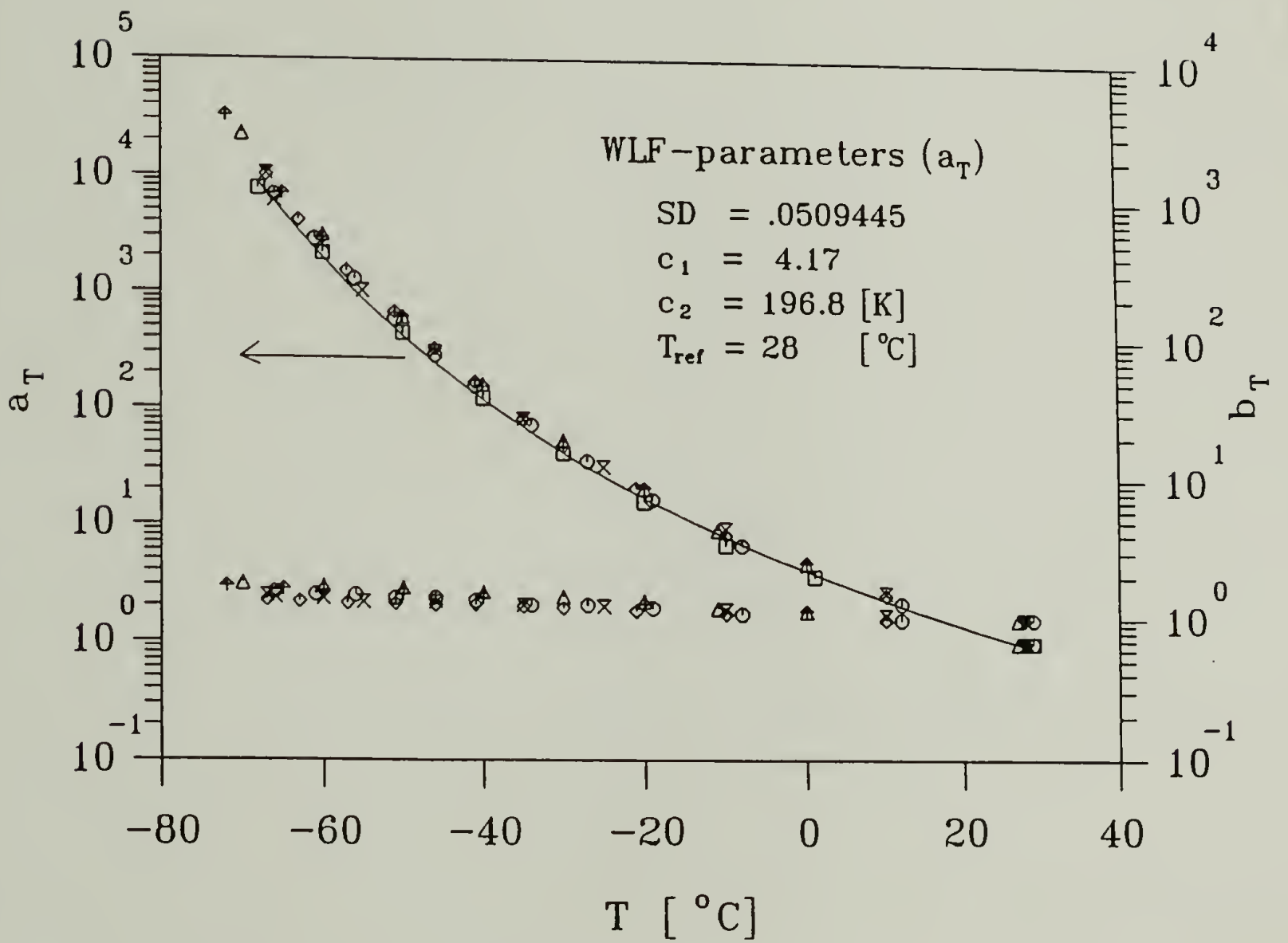


Figure 4.3 Time-temperature superposition horizontal shift factor (a_T) and vertical shift factor (b_T) of the dynamic data in figure 4.1. The WLF equation describes a_T as a function of temperature with the parameters given in the figure 4.1.

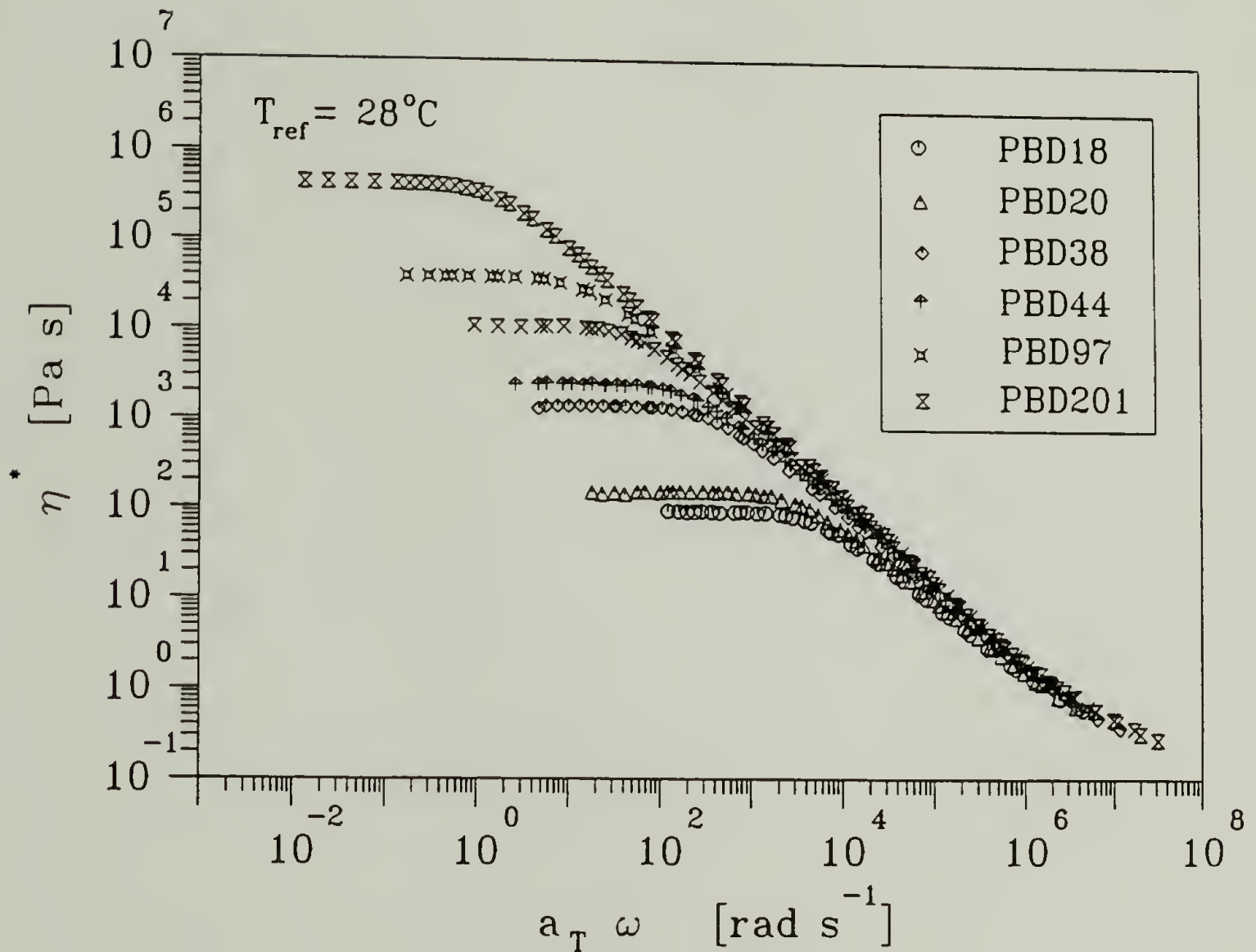


Figure 4.4 Complex viscosity (η^*) of the dynamic data in figure 4.1. The reference temperature is 28°C . The zero shear viscosity (η_0) is taken as the value of η^* in the long time region where η^* is independent of frequency.

Table 4.1 Zero shear viscosity values for PBD samples diluted with stoichiometric amounts of crosslinker (12 wt%). η_0 was obtained from η^* in the low frequency limit.

M_w [g/mole]	Bulk η_0 [Pa s]	Dilute η_0 [Pa s]
18100	89	36
20700	162	87
37900	1445	575
44100	2570	1096
70200	10965	4075
97000	38905	17782
201000	446684	-

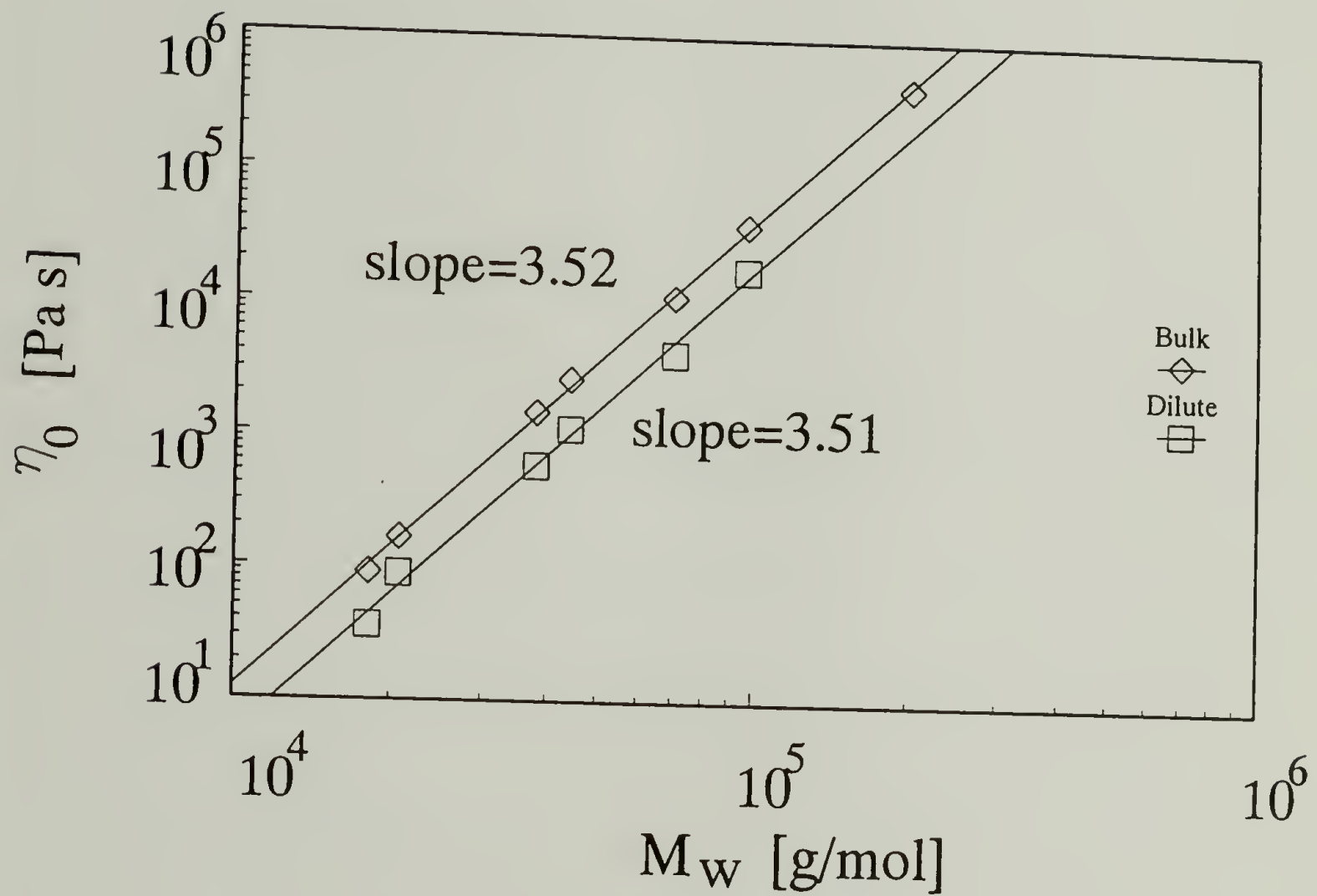


Figure 4.5 Zero shear viscosity (η_0) of bulk polybutadiene precursors and polybutadiene precursors diluted with a stoichiometric ($r=1$) amount of crosslinker ($\sim 12\text{wt}\%$). η_0 is taken as η^* in the low frequency limit. η_0 scales with M_w to the 3.52 and 3.51 for the bulk and diluted precursors respectively.

M_c where the viscosities begin to deviate from the scaling behavior of higher molecular weights. Data on the viscosity dependence of the molecular weight for many polymers show that the transition between the scaling exponent of 1 for $M_w < M_c$ to about 3.4 for $M_w > M_c$ can be somewhat broad (Berry and Fox, 1968).

4.2 Relaxation Time Spectrum of Bulk Polybutadienes (BSW-Spectrum)

Chemical details of macromolecules are important for the short time behavior, but have less significance at longer time scales. It is generally agreed that the entanglement and flow behavior of linear macromolecules can be modeled independently of chain chemistry. It therefore is expected that such materials are characterized by a unique relaxation time spectrum, $H(\lambda)$. Molecular dynamics theories predict the spectrum from models for the molecular motion and the averaged forces on the molecules (Rouse, 1953; de Gennes, 1979; Doi and Edwards, 1986; Bird, 1987; des Cloizeaux, 1990). Two well known predictions of $H(\lambda)$ are the spectrum of Rouse (1953) who proposed a bead-spring model which scales as $\lambda^{-1/2}$, and the spectrum which Doi (1974) derived from the reptation theory of de Gennes (1979) which scales as $\lambda^{1/2}$ at intermediate times with a sharp cut off at the longest relaxation time which scales with M_w to the power of 3. Doi combined this region with the Rouse spectrum at short times to give a spectrum described by two superimposed power laws. These theories provide insight into the meaning of macroscopically measured material functions and the associated parameters such as plateau modulus, G_N^0 , and longest relaxation time, λ_{max} , but lack quantitative agreement with experimental data such as the dynamic moduli, $G'(\omega)$ and $G''(\omega)$.

Experimentalists have also made substantial progress towards finding the relaxation spectrum of linear flexible macromolecules. Tobolsky (1960) proposed an empirical model for the relaxation spectrum based on stress relaxation data. He suggested that the relaxation modulus, $G(t)$, could be approximated by a spectrum with a distribution of relaxation times represented by "box-wedge" shape for $H(\lambda)$. The rubbery region is

described by the box. Parameters are given for the shortest and longest time and height of the box. The relaxation times of the box are dependent upon the molecular weight. The transition region is characterized by a wedge with slope of $-1/2$. Ferry (1980) reviewed several other empirical methods of approximating $H(\lambda)$ from rheological data. These methods not only involve the absolute values of material functions, but also their derivatives to arrive at approximations for $H(\lambda)$. Researchers have also investigated the merits of discrete relaxation time spectra. A review of current methods of evaluating discrete relaxation spectra from dynamic mechanical data has been presented by Orbey and Dealy (1991).

The relaxation time spectra of a linear flexible polymers with narrow molecular weight distribution above the entanglement molecular weight have been shown to be well represented by a superposition of two power laws (Baumgaertel et al., 1990). The form of the spectrum was proposed by Baumgaertel, Schausberger, and Winter (1990), hence the name BSW-spectrum. In this work, the parameters of the BSW-spectrum for polybutadiene were evaluated. Previous work focused on obtaining the best approximation of the data for individual samples of polystyrene, polybutadiene (Baumgaertel et al., 1990, 1992), polyisoprene, and polyethylene (Baumgaertel, 1991). In this study, a method is outlined for obtaining a single set of parameters which best approximates the entire range of data for all the molecular weights. The features of the spectrum which are common to all linear flexible polymers are clarified and the physical significance of the spectrum parameters are interpreted.

4.2.1 BSW-Spectrum and Its Properties

The BSW-spectrum, which is valid only for linear flexible polymers with molecules of (nearly) uniform length, may be written as

$$H(\lambda) = \begin{cases} n_e G_N^0 \left[\left(\frac{\lambda}{\lambda_c} \right)^{-n_g} + \left(\frac{\lambda}{\lambda_{\max}} \right)^{n_e} \right] & \text{for } \lambda \leq \lambda_{\max}, \\ 0 & \text{for } \lambda > \lambda_{\max}. \end{cases} \quad (4.1)$$

where G_N^0 is the plateau modulus, λ_{\max} is the longest relaxation time of the material, n_e and n_g are the slopes of the spectrum in the entanglement and glass transition zones respectively, and λ_c is the crossover time to the glass transition. The first term in the bracket stands for the glass transition region (as proposed by Tobolsky, 1960). The second term describes the self-similar relaxation in the entanglement region. The cut-off at λ_{\max} is the most simple way of introducing the long time behavior. A schematic of the BSW-spectrum and its parameters is presented in figure 4.6.

Using the BSW-spectrum, it is a simple matter to calculate other viscoelastic properties of interest such as zero-shear viscosity

$$\eta_0 = \int_0^{\lambda_{\max}} H(\lambda) d\lambda = \frac{n_e}{n_e + 1} G_N^0 \lambda_{\max} \quad (4.2)$$

or the recoverable compliance, J_e^0 ,

$$J_e^0 = \frac{1}{\eta_0^2} \int_0^{\lambda_{\max}} H(\lambda) \lambda d\lambda = \frac{1}{G_N^0} \left(1 + \frac{1}{n_e^2 + 2n_e} \right). \quad (4.3)$$

Another important property of the BSW-spectrum is its prediction of the high frequency asymptote of $G''(\omega)$ when the glass transition is neglected. It is seen from equation 3.24,

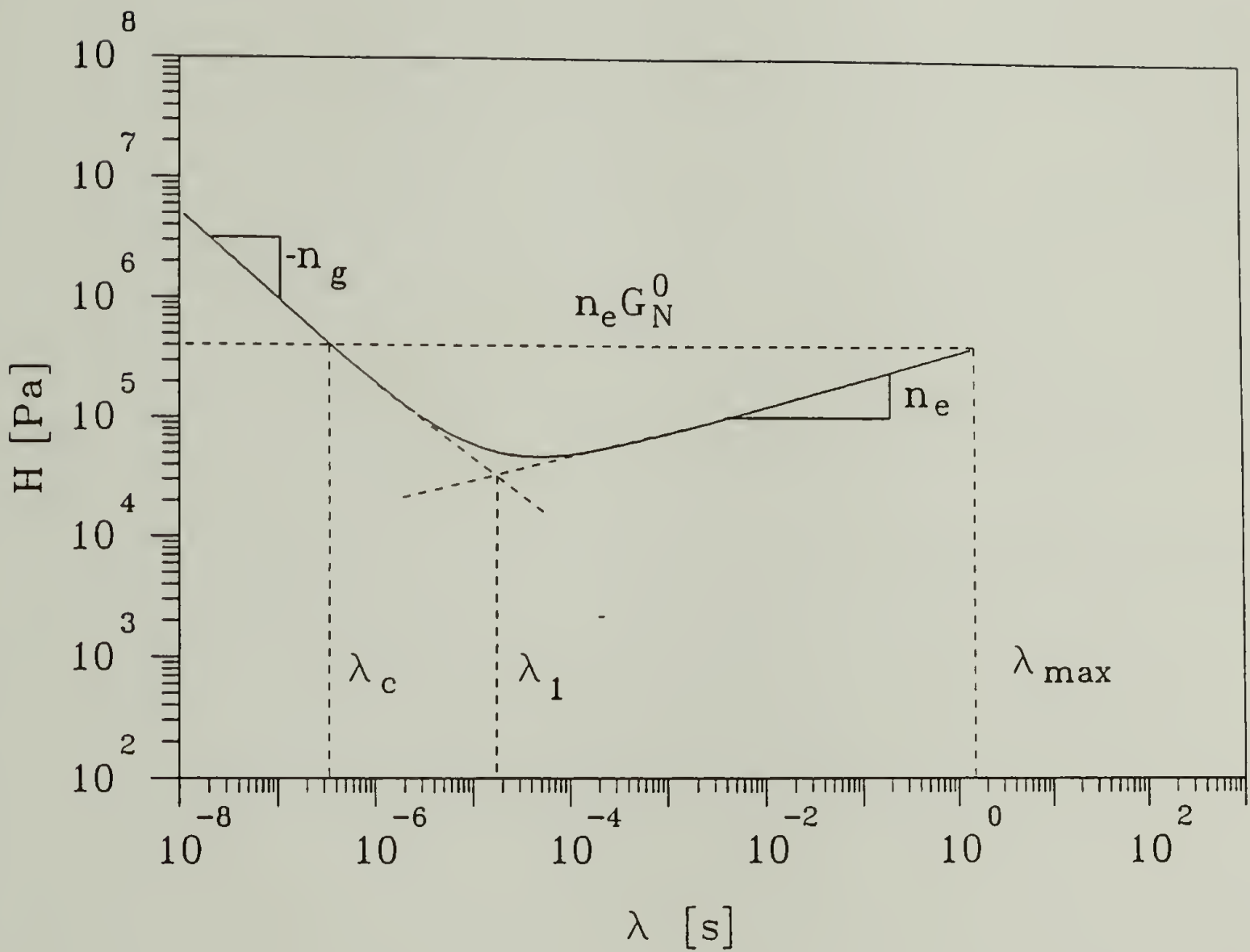


Figure 4.6 Schematic of the BSW-spectrum with labeled parameter. λ_1 represents the intercept of the asymptotes of the power laws from the entanglement and transition zones. λ_1 is found to decrease with decreasing M_w while λ_c is constant for all M_w 's.

$$\lim_{\omega \rightarrow \infty} G''(\omega) = \lim_{\omega \rightarrow \infty} \int_0^{\lambda_{\max}} n_e G_N^0 \left(\frac{\lambda}{\lambda_{\max}} \right)^{n_e} \frac{\omega d\lambda}{1 + (\omega\lambda)^2}, \quad (4.4)$$

$$= \frac{(n_e \pi/2)}{\cos(n_e \pi/2)} (\omega \lambda_{\max})^{-n_e}. \quad (4.5)$$

Thus the limiting slope of $G''(\omega)$ gives the same exponent value as the slope of the entanglement region of the BSW-spectrum, n_e . The parameter n_e is determined initially from the slope of $G''(\omega)$ in the entanglement regime. Though this is a close approximation, it is only precise in the limiting case of equation 4.5. Thus it is necessary to iterate on n_e to obtain a value consistent with equation 4.2.

4.2.2 Molecular Weight Dependence of BSW Parameters

Of the BSW parameters, n_e , n_g , G_N^0 , λ_c , and λ_{\max} , only λ_{\max} is assumed to have molecular weight dependence. It is proposed that the longest time, λ_{\max} , scales as

$$\lambda_{\max} = \lambda_c \left(\frac{M_w}{M_c} \right)^z \quad (4.6)$$

where the parameters λ_c and M_c are a crossover relaxation time and molecular weight respectively, and the parameter z is the scaling exponent. Equation 4.6 can be substituted into equation 4.1 to obtain

$$H(\lambda) = n_e G_N^0 \left[\left(\frac{\lambda}{\lambda_c} \right)^{-n_g} + \left(\frac{\lambda}{\lambda_c} \left(\frac{M_c}{M_w} \right)^z \right)^{n_e} \right] \quad \text{for } \lambda \leq \lambda_c \left(\frac{M_w}{M_c} \right). \quad (4.7)$$

This formulation shows explicitly the parameters necessary to describe linear flexible polymers above the entanglement molecular weight with low polydispersity.

Equation 4.6 can be substituted into equation 4.2 and combined with the well established scaling of η_0 with molecular weight (Berry et al., 1968),

$$\eta_0 = aM_w^z \quad (4.8)$$

to obtain an expression for the prefactor, a , in terms of BSW parameters,

$$\eta_0 = \frac{n_e}{n_e + 1} G_N^0 \lambda_c \left(\frac{M_w}{M_c} \right)^z. \quad (4.9)$$

The characteristic time, λ_1 , at which the asymptotes of the entanglement region and the glass transition region intersect (figure 4.6) could be chosen as a reference time instead of λ_c . While either time could be used, the advantage of using λ_c , is that it does not change for each molecular weight sample as λ_1 does. λ_1 observed to decrease with decreasing M_w . The reference time, λ_1 , is related in a straightforward manner to λ_c and M_c . Given the definition of the BSW-spectrum for the entanglement and glass transition regions it is clear that the two power laws intersect at $\lambda = \lambda_1$

$$n_e G_N^0 \left(\frac{\lambda_1}{\lambda_{\max}} \right)^{n_e} = n_e G_N^0 \left(\frac{\lambda_1}{\lambda_c} \right)^{-n_g}. \quad (4.10)$$

Rearrangement of equation 4.10 and introduction of equation 4.4 gives

$$\lambda_1 = \lambda_c \left(\frac{M_w}{M_c} \right)^{\frac{3.4n_e}{n_e + n_g}}. \quad (4.11)$$

Therefore, as $M_w \rightarrow M_c$, the times λ_c and λ_1 coincide. Whether one chooses to use λ_c or

λ_1 as the reference time, the choice simple fixes the spectrum at a reference point and does not suggest anything about the physics of the glassy relaxation behavior which is outside the scope of this study.

4.2.3 Procedure for Evaluating the BSW Parameters

4.2.3.1 Parameter Initialization

Before an iteration can begin, initial values of each parameter must be chosen.

The scaling exponent z: The zero shear viscosities from the dynamic data for each sample are plotted versus M_w and fit with a power law as shown in figure 4.5. The power law exponent is the value of the exponent z for the molecular weight dependence.

BSW slopes, n_e and n_g : The slopes of the glass transition and entanglement power laws of the BSW spectrum are evaluated next. For that purpose a line is fit to the entanglement region of the low modulus, G'' . Its slope gives an approximate value for n_e . A line is fit to the glass transition region of G'' to obtain an approximate slope n_g (see figure 4.7). The most accurate evaluation of slopes is possible from the highest molecular weight which has the most pronounced entanglement behavior.

The plateau modulus, G_N^0 : The initial estimate of G_N^0 is chosen to fix the entanglement power law on the y-axis such that the plateau region of G' matches the simulation, for the data of the highest molecular weight sample. For this initial estimate, G_N^0 was calculated from the empirical relation found for polybutadiene (Raju et al., 1981; Aranguren and Macosko, 1988)

$$G_N^0 = 3.56G_{\max}'' \quad (4.12)$$

where G_{\max}'' is the maximum peak value of G'' in the terminal zone.

The longest relaxation time, λ_{\max} and the crossover relaxation time, λ_c : Once the plateau modulus has been chosen, it is possible to obtain λ_{\max} by fixing the location

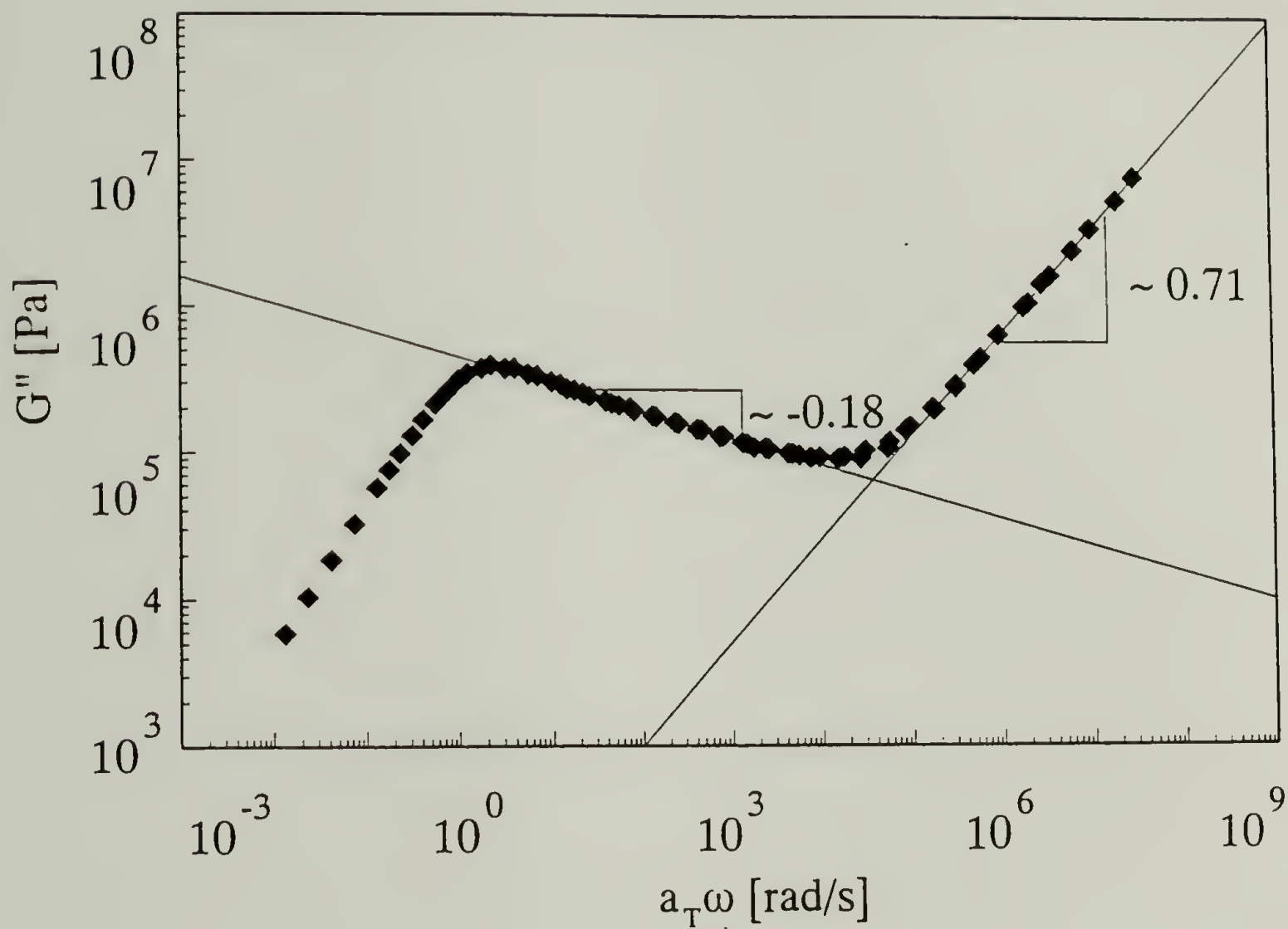


Figure 4.7 Loss moduli for sample PBD201. Power law fits through the entanglement zone and onset to glass transition zone give initial slope values of $n_e=0.18$ and $n_g=0.71$ respectively.

of the entanglement power law on the x-axis such that the terminal zone of the dynamic moduli data match the simulation. The crossover time, λ_c , is obtained by fixing the glass transition power law on the x-axis such that the glass transition zone of the dynamic moduli data match the simulation. Both of these parameters should be evaluated for each individual molecular weight sample. A simple rearrangement of equation 4.6 allows for calculation of M_c once λ_{max} and λ_c are known.

4.2.3.2 Iteration Procedure for Improving the Fit

The initial values obtained in steps 1 through 4 are substituted into equation 4.7 and the dynamic moduli from equations 3.19 and 3.20 are calculated. Iteration on the parameters n_c and n_g are done to obtain the best agreement in the shape of the loss modulus in the entanglement and transition region. The plateau modulus is iterated to give the best agreement to the height of G' in the entanglement region. Iteration of the other parameters is done improve the final agreement of the G' and G'' simulation with the dynamic data.

4.2.3.3 Final Parameter Evaluation

Once the parameters λ_c and M_c are obtained for each PBD sample, an average of all the values is calculated to get final values. It is the averaged values of λ_c and M_c which are used along with z , n_c , n_g , G_N^0 , and λ_{max} to perform the final simulation. The BSW parameters are given in Table 4.2.

4.2.4 Modeling Results

The spectra evaluated from the BSW model with parameters in table 4.2 are shown in figure 4.8. Figure 4.9 and 4.10 shows the dynamic moduli calculated from the BSW spectra in comparison to the data.

Table 4.2 BSW parameters for polybutadiene precursor polymers.

BSW Parameter	Parameter Value
G_N^0 [Pa]	1.65 E+6
n_e	0.23
n_g	0.73
λ_c [s]	4.04 E-7
M_c [g/mole]	2714
z	3.52

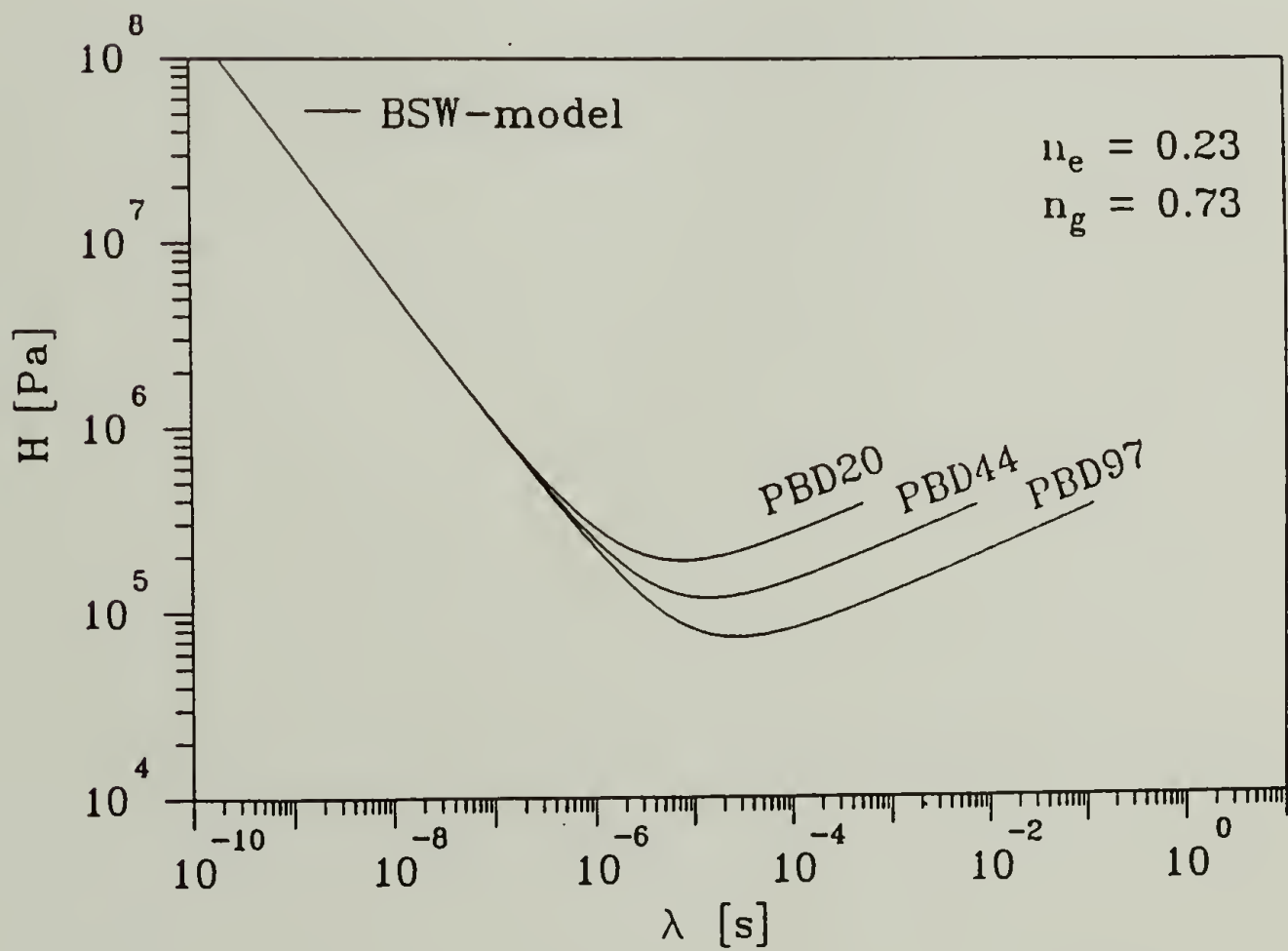
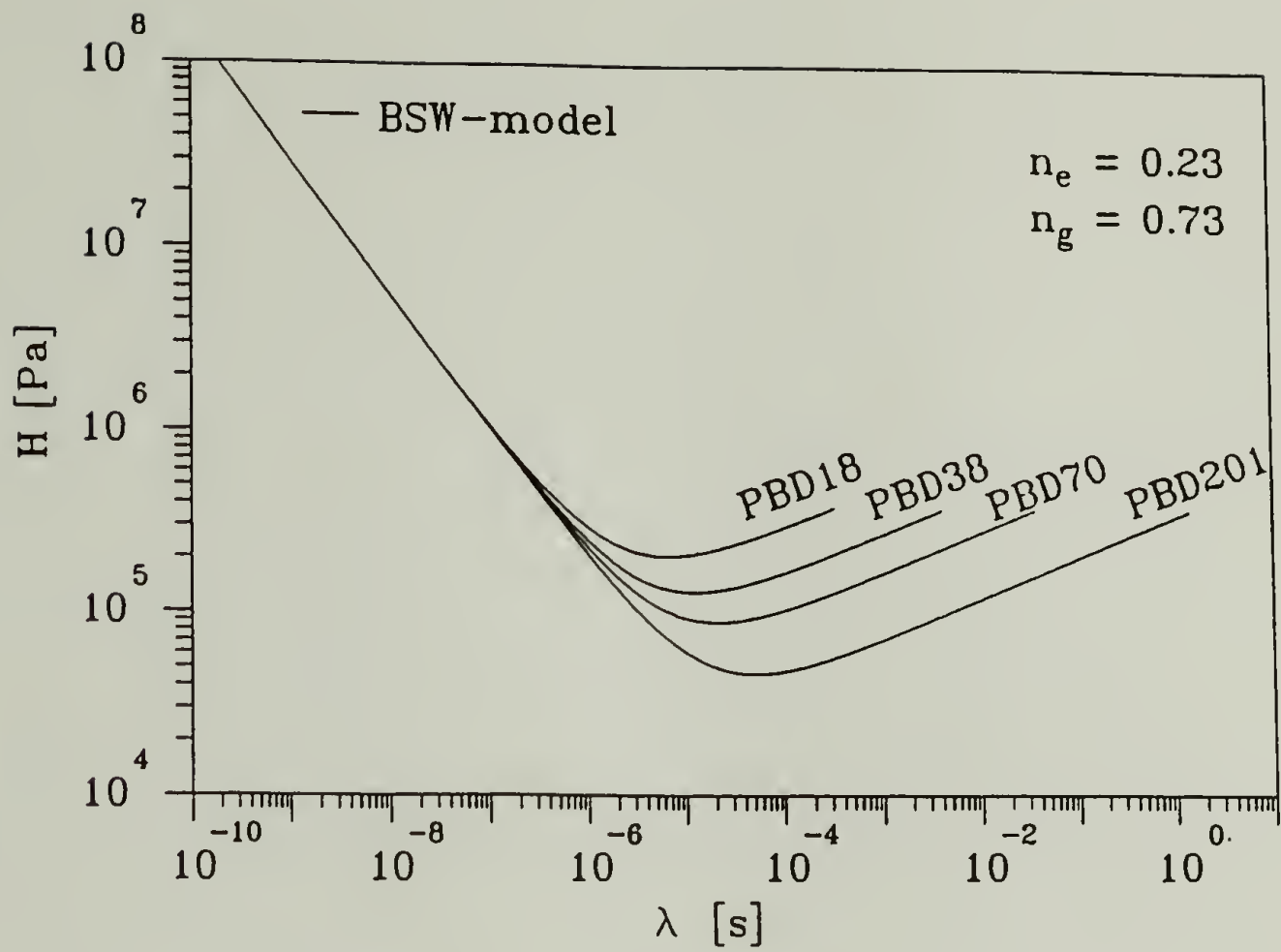


Figure 4.8 BSW-spectra calculated for the molecular weights of the polybutadiene samples with parameters in table 4.2.

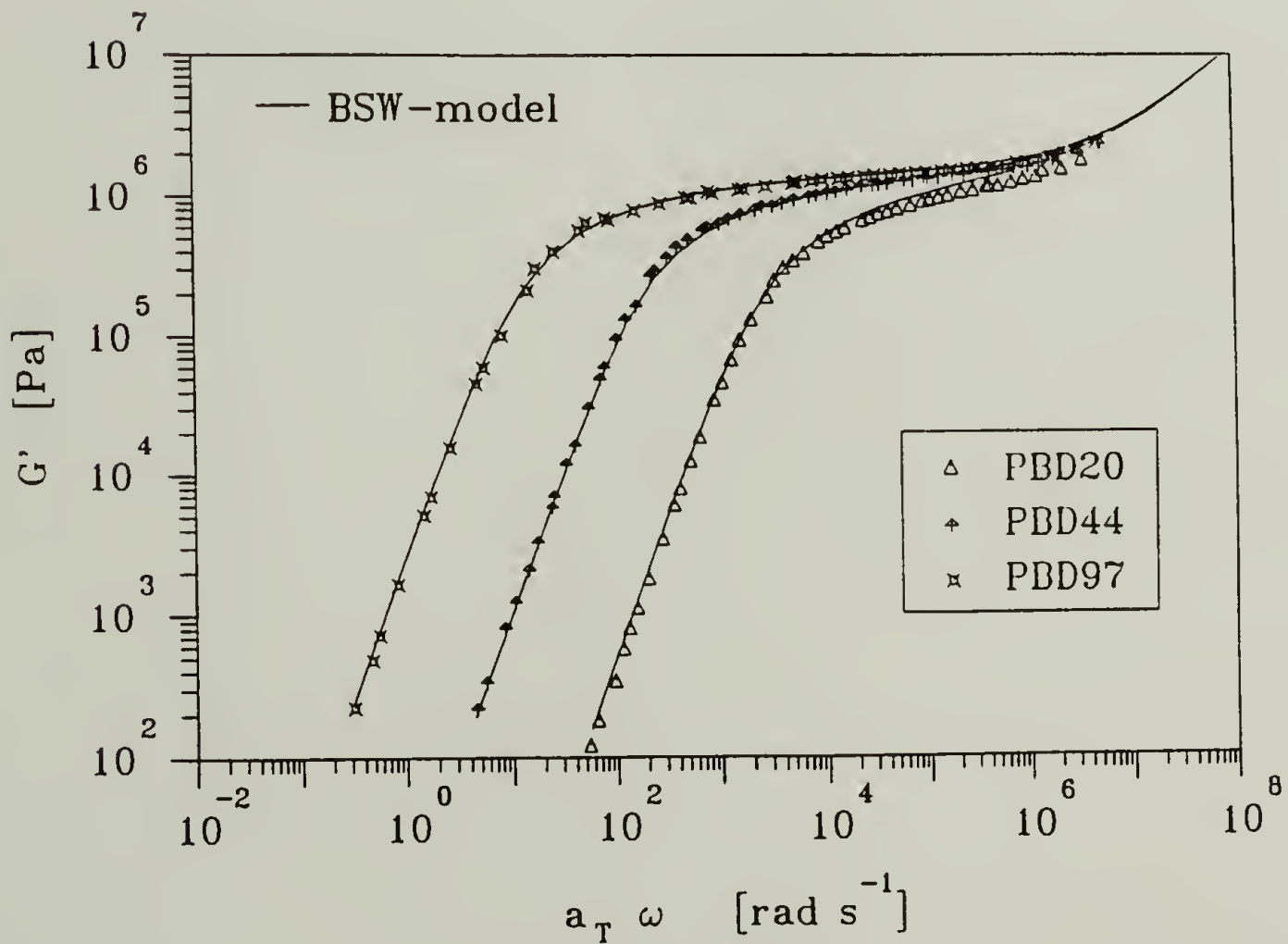
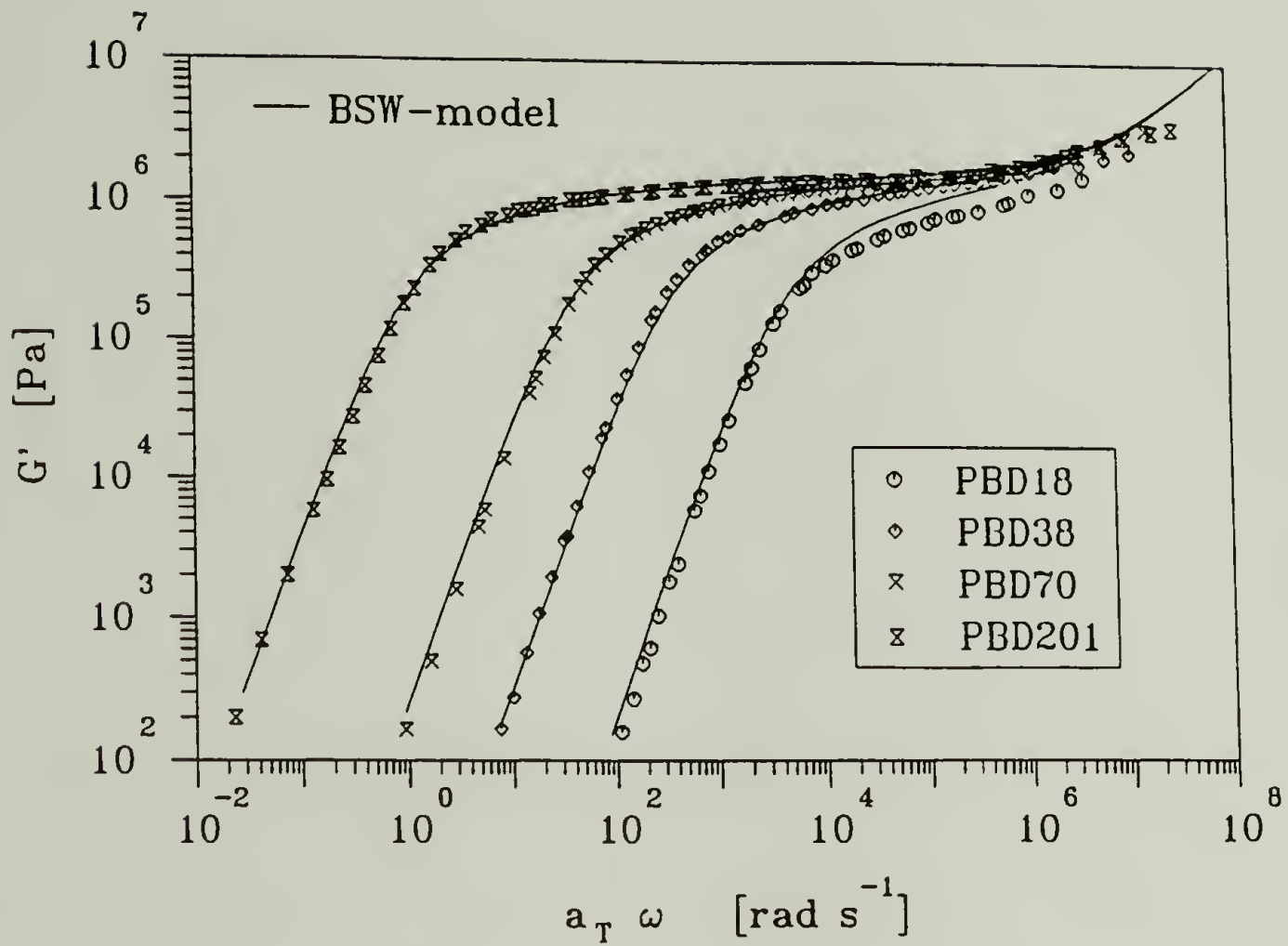


Figure 4.9 Comparison of the storage modulus (G') data of samples PBD18 through PBD97 with the storage modulus calculated from the BSW-spectra in figure 4.8. $T_{\text{ref}} = 28^\circ\text{C}$.

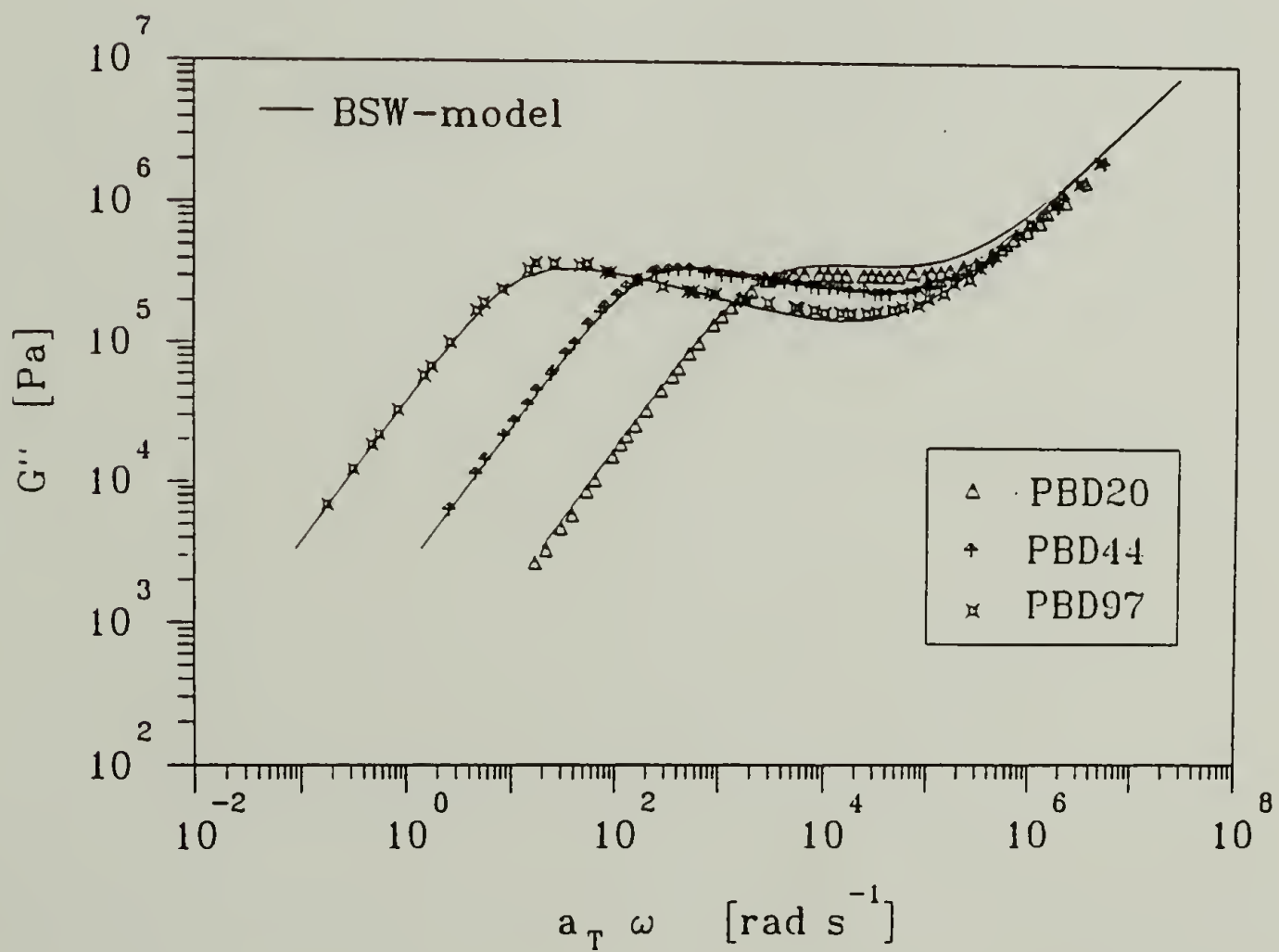
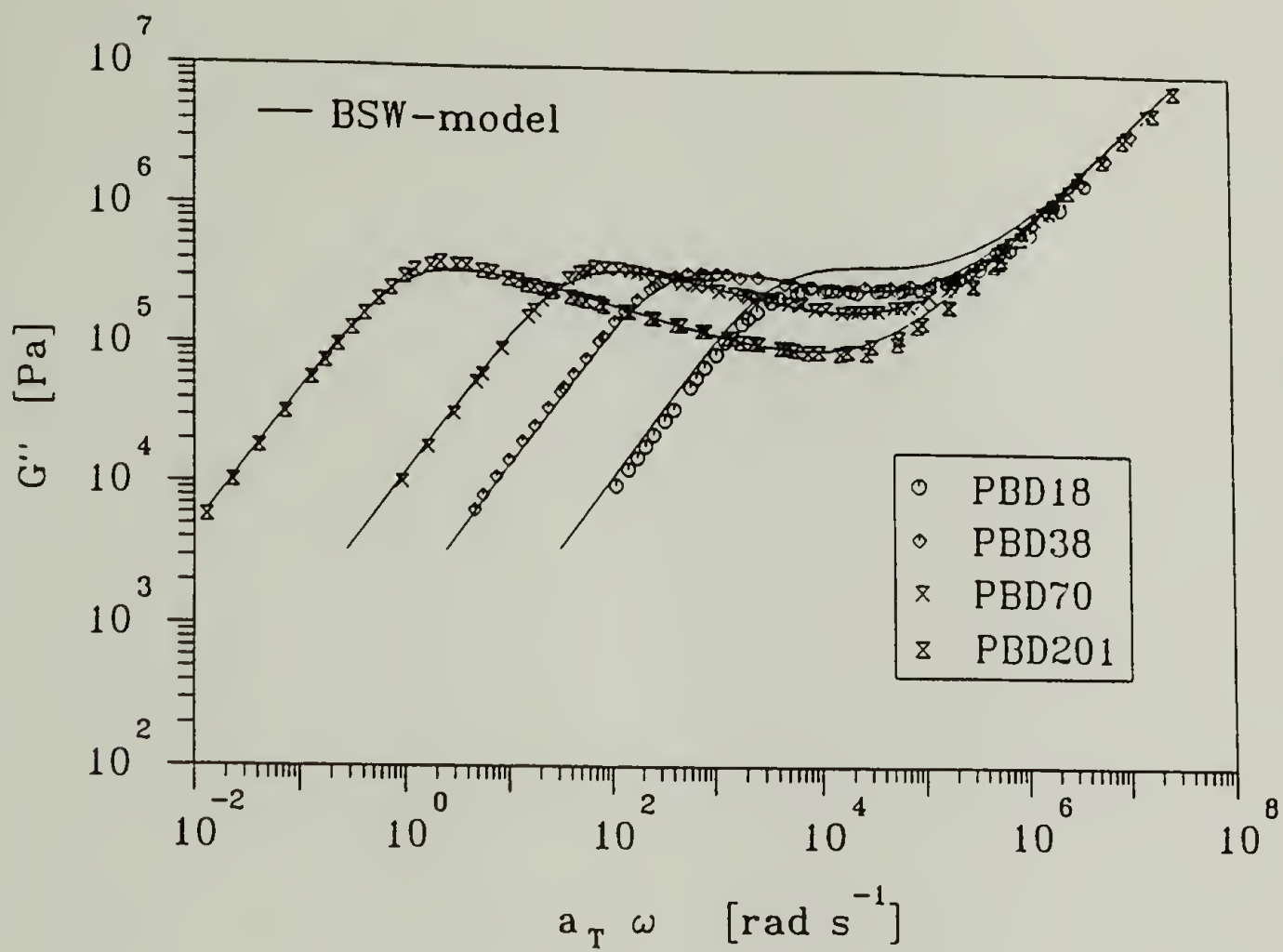


Figure 4.10 Comparison of the loss modulus (G'') data of samples PBD18 through PBD97 with the loss modulus calculated from the BSW-spectra in figure 4.8. $T_{\text{ref}} = 28^\circ\text{C}$.

4.2.5 Discussion

The results in figures 4.9 and 4.10 show that the dynamic moduli of polybutadiene of narrow molecular weight distribution are well described by the spectra proposed in figure 4.6 over a range of molecular weights. While these results are encouraging, it would be useful to analyze additional data on linear flexible polymers with different chemistry and to determine the range of parameter values for different materials. It has been found that the slope n_c is the same for polybutadiene and polystyrene (Jackson et al., 1993) and it would be useful to know whether this is a universal value.

One source of discrepancies between the data and the predicted moduli come from the scaling exponent, z . As described previously, z was obtained from a plot of η_0 versus M_w for all of the samples in this study. However, the lower molecular weight samples of polybutadiene may not scale with a 3.4 power but rather with a power between 1 and 3.4. If this is the case, then the lower molecular weights should not be included in the modeling and z should be obtained from the higher molecular weight samples only.

The parameters M_c and λ_c were previously introduced to describe the relaxation behavior of linear flexible polymers of narrow molecular weight distribution. By presenting these parameters in equation 4.6, it was possible to construct a unique expression for the prefactor, a , given in equation 4.8 in terms of these two parameters shown in equation 4.9. Their physical meaning is subject to interpretation, but one suggestion is that they correspond to the molecular weight at which entanglement begins. The definition of M_c as used in this analysis of G' and G'' data differs from the definition of M_c determined from viscosity data (see data compiled in Ferry, 1980). Accordingly, their values are slightly different. The values of M_c found from the BSW method agree with reported values within a factor of 2.

The modeling emphasizes the high molecular weight behavior, $M_w \gg M_c$. Significant deviations were found for the samples with molecular weight in the crossover

region, $M_w \approx M_c$. Our model seems to be too simple for capturing the details near M_c . Similar complications are known to occur with the molecular weight dependence of the shear viscosity in the crossover region. The rheological behavior near M_c should be studied further. This study can only be used as a first order approximation in this region. More data have to be analyzed in this fashion in order to obtain generic parameter sets for a wide range of polymers.

4.3 Relaxation Behavior of Diluted Precursor

It is a consequence of this two component system, requiring small crosslinker molecules and long precursor molecules, that the added crosslinker increases the mobility of the precursor molecules (Ferry, 1980). In this particular case, 12% by weight of crosslinker must be added in order to reach stoichiometrically balanced conditions. At this considerable amount, the crosslinker is fully compatible with the PBD. It acts as a plasticizer which lowers the zero shear viscosity (figure 4.5) but does not affect the molecular weight dependence for six diluted samples, PBD18 through PBD97. Figure 4.11 shows a comparison of the dynamic moduli of bulk PBD38 and PBD38 mixed with a stoichiometric amount of crosslinker. Dynamic data of the diluted precursor molecules PBD18 through PBD97 are shown in figure 4.12. Dilution also reduced the T_g by 3K from that of the bulk precursors to -94°C . The dilution effect of the crosslinker on the relaxation behavior of polybutadiene is important to include in the following considerations. The dynamic moduli of stopped samples at $r=1$ must be compared to the dynamic data of the precursor mixed with a stoichiometric amount of crosslinker.

4.3.1 Diluent Effect of Crosslinker on the BSW-Spectrum

The plasticizing effect that the crosslinker has on the prepolymer causes a vertical and horizontal shift of the data which lowers the plateau modulus and shifts the value of

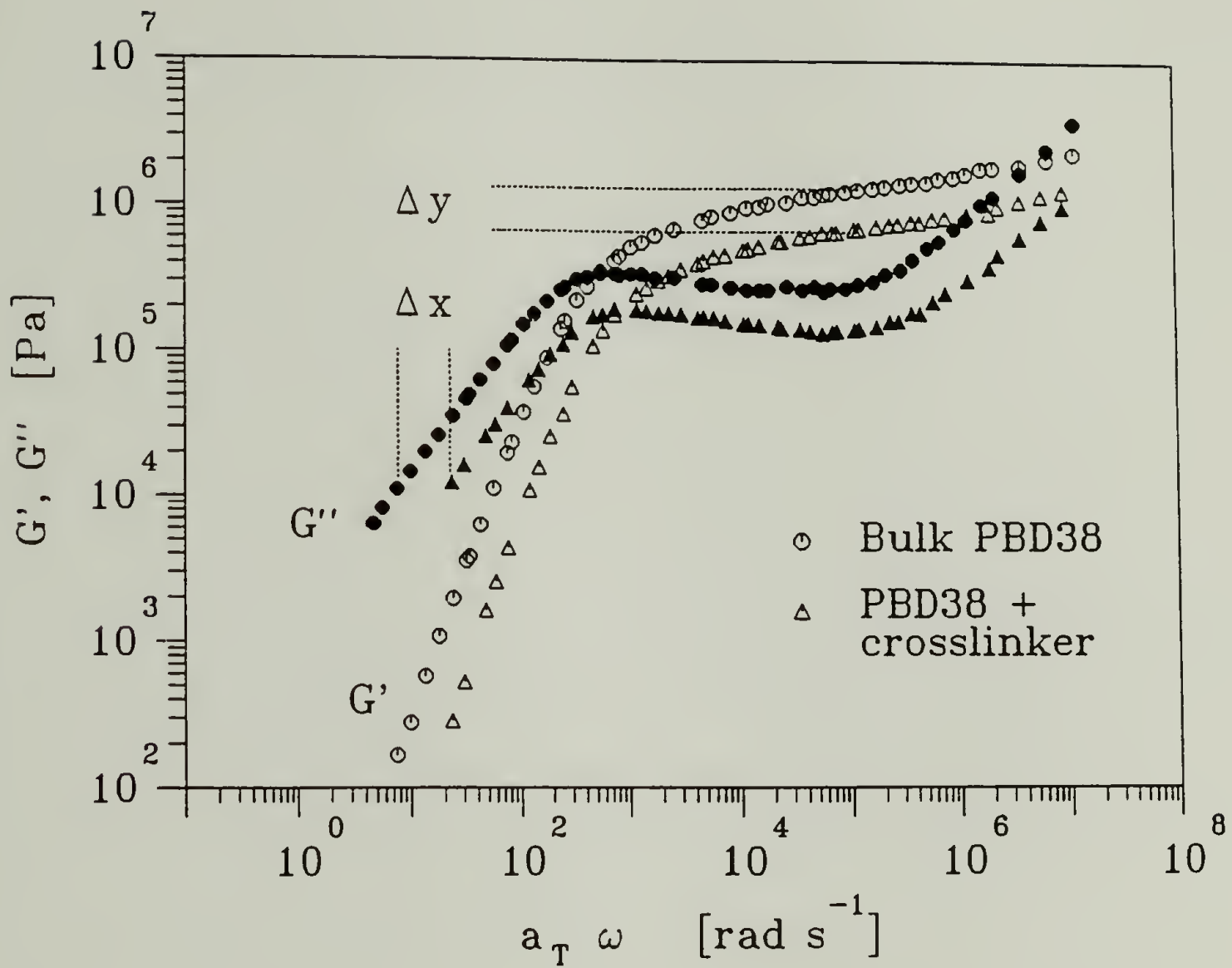


Figure 4.11 Dynamic moduli of bulk PBD38 and PBD38 mixed with stoichiometrically balanced amount (12 wt%) of crosslinker. The plasticizing effect of the crosslinker shifts the data vertically down and horizontally to higher frequencies.

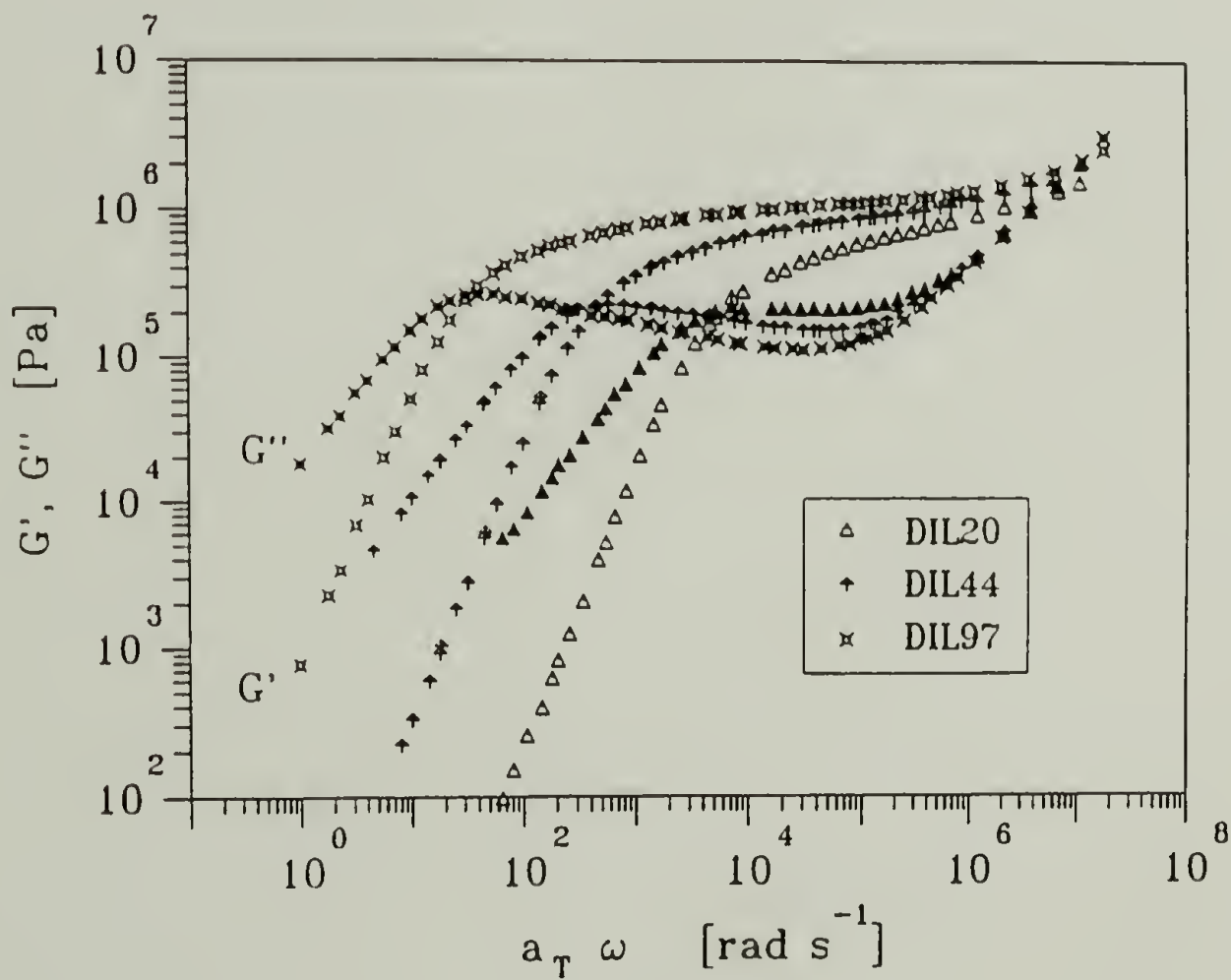
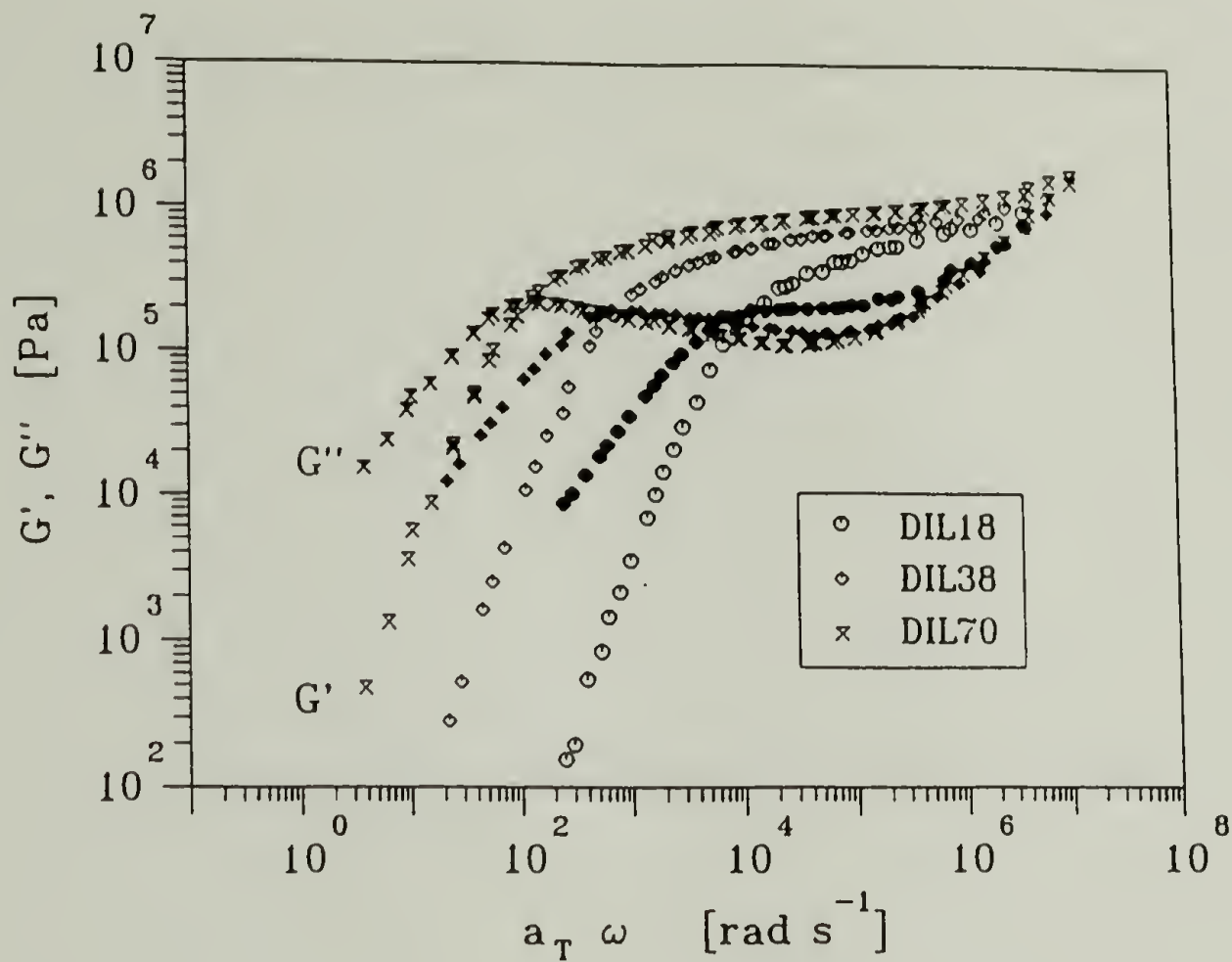


Figure 4.12 Dynamic moduli of PBD samples PBD18 through PBD97 diluted with stoichiometrically balanced amounts of crosslinker. $T_{ref} = 28^\circ\text{C}$.

λ_{\max} and λ_c to shorter times due to the increased molecular mobility. This shifting must be taken into account to obtain BSW parameters for the diluted sample before crosslinking so that the crosslinked samples can be compared to the diluted initial state, not the bulk precursors.

It was observed that the shape of the dynamic data and the relaxation spectra are not changed for samples with stoichiometrically balanced amounts of crosslinker in them. Thus, only a simple vertical and horizontal shift are applied to the data to account for the plasticization effect. Only at much lower concentrations of polymer (high solvent content), would the shape of the spectra be expected to change (Raju et al., 1981; Colby et al., 1991).

The vertical shift can be accounted for by examining the concentration dependence of the plateau modulus. It has been found for concentrated solutions ($c > \sim 0.25$ g/ml) of several polymers that G_N^0 is closely proportional to c^2 (Nemoto et al., 1942; Masuda et al., 1972; Graessley, 1974). Several other systems have shown that the concentration dependence of G_N^0 is slightly higher with values from 2.2 - 2.3 (Riande et al., 1975; Isono et al., 1978)

The plateau modulus for bulk polymers is given as (Ferry, 1980)

$$G_N^0 = \frac{\rho RT}{M_e} \quad (4.13)$$

where ρ is the density and M_e is the molecular weight between entanglements. Diluting the sample with solvent decreases the entanglement density. Consequently, M_e increases with increasing dilution. Therefore, for concentrated solutions, M_e should be proportional to (ρ/c) . The plateau modulus of the diluted polymer ($G_{N,d}^0$) can be expressed in terms of the plateau modulus and molecular weight between entanglements of the bulk polymer (G_N^0 and M_e) as (Graessley, 1974; Ferry, 1980)

$$G_N^0 = \frac{c^2 RT}{M_e \rho} = v^2 G_N^0 \quad (4.14)$$

where the volume fraction $v = c/\rho$.

However, deGennes (1976) has found that G_N^0 should be proportional to $c^{9/4}$. Further work needs to be done in this area. For this study equation 4.14 was used to account for the shift in G_N^0 .

Like M_e , the crossover molecular weight also increases with dilution and is proportional to v^{-1} . Experimentally, the relationship between M_c of the diluted polymer ($M_{c,d}$) and the bulk polymer (M_c) has been found for several polymers to be (Nakagasu and Fox, 1960; Berry and Fox, 1967; Graessley, 1974;)

$$M_{c,d} = \frac{M_c}{v} \quad (4.15)$$

Combining this relationship with equation 4.6 reduces the longest relaxation time for the diluted samples as

$$\lambda_{\max,d} = \lambda_c \left(v \frac{M}{M_c} \right)^z \quad (4.16)$$

The crossover time shifts by the amount v^z to give

$$\lambda_{c,d} = \lambda_c v^z \quad (4.17)$$

The shifting of the BSW-spectrum for the diluted samples can now be expressed as

$$H(\lambda) = n_e G_{N,d}^0 \left[\left(\frac{\lambda}{\lambda_{\max,d}} \right)^{n_e} + \left(\frac{\lambda}{\lambda_{c,d}} \right)^{-n_g} \right] \quad (4.18)$$

or in terms of the original parameters (before dilution) and the volume fraction (v) as

$$H(\lambda) = n_e v^2 G_N^0 \left[\left(\frac{\lambda}{v^z \lambda_{\max}} \right)^{n_e} + \left(\frac{\lambda}{v^z \lambda_c} \right)^{-n_g} \right]. \quad (4.19)$$

A schematic of the BSW-spectrum for the diluted precursors compared to the undiluted precursor is shown in figure 4.13.

The BSW parameters for the diluted samples were determined by using the parameters for the bulk uncrosslinked samples given in table 4.2. The value of v in equation 4.16 and 4.19 was optimized to fit the data. A value of v equal to 0.85 results in the best fit of the data. The value of v calculated from the amounts of crosslinker and precursor used was 0.87. The discrepancy between the two values of volume fraction is only 1.9%. Once the adjustments were made to the BSW parameters to account for the diluent, the single set of parameters was used for all of the diluted PBD samples. These values are given in table 4.3. Figure 4.14 shows a comparison of the dynamic moduli calculated from the BSW-spectrum modified for the dilution effect described in equation 4.19 and the data for six PBD precursors mixed with stoichiometric amounts of crosslinker.

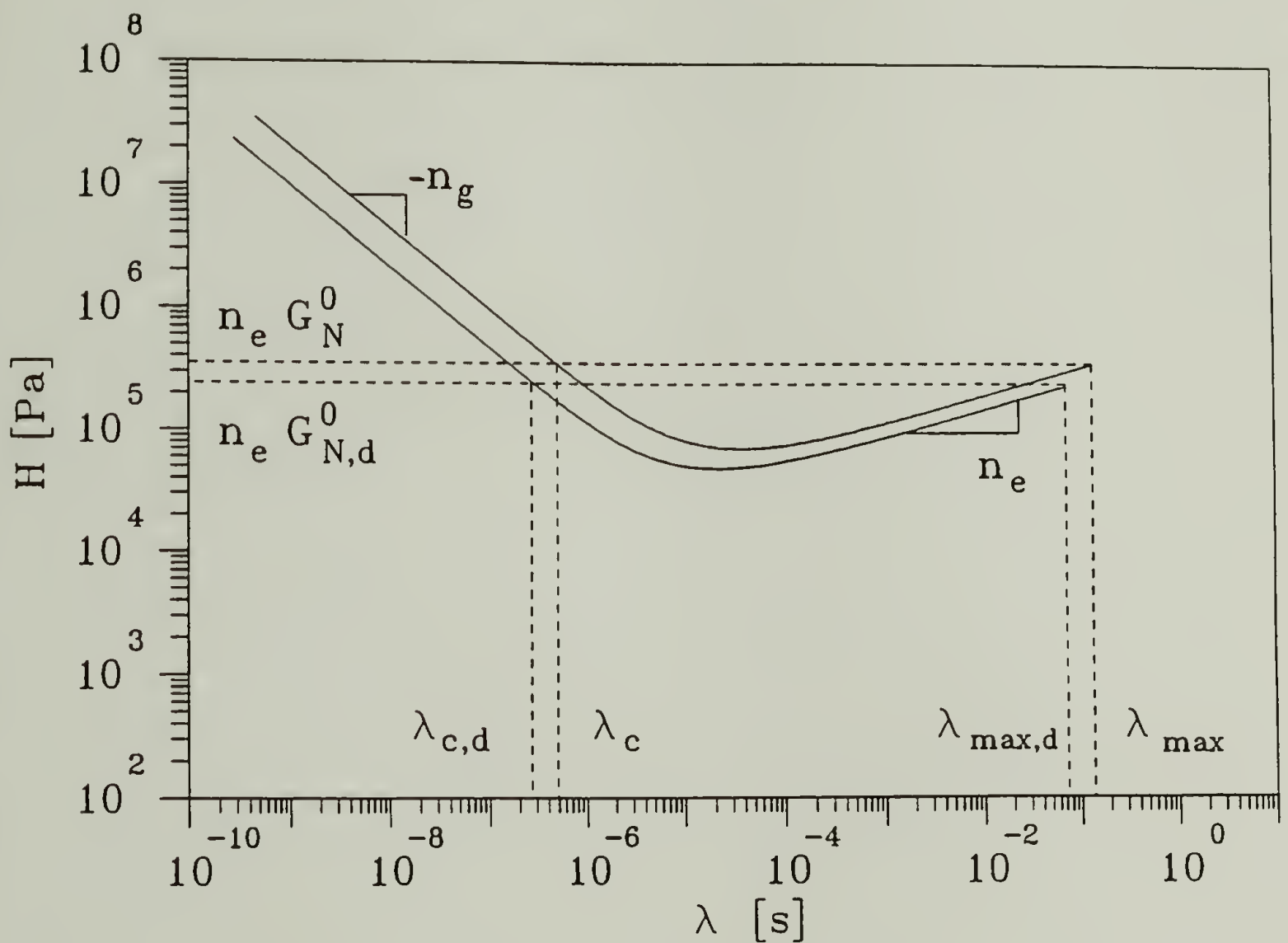


Figure 4.13 Schematic representation of the BSW-spectrum for bulk polymers compared to the BSW-spectrum of concentrated solution. Due to the dilution effect, the plateau modulus (G_N^0) and λ_{max} of the bulk material is shifted down to $G_{N,d}^0$ and $\lambda_{max,d}$ respectively.

Table 4.3 BSW parameters for polybutadiene precursor polymers diluted with a stoichiometric amount ($r=1$) of crosslinker.

BSW Parameter	Parameter Value
G_N^0 [Pa]	1.20 E+6
n_e	0.23
n_g	0.73
λ_c [s]	2.31 E-7
M_c [g/mole]	2714
z	3.51

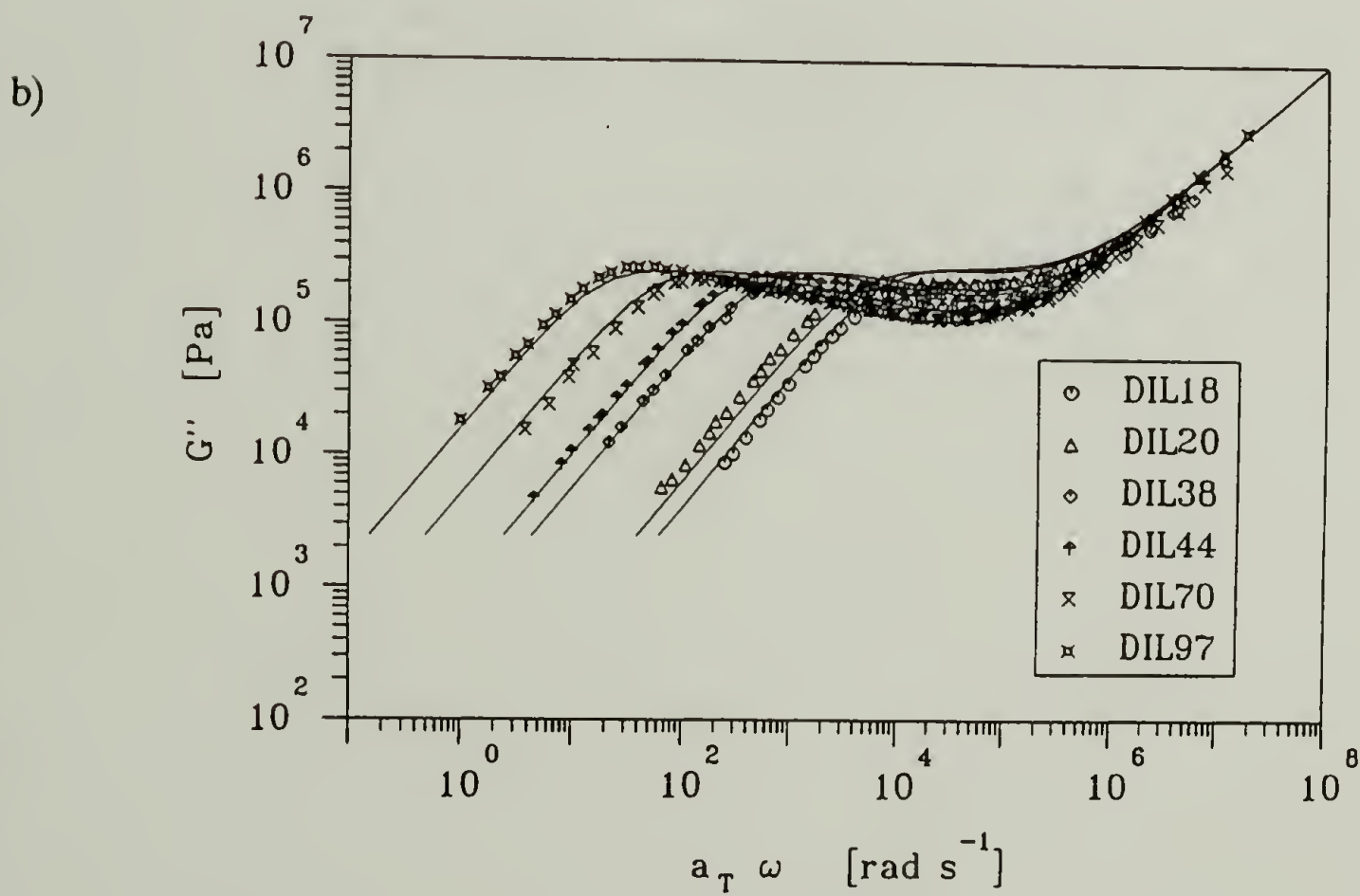
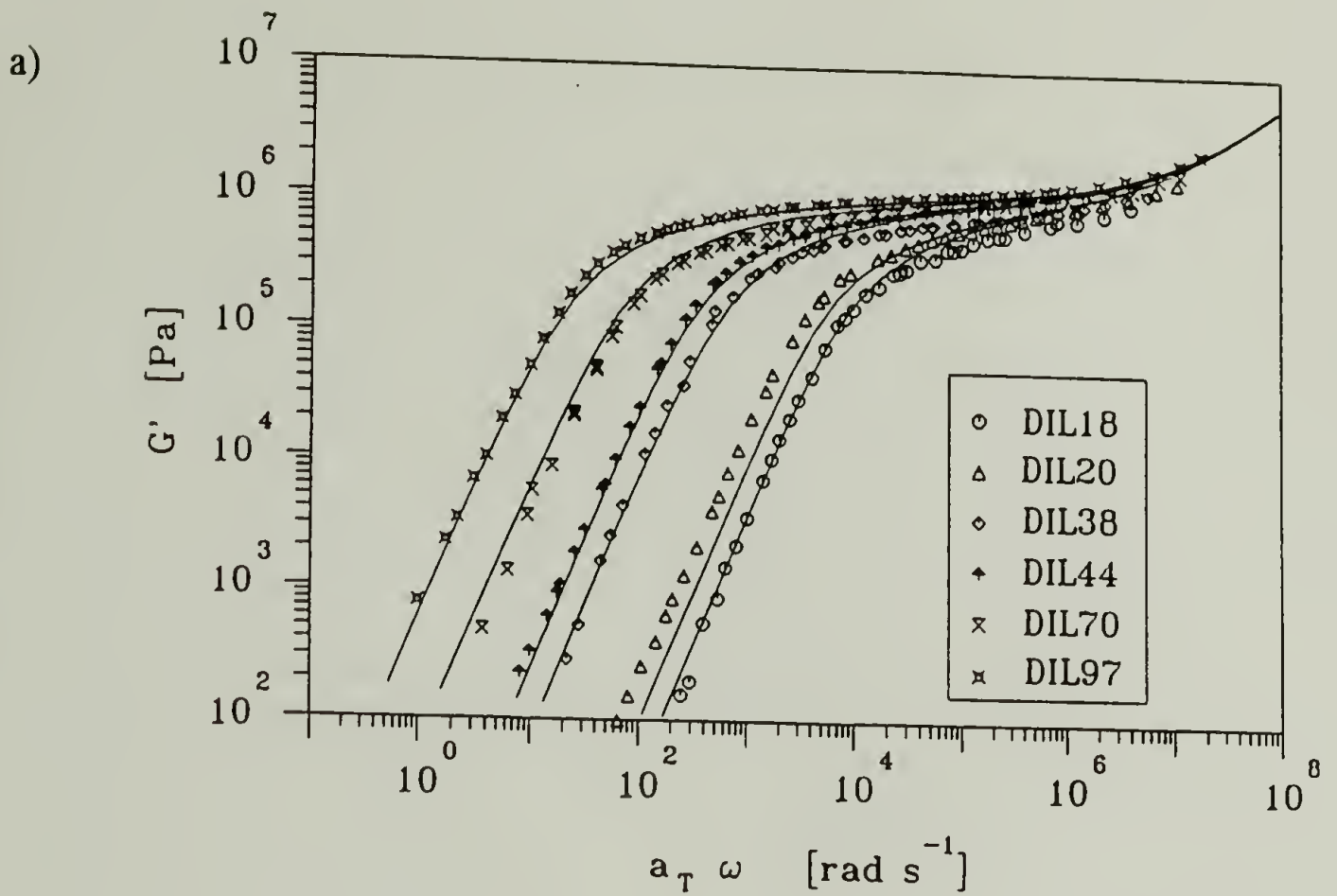


Figure 4.14 (a) Storage and (b) loss modulus data of diluted PBD samples PBD18 through PBD97. The modified BSW model accounting for the diluent effect is given by the solid line. $T_{ref} = 28^\circ\text{C}$.

CHAPTER 5

DYNAMIC MECHANICAL BEHAVIOR OF CROSSLINKING SAMPLES

5.1 Motivation

The changing mechanical properties of a crosslinking polymer can be used as a measure of the growing molecular structures during a crosslinking reaction. As molecular clusters grow in size the molecular weight distribution broadens, the viscosity and the relaxation times increase. When reaching the critical gel point, the weight average molecular weight and the viscosity diverge to infinity as described in chapter 1.

Very often, the critical gel time (t_c) has been estimated by measuring the viscosity under steady shear conditions as a function of reaction time and then extrapolating viscosity data where they diverge to infinity (Gonzalez-Romero and Macosko, 1985). However, this method turns out to be unreliable mainly for three reasons. First, chemical bonds of the larger clusters are being broken during the shear flow (Venkataraman and Winter, 1990). This rupturing process disturbs the network formation in some undefined way and consequently delays the time at which the gel point occurs. Second, due to the fact that the longest relaxation time of the polymer grows with increasing extent of reaction, longer and longer shearing times are required to reach steady shearing conditions. Near the gel point, steady shear can not be reached any more for this practical reason. Third, in approaching the gel point, the shear stress increases to such high values that the measurement must be stopped before reaching the liquid-solid transition in order to avoid overloading of the rheometer transducer. In summary, only a crude estimate of the gel time can be made from viscosity data. A more reliable method is known and will be explored here.

The problems with viscosity measurements in gel point detection can be avoided by using Dynamic Mechanical Spectroscopy which allows measurement of the dynamic shear moduli (G' , G'') during the crosslinking reaction. Since the sample is probed in the

linear viscoelastic range, there is no risk of rupturing the evolving structure. The whole curing process can be monitored from the initial liquid stage through the gel point to the final stage of the fully cured polymer.

Chambon and Winter (1985, 1986, 1987) have shown that polymers at the gel point relax with a characteristic relaxation pattern. The frequency dependence of the dynamic shear moduli of critical gels discussed in chapter 1 is given by equations 1.5 through 1.7. By using the results of these equations, the technique of Consecutive Frequency Sweeps (CFS), discussed in chapter 3, was used to directly monitor the evolution of the mechanical behavior during crosslinking. This experiment provides important information that characterizes the critical gel: the gel time t_c , the parameter S (gel strength) and n (relaxation exponent). The experiment continues through the critical transition point without having to extrapolate data as would be required in viscosity measurements.

CFS has been used previously to measure critical gel properties for short and intermediate precursor molecules below their entanglement molecular weight ($M_w < M_c$) (Scanlan and Winter, 1991; Izuka et al., 1992; Lairez et al., 1992). Other similar dynamic mechanical rheological techniques have been used to monitor the evolution of crosslinking samples with precursors below their M_c (Holly et al., 1988; Muller et al., 1991). The absence of entanglements has made the detection of the gel point a rather simple task because the frequency window probed always includes the terminal zone where the long time relaxation behavior of polymer molecules occurs. It will be shown that at the gel point it is the terminal zone where the characteristic power law relaxation pattern is observed. Therefore, in order to monitor the onset of gelation, one needs to select a rheological frequency window that is low enough so that the terminal zone can be observed.

The objective in this section of the study was to determine critical gel properties of various precursor compositions. The experimental limitation of the CFS method is also explored in relation to applying it to highly entangled precursor molecules with increasing molecular weights.

5.2 Experimental Procedure

Isothermal CFS experiments were performed on polybutadiene samples PBD18 through PBD97. PBD201 was not used because the viscosity was so high that it was impossible to mix in crosslinker and catalyst solution homogeneously in a period of time short enough to make CFS measurements. Samples for CFS experiments were prepared as described in section 2.5. Reacting samples were placed onto 25 mm parallel disks in either the RDS 7700 or RMS 800. Gap settings were usually chosen between 0.5 mm and 1.0 mm. The highest initial strain ($\gamma = 0.25$) was used to achieve reasonable torque values for the lowest molecular weight precursors which have a relatively low initial viscosity. For higher precursor molecular weights (e.g. PBD44, PBD70, PBD97) lower initial strain values could be used due to the higher initial viscosity. As the reaction proceeded for all samples, the strain level was decreased so that in the vicinity of the gel point the strain level was ≤ 0.1 .

Frequency windows from 1 rad/s to 316 rad/s were scanned on the RDS 7700. The RMS 800 has a 100 rad/s upper frequency limit. Two data points per decade were measured. Scans were performed by using the Frequency/Temperature sweep test option of the Rhios operating software of Rheometrics. In this option, the temperature changes were suppressed by setting the temperature step to zero. With these programmed parameters, the computer performs frequency scans over and over at the same temperature. Measurements were made for samples in the stoichiometric range from $0.25 < r < 3.0$. All samples were cured at $28 \pm 0.5^\circ\text{C}$ in an air atmosphere.

5.3 Data Analysis

5.3.1 Conversion of Raw Data Files to IRIS Format

Raw data files must be converted to IRIS format first before "Gelpro" can be used to analyze the collected CFS data. Upgrades in any of the current software applications (Rhios, IRIS, "Gelpro") may make the following procedure of file conversion in its present form obsolete in the future.

Several simple steps must be taken to convert raw data files to IRIS format. First, essential data is needed for the "Gelpro" program to analyze. These data are the frequency, G' , G'' , and time. To make sure that these data are included in the conversion, the printing parameters in Rhios must have the correct settings. The following selections should be chosen for the two blocks of file printing parameters and will insure that the files converted will contain the necessary information for "Gelpro" analysis:

Block 1	12	1	2	11	5
Block 2	0	0	0	0	0

The user can select any parameter for the fifth column in block 1. Any parameter can be used in block 2. Only the first four parameters in block 1 represent the data needed.

Second, once the printing parameters have been set, the raw data files must be converted in Rhios as printout data files with the extension (.PAD). The conversion will automatically give the files the .PAD extension.

Third, once the .PAD files have been made, they must be moved from the default directory (i.e. C:\) to any IRIS notebook (i.e. a directory in IRIS with rheological data). The .PAD files can be directly sent into an IRIS notebook by specifying the entire path and filename when creating the .PAD file in Rhios.

Finally, one must enter IRIS and open the directory where the .PAD files are. IRIS will automatically convert the .PAD files to .DDD files (IRIS standard format for dynamic data). The .DDD files can now be read by "Gelpro" for data analysis.

5.3.2 "Gelpro" Analysis of CFS Data

Analysis of the CFS data was performed by using "Gelpro" software. In this program, one chooses the CFS data file to be analyzed which is in IRIS format. The data is then sorted by frequency. The result is a plot of G' , G'' versus time for each individual frequency scanned.

Once the data is sorted, the curves are then smoothed with a fitting spline. An example of sorted and smoothed data is shown in figure 5.1. When the data is smoothed, it can then be interpolated at any reaction time over the frequency window probed even if a data point was not measured at the precise moment chosen. The time chosen to calculate G' , G'' must however be within the range of the time measured for the CFS experiment.

To determine the instant of gelation, $\tan \delta$ is plotted as a function of time for the frequencies probed (figure 5.2). Intersection of the $\tan \delta$ curves indicates the time at which the dynamic data exhibit power law over the frequency window, hence the gel point. The point of intersection is determined by inspection. The value of the gel time is taken off of the screen by using the Data/Value graphics option. One can be more precise about the point of intersection by making the y-scale linear instead of logarithmic and zooming in on the crossover region.

It should be noted that the time equal to 0 plotted in the CFS data is assigned to the beginning of the rheological experiment after mixing and loading the sample into the rheometer. Therefore, the total time to reach the gel point can be determined by simply

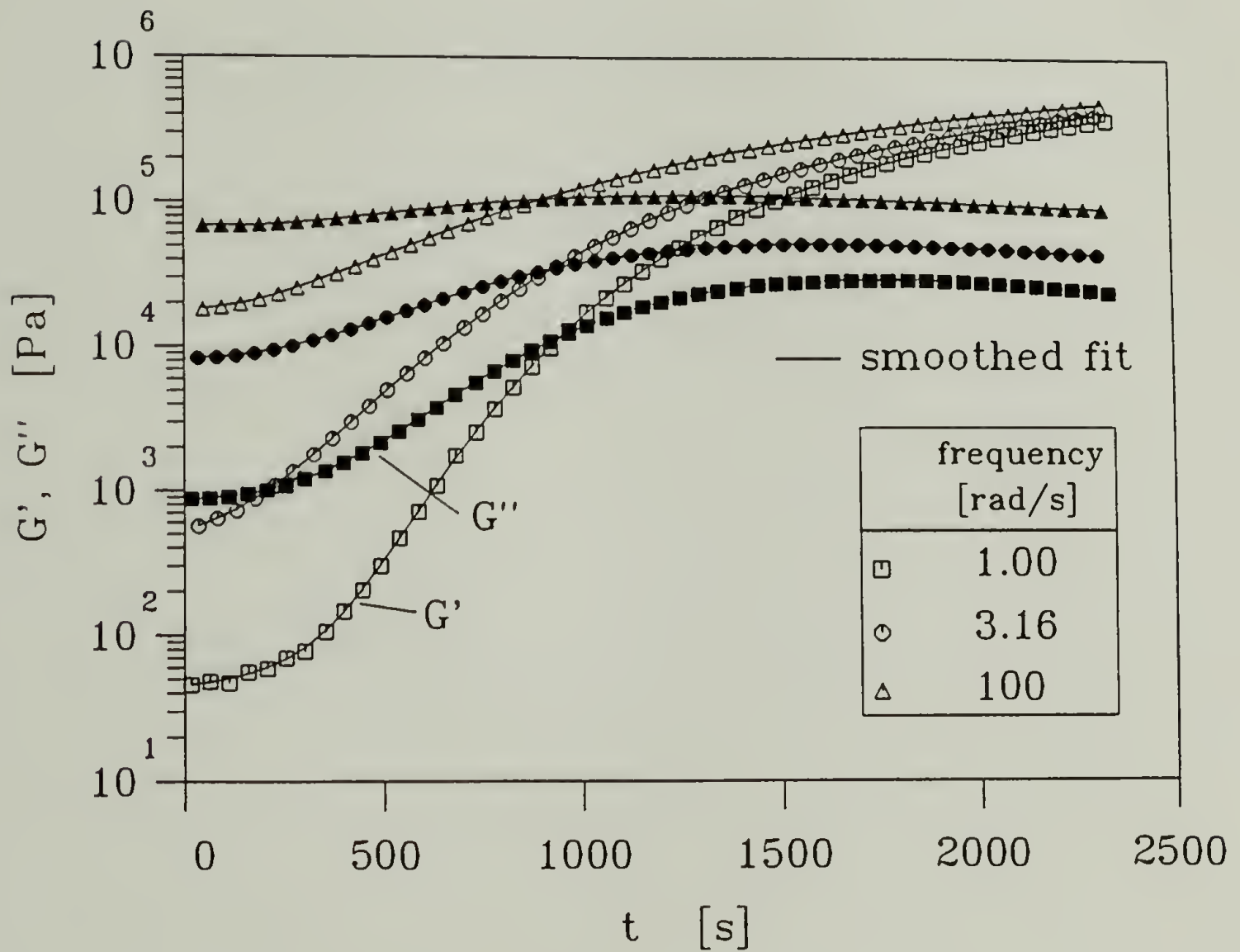


Figure 5.1 Evolution of G' , G'' versus reaction time for PBD38 at stoichiometric conditions at 28°C . The data are sorted with "Gelpro" by frequency. The solid line represents the smoothed fit of the data. Symbols are actual data points.

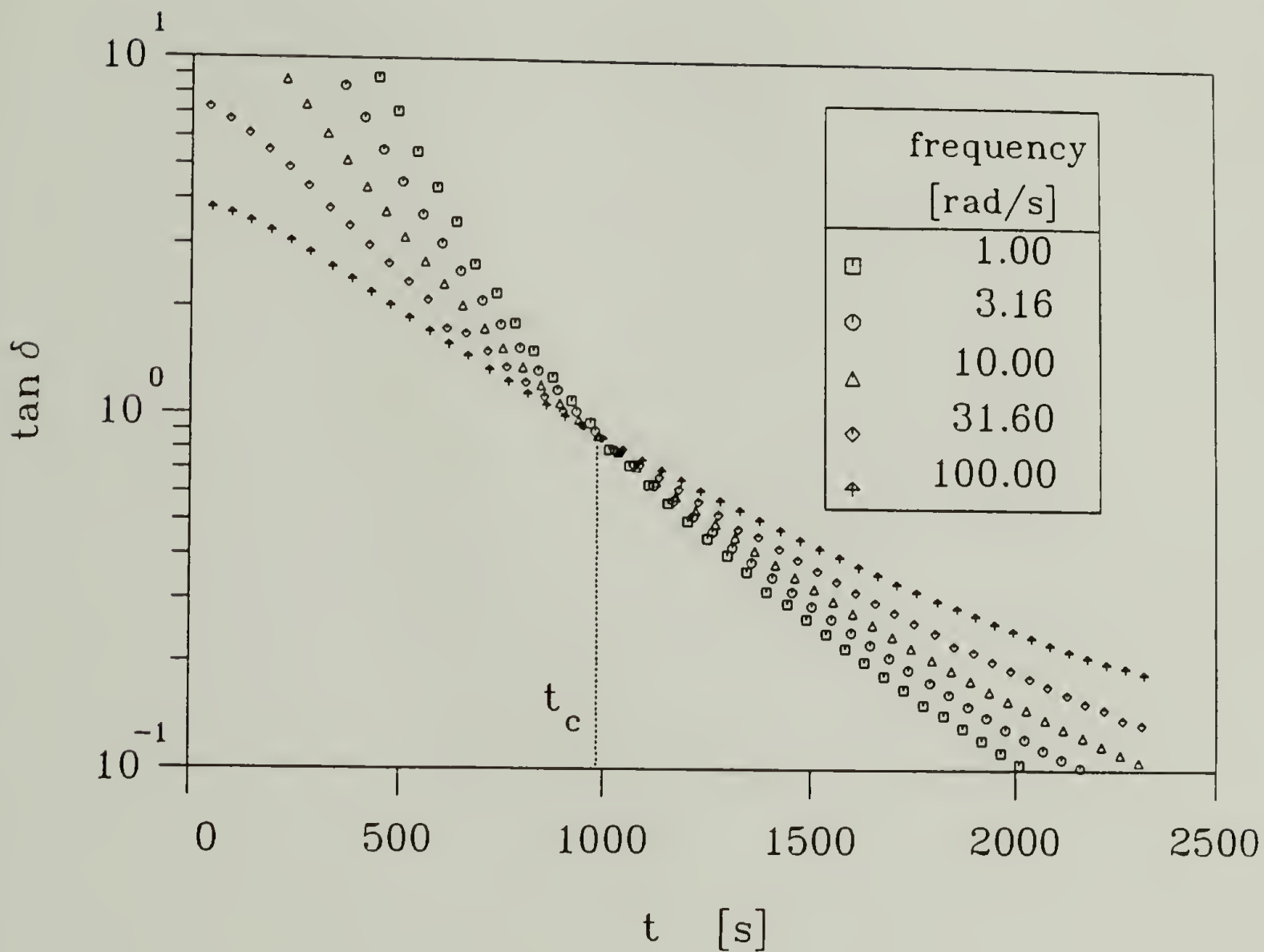


Figure 5.2 CFS data showing the evolution of $\tan \delta$ during the reaction time for PBD38 at stoichiometric conditions at 28°C. The frequency range of the window is from 1 to 100 rad/s. t_c indicates the critical gel time.

adding the time of mixing and loading. However, the time used to calculate the dynamic moduli at the gel point is taken from the time at the intersection of the $\tan \delta$ curves. This issue will be discussed in greater detail in chapter 7.

The error in determining the exact instant of the gel time mostly originated from scatter which slightly smeared out the intersection point of all of the $\tan \delta$ curves. Therefore, the time chosen to be t_c was the point where all the $\tan \delta$ curves came closest to intersecting. The error was found to be greatest when the reaction was extremely slow (see figure 5.3). In this case, the smearing effect was more pronounced and the observed gel time was in error by approximately ± 60 seconds. When the reaction was rapid, a sharp intersection usually resulted which gave an error in t_c of approximately ± 15 seconds.

Many times the data at the highest frequency, 316 rad/s, at the gel point did not intersect with the rest of the frequencies and was not taken into consideration to determine t_c . This may be due to some type of flow instability which may occur at such high frequencies which results in poor reliability of the data taken at these highest frequencies (i.e. ≥ 100 rad/s).

Once the gel time was determined, "Gelpro" was used to calculate dynamic data at times in the vicinity of the gel point. Figure 5.4 shows an example of G' , G'' interpolated for a time before, at, and after t_c . The gel point is given by the power law behavior in G' , G'' which is also displayed by the independence of $\tan \delta$ and the normalized phase angle, $2\delta/\pi$, with frequency as shown in figures 5.5 and 5.6 respectively.

Interpolated CFS data at the gel point gives excellent agreement with stopped sample data. Figure 5.7 shows a comparison of dynamic data calculated at t_c from CFS data was compared to a master curve constructed from a stopped sample near the gel point. This agreement shows that data interpolated from *in-situ* measurements gives essentially the same result as samples in which the reaction was stopped and are therefore representative of samples at the gel point.

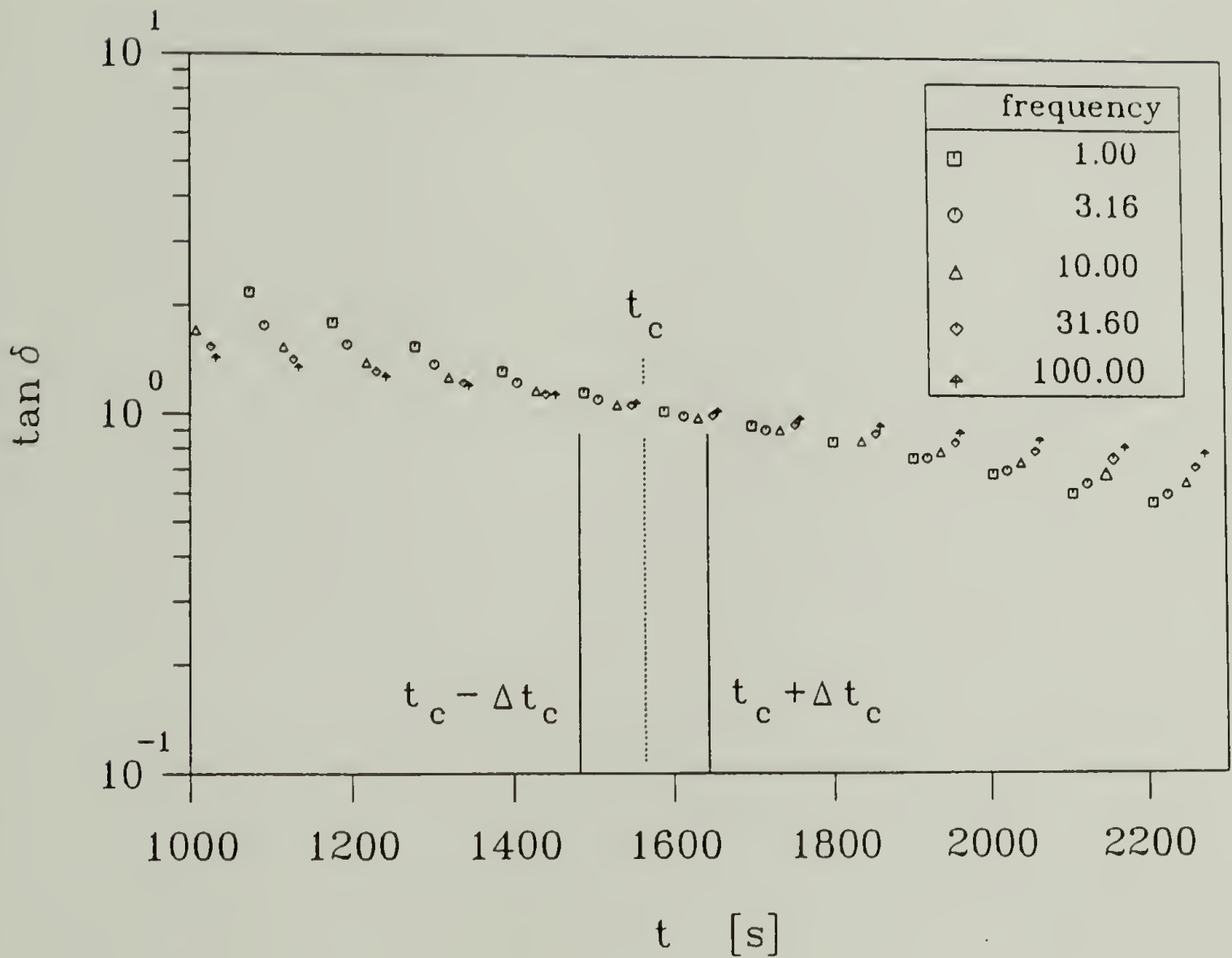


Figure 5.3 CFS data for PBD18 at $r=0.25$ at 28°C . Slow reactions tend to smear out the intersection point of $\tan \delta$ making determination of t_c more difficult. Error bars in t_c are given by Δt_c . Δt_c becomes smaller as the rate of gelation increases.

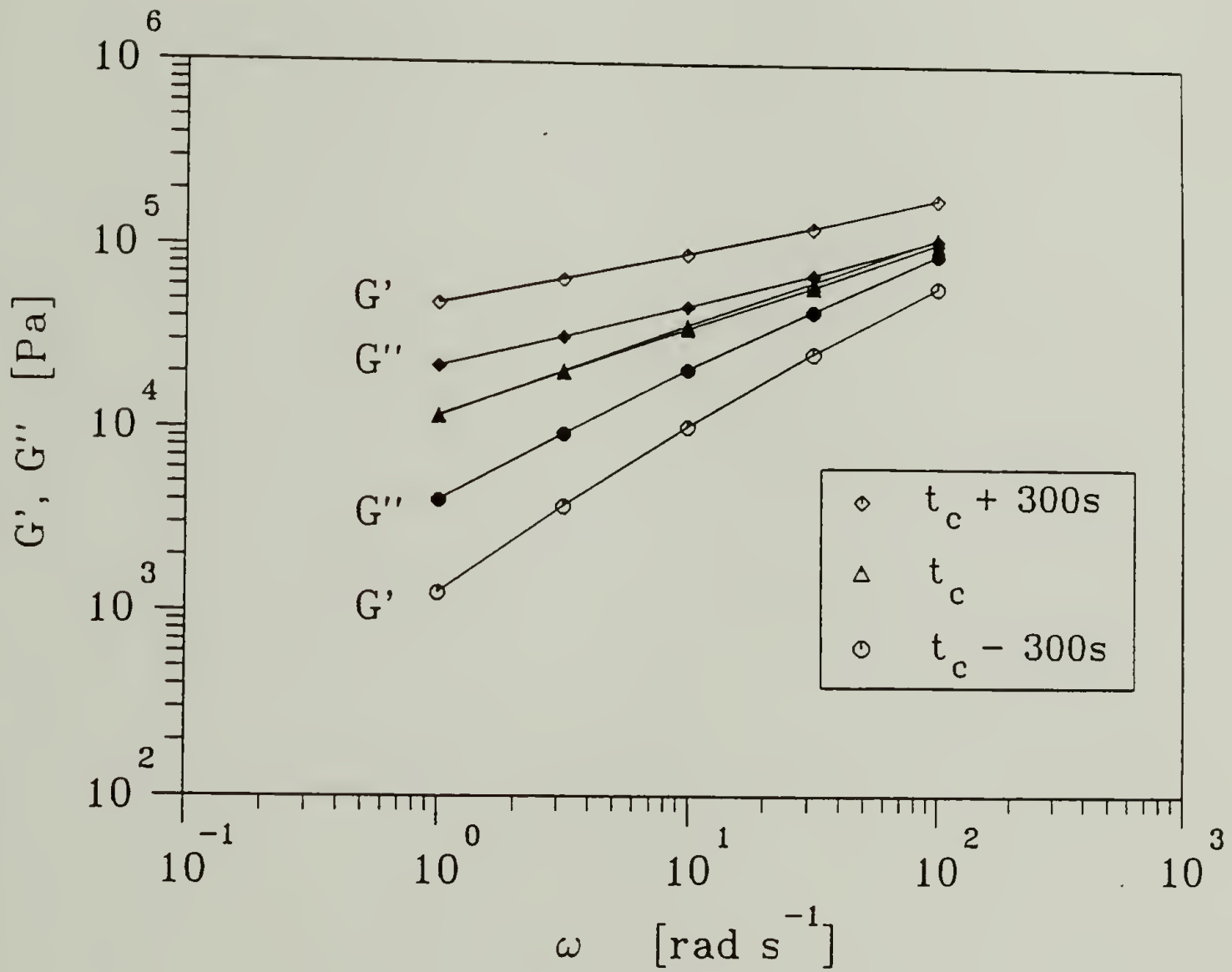


Figure 5.4 "Gelpro" interpolated dynamic moduli at three times in the vicinity of the gel point from the smoothed curve data of PBD38 at stoichiometric conditions at 28°C . The symbols are interpolated data points. The solid line only serves to connect the points and is not a fit to the data.

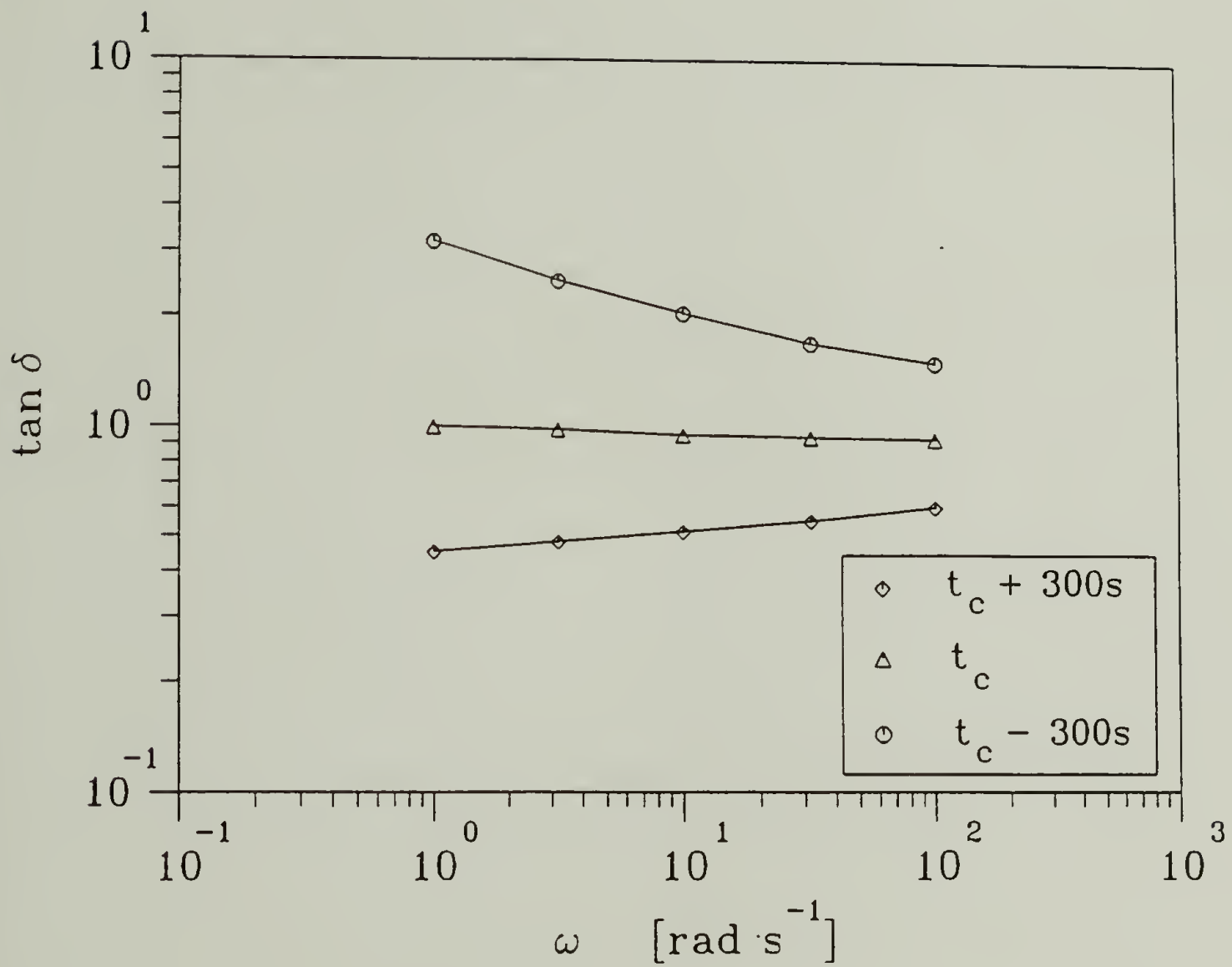


Figure 5.5 Tan δ of interpolated data in figure 5.4. At the gel point, $\tan \delta$ is independent of frequency with a value close to 1. The solid line connects the interpolated data points and is not a fit.

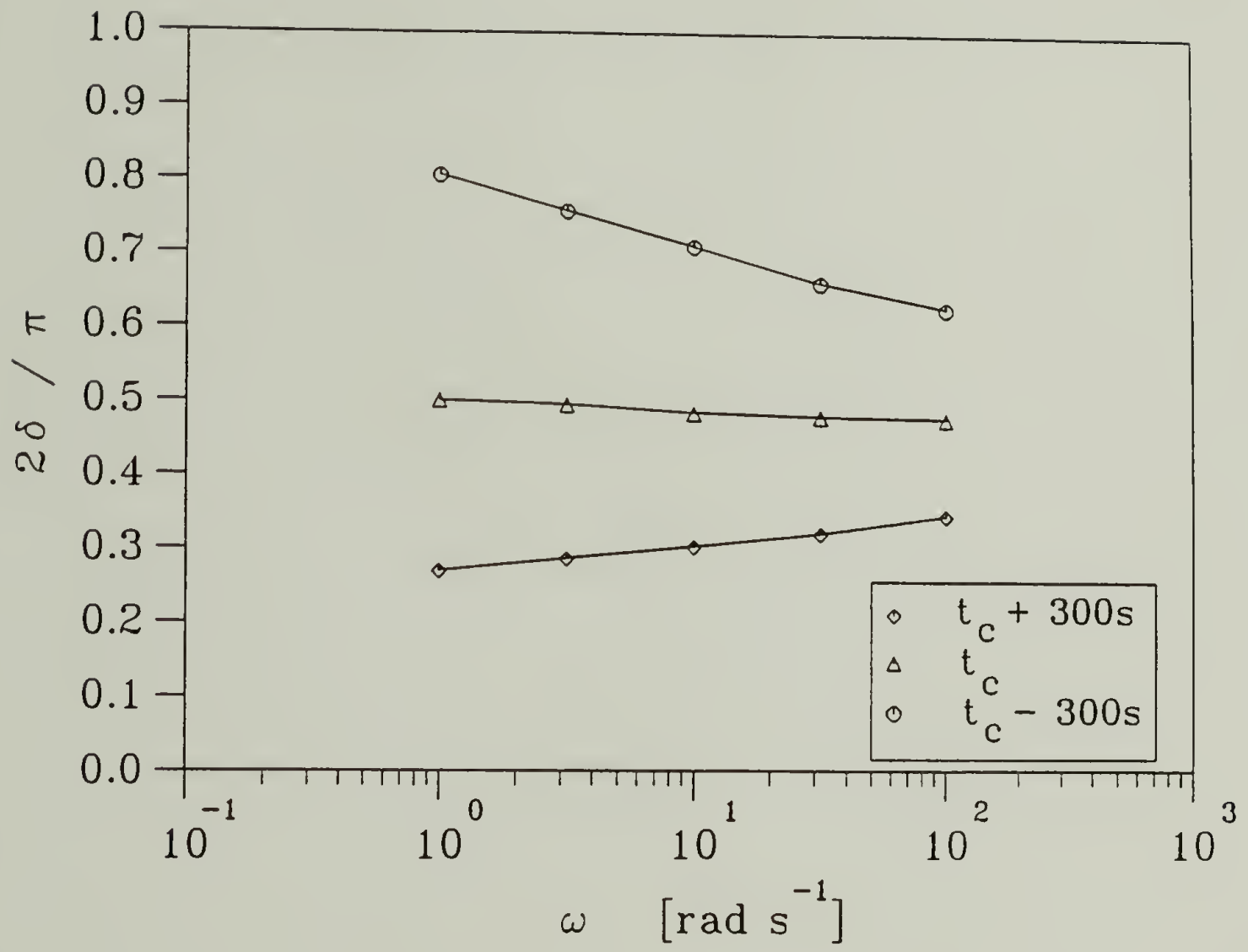


Figure 5.6 Normalized phase ($2\delta/\pi$) of interpolated data in figure 5.4. At the gel point, $2\delta/\pi$ gives the exponent $n = 0.5$. The solid line connects the interpolated data points and is not a fit.

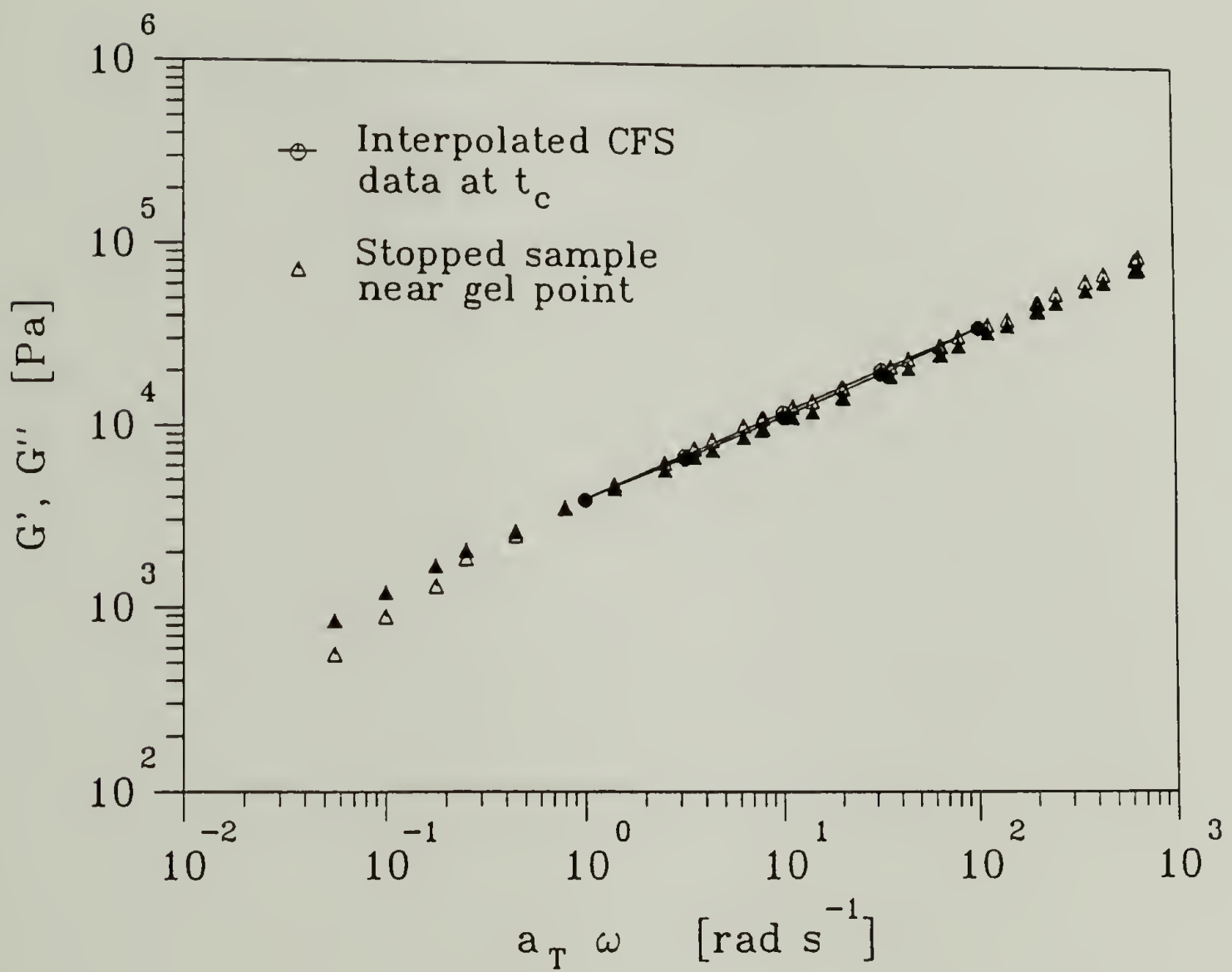


Figure 5.7 Comparison of interpolated G' , G'' data points calculated by Gelpro at t_c to G' , G'' of stopped sample. The stopped sample and CFS sample are both PBD18 at $r=1$ measured at 28°C .

The gel strength was calculated by using equation 1.6 and interpolated dynamic data at t_c . First, the values of n at each frequency were calculated by using equation 1.7. Once this was done, the values of $\Gamma(1-n)$ for each frequency were taken from a gamma function table. In the final step, G' is taken at each frequency to calculate a value of S at each frequency. An average value of S and n was reported for each data set.

5.4 Results of CFS Measurements

CFS measurements were made for samples PBD18 through PBD97. CFS data for all samples with balanced stoichiometry are shown in figures 5.8 and 5.9. Only one measurement of PBD20 at $r=1$ was made. All of sample PBD20 was used up performing earlier experiments before the sample preparation technique was refined to give good data. Critical gel properties could not be calculated for sample PBD97 as will be discussed later.

CFS measurements yielded data where all of the $\tan \delta$ curves intersected at the gel point for PBD18 (1-100 rad/s), PBD20 (1-316 rad/s), and PBD38 (1-100 rad/s) (figure 5.8). For samples PBD44, PBD70, and PBD97, all of the $\tan \delta$ curves (1-316 rad/s) do not intersect (figure 5.9). In these last three cases, the lowest frequencies intersect at one time, but the highest frequencies do not intersect with the lowest frequencies. This effect appears to be more pronounced as the molecular weight of the precursor increases from PBD44 to PBD97.

The gel strength is plotted as a function of stoichiometry in figure 5.10. S was found to decrease slightly with increasing amount of crosslinker. The value of the relaxation exponent is shown as a function of r in figure 5.11. The values of n were found to stay in the narrow range $0.41 < n < 0.53$ and remained insensitive to stoichiometric ratio over the precursor molecular weights examined. A summary of the CFS results are given in table 5.1.

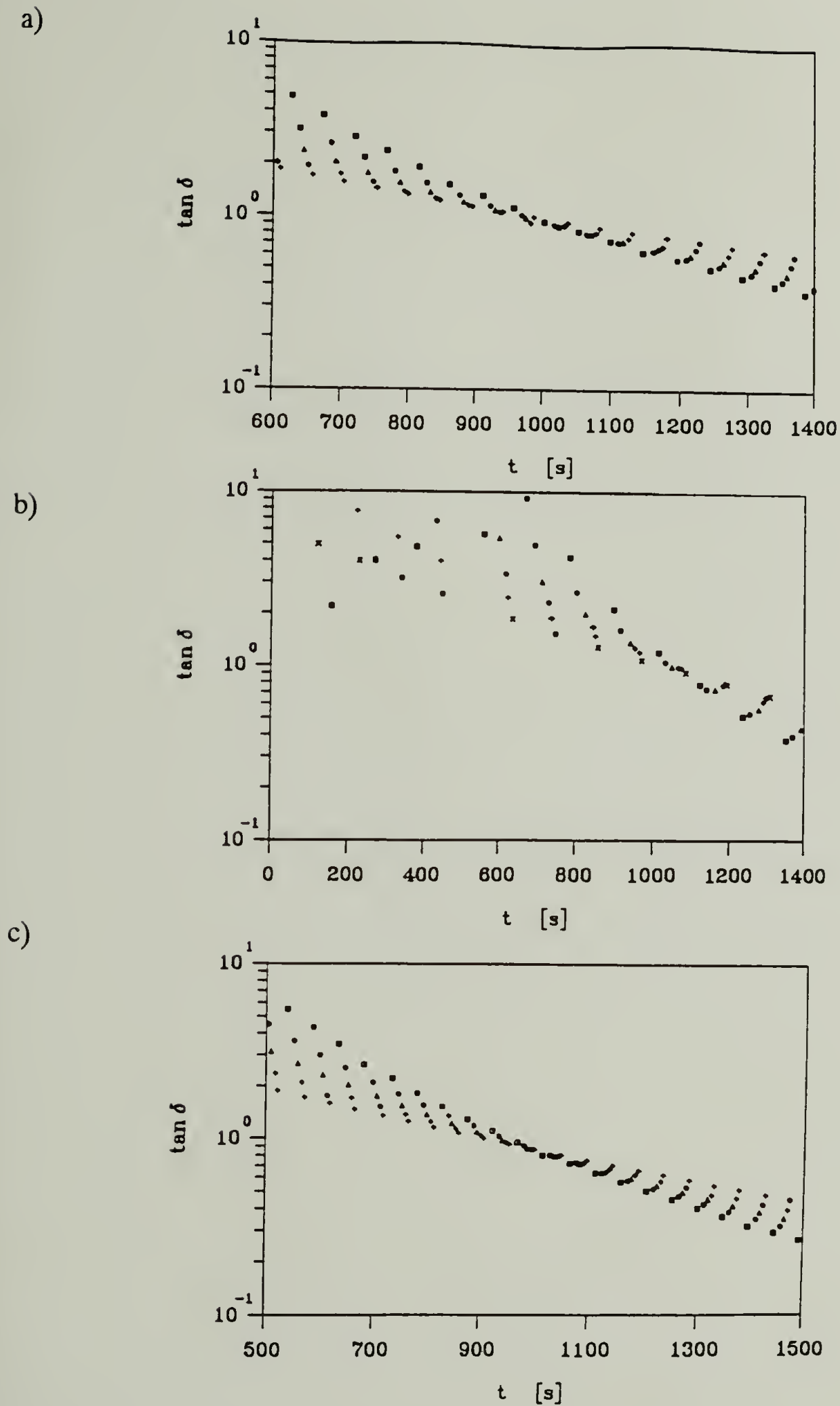


Figure 5.8 CFS data showing $\tan \delta$ versus reaction time in the vicinity of the gel point for samples (a) PBD18 (b) PBD20 (c) PBD38. All measurements were carried out at balanced stoichiometry with a temperature of 28°C .

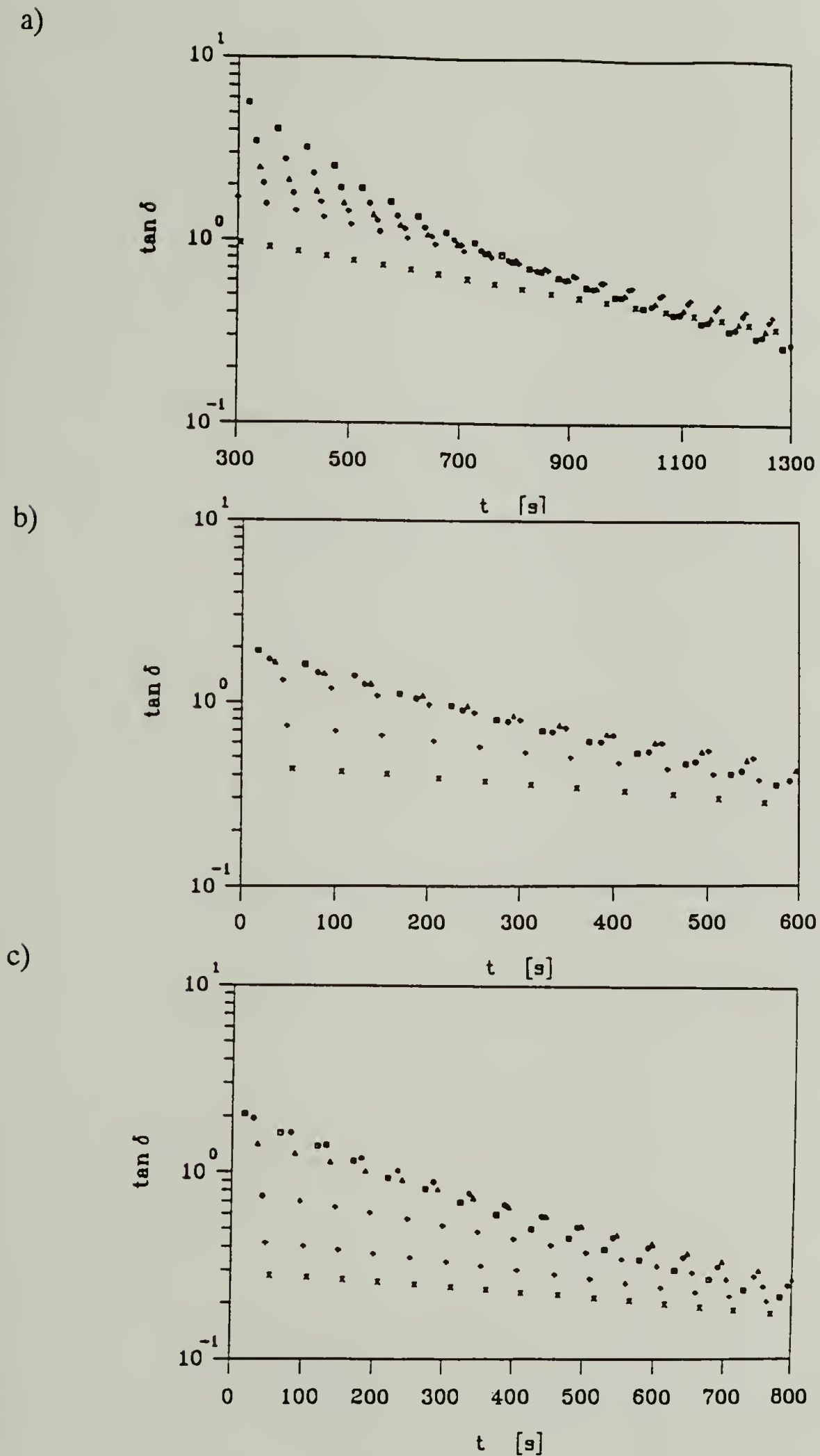


Figure 5.9 CFS data showing $\tan \delta$ versus reaction time in the vicinity of the gel point for samples (a) PBD44 (b) PBD70 (c) PBD97. All measurements were carried out at balanced stoichiometry with a temperature of 28°C .

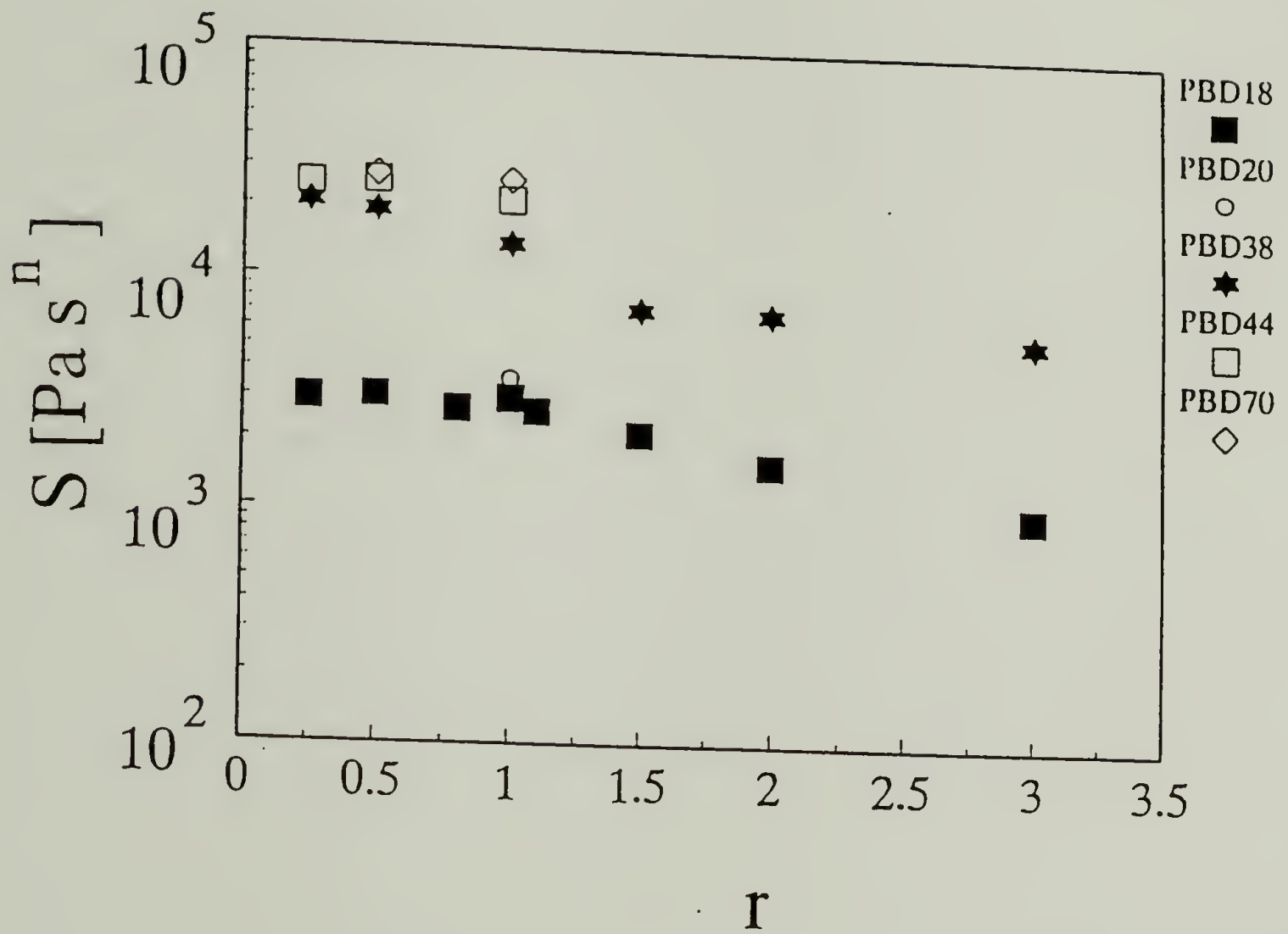


Figure 5.10 Critical gel strength (S) versus stoichiometric ratio (r) for samples PBD18 through PBD70. All measurement were made at 28°C .

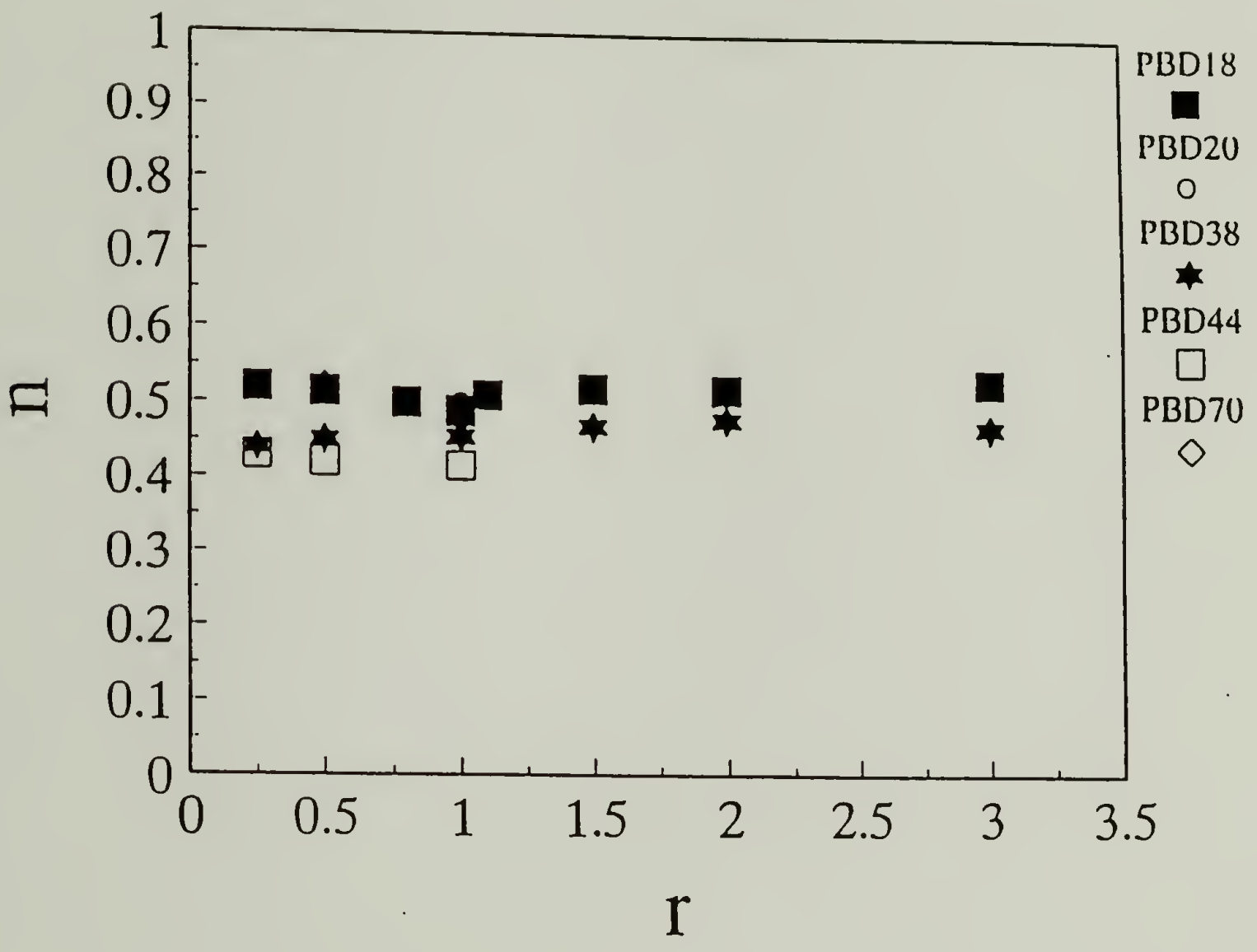


Figure 5.11 Critical relaxation exponent (n) versus stoichiometric ratio (r) for samples PBD18 through PBD70.

Table 5.1 Summary of critical gel strength, S , and critical relaxation exponent, n , for PBD gel samples for five precursor molecular weights at various stoichiometric ratios, r . All data was taken at 28°C.

Sample	r	S (Pa · s ^{n})	n
PBD18	0.25	3000	0.52
	0.5	3100	0.51
	0.8	2700	0.50
	1.0	3000	0.49
	1.1	2700	0.51
	1.5	2200	0.52
	2.0	1600	0.52
	3.0	980	0.53
PBD20	1.0	3700	0.50
PBD38	0.25	20900	0.44
	0.5	19400	0.45
	1.0	13700	0.45
	1.5	7500	0.47
	2.0	7300	0.48
	3.0	5700	0.47
PBD44	0.25	25300	0.43
	0.5	26200	0.42
	1.0	19900	0.42
PBD70	0.5	27800	0.52
	1.0	24800	0.49

5.5 Sources of Error

5.5.1 Mutation Number (N_{mu})

As mentioned earlier in section 3.2.2, there is error involved when taking measurements of the dynamic moduli as the material is evolving. This error is represented by the mutation number N_{mu} . N_{mu} for G' and G'' can be represented by

$$N_{\text{mu}}(G') = \frac{1}{G'} \frac{\partial G'}{\partial t} \Delta t \quad (5.1)$$

$$N_{\text{mu}}(G'') = \frac{1}{G''} \frac{\partial G''}{\partial t} \Delta t. \quad (5.2)$$

The values of $\frac{1}{G'} \frac{\partial G'}{\partial t}$ and $\frac{1}{G''} \frac{\partial G''}{\partial t}$ are calculated by Gelpro at t_c for the frequencies scanned. $\frac{1}{G'} \frac{\partial G'}{\partial t}$ is greater than $\frac{1}{G''} \frac{\partial G''}{\partial t}$ since G' increases at a higher rate during crosslinking than G'' does (see figure 5.1). Figure 5.12 shows an example of these values for sample PBD38 at balanced stoichiometry. Multiplying these values by Δt (time of measurement) gives the mutation number. Only the mutation number for G' at the lowest frequency is reported. This is where the largest error will occur. All values of N_{mu} will become lower at higher frequencies as seen in figure 5.12. At a frequency of 1 rad/s, Δt is equal to 13 s to 16 s. N_{mu} at 1 rad/s at 28°C ranged from $0.04 < N_{\text{mu}} < 0.13$ for the samples with the slowest to fastest rates of gelation respectively. The sample with the slowest rate of gelation was PBD18 at $r=0.25$ while the fastest rate of gelation was sample PBD38 at $r=3.0$.

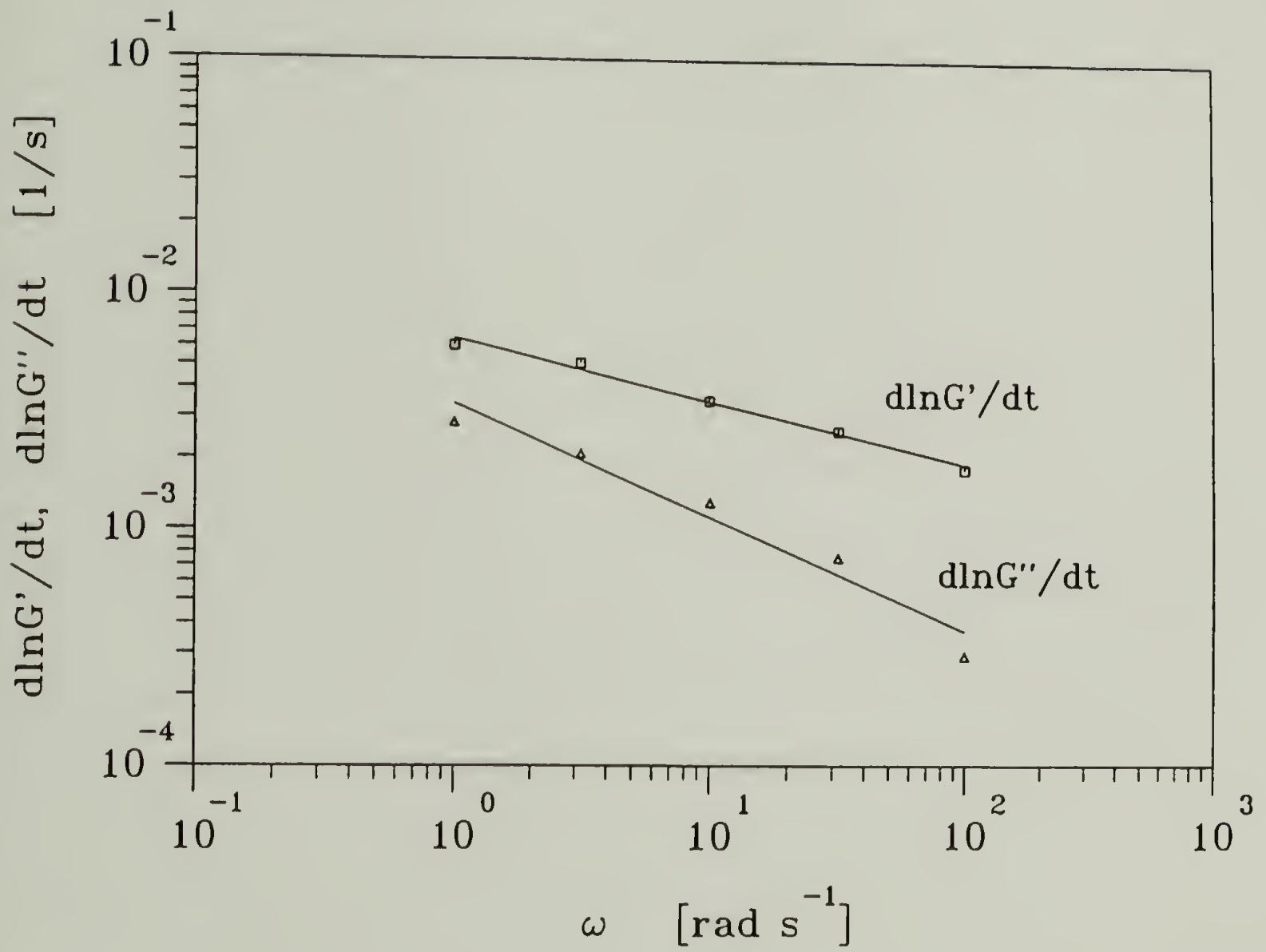


Figure 5.12 Rate of change the dynamic moduli at t_c versus frequency at 28°C for sample PBD38 at balanced stoichiometry.

5.5.2 Sample Homogeneity

Some experiments for the lowest molecular weight precursor, PBD18, gave CFS data where the lowest one or two frequencies did not cross with the other higher frequencies at all (figure 5.13). This gives evidence of inhomogeneous gelation where some sections of the material go through the liquid-solid transition before others. When these inhomogeneous samples were visually inspected, they were observed to be more solid in the center of the sample than at the outer edge. There appeared to be a ring of only slightly cured material, about 1mm thick, around the edge of the sample. This suggests that there was most likely a temperature gradient throughout the entire diameter of the plate, possibly due to poor air circulation around the sample plates. Such types of inhomogeneities were also observed by Scanlan (1990) when performing CFS measurements on curing PDMS samples.

Attempts were made to reduce the chances of inhomogeneity. Sample plates were preheated to the desired temperature needed for CFS measurement. The air flow pressure through the environmental chamber was made sufficiently high (≥ 35 psi). It was made sure that the plates were clean. The sample gap was kept small (~ 0.5 mm) to reduce possibility of temperature gradient through the sample thickness. However, even when these precautions were taken, some samples still showed signs of inhomogeneity. Curiously, samples did not show inhomogeneity when the oven was not used, i.e. when the samples were cured at ambient conditions. Once again, this may indicate that at times there is poor air circulation in the environmental chamber.

Sample inhomogeneity posed quite a frustrating experimental problem of which the cause was never exactly discovered. Samples that were found to be inhomogeneous were not accepted for critical gel analysis and the experiment was repeated.

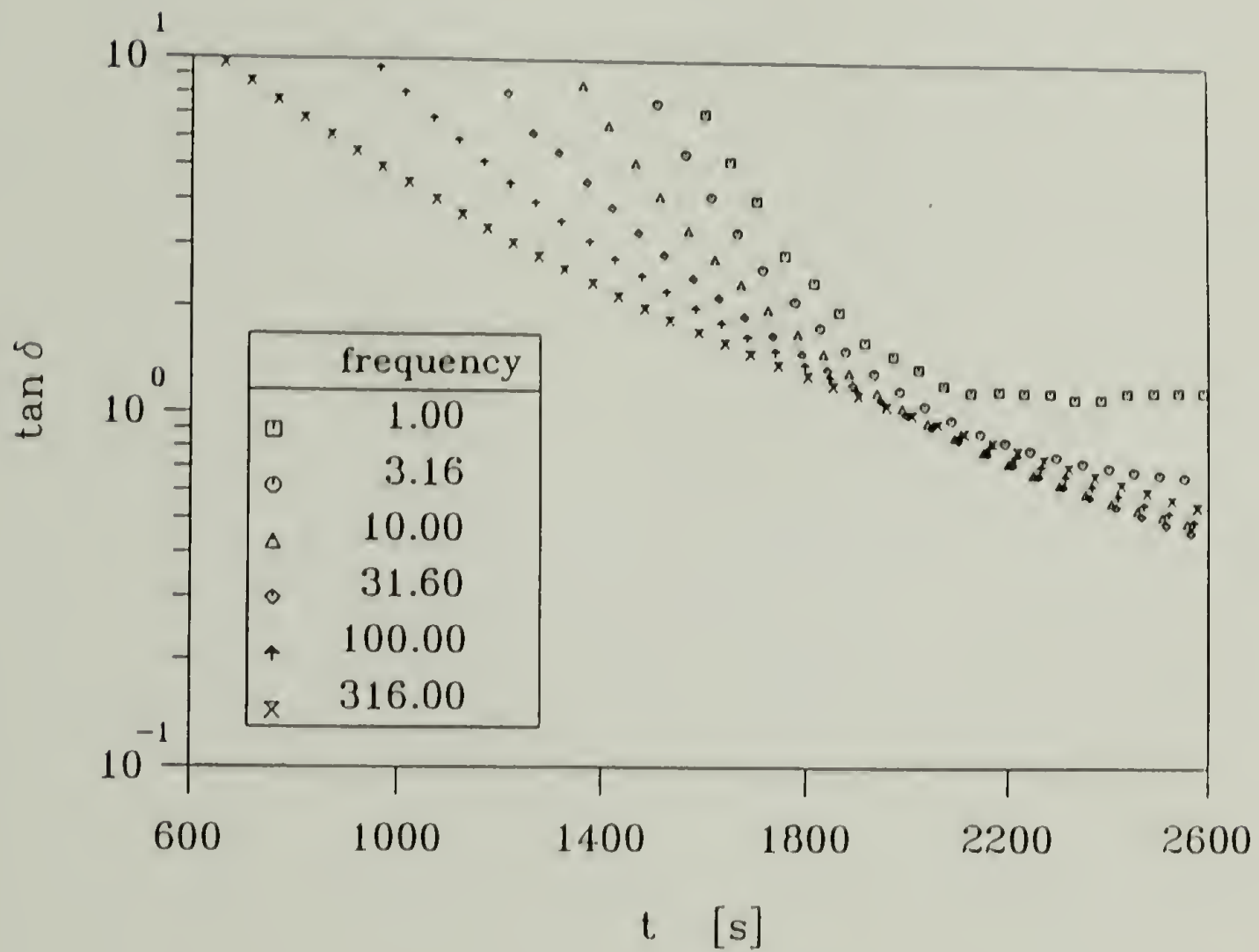


Figure 5.13 CFS data illustrating an example of the inhomogeneous cure of PBD18, $r=1$, at 28°C . The lowest two frequencies do not intersect with the other frequencies.

5.6 Discussion

5.6.1 Effect of Physical Entanglements on Gel Point Detection

Figures 5.8 and 5.9 show that as the molecular weight of the precursor increases from PBD18 to PBD97, the detection of the gel point by CFS becomes increasingly difficult. It appears that the gel point is not reached due to the failure of the $\tan \delta$ curves to intersect at a single time. The effect first becomes obvious for PBD44 and is most pronounced for PBD97. For PBD97, the lowest three frequencies intersect near 250 s but the three highest frequencies do not.

Figures 5.14 and 5.15 show interpolated dynamic data at three times in the vicinity of where the lowest three frequencies intersect for PBD97. As seen in figure 5.14, $\tan \delta$ is not independent of frequency at the proposed $t_c = 250$ s. It appears that the gel point has not been reached or that the sample is inhomogeneous. However, when the dynamic moduli are examined in figure 5.15, it is seen that the three highest frequencies appear to be probing the entanglement regime. This is evidenced by the appearance of the onset of the plateau modulus in G' . The dynamic data in the entanglement region show hardly any change during gelation. The three lowest frequencies probe the terminal zone and therefore display the same evolution of G' , G'' to power law at the gel point as was observed for the lower molecular weight precursors.

For gel point detection by CFS, each polymer seems to have an upper frequency limit depending on the molecular weight of the precursor denoted by $\omega_0 \sim 1/\lambda_0$ as discussed in chapter 1 (Scanlan and Winter, 1991). ω_0 occurs approximately at the G' , G'' crossover point in the terminal zone for the unreacted precursor which is approximately 30 rad/s for PBD97. As the length of the entanglement plateau increases with precursor molecular weight, the terminal zone is pushed toward lower frequencies thus moving ω_0 to lower values. At relatively low precursor molecular weight, the terminal zone is well within the CFS frequency window since ω_0 is higher than the highest frequency scanned by CFS and power law is easily observed at the gel point. As the precursor molecular

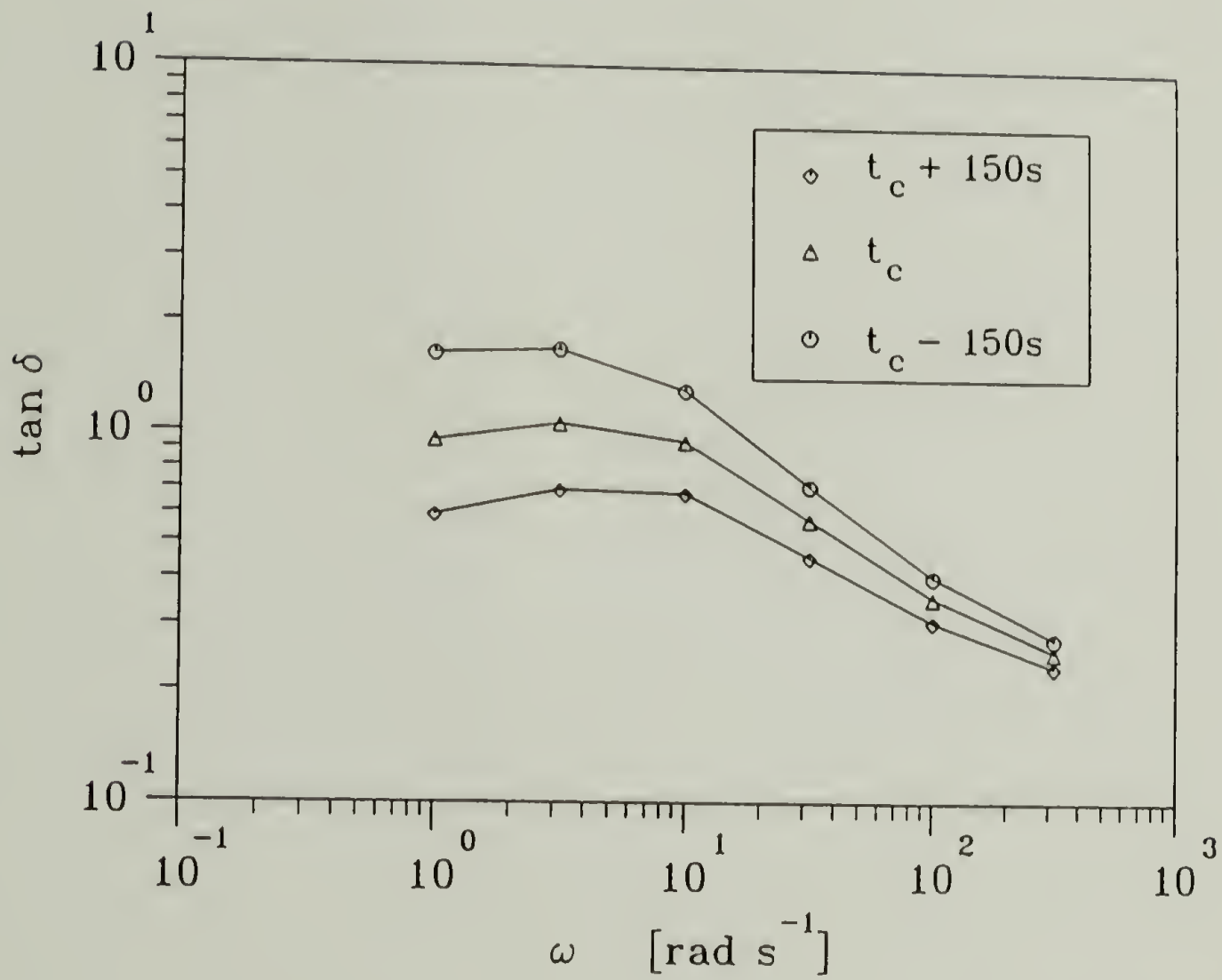


Figure 5.14 Interpolated $\tan \delta$ data points at three times in the vicinity of t_c for the gelation of PBD97 at $r=1$ and 28°C . Solid lines connect the interpolated data points and are not fits to the data.

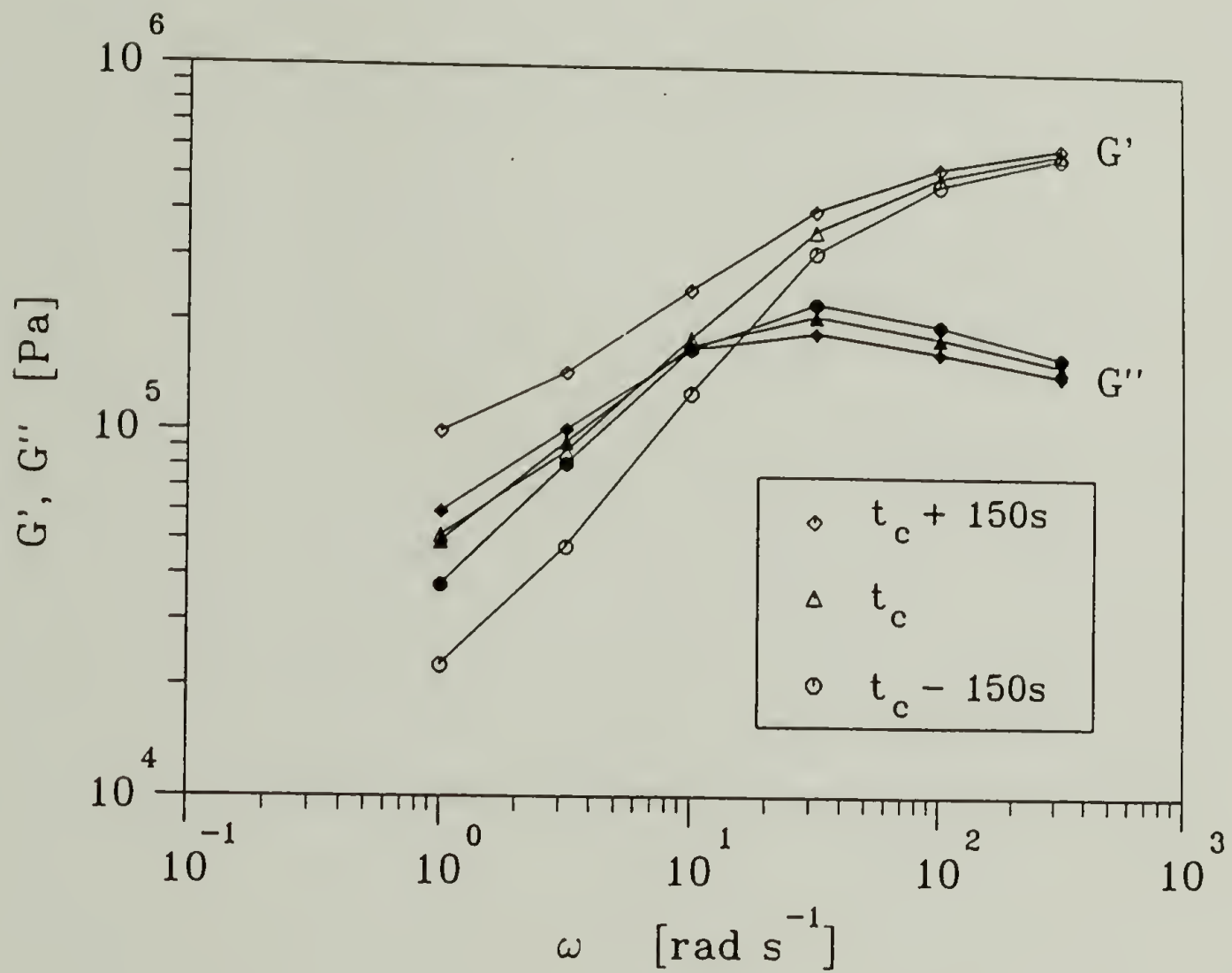


Figure 5.15 Interpolated dynamic moduli for the same conditions as in figure 5.14. Solid lines connect the interpolated data points and are not fits to the data.

weight increases the value of ω_0 begins to fall within the CFS window. Ultimately, at very high precursor molecular weight, the terminal zone occurs at such low frequencies that it is below the observable CFS frequency window.

Figure 5.16 shows the CFS frequency window in relation to the dynamic moduli of the precursor materials. The terminal zones of PBD18 and PBD44 are within the CFS window. However, only half the terminal zone of PBD97 is captured by the CFS window. If PBD201 were analyzed, all $\tan \delta$ curves would have values <1 and would never intersect because the entire terminal zone is outside the CFS window.

From a materials point of view, the upper frequency limit is fixed, however there is no lower frequency limit. The lower limit is determined by the limitations of the rheometer motor, sensitivity of the transducer at low frequencies, and the kinetics of the reaction. Probing frequencies higher than ω_0 using CFS will decrease the effectiveness of detecting the gel point.

In summary, from the results of the CFS data it is clear that the typical power law relaxation pattern for precursors with entanglements exists at low frequencies. Therefore, in order to observe the onset of gelation by dynamic means one must choose a frequency window that is within the terminal zone of the precursor. In analyzing this region, it is evident that the evolution of the relaxation pattern becomes similar to those of other systems using precursors of low molecular weight (i.e. $M_w < M_c$) (Chambon and Winter, 1985, 1986, 1987; Scanlan and Winter, 1991; Holly et al., 1988, Muller et al., 1991, Adolf and Martin, 1990; Izuka et al., 1991; Lairez et al., 1992). With low molecular weight precursors, detection of the gel point is relatively easy because the terminal zone was readily accessible and no entanglement effect could interfere

The gel transition can be measured for highly entangled polymers by rheological means. However, an exceedingly high initial molecular weight before crosslinking requires experimental frequencies which are so low that the time for taking a single rheological data point would exceed the gel time (i.e. $N_{mu} \gg 1$). Here the limiting precursor

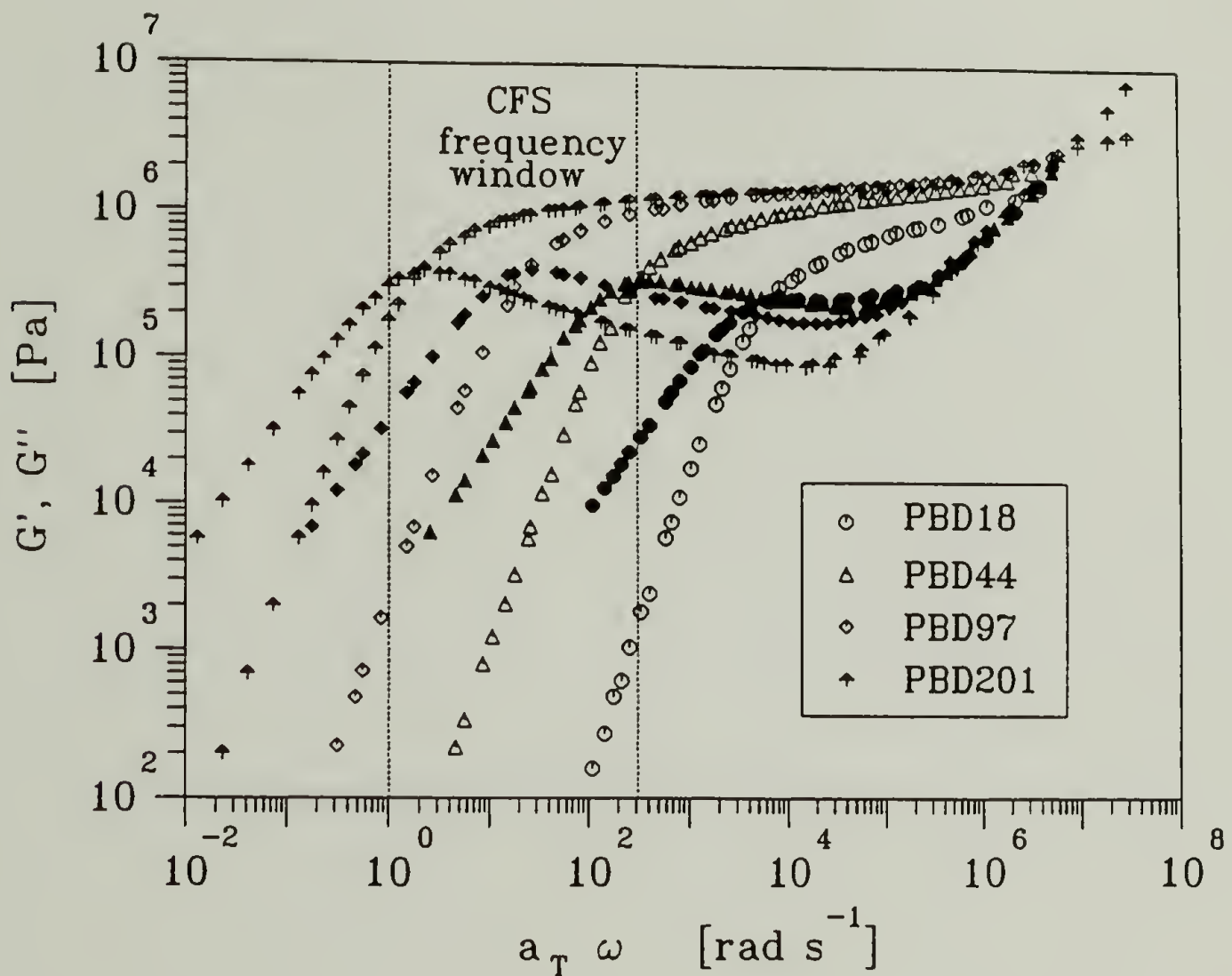


Figure 5.16 Master curves of bulk PBD18, PBD44, PBD97, and PBD201 precursors at $T_{\text{ref}} = 28^{\circ}\text{C}$. The dotted lines give the upper and lower values of the frequency window scanned with the CFS technique. As the precursor molecular weight increases, more of the entangle region enters into the CFS window thus making gel point detection more difficult.

molecular weight is approximately 70,000 to 80,000 g/mole. Attempts can be made to push the frequency window to lower values. However, this requires slowing the reaction down by decreasing the temperature or using less catalyst or crosslinking agent, etc.

5.6.2 Effect of Stoichiometry on the Gel Strength

The effect of stoichiometry on the critical gel properties has been reported for several endlinking systems. In each case the stoichiometric ratio had a significant effect on the critical gel strength, S , and the relaxation exponent, n . Winter et al. (1988) reported for an endlinking polypropylene oxide that the gel strength was sensitive to small variations in r . They reported that for $0.5 < r < 2.0$, S increased approximately by 1.5 decades from 500 to 20,000 Pa sⁿ. For an endlinking PDMS system, Scanlan and Winter (1991) observed that S varied by about 1 decade from 8000 to 50,000 Pa sⁿ for a higher molecular weight precursor above M_c for $0.5 < r < 3.0$. S appeared to be sensitive to a crosslinker deficiency (i.e. $r < 1$) and insensitive to an excess of crosslinker. Izuka et al. (1992) found that for an endlinking polycaprolactone that S ranged from 100 to 19,000 Pa sⁿ for $0.61 < r < 1.76$.

In this study it was found that the gel strength is relatively insensitive to stoichiometric ratio. In figure 5.10, S is shown, for PBD18, to decrease with increasing crosslinker content from 3200 to 980 Pa sⁿ over the range of $0.25 < r < 3.0$. For PBD38, S decreased with increasing crosslinker content from 21,000 to 6000 Pa sⁿ over the same stoichiometric range. This type of effect of stoichiometry on S for vulcanized polybutadiene is quite different from that observed for studies using endlinking systems where large changes in S were observed for relatively small changes in stoichiometry.

The relative insensitivity of gel strength to stoichiometric ratio may be due to a diluent effect caused by the crosslinker. Scanlan and Winter (1991) studied S as a function of the concentration of inert medium-length and high-length PDMS diluents

mixed into crosslinking PDMS. Their results show that S decreases by less than one decade up to approximately 30 to 40% diluent at constant r .

Since the results of this study show the same qualitative trend as those found for diluted PDMS, it is proposed that the same type of dilution effect may be experienced here. The source of diluent in this system comes from the unreacted crosslinker at the gel point. By using calculations of classical gelation theory of Flory(1941, 1953) and Stockmayer (1943) it was found that there is a significant amount of unreacted crosslinker in the material at the gel point due to the high functionality of the polybutadiene precursor molecules. Initially, 12% and 28% by weight of crosslinker must be added to achieve conditions of $r=1.0$ and 3.0 respectively. At the gel point, at $r=1$, it is calculated that 21% of the silane has been converted, and for $r=3.0$ at the gel point, only 12% of the silane is converted. Therefore, most of the crosslinker is still unreacted at the gel point acting as a diluent.

5.6.3 Effect of Stoichiometry on the Critical Relaxation Exponent

Studies with endlinking systems have shown that the relaxation exponent, n , is sensitive to stoichiometry. Various values of n have been reported for a range of stoichiometric ratios for several systems. The results are summarized in table 5.2.

Quite surprisingly, the results of this study have revealed that the value of n was independent of stoichiometric ratio for all precursor molecular weights examined. For five precursor molecular weights, samples PBD18 through PBD70 crosslinked with stoichiometric ratios of $0.25 < r < 3.0$, the relaxation exponent was found to be in the narrow range of $0.41 < n < 0.52$. The values of n found are close to 0.5 as has been observed by other authors.

The same insensitivity of n to r has also been observed in Scanlan's diluent studies of critical gels (Scanlan and Winter, 1991). They found that n is insensitive to the concentration of diluent of medium and long length chains up to some weight percent of

Table 5.2. Reported results found for the critical exponent, n , for different systems over a wide range of stoichiometric ratios. $r < 1$ denotes a crosslinker deficiency.

Reference	System	r	n
Chambon et al. (1986)	Polypropylene oxide/ isocyanate	1	1/2
Winter et al. (1988)	Polpropylene oxide/ isocyanate	$r < 1$ $r \geq 1$	$1/2 < n < 2/3$ 0.5
Adolf and Martin (1990)	Polydimethylsiloxane	0.45 0.52 0.80	0.65 0.56 0.51
Scanlan and Winter (1991)	Polydimethylsiloxane	$r < 1$ $r \geq 1$	$0.5 < n < 0.7$ 0.5
Izuka et al. (1992)	Polycaprolactone/ isocyanate	$0.61 < r < 1.76$	$0.3 < n < 0.67$
Muller et al. (1992)	Polyethylene oxide/ isocyanate	$r < 1$ $r \geq 1$	2/3 1/2
Lairez et al. (1992)	Epoxy/amine	1	0.64

diluent. For a medium length chain diluent, n remained close to 0.45 up to 30% diluent. For a long length chain diluent, n remained close to 0.35 up to 50% diluent. At higher concentrations of diluent, n was observed to increase approaching a value of 1 as the diluent approached 100% concentration.

This dilution effect could possibly be eliminated by using some other type of crosslinking mechanism such as peroxide or u.v. curing agent. For these systems, only a small amount of crosslinking agent would need to be introduced to crosslink the sample and the diluent effect could be removed. However, the control over stoichiometry would be lost.

5.6.4 Effect of Stoichiometric Window on Critical Gel Properties

As just discussed, one possible explanation for the insensitivity of the critical gel strength and exponent with stoichiometric ratio could be due to a diluent effect of the crosslinker. However, another possible explanation for this observation is based on the limited stoichiometric window for gelation.

According to branching theory, Flory (1941, 1953) defines an upper and lower bound for the stoichiometric ratio in which the gel point can be successfully reached. The lower bound is

$$r_l = \frac{1}{(f-1)(g-1)} \quad (5.3)$$

where f is the functionality of the polybutadiene and g is the functionality of the crosslinker. The upper bound is defined as

$$r_u = \frac{1}{r_l} \quad (5.4)$$

If crosslinking is attempted outside these critical values of r , the infinite cluster will never be reached. When $r < r_l$, too little crosslinker is used and the largest cluster will never be able to reach infinite size. When $r > r_u$, then the crosslinker will ultimately endcap all of the precursor reactive sites and the largest cluster will never be able to reach infinite size.

For low functionality endlinking systems, the entire range of stoichiometric ratios could be examined. For example, for gelation to be successful for a system where $f=2$ and $g=4$, (Chambon and Winter, 1985) the stoichiometry must be within the range $0.33 < r < 3.0$. For high functionality systems, this range is widened dramatically. Though it appears that a wide range of stoichiometric ratios was used for this study, it was not possible to examine the entire range of stoichiometric ratios described above for successfully reaching the gel point. Due to the high functionality of the precursor molecules, the stoichiometric window is $0.043 < r < 22.8$ for PBD18 and from $0.007 < r < 133$ for PBD97. The values of r explored in this study, from $0.25 < r < 3$, are only a fraction of this large range and could be a reason why the critical exponent and the gel strength were close to being independent of r . Here, it would be almost impossible to successfully measure samples with stoichiometries much greater than 4 because the crosslinker concentration would be so high that the viscosity of the mixture would be too low to measure experimentally.

CHAPTER 6

EVOLUTION OF MECHANICAL PROPERTIES DURING GELATION

A combination of CFS measurements and rheometry on stopped samples is needed to obtain the characteristic critical gel parameters t_c , S , and n . CFS accesses only 2 to 2.5 decades of frequency and does not provide insight to the relaxation behavior of critical gels on time scales outside of this narrow window. Stopping of the crosslinking reaction at intermediate states of conversion has the advantage over CFS in that the experimental frequency window can be extended through time-temperature superposition. This makes it possible to examine changes which take place in the terminal, entanglement, and onset to glass transition relaxation zones as chemical crosslinks are added. Ultimately, with such measurements it will be possible to propose a form of the relaxation time spectrum over these three viscoelastic regions for critical gels with entanglements.

Results from CFS measurements have shown that the stoichiometric ratio has little effect on both the relaxation exponent and the gel strength. Therefore, it was not necessary to examine the rheological behavior of stopped critical gels over a range of stoichiometric ratios. It was sufficient to measure the relaxation behavior of stopped samples with balanced stoichiometry ($r=1$).

6.1 Experimental Procedure

6.1.1 Rheological Measurements

Samples were prepared as described in section 2.5. Reacting mixtures were put into a 25mm removable disk mold. The mold is comprised of a disk and an aluminum ring which was machined to fit tightly around the outside of the disk (see figure 6.1). A rubber O-ring (Parker Seal Co.) was used to seal the gap between the and outside of the

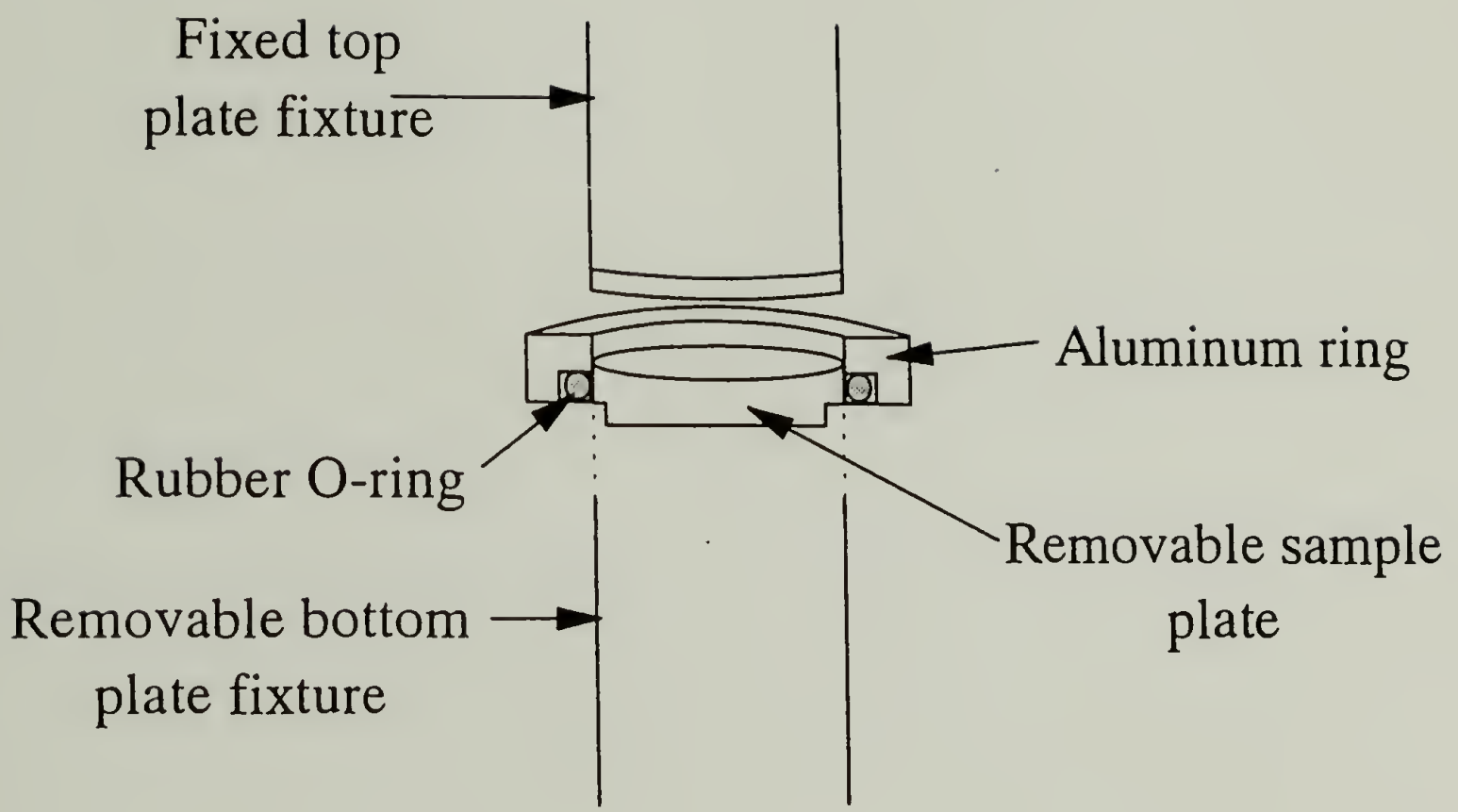


Figure 6.1 Schematic of the removable sample mold used for stopped samples.

disk. The ring could be moved up and down in order to adjust the desired mold depth setting with the aid of a depth micrometer (Starrett Co.). Mold settings for a sample thickness of 0.6 mm was used.

It was important to use rubber O-rings cured by peroxide and not by sulfur. As mentioned in chapter 2, trace amounts of sulfur can poison the hydrosilation reaction and cause inhomogeneous curing of the sample in areas in contact with the rubber O-ring. The poisoning of hydrosilation curing reactions in contact with sulfur-containing rubber products has been reported (Valles and Macosko, 1979).

Before the reacting sample was placed into the mold, the removable disk alone was fastened to the fixture and loaded into the rheometer so that the initial zero gap could be set with the top plate at the reference temperature of 28°C. A fixed 25mm diameter disk was used for the top plate.

The reacting sample was put into the mold and allowed to cure at ambient temperature. To test the progress of the reaction, the sample was probed every few minutes by touching a portion of it with the tip of a microspatula. Near the gel point, the material appeared viscous with a "stringy" consistency by visual inspection. At this point, the hydrosilation reaction was stopped by spraying the TMEDA poison solution described in section 2.4 on the surface of the sample. This technique, although it seems quite unsophisticated, worked well to obtain samples near the gel point. A similar technique to test the progress of gelation has been used by others (Chambon and Winter, 1985; Gonzalez-Romero and Macosko, 1985).

After applying the poison solution, the effectiveness of stopping the reaction was tested by measuring the dynamic moduli from 1 to 316 rad/s as a function of time for one hour. The time sweep data in figure 6.2 shows that the crosslinking reaction has been stopped. This is concluded from the fact that the dynamic moduli remain constant over the time measured.

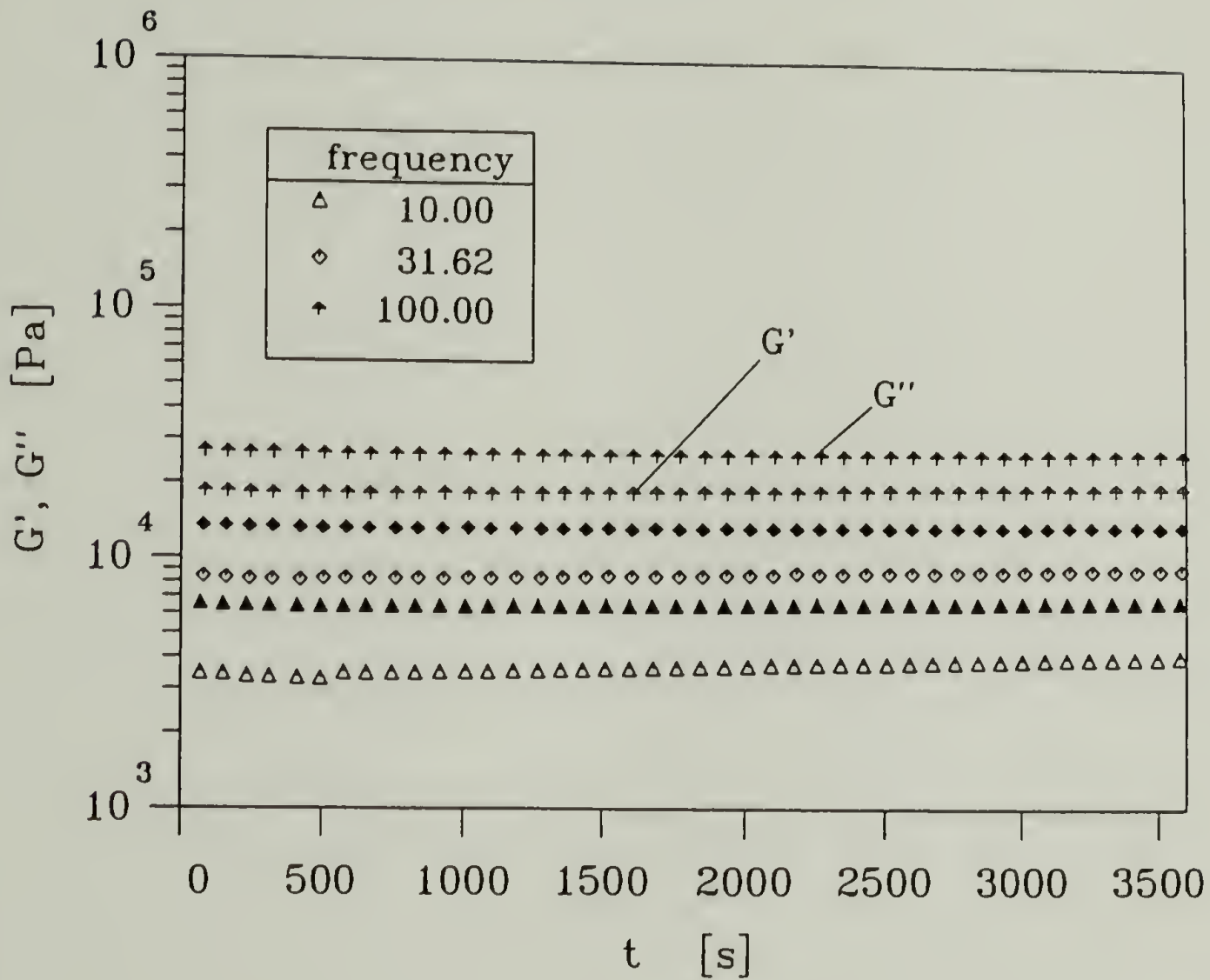


Figure 6.2 CFS data showing G' , G'' of PBD18 at 28°C as a function of time for three frequencies after spraying on poisoning solution to stop the reaction.

The small amount of solvent introduced by the poison solution was not enough to shift the dynamic data any significant amount by the dilution effect. Figure 6.3 shows a master curve of sample PBD38 plus $r=1$ amount of crosslinker and PBD38 with $r=1$ amount of crosslinker sprayed with poison solution. The stopped samples were not vacuum stripped because large air bubbles were found to be produced under vacuum. High temperature could not be used to evaporate any residual solvent because it was observed that the reaction was reinitiated, although to a slow rate of gelation, at temperatures at $T = 50^{\circ}\text{C}$.

Five minutes after poisoning, the stopped samples were loaded into the RDS7700 for measurements at frequencies from 1 to 500 rad/s and temperatures from 28°C to -75°C in an air atmosphere. The initial sample thickness was slightly less than 0.6mm due to the fact that the sample became squeezed when the top plate was brought down. For every decrease in temperature by 10K, the programmed gap setting was increased by 0.01mm to account for thermal expansion of the rheometer fixtures. All data were shifted into master curves by time-temperature superposing using the standard IRIS software.

6.1.2 Spectroscopic Measurements

F.T. Raman spectroscopy measurements were made with a Bruker instrument model IFS-88 with F.T. Raman module FRA 106 attachment. The laser source used was a CVI Nd:YAG laser with a wavelength of $1.06\ \mu\text{m}$. All data were analyzed with Labcalc (Galactic Industries Corp.) software. The scattered data was collected at 180° to the sample.

Four samples of mixtures of PBD18 and crosslinker with ratios of $r=0.25, 0.5, 0.75,$ and 1.0 were analyzed by F.T. Raman to show the linear dependence of the intensity of the silane peak with silane concentration. All four samples were placed into glass screw capped vials and placed into the beam for measurement without any further sample preparation. Each sample was measured with 200 scans at 4cm^{-1} resolution at a laser

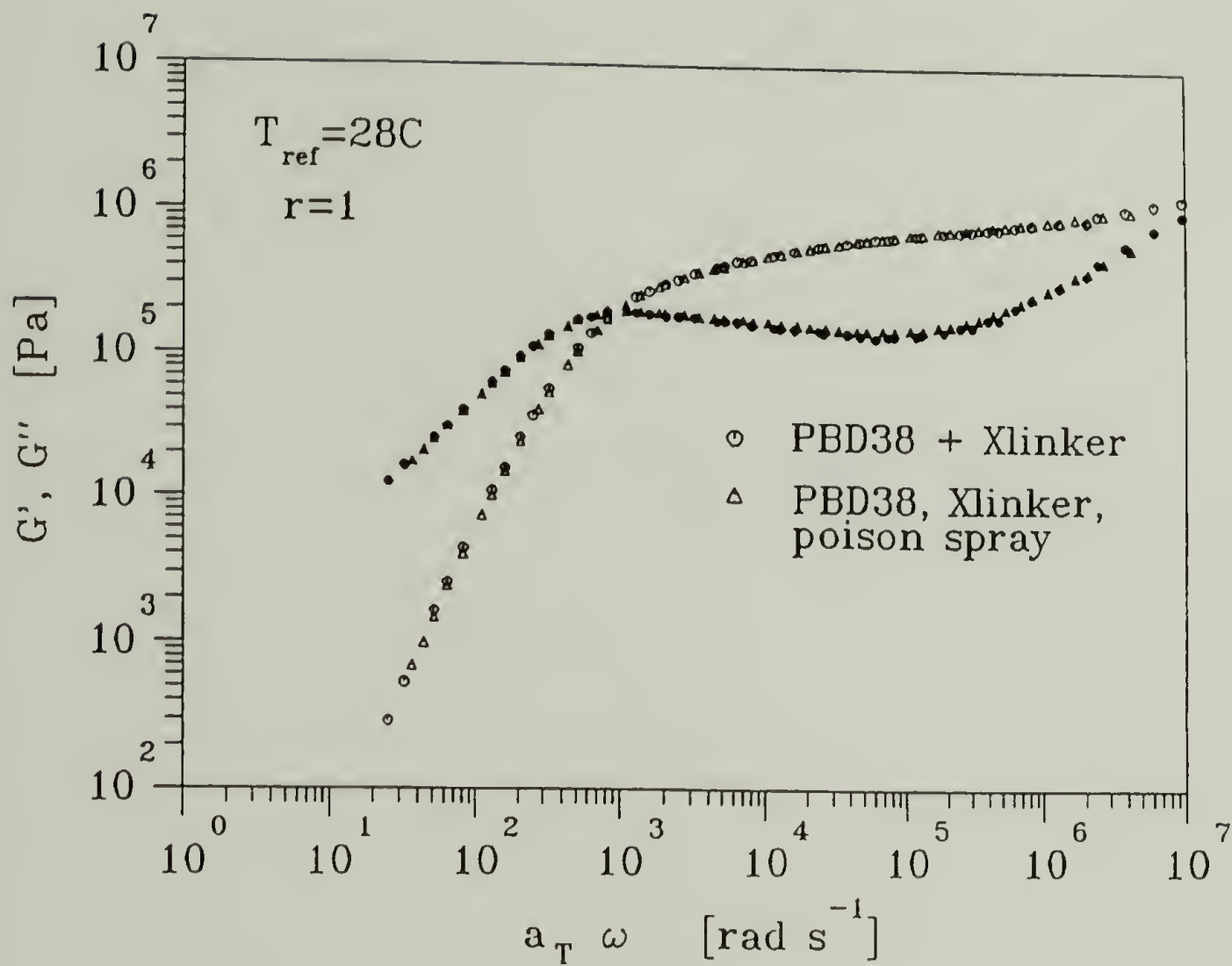


Figure 6.3 Dynamic data master curves of sample PBD38 mixed with stoichiometric amount of crosslinker. One of the samples has been sprayed with poison solution (<2wt%). Open symbols represent G' and filled symbols represent G'' . $T_{\text{ref}} = 28^\circ\text{C}$.

power of 200 milliwatts. The peak heights of silane at 2120cm^{-1} were normalized by the peak on occurring at 1437cm^{-1} . Figure 6.4 shows the linear dependence of the normalized peak height versus r .

The extent of reaction of three stopped samples at of PBD20 at $r=1$ were measured directly by F.T. Raman. Measurements were made by aiming the laser at ten locations on the sample which was in the stopped sample mold so that an average extent of reaction could be calculated. The removable plate surface was polished to mirror-like quality to get good reflection of the laser and improved quality of the scattered data. Sample mold had to be mounted vertically to expose the surface of the sample to the laser. The vertical geometry made it necessary to rotate the mold after every measurement to compensate for the minor amount of sample flow of the highly viscous material so that the sample would not flow out of the mold.

To determine the extent of reaction, a measurement of the initial mixture of crosslinker and PBD20 was first made. The initial ratio of the silane peak at 2120cm^{-1} was normalized with the peak at 1585cm^{-1} . The peak at 1585cm^{-1} was chosen as a normalization peak because it is due to the aromatic $\text{C}=\text{C}$ stretch of the crosslinker and represents a bond that does not take part in the crosslinking reaction. The extent of reaction was calculated by the equation

$$P_{\text{SiH}} = \frac{R_0 - R_t}{R_0} \quad (6.1)$$

where R_0 is the initial normalized peak height ratio and R_t is the normalized peak height ratio of SiH at some reaction time t . Figure 6.5 shows the F.T. Raman spectra of three stopped samples of PBD20.

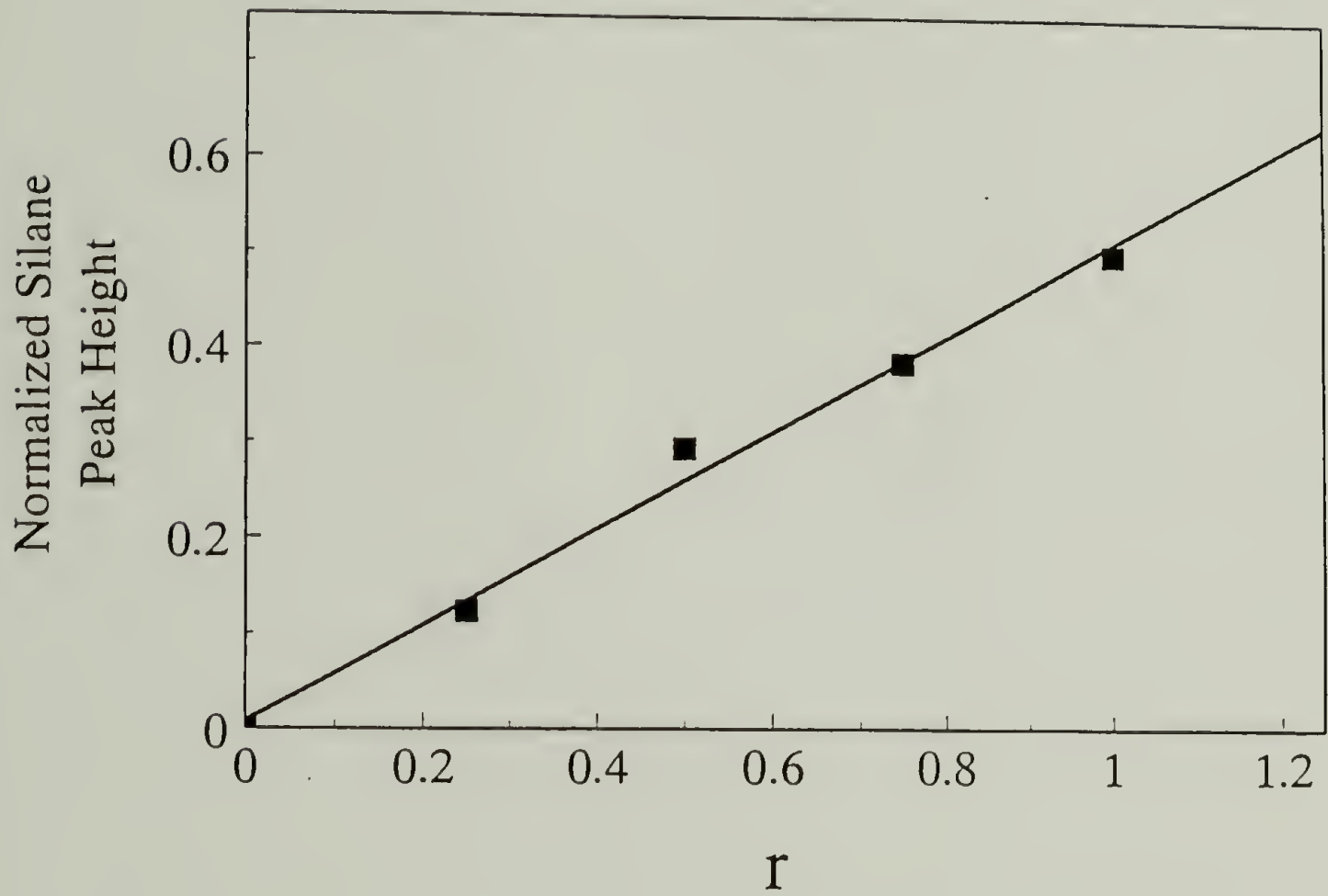


Figure 6.4 F.T. Raman calibration curve showing the linear dependence of the normalized silane peak intensity as function of stoichiometric ratio (r).

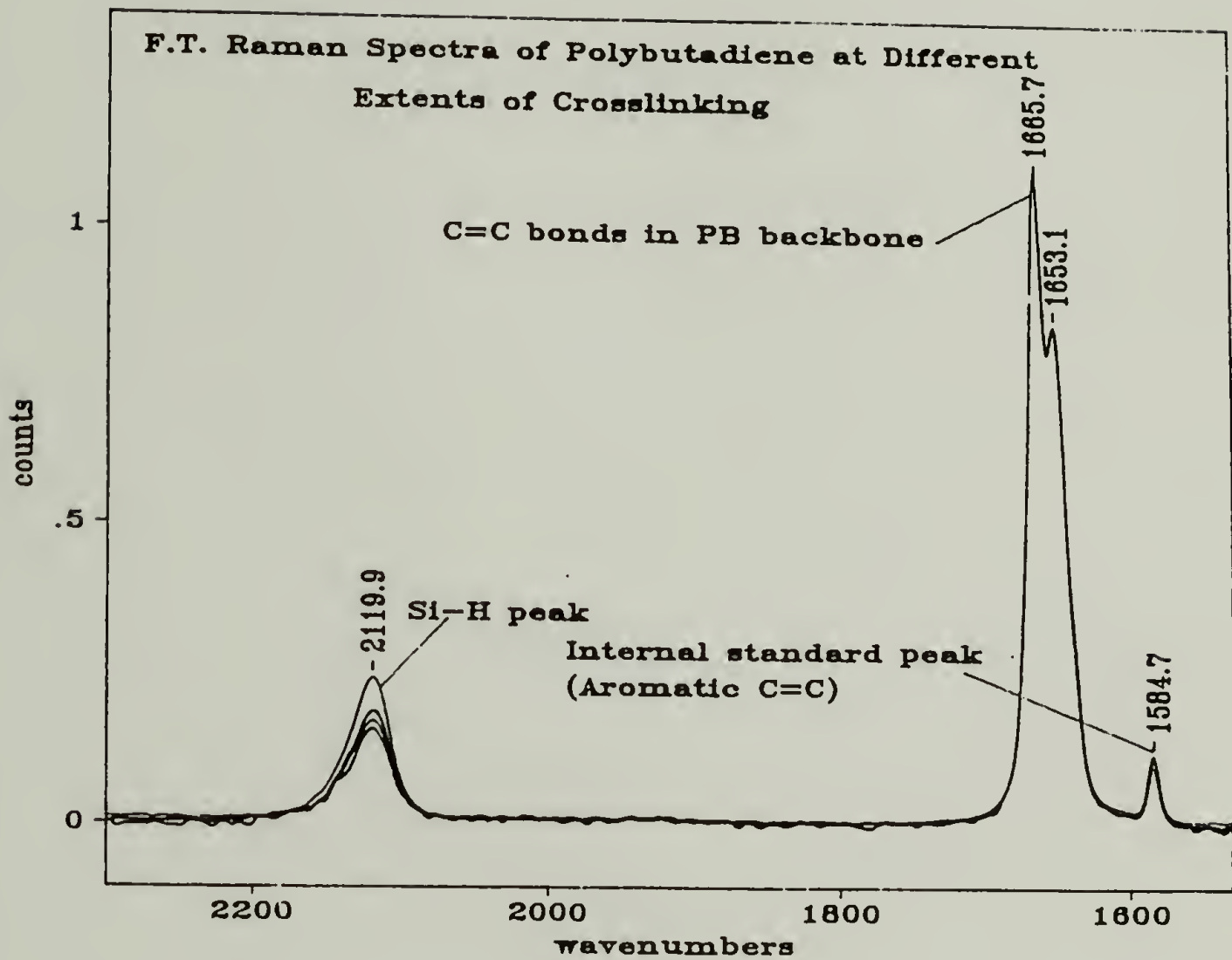


Figure 6.5 F.T. Raman spectra of three stopped PBD20 samples compared to the initial uncrosslinked material. Conversion of silane is seen by the decreasing peak intensity at 2120cm^{-1} .

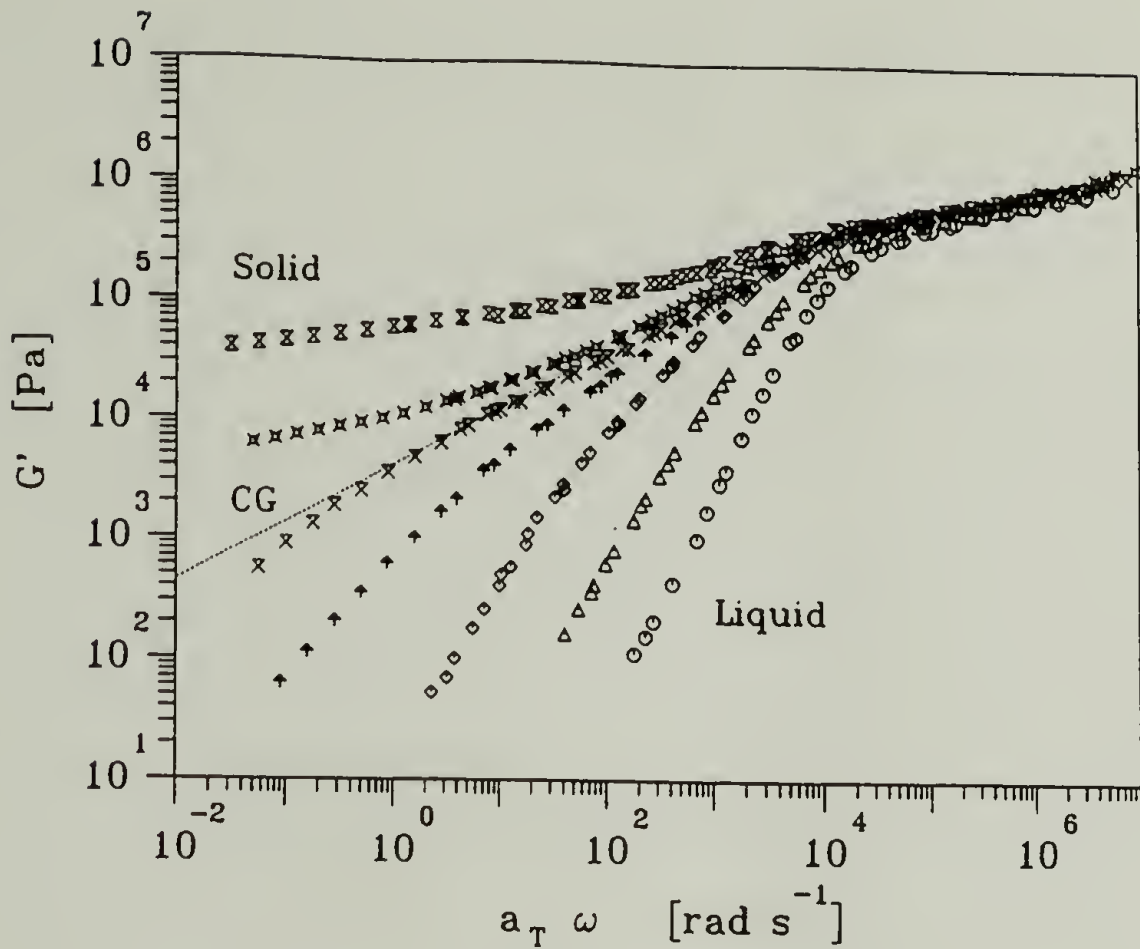
6.2 Rheological Results of Stopped Samples

G' and G'' master curves of PBD18 samples stopped at increasing extents of reaction are shown in figure 6.6. The initial uncured sample is a stoichiometric mixture of precursor and crosslinker. Figure 6.6a shows the evolution of the storage modulus (G') at increasing extents of reaction. By adding chemical crosslinks, the longest relaxation time increases and the relaxation behavior in the terminal zone changes dramatically. The slopes of G' and G'' decrease (from 2 and 1, respectively) and approach 0.5 near the gel point, see figure 6.6. Beyond the gel point, an equilibrium modulus (G_e) develops as an asymptote at low frequencies. The entanglement plateau and the onset to the glass transition are only slightly affected in shape by the addition of chemical crosslinks. Only at much higher crosslink density were the entanglement and glass transition region observed to change shape.

The plateau modulus of G' in the entanglement regime increases slightly with increasing extents of reaction. The data sets show a small but systematic increase. This phenomenon may be due to several factors. First, as the reaction proceeds, some of the crosslinker molecules attach to the PBD chains and reduce their plasticizing effectiveness. Therefore, the effective solvent concentration of the solution decreases and according to equation 4.14, the plateau modulus increases. Second, the plateau modulus may increase due to trapped entanglements. In fully cured samples, chemical crosslinks add to the physical entanglements which results in an equilibrium modulus which is higher than the plateau modulus of the uncrosslinked material (Aranguren and Macosko, 1988; Dossin and Graessley, 1979). Experimental problems give rise to additional uncertainty since stopped samples past the gel point become difficult to load into the rheometer and sometimes do not completely fill the entire gap between the plates. Incomplete filling of the gap would result in actually lowering the measured dynamic moduli.

Figure 6.6b shows the evolution of the loss modulus (G'') as the crosslink density increases. It is evident that the addition of chemical crosslinks has only very little effect on

a)



b)

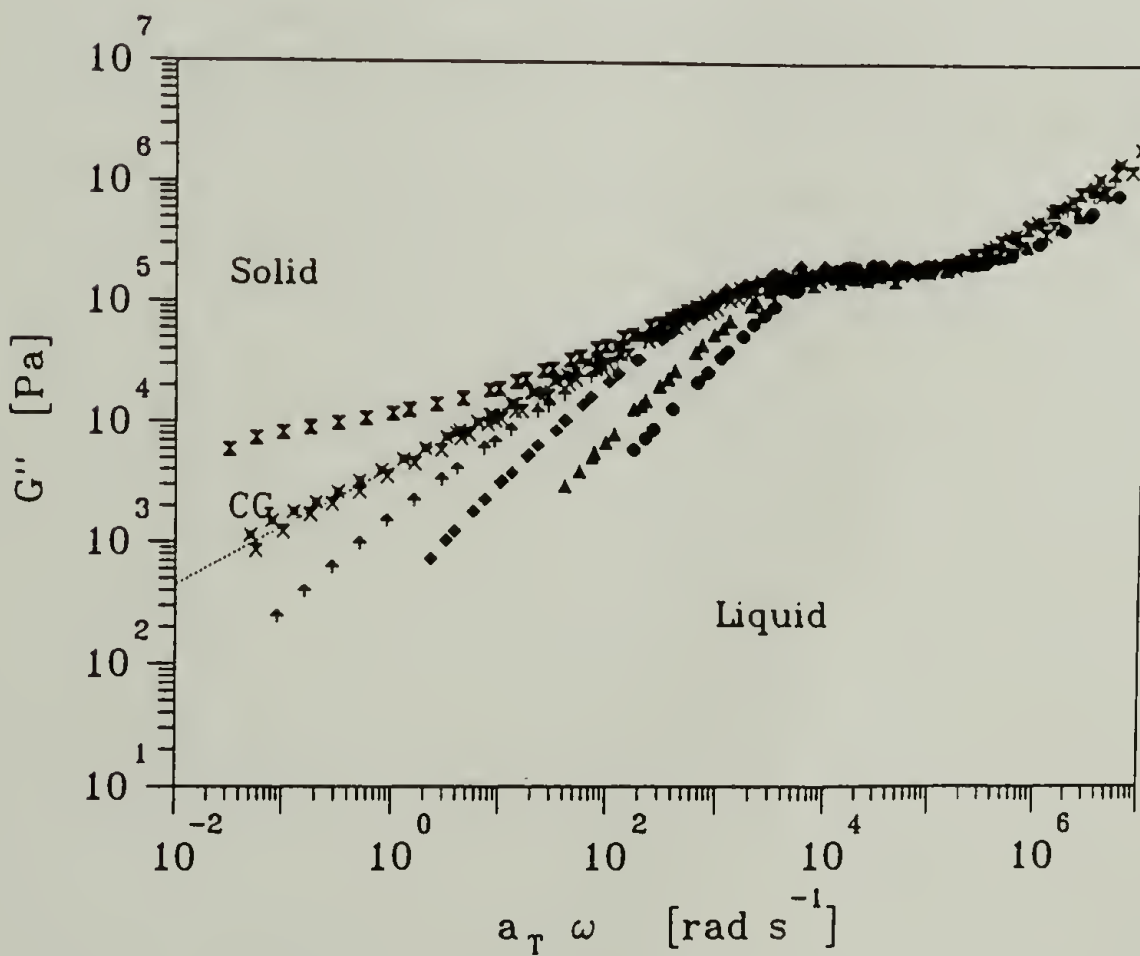


Figure 6.6 Evolution of master curves of (a) the storage modulus (G') and (b) the loss modulus (G'') of PBD18 stopped samples. The power law of the critical gel (CG) is given in the terminal zone. All samples are at balanced stoichiometry. $T_{ref} = 28^{\circ}\text{C}$.

the onset of the glass transition region. However, crosslinking has the effect of lowering the slope of G'' in the entanglement region at intermediate frequencies.

The shift factors of each of the stopped PBD18 samples were found to obey WLF behavior (figure 6.7). All of the samples were found to have very nearly the same shift factors. At the gel point, it became difficult to shift the data near the reference temperature since $\tan \delta$ is independent of frequency in the terminal zone. Therefore, for samples near the gel point, the data taken at temperatures just below the reference temperature were assigned the same shift factors as stopped samples well before the gel point. Once the terminal zone part of the master curve was constructed, the remaining data at lower temperatures that probed the entanglement zone could be easily shifted to complete the master curve.

Figure 6.8 shows the evolution of $\tan \delta$ for the data shown of figure 6.6. Near the gel point $\tan \delta$ at low frequencies become independent of frequency and adopts a value close to 1. The same data can be expressed as the normalized phase angle $\left(\frac{2\delta}{\pi}\right)$, see figure 6.9. At the gel point, $\left(\frac{2\delta}{\pi}\right)$ is equal to the critical exponent n as described by equation 1.7. For the stopped sample near the gel point, a power law region for nearly 3 decades (~ 1 to 1000 rad/s) gives a value of $n = 0.46$ which is close to 0.5.

Figure 6.10 shows the evolution of the relaxation time spectrum, $H(\lambda)$, during crosslinking for PBD18 at increasing extents of reaction calculated with standard IRIS software as discussed in chapter 3. The spectrum develops modes of relaxation at times longer than $\lambda_{\max,d}$ of the uncrosslinked precursor as the extent of reaction increases. This trend continues up to the gel point where at the true gel point the longest relaxation time of the system, λ_{\max} , will approach ∞ .

Critical gels were prepared with stoichiometric amounts of crosslinker for samples PBD18 through PBD97. For comparison, figure 6.11 shows both the dynamic data of a

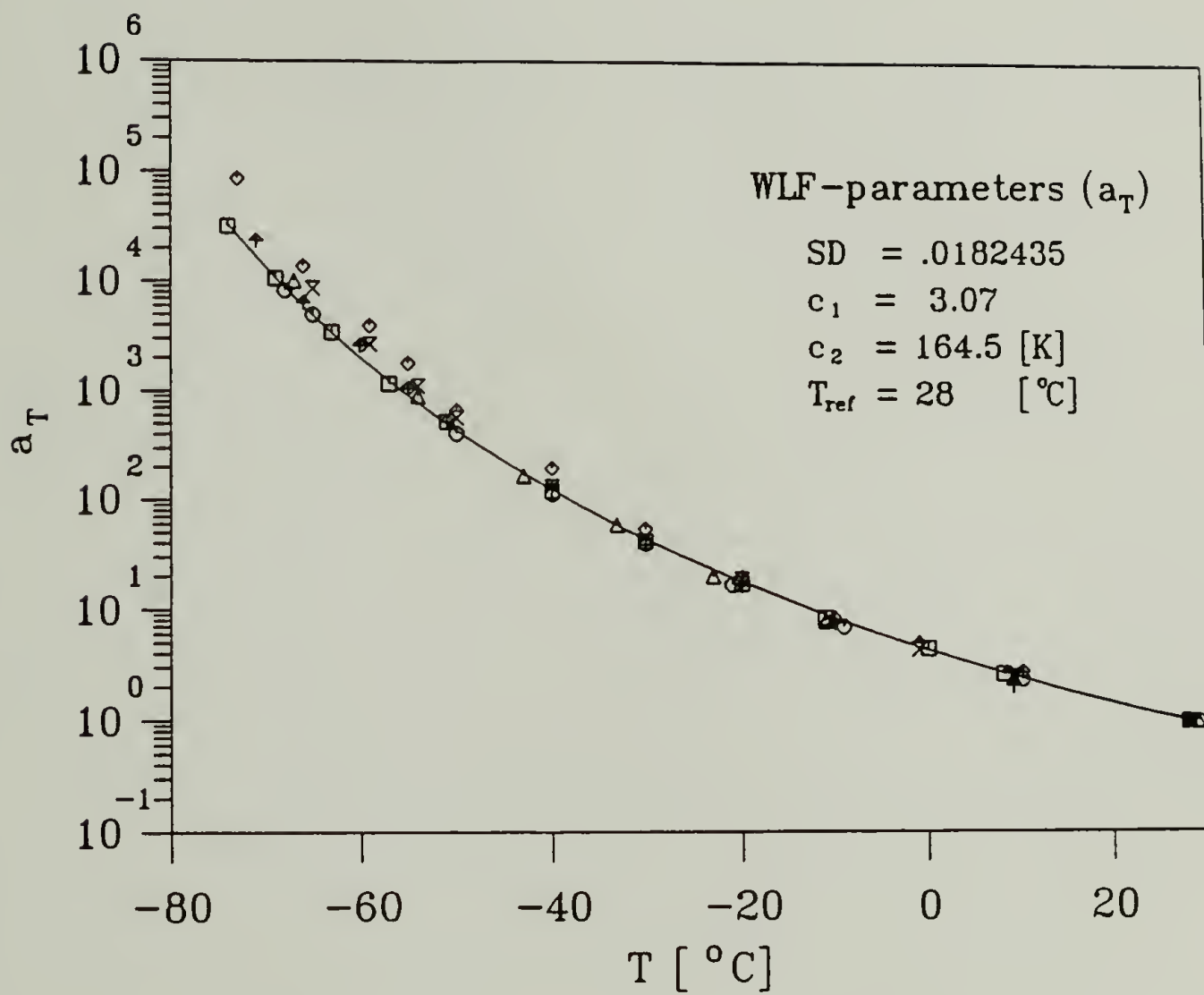


Figure 6.7 Horizontal shift factor (a_T) for the stopped PBD18 samples of figure 6.6. The WLF parameters are given in the figure.

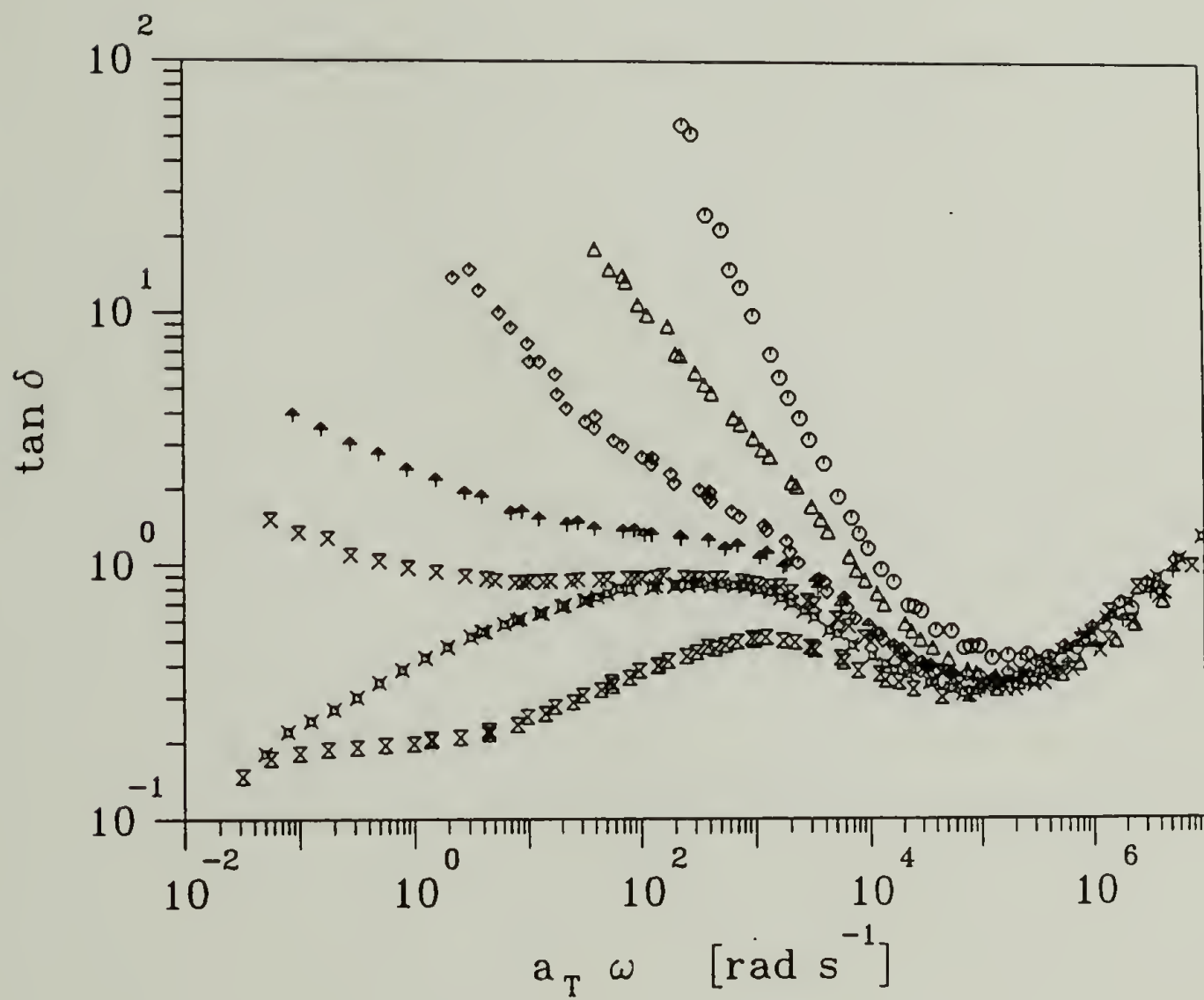


Figure 6.8 Tan δ master curves of dynamic data in figure 6.6.

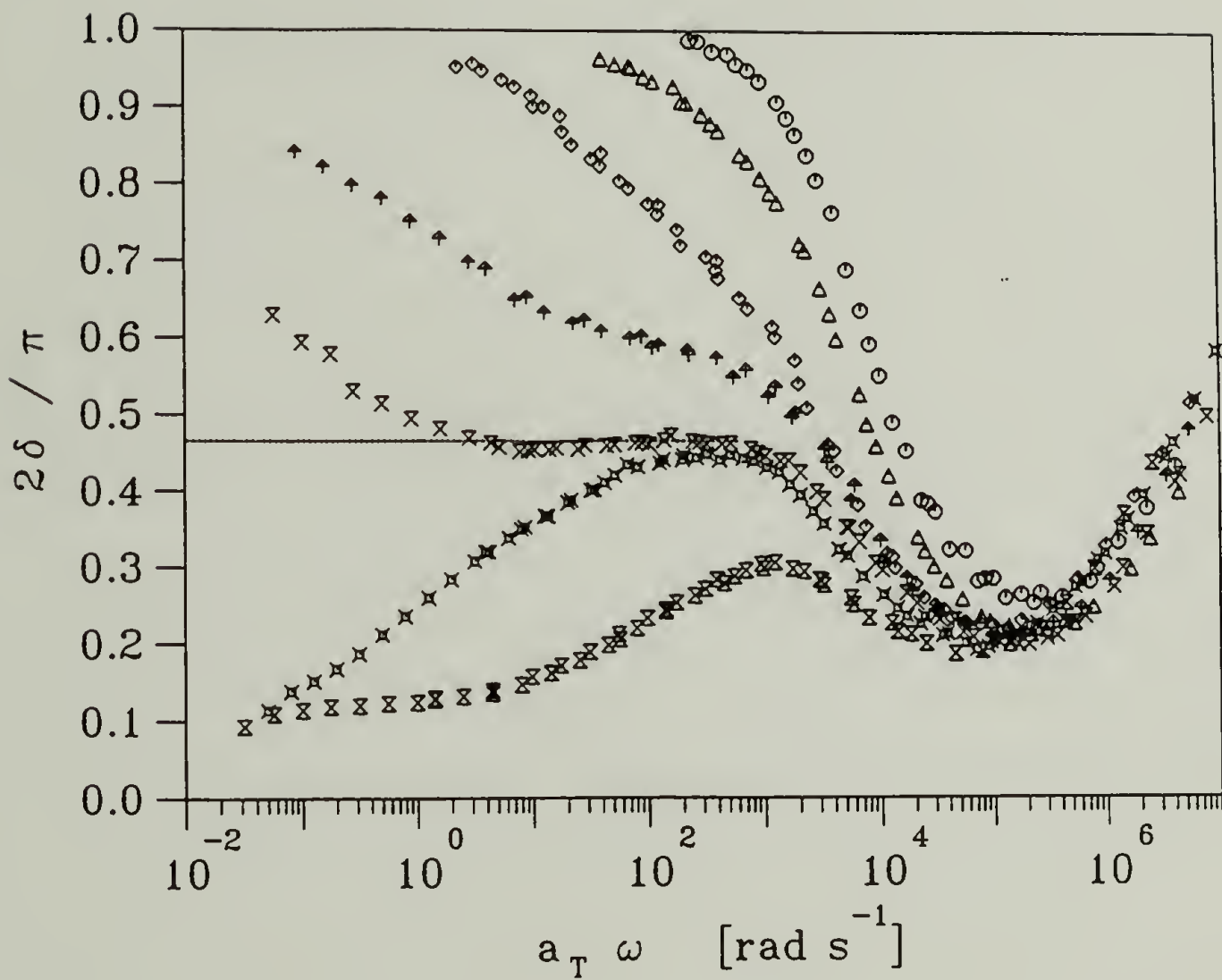


Figure 6.9 Normalized phase angle ($2\delta/\pi$) of $\tan \delta$ data given in figure 6.8.

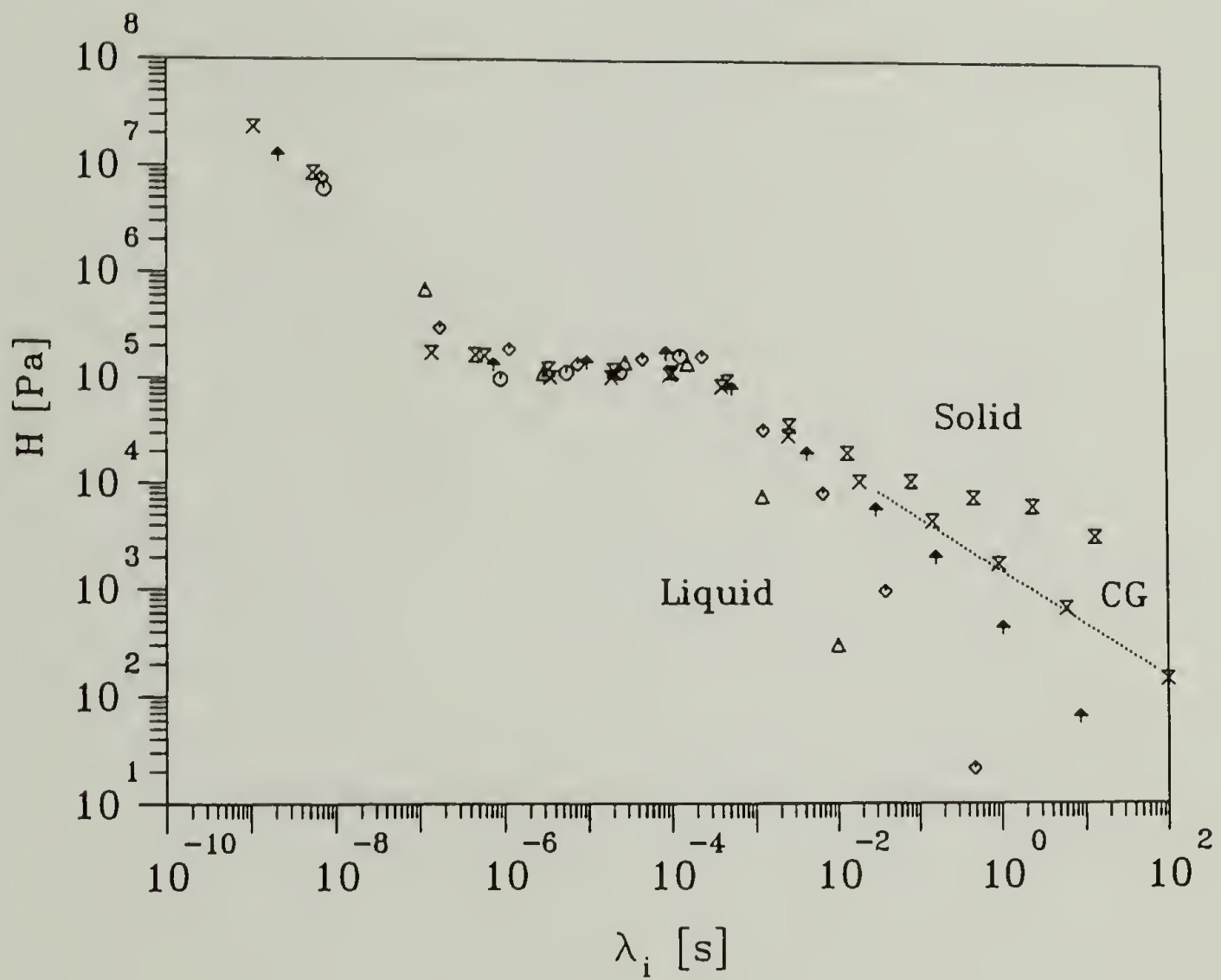


Figure 6.10 Evolution of the relaxation time spectrum calculated by IRIS software for the dynamic data in figure 6.6.

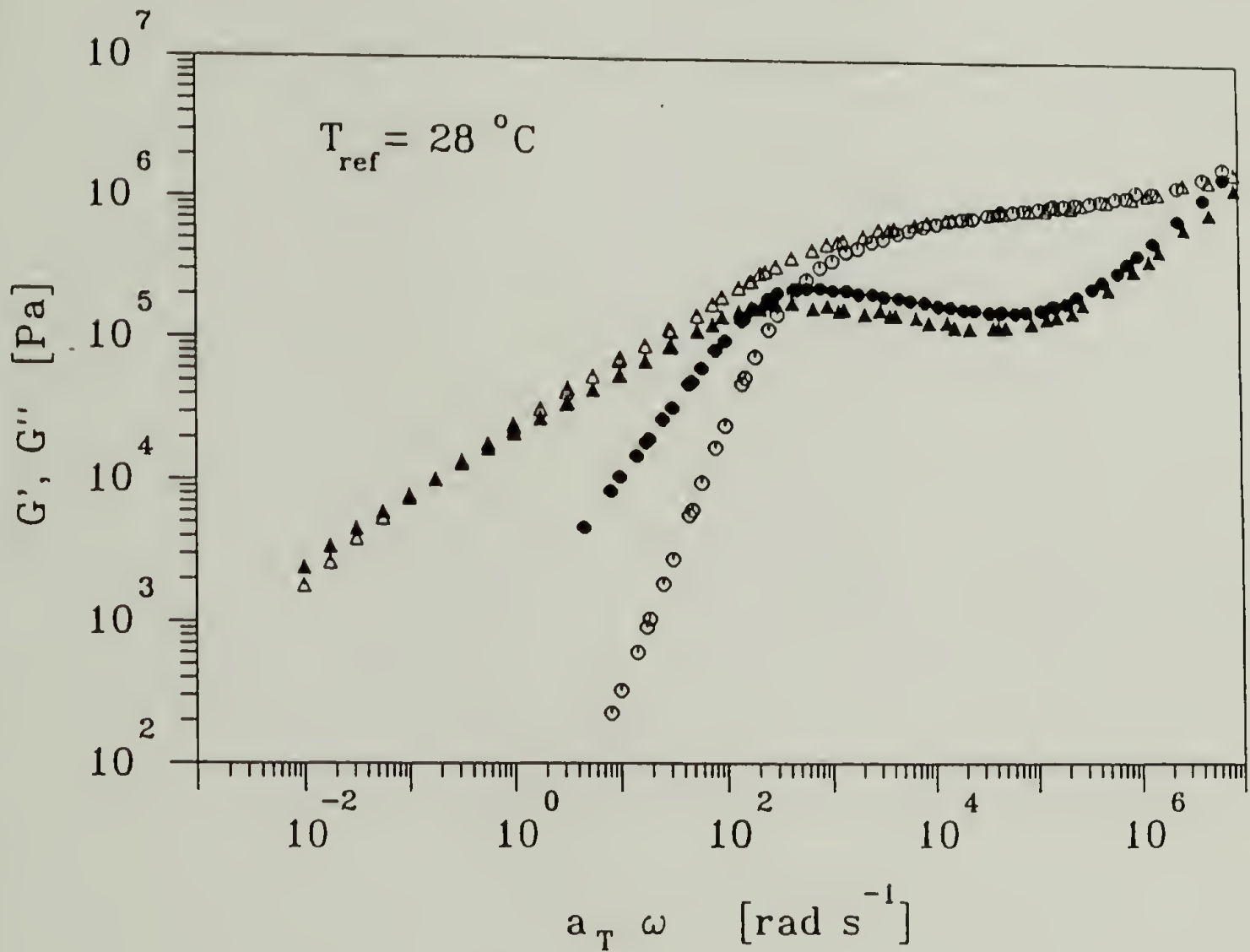


Figure 6.11 Dynamic data master curves showing the comparison of PBD44 critical gel to the precursor state of PBD44 mixed with $r=1$ amount of crosslinker. Open symbols represent G' and filled symbols represent G'' . $T_{ref} = 28^\circ\text{C}$.

stopped sample of PBD44 near the critical gel point and of the uncrosslinked mixture of PBD44 precursor and crosslinker. The relaxation dynamics in the entanglement region and the onset of the glass transition remain virtually unaffected by the gelation process except for a decrease in the slope of G'' at intermediate frequencies. The onset to the glass transition region is hardly affected. Figure 6.12 shows the dynamic moduli of stopped PBD samples near the gel point. The experiments were performed at a reference temperature of 28°C. The power law behavior at the gel point only occurs in the terminal zone and the slope of the power law is close to 0.5 for all samples. The corresponding $\tan \delta$ and normalized phase angle are shown in figure 6.13. Figure 6.14 shows the relaxation time spectra calculated with IRIS for data in figure 6.12. Three distinguished regions of power law behavior: one at short times for the glass transition, one at intermediate times for the entanglement region, and one in the terminal zone for the critical gel behavior. The shift factors for all the critical gels, shown in figure 6.15, were found to obey WLF behavior and are the same for all precursor molecular weights studied.

6.3 Critical Extent of Reaction at the Gel Point

Figure 6.16 shows the evolution of $\tan \delta$ of stopped PBD20 samples. The extents reaction of three of the samples, measured by F.T. Raman, are labeled. The extent of reaction for the sample near the gel point is 0.204 ± 0.006 . The extents of reaction for the samples before and after the gel point are 0.175 ± 0.006 and 0.240 ± 0.006 respectively.

The classical theory of gelation (Flory, 1953) was used to predict the critical extent of reaction at the gel point, p_c . p_c of SiH is given by the equation

$$p_{c, \text{SiH}} = \frac{1}{\sqrt{r(f-1)(g-1)}} \quad (6.2)$$

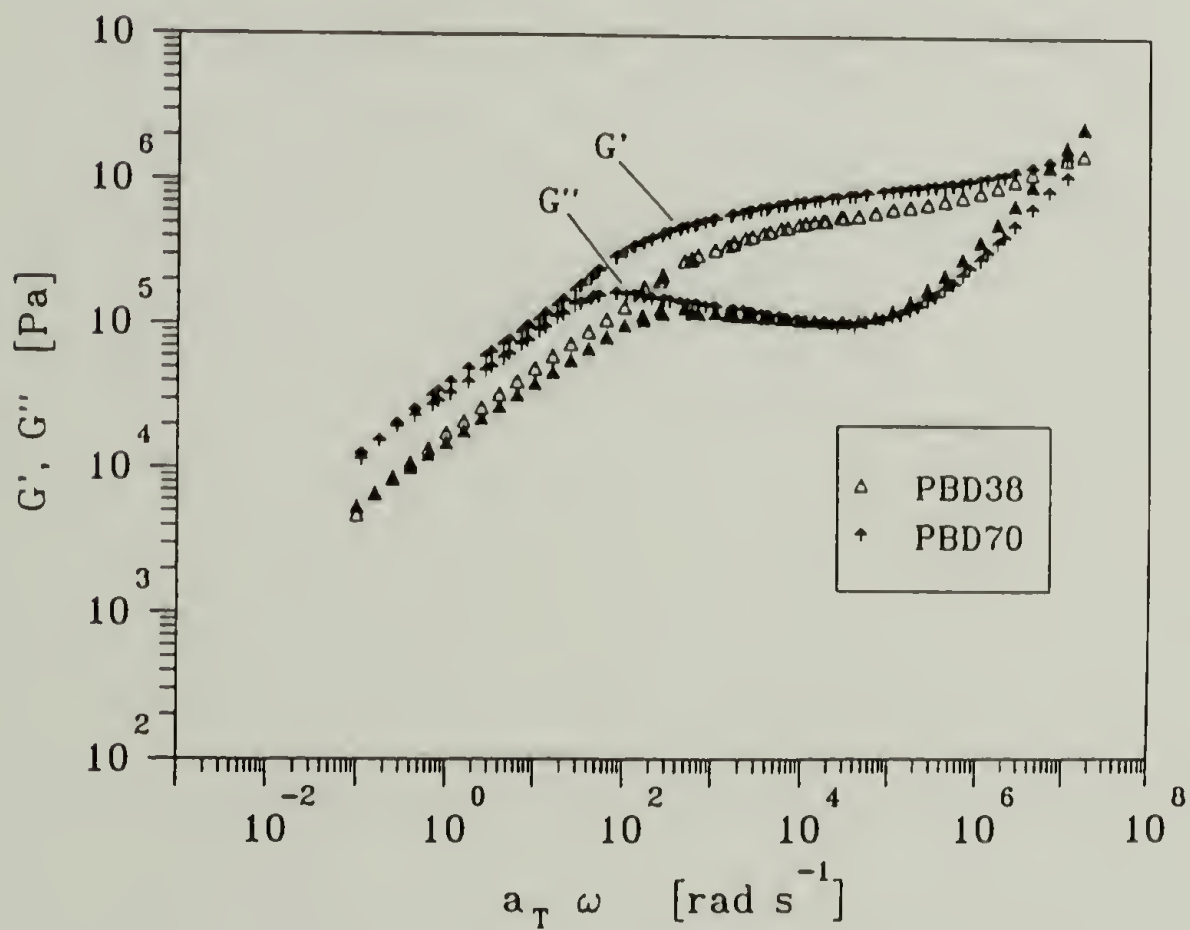
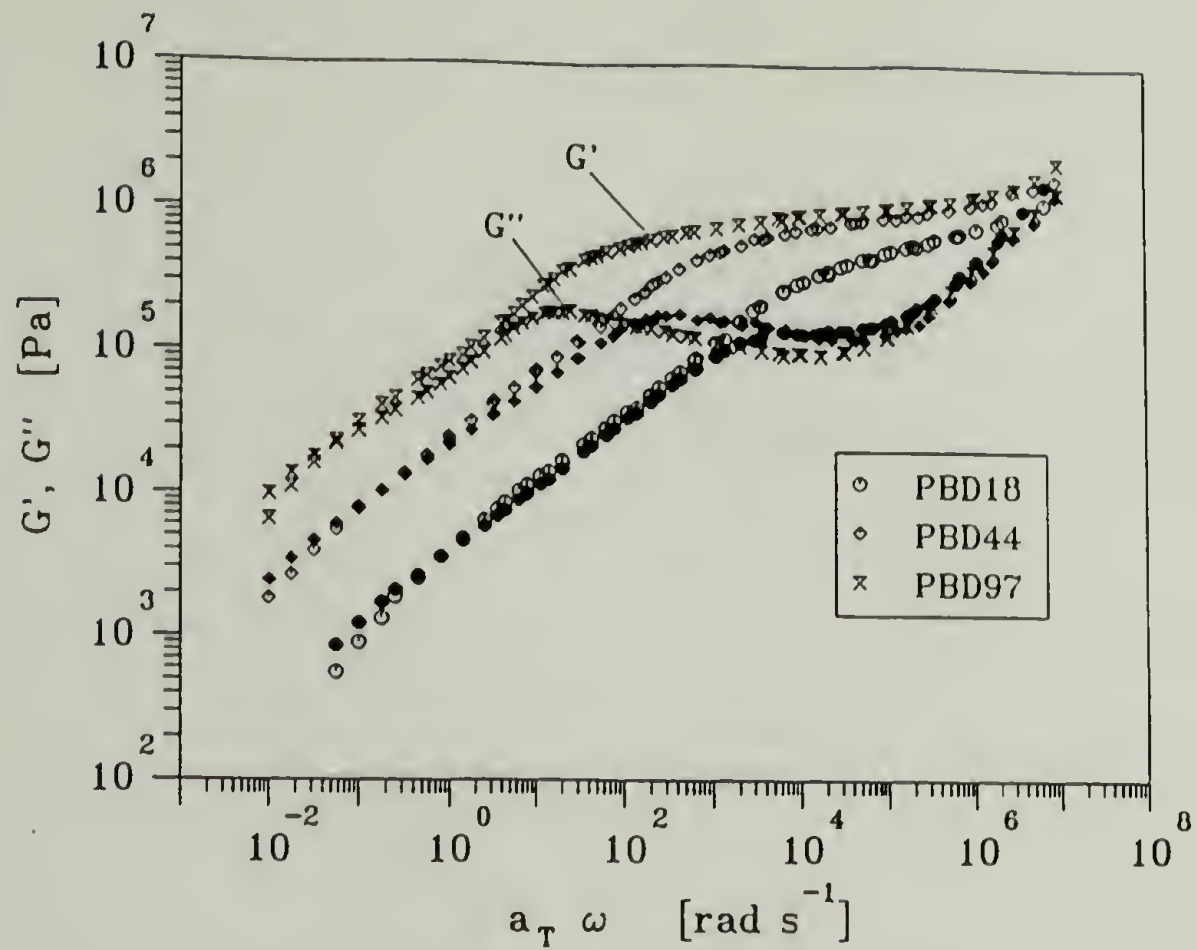
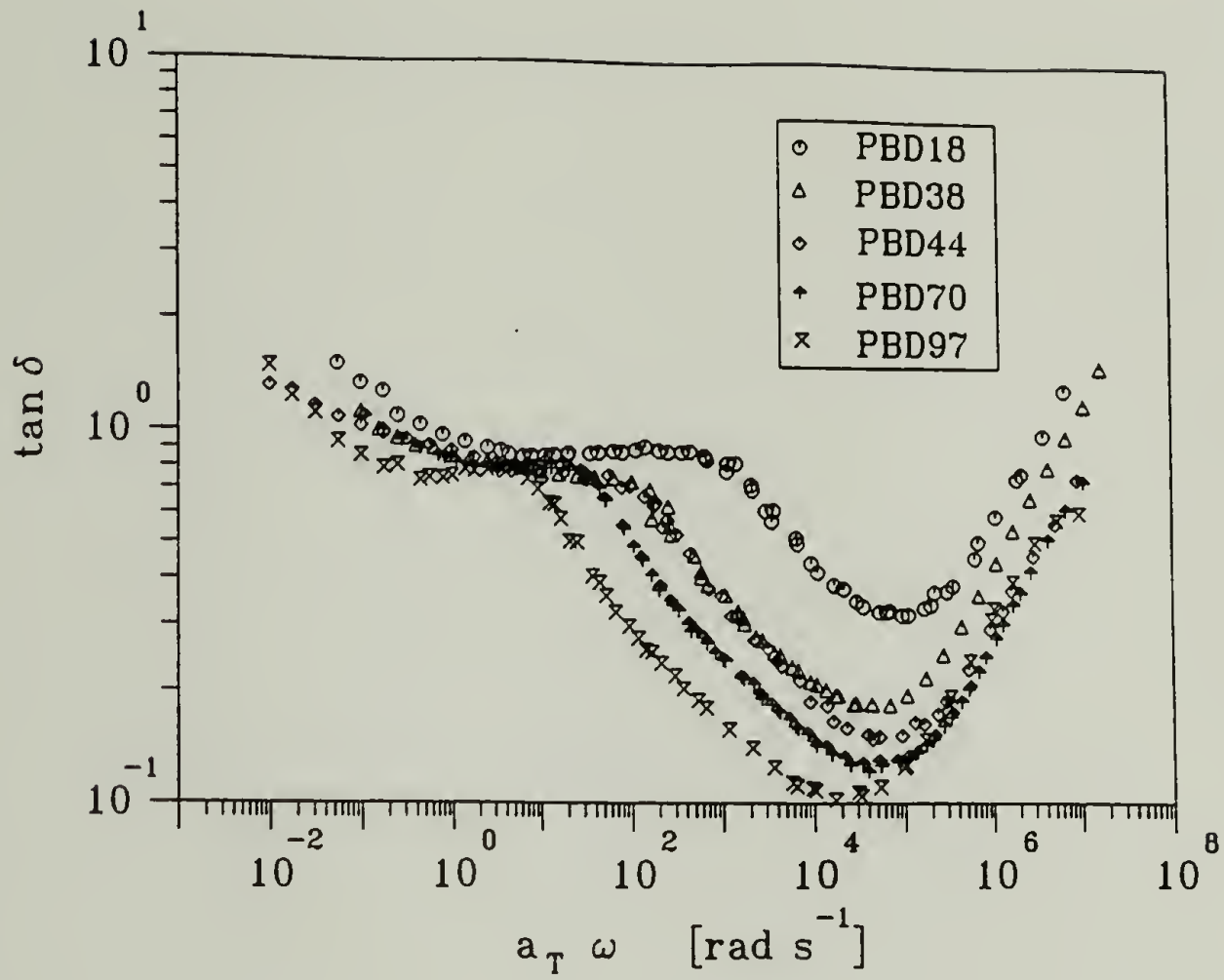


Figure 6.12 Dynamic data master curves of stopped samples near the critical gel point. Open symbols represent G' and filled symbols represent G'' . $T_{\text{ref}} = 28^\circ\text{C}$.

a)



b)

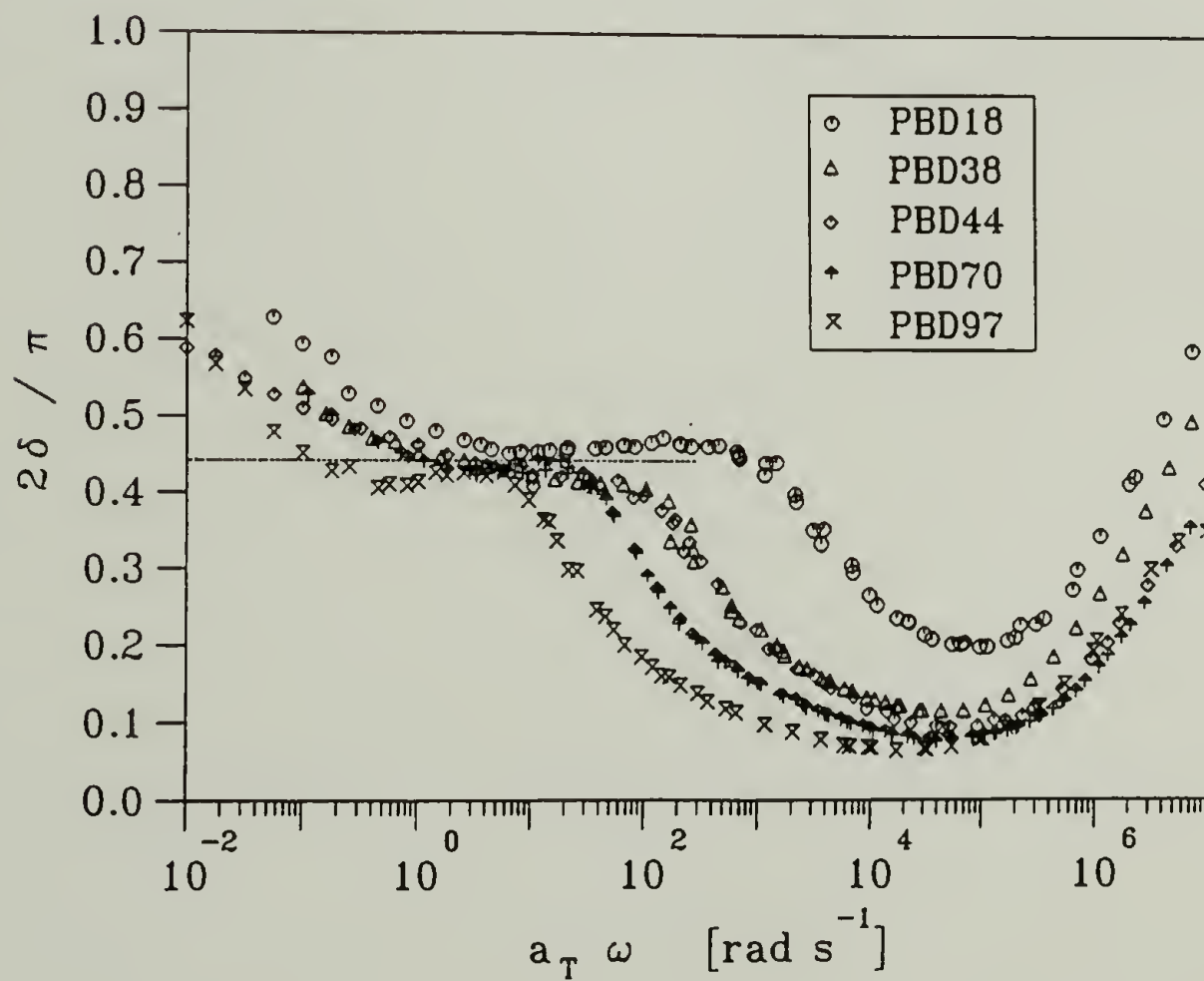


Figure 6.13 Master curves of (a) $\tan \delta$ and (b) normalized phase angle ($2\delta/\pi$) for dynamic data in figure 6.12.

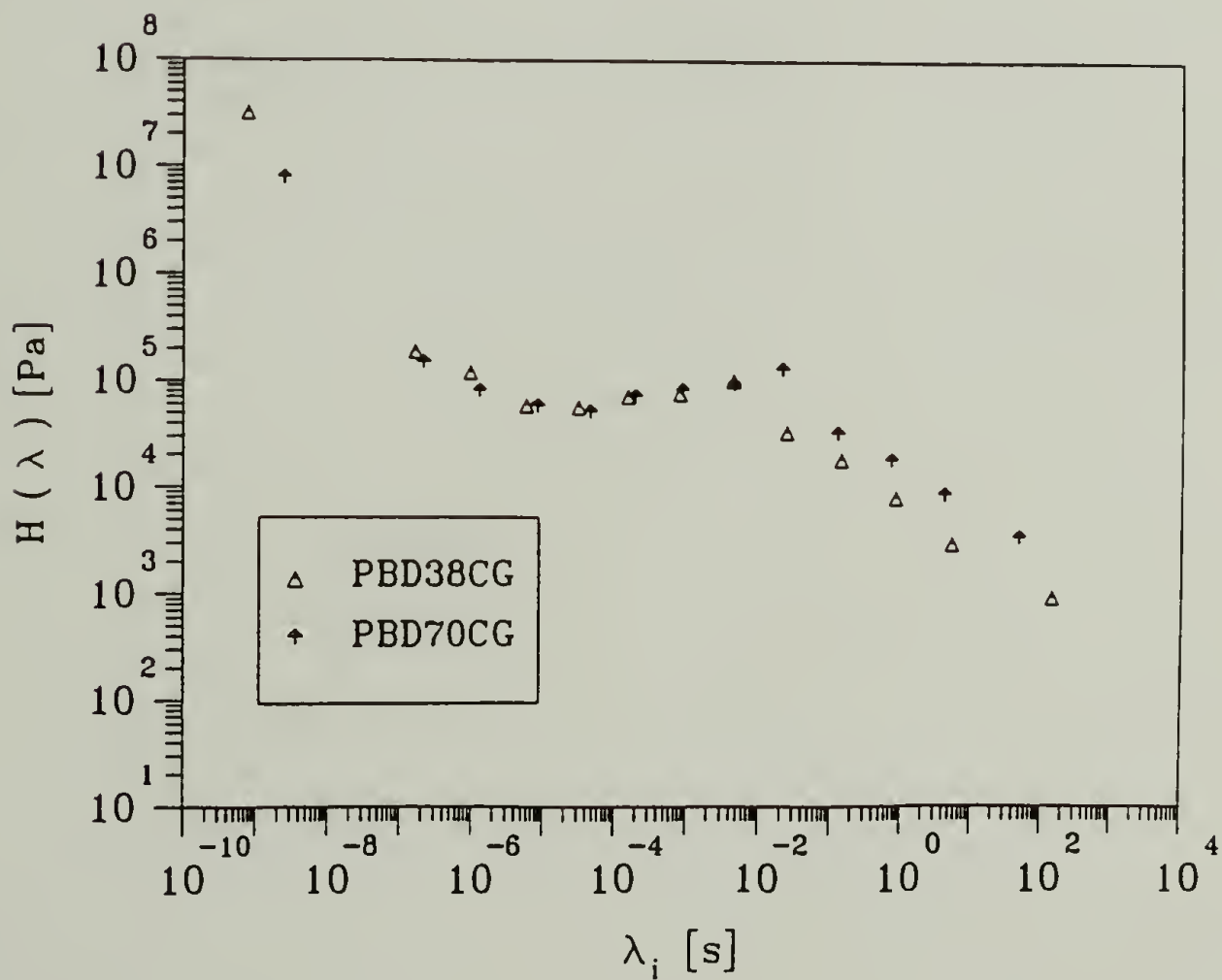
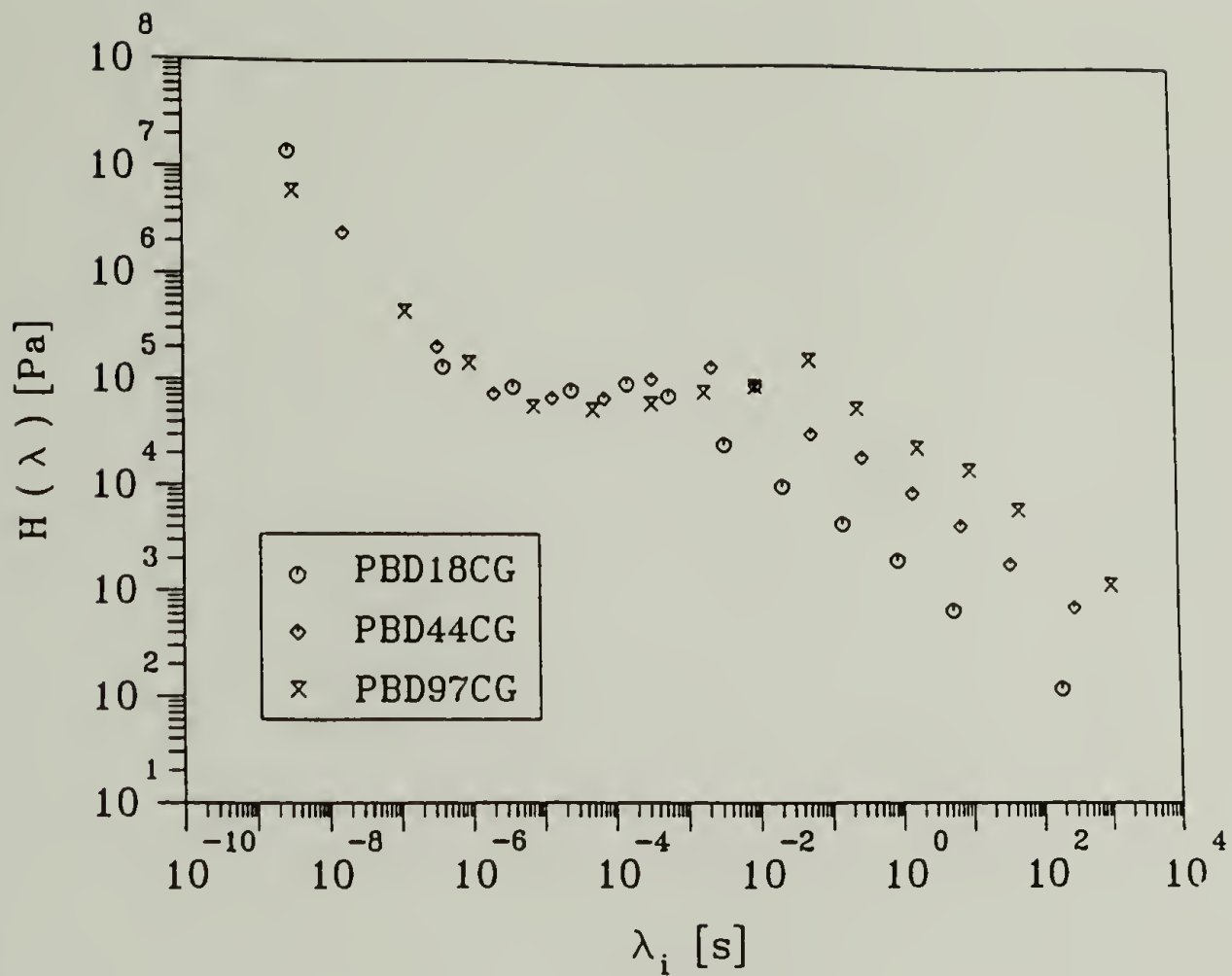


Figure 6.14 Relaxation time spectra of stopped critical gel samples calculated with IRIS software.

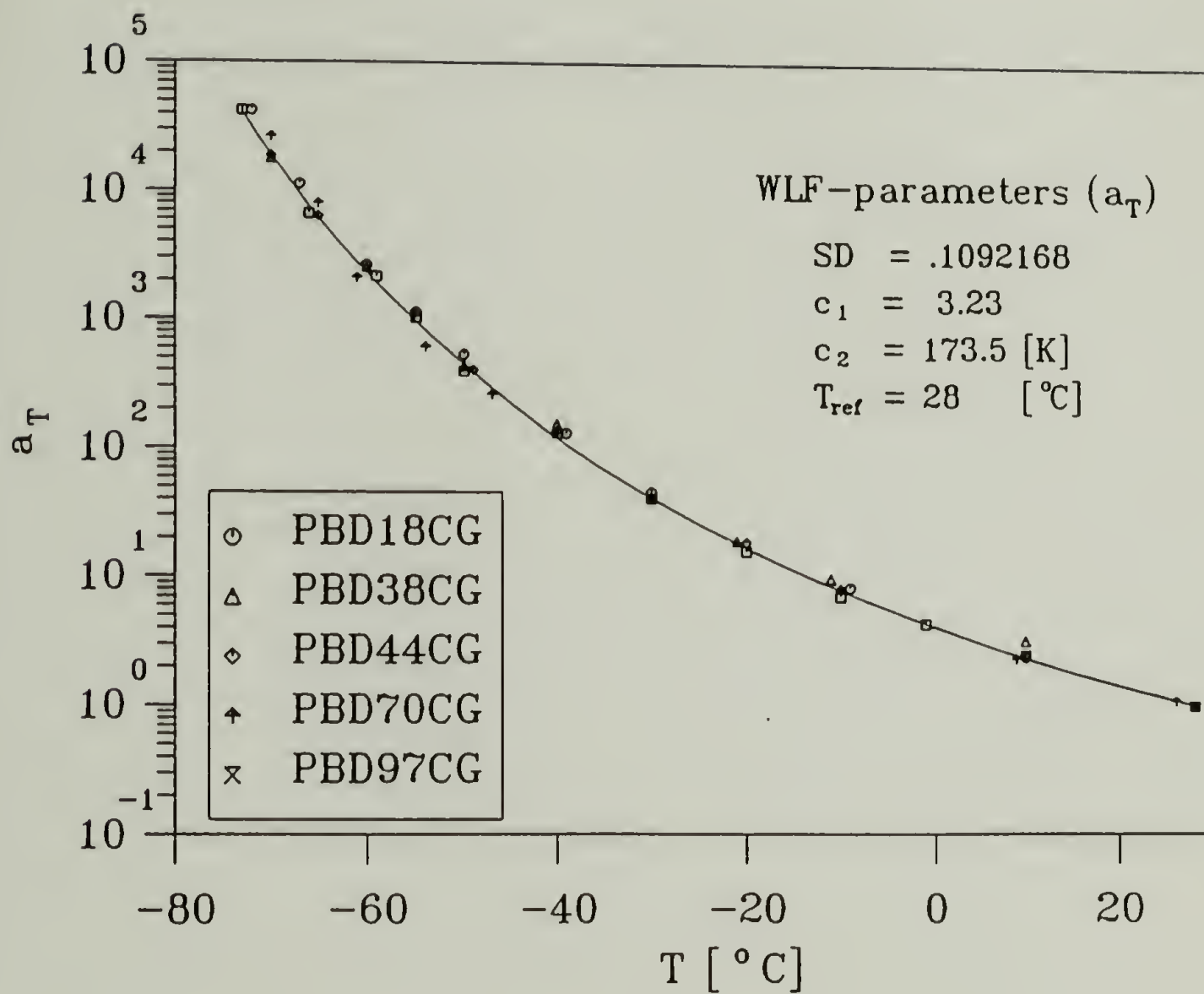


Figure 6.15 Horizontal shift factor (a_T) of stopped critical gel samples. a_T can be described by WLF behavior with the parameters in the figure.

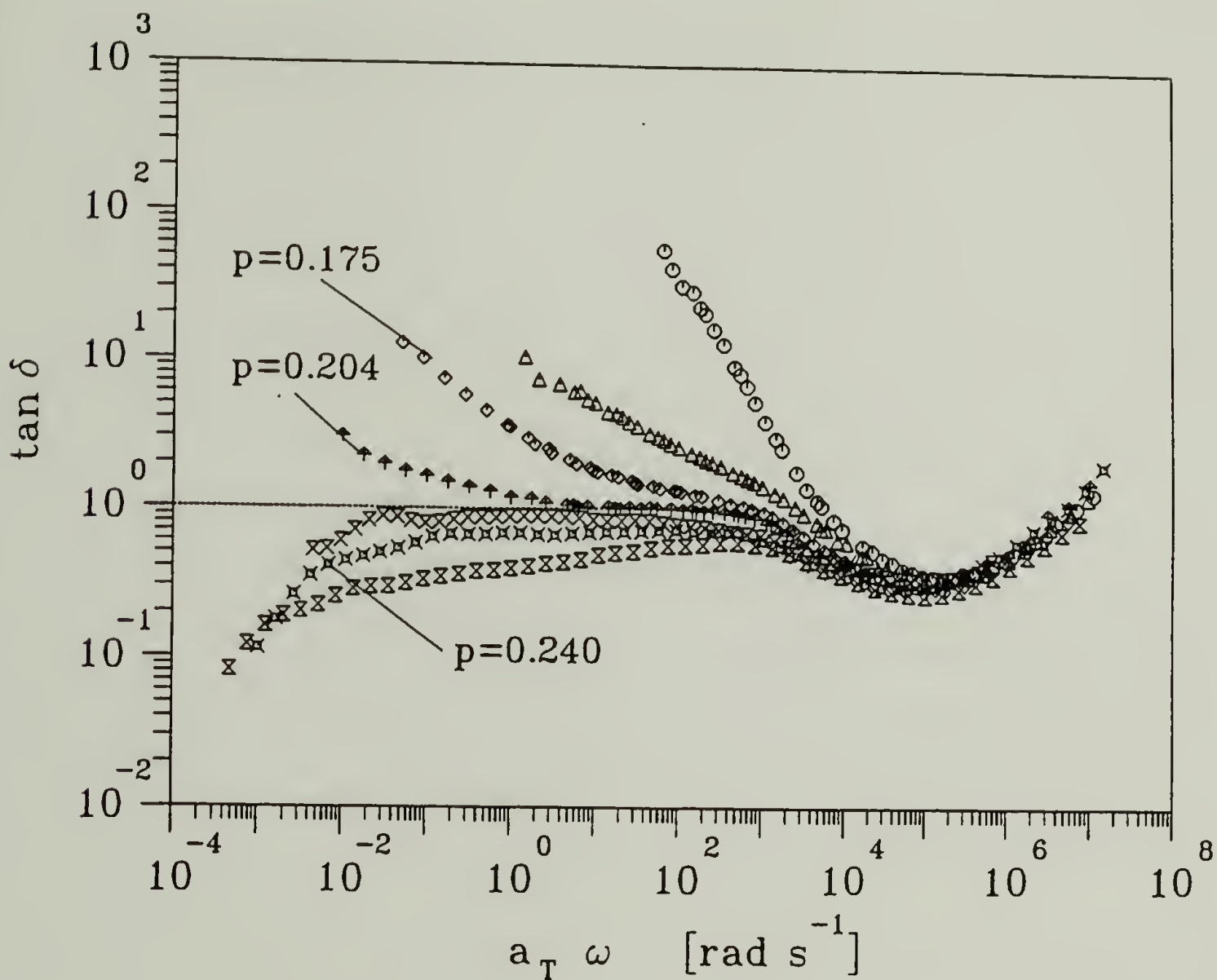


Figure 6.16 Evolution of $\tan \delta$ master curves of stopped PBD20 samples at balanced stoichiometry. $T_{\text{ref}} = 28^\circ\text{C}$. The extent of reaction (p), measured by F.T. Raman spectroscopy, of three of the samples are labeled.

where f is the functionality of the polymer, g is the functionality of the crosslinker, and r is the stoichiometric ratio defined in equation 2.3. For this experiment, $r=1$, $g=2$, and equation 6.2 simplifies to

$$p_{c,SiH} = \frac{1}{\sqrt{f-1}} \quad (6.3)$$

This expression is commonly used for crosslinking materials of low functionality (i.e. f and $g < 10$) however, it also applies to random crosslinking polymer chains as in this case (Brotzman and Flory, 1987).

By using equation 6.3, $p_{c,SiH}$ was calculated to be 0.186 (i.e. 18.6%) which is in close agreement with the measured value of 0.204. The fact that the measured value of $p_{c,SiH}$ is higher than the predicted value is most likely due to wasteful chemical side reactions and loop formations which are not accounted for in Flory's model but are always present in real chemical crosslinking systems (Flory, 1953). Side reactions and loops use up the reactive sites without forming effective elastic crosslinks however they are still measured as converted bonds. Therefore, when taking this point into consideration, p_c would be expected to be higher than the predicted value.

The number of effective crosslinks per chain is given by the crosslinking index, ξ , defined as

$$\xi = \alpha f \quad (6.4)$$

where α is the branching coefficient (Flory, 1953). At the gel point, the critical crosslinking index, ξ_c , is given by (Flory, 1953)

$$\xi_c = \alpha_c f \quad (6.5)$$

where

$$\alpha_c = r p_c^2 = \frac{1}{(f-1)(g-1)} \quad (6.6)$$

From equation 6.5 ξ_c was predicted to be 1.026. Using the data obtained from F.T. Raman, ξ_c was calculated to be 1.26. Valentine et al. (1968) who measured the crosslinking index to be 1.2 for a peroxide cured polybutadiene near the gel point of precursor molecular weight equal to 180,000 and vinyl content of 7%.

6.4 Relaxation Behavior at the Gel Point

The dynamic moduli of the PBD samples, stopped close to the critical gel point, clearly show three regions of viscoelastic behavior (see figure 6.12). At long times, G' and G'' are nearly parallel and their slopes are close to 0.5. The intermediate frequencies are governed by entanglements and the high frequencies by the glass transition. The same behavior in the three viscoelastic regions can be seen in $H(\lambda)$. From these data it is proposed here that the entire spectrum can be described by three power laws. The short and intermediate time represent the glass and entanglement region and the long time represents the critical gel behavior.

Data obtained from stopped samples reveals several interesting aspects about the rheological behavior of critical gels with entanglements. First, it was surprising to see that the entanglement region change so little during the initial crosslinking period. It is interesting to note that as the molecules are crosslinked and become longer, one might expect that the plateau zone (entanglement region) may extend out to lower frequencies. Such a trend is seen for the bulk precursors as shown in chapter 4. However, this does not occur and the entanglement regime remains approximately the same length even though the molecules are getting longer. This may be explained in the following manner.

A critical gel consists of many different species of molecular clusters: precursor molecules, dimers (two precursor molecules), trimer, tetramers, etc. and one largest

cluster that spans the entire sample size with an infinite relaxation time and molecular weight. Flory (1953) and Stockmayer (1952, 1953) have reported statistical results for the weight fraction of each of these species at different extents of reaction or degrees of crosslinking. They have shown that as the gelation process proceeds, the weight fraction of the precursor is always greater than that of any one of the other species up to the gel point. Shortly after the gel point, the weight fraction of the infinite cluster rises sharply as crosslinking continues until it becomes larger than any other species in the sol (material before the gel point) including the monomer. Therefore at the gel point, the precursor molecules are still the most abundant species and will ultimately dominate the rheological behavior. Thus the length of the plateau region would be determined by the precursor molecule and thus remain approximately the same length.

A related molecular weight effect has been observed in a study by Watanabe and Kotaka (1984) with blends of entangled monodisperse polymers of different molecular weight. In the simplest case of binary blends of a 36,000 g/mole polystyrene blended with smaller weight fractions of a 407,000 g/mole polystyrene, they found that the dominating relaxation behavior at intermediate and high frequencies came from the lower molecular weight polymer which had the highest weight fraction. The frequency range of the plateau in G' was found to be essentially the same length even when up to 20% of the high molecular weight polystyrene was blended in. The higher molecular weight polymer only affected the long relaxation time behavior of the lowest frequencies within the terminal zone of the small molecular weight polymer.

Another explanation for not seeing a dramatic change in the entanglement region is due to the fact that at the gel point the entanglement density is significantly higher than the chemical crosslink density. Since the functionality of the precursor is so high, few chemical crosslinks per chain are needed to reach the gel point. This is reflected in the value of ξ_c which was found to be only 1.26 for PBD20. For PBD20 the number of

entanglements per chain can be calculated by dividing M_w by M_e where M_e , the molecular weight between entanglement points is (Ferry, 1980)

$$M_e = \frac{\rho RT}{G_N^0}. \quad (6.7)$$

For PBD20, the amount of entanglements per chain is 15 and the amount of chemical crosslinks added per chain is 1.26. Therefore, at most, only an 8% increase in the plateau modulus would be observed at the gel point. This value is very close to the experimental error involved with measuring dynamic data of stopped samples near the gel point.

The second interesting observation made in this study was that the critical relaxation exponent was close to 0.5 for all precursor molecular weights examined. It has been reported that the value of n was effected by the precursor molecular weight for endlinking systems (Izuka et al., 1992; Scanlan and Winter, 1991). The independence of n with precursor molecular weight found in this study may be due to the fact that the crosslinking mechanism occurs by vulcanization rather than by endlinking.

During vulcanization, clusters grow by precursor polymers connecting at random sites along the backbone of the chain as opposed to at the ends as in endlinking. The mechanism of cluster growth should be identical for all polymers irrespective of their initial length before crosslinking. Therefore, at the gel point, the largest cluster along with all other clusters of smaller sizes, should have very similar structures, i.e. the distance between all crosslinks is random and not determined by precursor molecular weight. The only structure in the critical gel that depends upon precursor molecular weight is the most abundant species; the unreacted precursor polymer. If this is true, then it would be expected that the rate of stress relaxation of critical gels, characterized by n , should be independent of precursor molecular weight for vulcanizing systems.

6.4.1 Empirical Relaxation Time Spectrum for Highly Entangled Critical Gels

For the following data analysis, we propose a simple framework which captures the essential features of the observed spectra. More detailed analysis will have to follow. A change in notation has to be introduced at this time. The longest relaxation time of the mixture of precursor and crosslinker, $\lambda_{\max,d}$, will be called $\lambda_{p,d}$ (diluted precursor) and it will serve as a reference time scale for describing the evolving molecular dynamics during crosslinking. The longest relaxation time of the crosslinked material, given by λ_{\max} , characterizes the largest cluster (Rubenstein et al., 1990). λ_{\max} becomes longer than $\lambda_{p,d}$ as soon as crosslinks are added. As the material approaches the gel point, $\lambda_{\max} \rightarrow \infty$. After the gel point, as described earlier, the material is comprised of the infinite cluster and many smaller clusters. λ_{\max} after the gel point characterizes the largest cluster that is not connected to the infinite cluster. This value begins to decrease rapidly as the extent of reaction increases past the gel point. This observation has been made by Valentine et al. (1968) who investigated the relaxation behavior of crosslinked high molecular weight polybutadienes.

For getting started it is realized that the spectrum of the precursors is hardly changed at all by the crosslinking, but that a long time tail is added which follows the Chambon-Winter spectrum characteristics. In the simplest case, a CW-spectrum would be added to the BSW-spectrum of the diluted samples. This spectrum can be represented as

$$H(\lambda) = \begin{cases} n_e G_{N,d}^0 \left[\left(\frac{\lambda}{\lambda_{p,d}} \right)^{n_c} + \left(\frac{\lambda}{\lambda_{c,d}} \right)^{-n_g} \right] & \text{for } 0 < \lambda < \lambda_{\max,d} \\ n_e G_{N,d}^0 \left(\frac{\lambda}{\lambda_{p,d}} \right)^{-n} & \text{for } \lambda_{p,d} < \lambda < \infty \end{cases} \quad (6.8)$$

Figure 6.17 shows a schematic representation of the spectrum in equation 6.8.

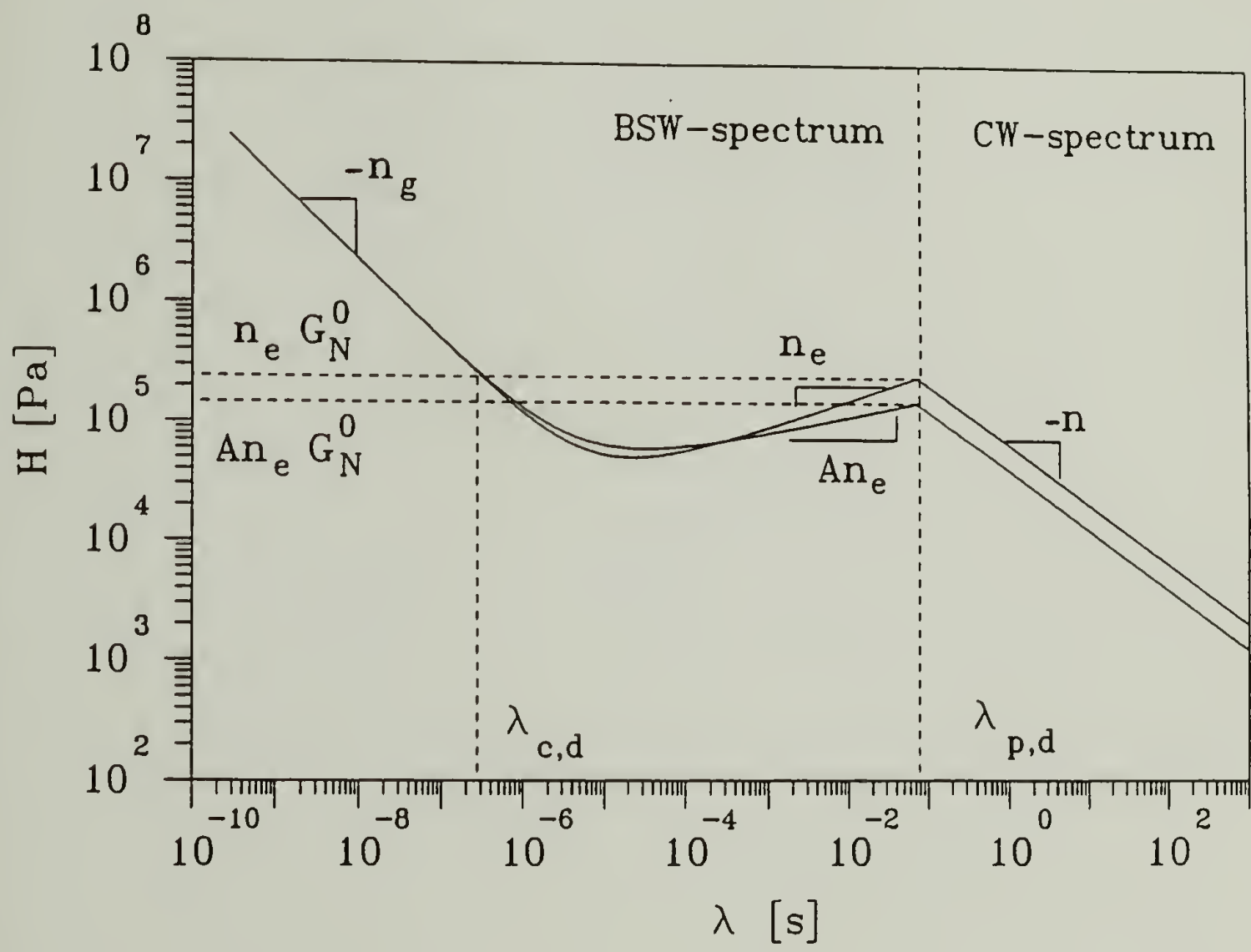


Figure 6.17 Schematic representation of the model spectra for entangled critical gels. Comparison is shown for the simple superposition of BSW-spectrum of the precursor and CW-spectrum, and the modified spectra with decreased slope in the entanglement region.

The short time limit for power law behavior denoted by λ_0 in equation 1.3 occurs at the onset of the rubbery regime for entangled polymers, $\lambda_0 \equiv \lambda_{p,d}$. For precursors of molecular weight below M_c , this value would indicate the time for the crossover to the glass transition since no physical entanglements are present (Scanlan and Winter, 1991; Izuka et al., 1992). For entangled polymers, λ_0 is equal to the longest relaxation time of the precursor. The longest relaxation of crosslinked system approaches infinity as the system approaches the true gel point.

Recently, Rubenstein et al. (1990) proposed a theoretical description for the relaxation of entangled polymers near the gel point based on molecular motions and Flory-Stockmayer percolation. They also proposed a separation between the relaxation behavior of the entanglement zone and the power law zone in $G(t)$. The time which characterized the division between these two zones is equivalent to here to λ_0 .

The simple framework in equation 6.8, allows for the analysis of the entanglement region in greater detail. The slope n_e was observed to decrease from 0.23 to 0.12 during the initial crosslinking period up to the gel point. The change in slope might be due to the broadening of the molecular weight distribution. A better fit of the data can be achieved by accounting for the change in slope in equation 6.8. The form of the relaxation spectrum with entanglements can then be written as

$$H(\lambda) = \begin{cases} n_e G_{N,d}^0 \left[A \left(\frac{\lambda}{\lambda_{p,d}} \right)^{An_e} + \left(\frac{\lambda}{\lambda_{c,d}} \right)^{-n_e} \right] & \text{for } 0 < \lambda < \lambda_{p,d} \\ n_e G_{N,d}^0 A \left(\frac{\lambda}{\lambda_{p,d}} \right)^{-n} & \text{for } \infty > \lambda > \lambda_{p,d} \end{cases} \quad (6.9)$$

The slope of the entanglement regime is equal to An_e where A is an empirical constant between 0 and 1. Here we find a value of $A = 0.52$ fits best. For the uncrosslinked

samples $A=1$. Figure 6.17 shows a comparison of the schematic representation of the spectrum in equation 6.8 to the spectrum in equation 6.9. Figure 6.18 shows a comparison of the dynamic data of PBD97 stopped near the gel point to the model represented by equations 6.8 and 6.9. Figure 6.19 shows the calculated values of $H(\lambda)$ from equation 6.9 for all precursors except PBD201. The parameters of the spectrum for the critical gel model are given in table 6.1. Figure 6.20 shows how the prediction of equation 6.9 compares to the stopped sample data near the gel point for all precursors.

An interesting result of the form of the spectrum proposed here for the entangled critical gel is a new interpretation of the value of G_0 described in equations 1.3 and 1.4. Scanlan and Winter (1991) proposed that G_0 and λ_0 are characteristic of the prepolymer. Consequently, the gel strength is related to these parameters by

$$S = G_0 \lambda_0^n. \quad (6.10)$$

It was suggested that since n is limited to $0 < n < 1$, S was constrained to

$$G_0 \lambda_0 < S < G_0 \quad (6.11)$$

where G_0 was speculated to be the plateau modulus of the precursor and $G_0 \lambda_0$ to be the zero shear viscosity of the precursor polymer.

From the results of this work, it has been found that the upper and lower limits of S are related to the plateau modulus and the viscosity of the precursor. With the form of the spectrum proposed in equation 6.9 it was possible to specifically determine G_0 as a function of the plateau modulus of the precursor. G_0 was determined by first setting the CW-spectrum of equation 1.3 equal to the CW type spectrum described by equation 6.9 at times longer than $\lambda_{p,d}$ giving

$$H = \frac{G_0}{\Gamma(n)} \left(\frac{\lambda}{\lambda_0} \right)^{-n} = A n_c G_N^0 \left(\frac{\lambda}{\lambda_{p,d}} \right)^{-n}. \quad (6.12)$$

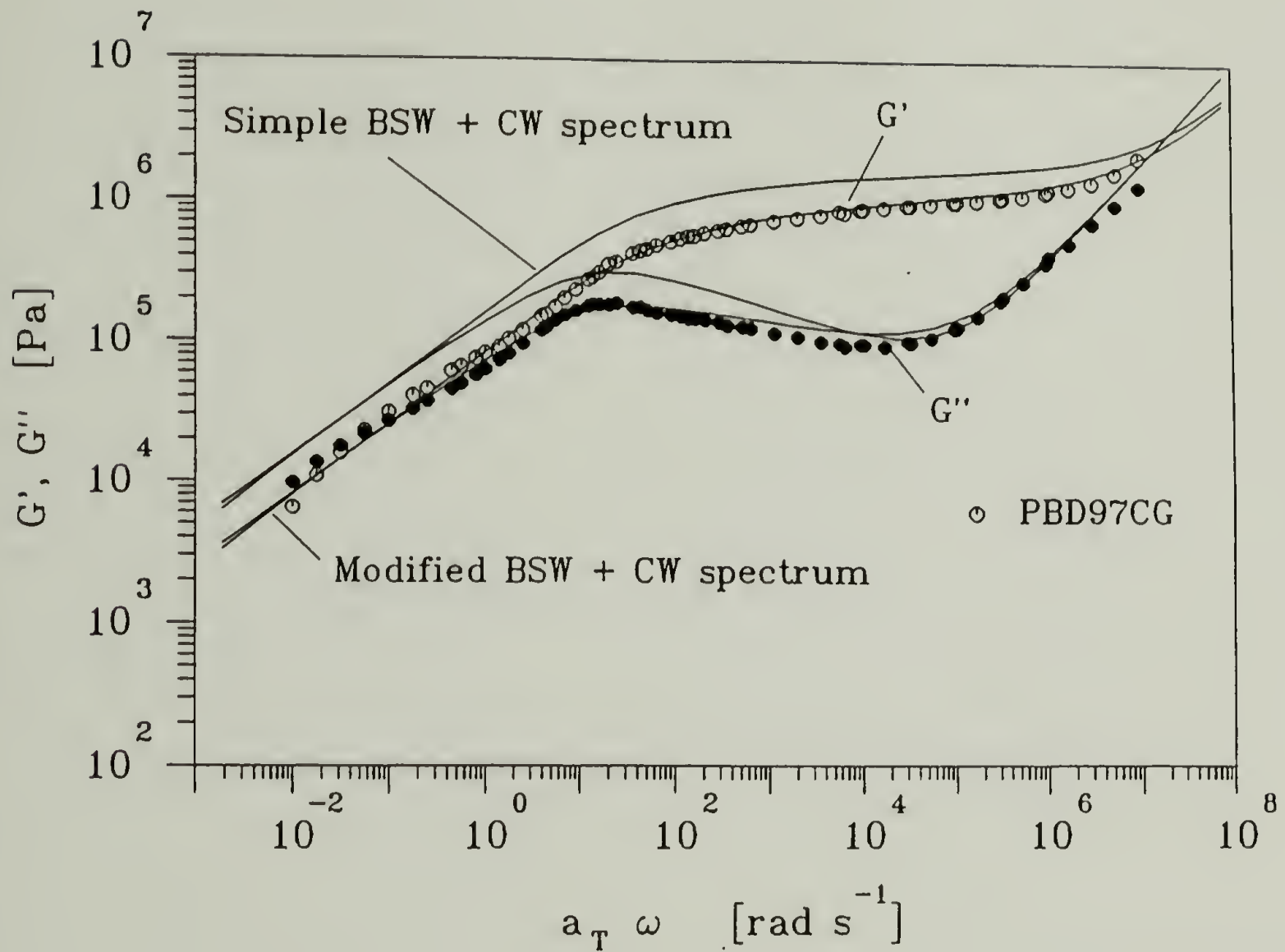


Figure 6.18 Calculated dynamic moduli from the model gel spectra in equation 6.8 (simple BSW-CW-spectrum) and modified gel spectra model in equation 6.9 for a sample with precursor M_w of 97000 g/mole. The experimental dynamic data of stopped PBD97 critical gel is shown in comparison to the model. $T_{ref} = 28^\circ\text{C}$.

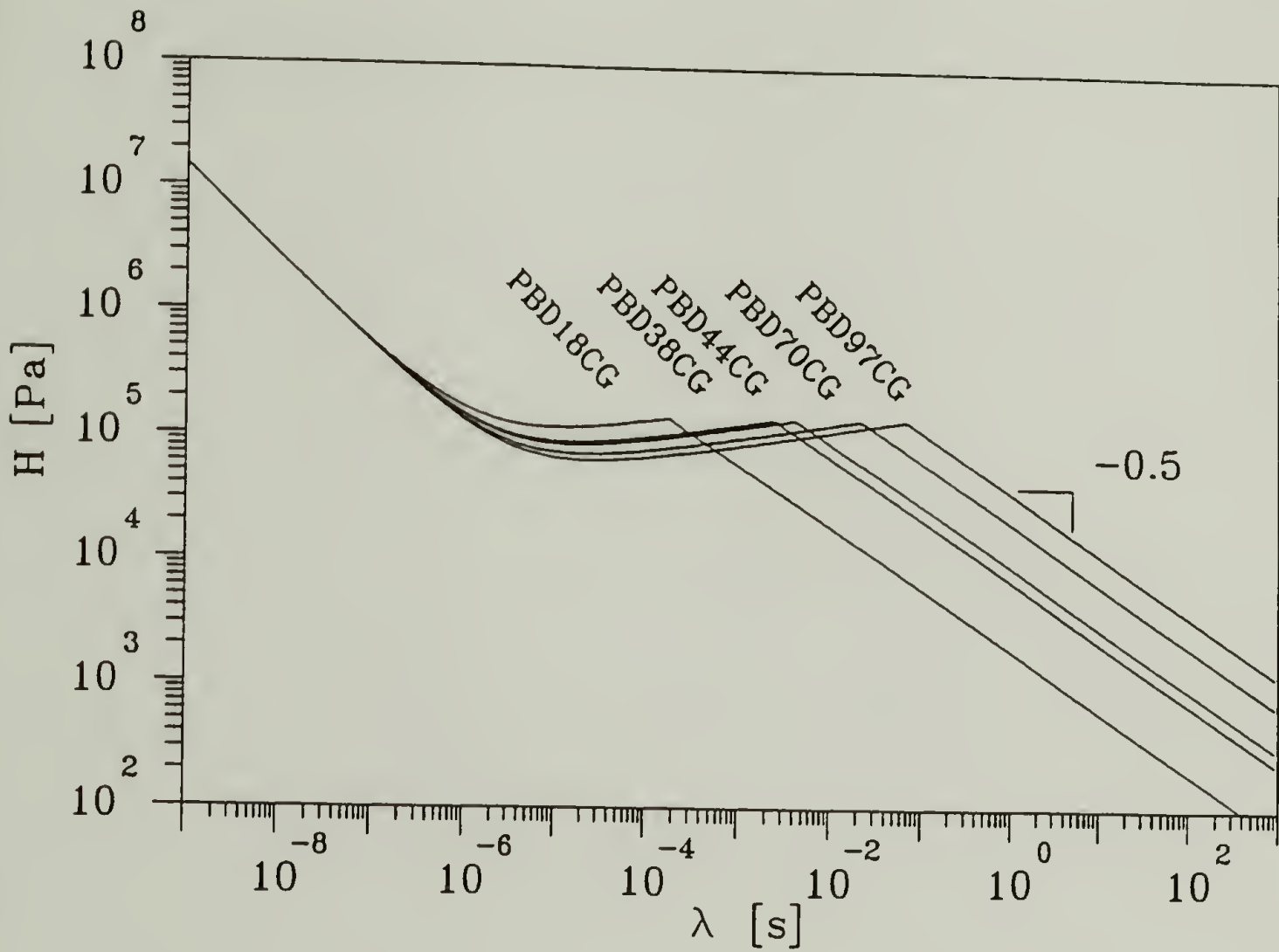


Figure 6.19 Relaxation time spectra calculated with the gel model of equation 6.9 and parameters in table 6.1 for precursors PBD18 through PBD97.

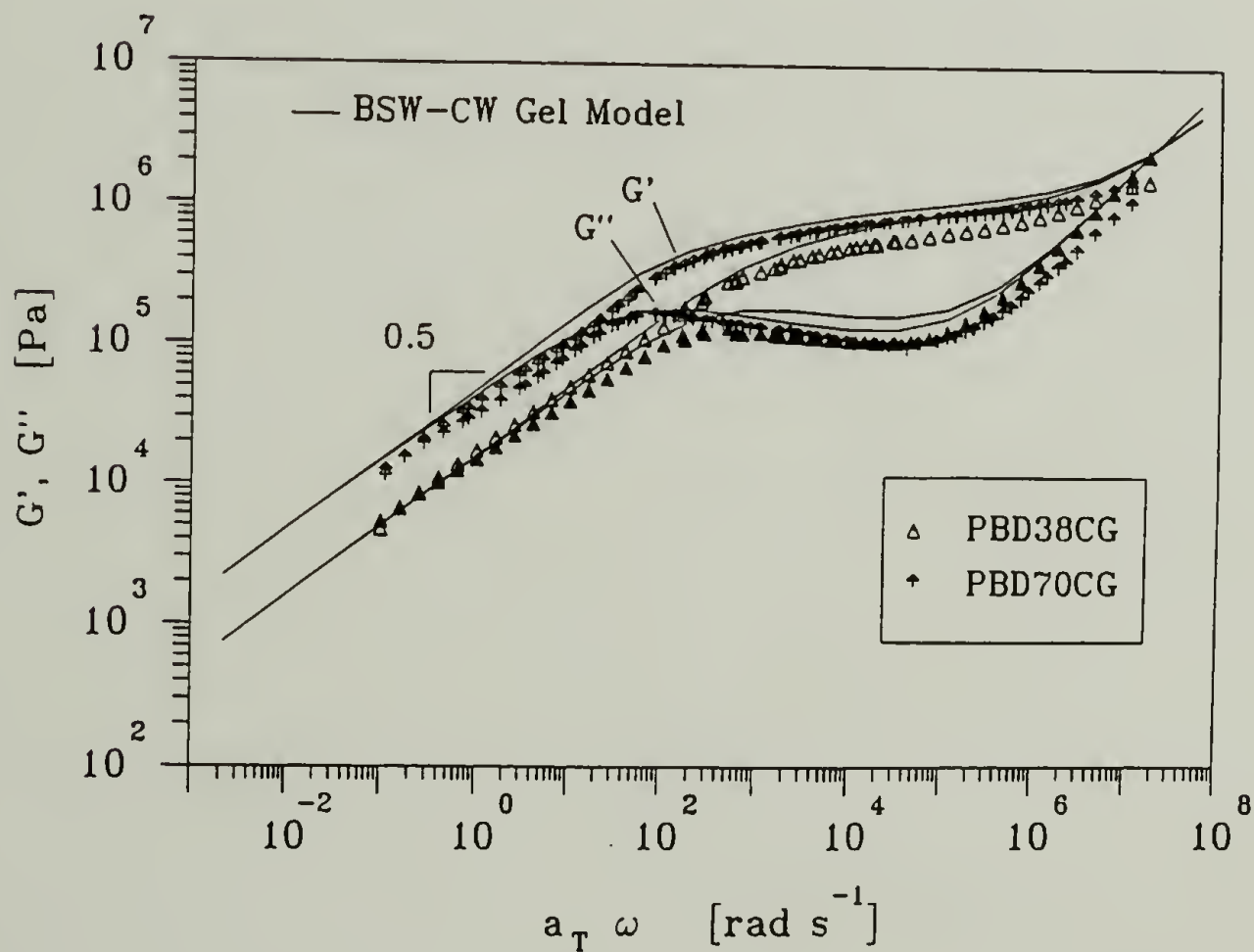
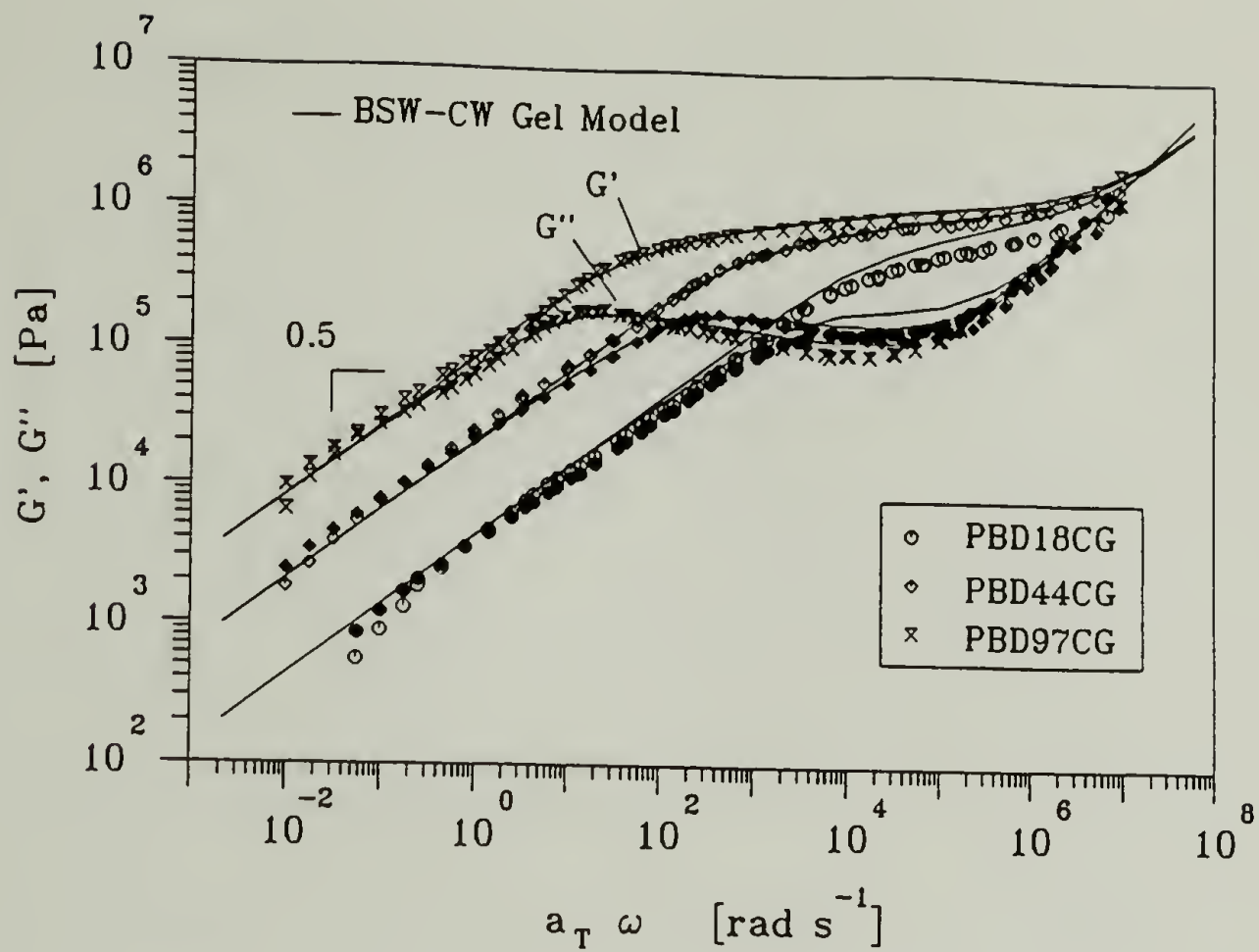


Figure 6.20 Dynamic moduli calculated with the BSW-CW gel model spectra in figure 6.19 compared to experimental data of stopped samples near the critical gel point. $T_{ref}=28^{\circ}\text{C}$.

Table 6.1 Parameters for the BSW-CW gel model.

BSW-CW Parameter	Parameter Value
G_N^0 [Pa]	1.20 E+6
A	0.52
n_c	0.23
n_g	0.73
n	0.5
λ_c [s]	2.31 E-7
M_c [g/mole]	2714
z	3.51

From this relation, λ_0 is given by the longest relaxation time of the precursor, $\lambda_{p,d}$. G_0 is therefore given by

$$G_0 = An_e G_N^0 \Gamma(n). \quad (6.13)$$

By using the parameters given in table 6.1 with a value of $n=0.5$, G_0 is calculated to be $2.55 \text{ E}+5 \text{ Pa}$. Figure 6.21 shows that $G_0 = 2.55 \text{ E}+5 \text{ Pa}$ is indeed the upper limit of the power law relaxation behavior of stopped samples near the critical gel point. A result of equation 6.13 is that the gel strength becomes

$$S = An_e G_N^0 \Gamma(n) \lambda_{p,d}^n \quad (6.14)$$

and $G(t)$ becomes

$$G(t) = An_e G_N^0 \Gamma(n) \left(\frac{t}{\lambda_{p,d}} \right)^{-n}. \quad (6.15)$$

From this analysis it has been found that the upper limit of critical gel behavior for entangled polymers is determined by a function of the plateau modulus and the longest relaxation time of the precursor polymer. The upper value of the modulus of the gel power law behavior is given by equation 6.13 which corresponds to the shortest time of the gel power law behavior given by the longest relaxation time of the precursor polymer.

Other results have been reported by those working in the field of branched polymers. Roovers (1984) observed a slope near 0.5 in the terminal zone for H-shaped polystyrenes. Similar results were found for comb shaped (Roovers and Graessley, 1981) and star shaped polystyrenes (Graessley and Roovers, 1979). Theoretical aspects of the relaxation behavior of H-shaped polymers have also been examined (McLeish, 1988).

Rubenstein et al. (1990) theoretically predicted a power law region which occurs above λ_0

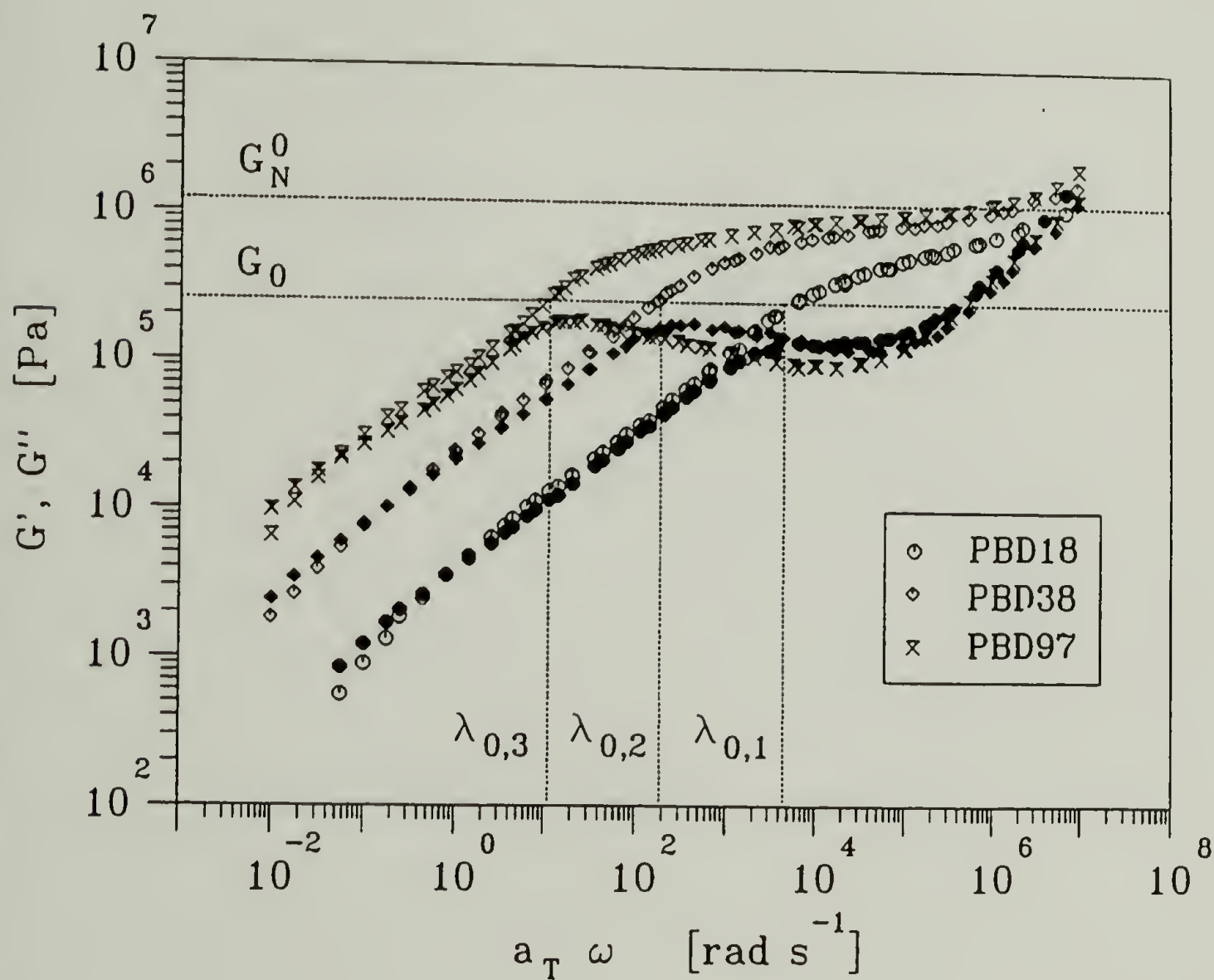


Figure 6.21 The characteristic modulus G_0 marks the upper limit observed for critical gel power law behavior. G_0 is calculated to be $2.55 \text{ E}+5$ Pa with equation 6.13. The corresponding characteristic shortest relaxation times of the power law behavior are given by $\lambda_{0,1}$, $\lambda_{0,2}$, and $\lambda_{0,3}$ for samples PBD18, PBD38 and PBD97 respectively.

for critical gels with entanglements. They predicted an exponent of 0.67. This is slightly higher than the value of n found in this study to be near 0.5.

6.4.2 Precursor Molecular Weight Dependence of S

It has been reported that the precursor molecular weight influences the gel strength (Chambon et al., 1986; Scanlan and Winter, 1991; Izuka et al., 1992). Chambon et al. (1986) found that for three endlinking polypropylene oxide precursors of different molecular weight all below M_c , the gel strength decreased with increasing precursor molecular weight. It was proposed that this result was due to the fact that the crosslink density decreases with increasing precursor molecular weight. This results in a softer gel characterized by a lower value of S . It should be noted however, that for their system, the T_g 's of the gels increased with decreasing precursor molecular weight. Therefore, the results that they found may not be conclusive since experiments were performed on samples that did not have the same glass transition temperature.

This trend was found to be just the opposite as the molecular weight of the precursors becomes high enough to contain physical entanglements. In the study by Scanlan and Winter (1991), two precursor molecular weights were used; one below M_c and the other approximately $5xM_c$. They found that S for the higher molecular weight precursor was about 1 order of magnitude higher than that of the lower molecular weight precursor at the same value of r . This observation was attributed to the presence of physical entanglements.

A similar result was reported by Izuka et al. (1992) who studied gelation for five precursor molecular weights. Two were just below M_c , the other three were slightly above M_c . For all precursors it was found that the gel strength increased with increasing molecular weight at constant r .

The results of this study have also found that the gel strength increases with increasing precursor molecular weight. Qualitatively, this trend agrees with those

reported in the previous studies mentioned (Scanlan and Winter, 1991; Izuka et al., 1992). Remarkably, it was found that the value of S increased with the precursor molecular weight in a well behaved manner that can be described by a scaling relationship. Figure 6.22 shows the values of S determined by CFS and for stopped samples versus precursor molecular weight. The slope of these power laws have experimentally been found to be 1.76 and 1.80 for CFS and stopped sample data respectively. A derivation of an expression has been worked out to describe this scaling relationship.

To begin, the result of equation 6.9 is used in conjunction with the result that n is independent of precursor molecular weight. Therefore, as shown in figure 6.19, $H(\lambda)$ of the critical gels of increasing precursor molecular weight in the terminal zone will be a set of power law spectra with the same slope (i.e. $-n$). From equation 6.9 it is proposed that the CW-spectrum intersects the BSW-spectrum at λ_0 (i.e. $\lambda_{p,d}$). Therefore, the value of H at the intersection point is the same for the CW-spectrum and the BSW-spectrum (see figure 6.17). For critical gels of two different precursor molecular weights, the value of H at the intersection point is

$$An_e G_N^0 = H = \frac{S_1}{\Gamma(n)} \lambda_1^{-n} \quad (6.16)$$

$$An_e G_N^0 = H = \frac{S_2}{\Gamma(n)} \lambda_2^{-n} \quad (6.17)$$

where λ_1 and λ_2 are $\lambda_{p,d}$ of precursors 1 and 2 of with molecular weights of M_1 and M_2 respectively.

From equations 6.16 and 6.17, the relationship between S and $\lambda_{p,d}$ is

$$\frac{S_1}{S_2} = \left(\frac{\lambda_1}{\lambda_2} \right)^n \quad (6.18)$$

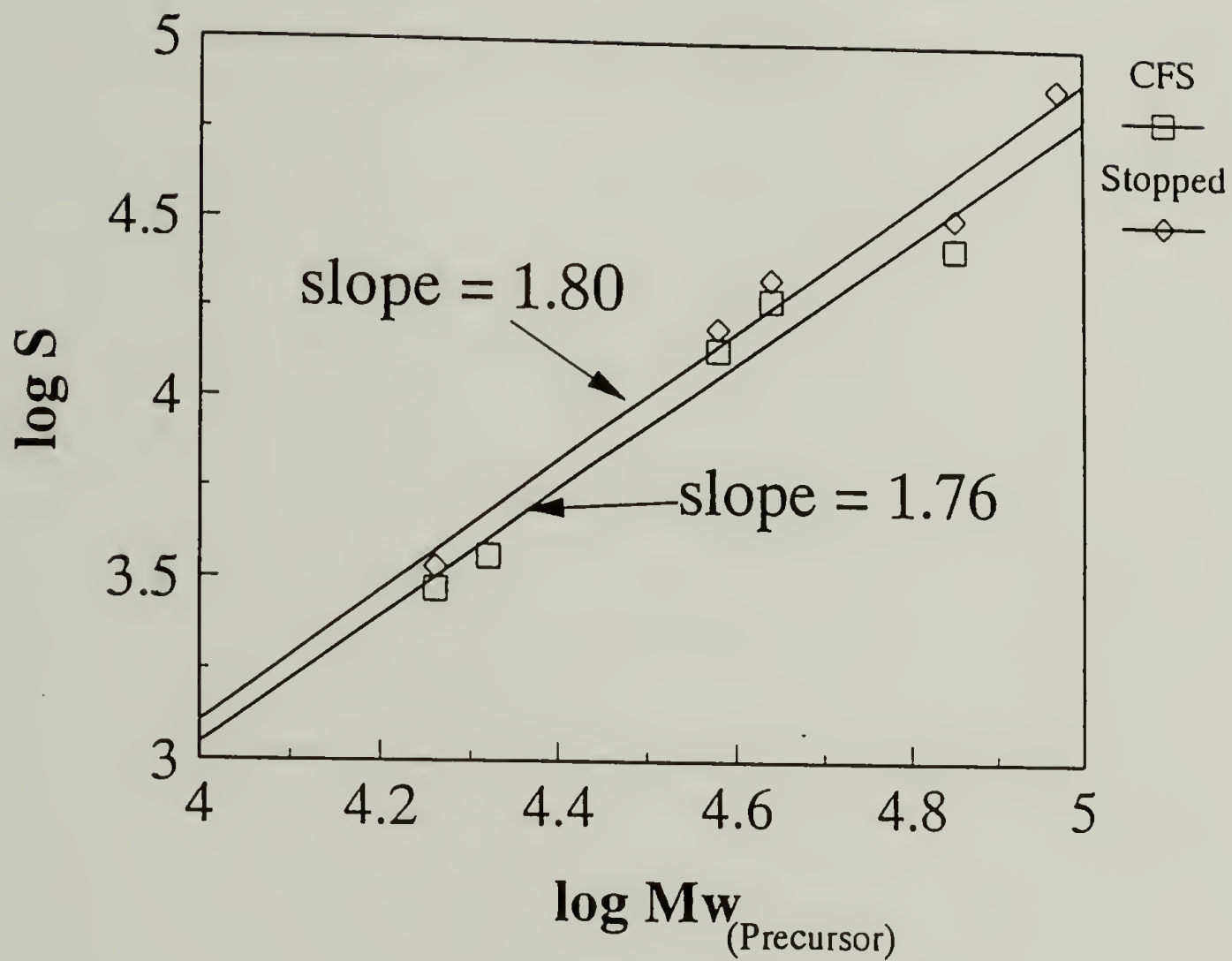


Figure 6.22 Scaling relationship of gel strength (S) with the precursor M_w . The slopes are 1.76 and 1.80 for gel strengths calculated from CFS and stopped sample data respectively.

It is known that $\lambda_{p,d}$ scales with the precursor M_w described by equation 4.16. By substituting 4.16 into equation 6.18 the result is

$$\frac{S_1}{S_2} = \left(\frac{\lambda_c \left(\frac{M_1}{M_c} \right)^z}{\lambda_c \left(\frac{M_2}{M_c} \right)^z} \right)^n \quad (6.19)$$

which reduces to

$$\frac{S_1}{S_2} = \left(\frac{M_1}{M_2} \right)^{zn} \quad (6.20)$$

or more generally to

$$S \sim M^{zn}. \quad (6.21)$$

A value of n equal to 0.5 and z equal to 3.51 will give a predicted exponent of 1.76 which is in excellent agreement with our experimental results found of 1.76 and 1.80 for CFS and stopped sample data respectively.

6.5 Mechanical Properties of Fully Cured Networks

6.5.1 Experimental Procedure

Fully cured samples were prepared by allowing samples used for CFS analysis to react for a total of 8 to 12 hours at 28°C under an air atmosphere. At this point, the reaction was considered to have reached its highest possible conversion ($p \rightarrow 1$) as was evidenced by the constant dynamic modulus as a function of reaction time. The complex modulus of the fully cured material was measured from 0.01 to 100 rad/s at 28°C with < 3% strain. The T_g of fully cured samples with balanced stoichiometry were measured by DSC.

6.5.2 Fully Cured Networks at Balanced Stoichiometry ($r=1$)

Figure 6.23 shows G^* for fully cured samples at balanced stoichiometry of all PBD samples except PBD20. The value of G^* at 0.01 rad/s was taken to be the equilibrium modulus, G_e . All of the samples have been found to have close to the same equilibrium modulus, and T_g within two degrees. The results are given in table 6.2. The T_g of the fully cured samples were found to increase by an average of 14K from the T_g of the precursor and crosslinker mixture. The increase in T_g is due to the fact that molecular motion is restricted by the chemical crosslinks (Ferry, 1980).

The fact that the equilibrium moduli are practically the same for the five precursor molecular weights suggests that they all have the same crosslink density as shown by classical rubber elasticity theory (Ferry, 1980)

$$G_e = \frac{\rho RT}{M_{\text{chem}}} \quad (6.22)$$

where ρ is the density of the crosslinked rubber and M_{chem} is the molecular weight between chemical crosslinks. Since all of the precursors have the same concentration of reactive sites ($\sim 8\%$ vinyl units) per chain, it is expected that they all would have the same crosslink density at fully extent of reaction and thus the same value of G_e . In the case of crosslinking by vulcanization, this is what should occur. However, in the case of endlinking, M_{chem} is determined by the precursor M_w and thus G_e would decrease with increasing molecular weight.

This is useful information to know for reactive polymer processing. By using a vulcanization crosslinking mechanism, a material can be made with the same G_e and T_g by using either a low or high molecular weight precursor. However, the lower molecular weight polymer would be easier to process before crosslinking due to the fact that its viscosity is lower.

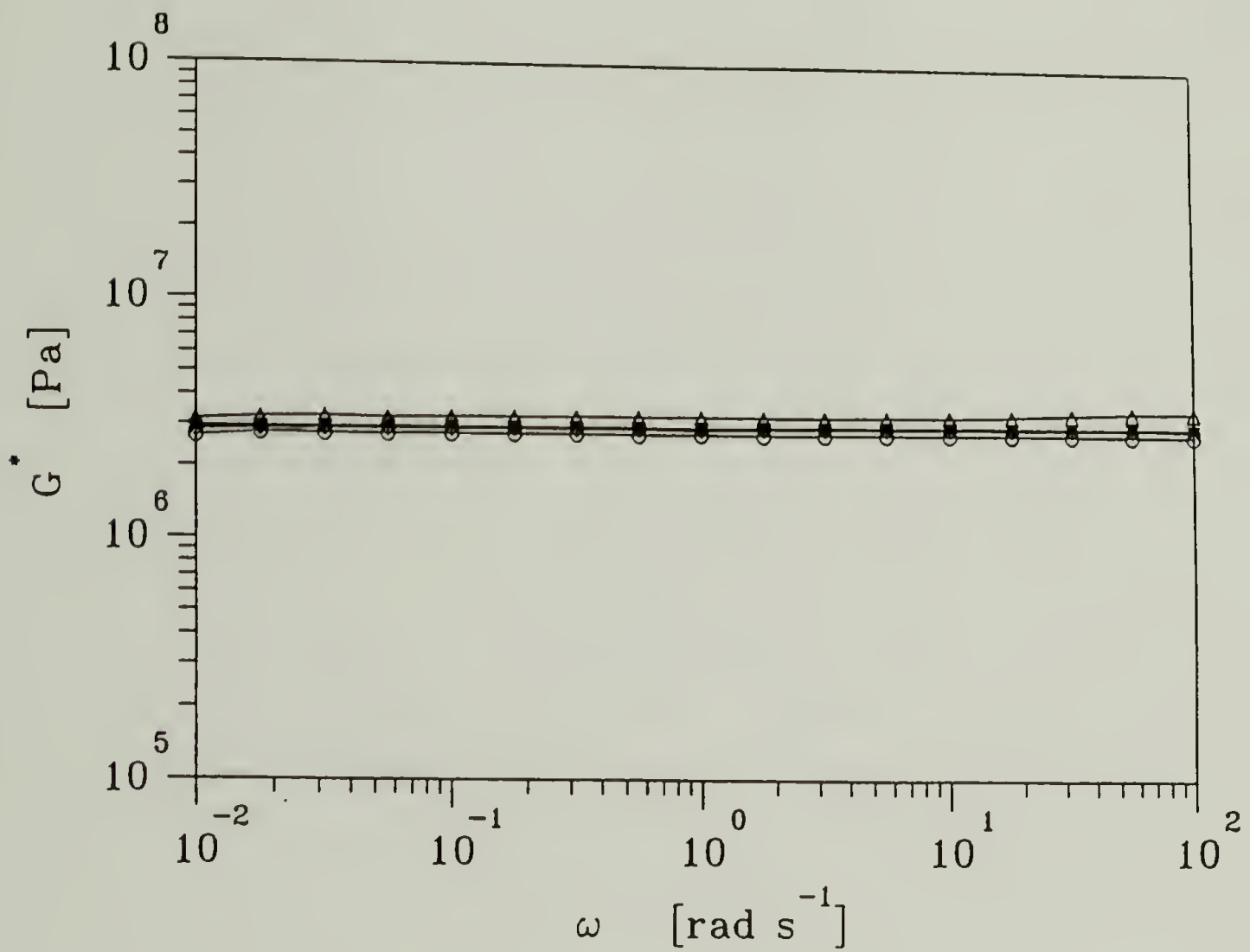


Figure 6.23 Complex modulus of fully cured samples PBD18, PBD38, PBD44, PBD70, and PBD97 at balanced stoichiometry. Measurements were made at 28°C.

Table 6.2 Final network properties of fully cured samples with balanced stoichiometry ($r=1$). G_c is taken as $G^*(\omega)$ at 0.01 rad/s. $G^*(\omega)$ measurements were made at 28°C.

Fully Cured Sample	G_c [MPa]	T_g (°C)
PBD18	2.73	-81
PBD38	3.24	-80
PBD44	2.87	-80
PBD70	2.96	-80
PBD97	2.93	-79

The value of G^* was observed to be approximately $2G_N^0$ of the uncrosslinked precursor. This is due to the presence of trapped entanglements (Ferry, 1980). The effect of trapped entanglements in polybutadiene networks cured by hydrosilation has been investigated by Aranguren and Macosko (1988). Earlier work on trapped entanglements in polybutadiene systems cured by peroxides (Maekawa et al., 1965; Ferry et al., 1964; Dickie and Ferry, 1966) and radiation (Dossin and Graessley, 1979) have been reported.

6.5.3 Fully Cured Networks at Imbalanced Stoichiometry ($r \neq 1$)

The complex modulus of fully cured samples was measured for values of r in the range of $0.1 < r < 3.0$. The results are given in table 6.3. Figure 6.24 shows the complex modulus of fully cured samples of PBD18 at increasing values of r . The values of G_e for PBD 18 are shown graphically in figure 6.25. The maximum value of G_e was found to be at $r=1.1$ which is slightly higher than the value of $r=1$ expected if no competing side reactions are present. Aranguren and Macosko (1988) also found a maximum value of G_e close to $r=1$ for the hydrosilation cure of polybutadiene. The maximum value of G_e for $r=1$ was predicted by computer simulation (Leung and Eichinger, 1984) for endlinking systems. Others have observed that the maximum elasticity of fully crosslinked networks is obtained at values of stoichiometry slightly higher than unity (Macosko and Benjamin, 1981; Macosko and Saam, 1987; Chambon and Winter, 1987; Venkataraman et al., 1989; Izuka et al., 1992). This discrepancy can be attributed to the fact that the chemical reaction is not ideal. Predictions of mechanical properties with stoichiometric ratio do not take into account wasteful side reactions which cause a decrease in the amount of effective elastic junctions created.

The asymmetric shape of the curve of G_e with r shown in figure 6.25 has also been observed by others (Macosko and Benjamin, 1981; Chambon and Winter, 1987; Venkataraman et al. 1989, ; Izuka et al., 1992). This pattern qualitatively agrees with the

Table 6.3 Equilibrium modulus (G_e) of fully cured PBD samples as a function of stoichiometric ratio (r). G_e is taken as $G^*(\omega)$ at 0.01 rad/s. Measurements were made at 28°C.

Sample	r	G_e [Pa]
PBD18	0.10	7.56 E+4
	0.25	6.03 E+5
	0.50	1.30 E+6
	0.80	1.75 E+6
	1.0	2.73 E+6
	1.1	2.90 E+6
	1.1	2.90 E+6
	1.5	2.90 E+6
	2.0	1.58 E+6
	3.0	1.36 E+6
PBD38	0.25	1.21 E+6
	0.50	1.85 E+6
	0.80	2.82 E+6
	1.0	3.24 E+6
	2.0	1.58 E+6
	3.0	1.38 E+6
PBD44	0.25	1.18 E+6
	0.50	1.83 E+6
	1.0	2.87 E+6
PBD70	0.5	2.11 E+6
	1.0	2.96 E+6
PBD97	0.5	2.25 E+6
	1.0	2.93 E+6

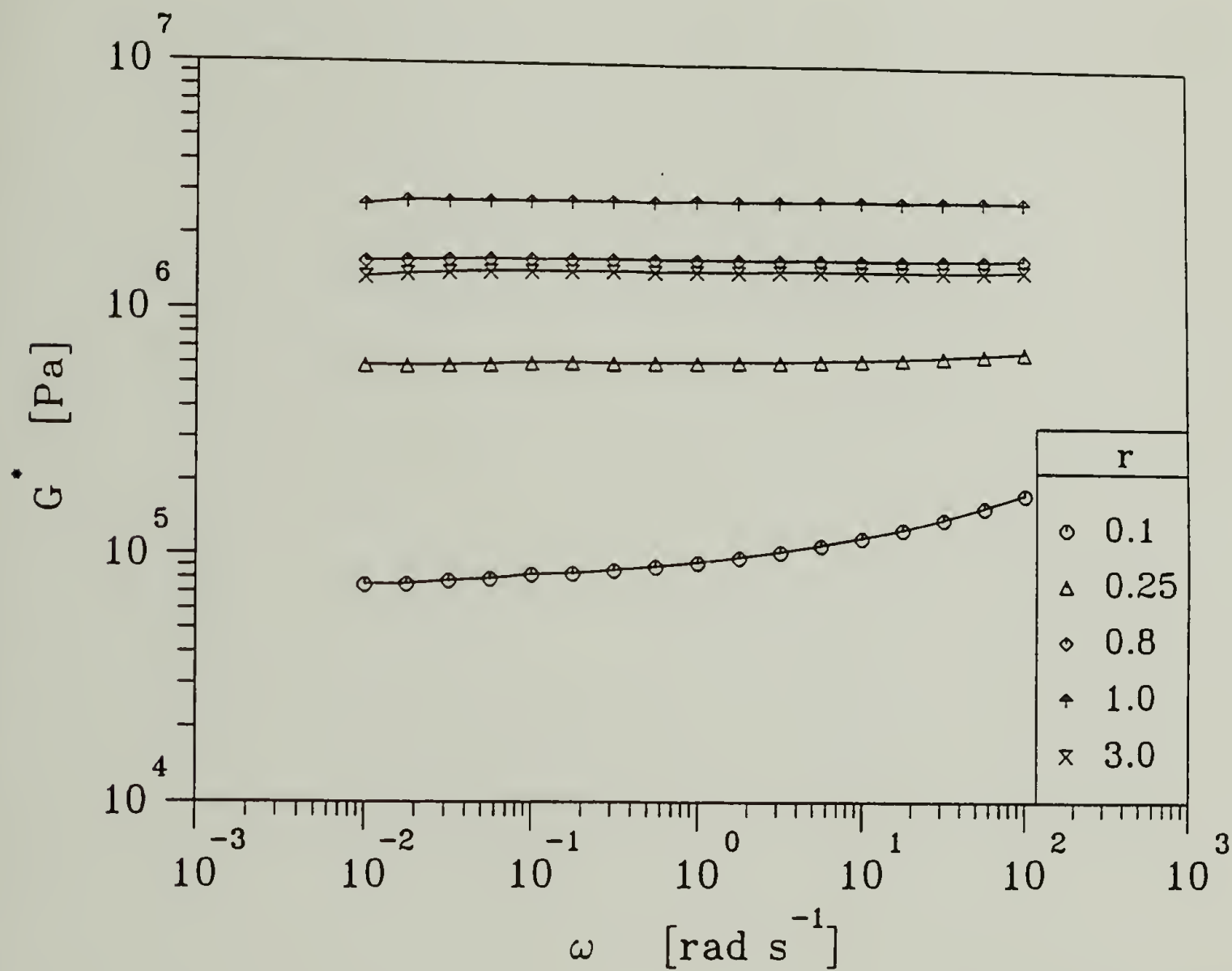


Figure 6.24 Complex modulus (G^*) of fully cured PBD18 samples at different values of stoichiometric ratio (r). Measurements were made at 28°C .

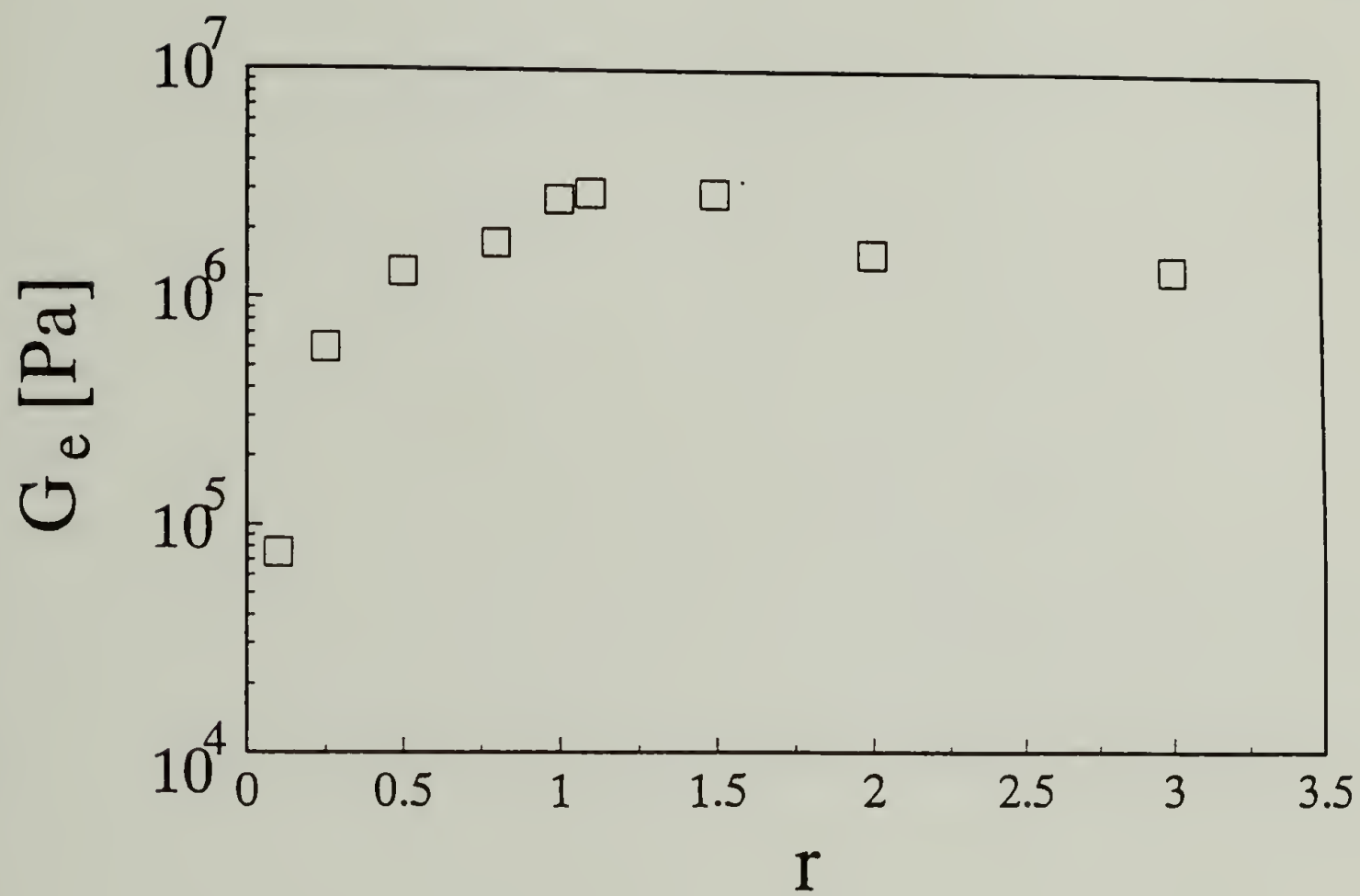


Figure 6.25 Equilibrium modulus (G_e) of fully cured PBD18 as a function of stoichiometric ratio (r). G_e is taken as G^* at 0.01 rad/s.

results of Leung and Eichinger (1984) who proposed that crosslinker deficient mixtures produce less effective network structures than networks made from mixtures with excess crosslinker.

6.5.4 Bubble Formations in Fully Cured Samples

There was some concern about what the effect the presence of many tiny air bubbles ($\sim 5\text{-}10\mu\text{m}$) found in the fully cured materials would be on G_e . The air bubbles were introduced by "whipping" air into the sample when stirring the precursor and crosslinker during the mixing stage. Due to the viscosity of the sample, the air bubbles can not leave the sample easily and as the viscosity of the material increases during reaction, it becomes even more difficult for the air bubbles to leave the sample. Ultimately, past the gel point, the air bubbles get locked into the structure. It was thought that the air bubbles would reduce the modulus of the sample in the same manner that a foam does.

To test the effect of the bubbles on the modulus, two samples of fully cured PBD18 samples were prepared without bubbles. Samples without bubbles were prepared by mixing $1/3$ the amount of catalyst used for all other experiments with the precursor. Vacuum stripping was used to remove the toluene as described in chapter 2. After the first vacuum stripping, a stoichiometric amount of crosslinker was added and mixed for 6 minutes. The sample was vacuum stripped again, this time at room temperature, to draw out the air bubbles. The reduced amount of catalyst, slowed the reaction down enough so that the sample would have time to be vacuum stripped for the second time without going through the gel point. Once the bubbles were removed, the sample was loaded into the rheometer, without any further mixing, for final curing. The complex modulus of the fully cured sample was then measured and compared to the modulus of a fully cured sample with bubbles (see figure 6.26).

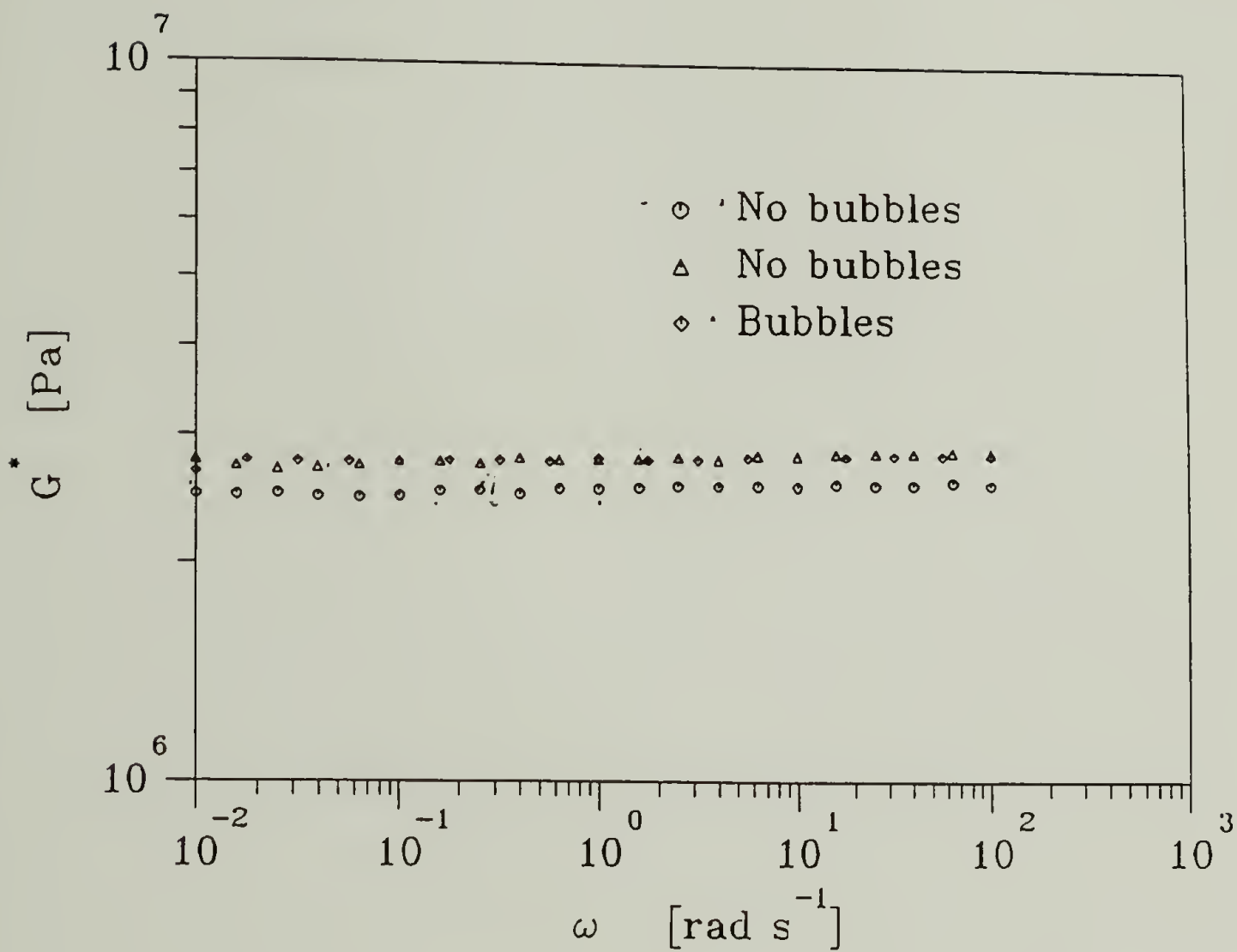


Figure 6.26 Complex modulus (G^*) for fully cured samples with and without tiny air bubbles. Measurements were made 28°C with balanced stoichiometry.

From the data it was observed that the concentration and size of the air bubbles present did not effect the modulus of the fully cured samples. Air bubbles may effect the shear modulus of the fully cured materials however, the small error that they cause appears to fall within the experimental scatter and error limits in the reproducibility of measurements made on fully cured samples.

CHAPTER 7

KINETIC STUDY OF GELATION

In chapters 5 and 6, the critical gel parameters S and n were examined in detail. It is the gel strength and the relaxation exponent that define the mechanical behavior of the critical gel. However, when working with crosslinking materials it may also be necessary to know the time it takes to reach the critical gel point in addition to the mechanical properties of the material at the liquid-solid transition.

For a variety of systems, many factors can influence the rate of crosslinking such as temperature, amount of catalyst or crosslinking agent, radiation dosage, chemical inhibitors, etc. In this study, it was found that the rate of gelation was also affected by the composition of the precursor materials. Results will be presented that show specifically how the gel time is affected by the precursor composition. A simple kinetic model will be proposed that is able to predict the critical gel time for isothermal gelation of polybutadiene at various temperatures as a function of stoichiometric ratio and functionality of the polybutadiene chain.

7.1 Experimental Procedure

7.1.1 Rheological Measurements

The gel time was measured with the CFS technique. Samples were prepared as described in section 2.5. Once the desired amount of crosslinker was added, the samples were mixed at ambient conditions for 6 minutes and then loaded in between the preheated 25mm fixed plates of the RDS 7700. Samples were cured at 28°C, 34°C, and 40°C. A nitrogen atmosphere was used for the experiments at 34°C and 40°C and air for experiments at 28°C. Cure temperatures in the rheometer were controlled to within $\pm 0.5^\circ\text{K}$. The time of loading and mixing was kept constant at 7min and 30sec for cure

temperatures of 34°C and 40°C. For experiments performed at a cure temperature of 28°C, the mixing and loading time was 10 minutes.

Since temperature affects the rate of reaction, the ambient temperature of the room is important to take into consideration during the mixing phase. If the room temperature on two separate days differs greatly by e.g. 5K, then the measured gel time can be quite different for the two runs even if the composition of the samples is identical. To minimize this effect, experiments were performed over a period of time in which the room temperature did not vary appreciably. For samples cured at 34°C and 40°C, the room temperature was $25.5 \pm 1.5^\circ\text{C}$. For samples cured at 28°C the room temperature was $21.5 \pm 1.5^\circ\text{C}$. Gel time data were not accepted for experiments which were at room temperatures outside this 1.5K temperature tolerance.

The reproducibility of measured gel times for samples with identical stoichiometry and precursor molecular weight at 28°C was found to be within 100 s. The average gel time was reported when more than one measurement was made for a particular precursor composition. More sophisticated sample preparation techniques that allow better control of the mixing temperature may have to be devised in the future if more precise kinetic results are needed.

7.1.2 F.T.i.r. Measurements

F.T.i.r. spectroscopy was used to measure the curing kinetics of PBD18. F.T.i.r. measurements were made on an IBM 98 Fourier Transform infrared spectrometer. Samples were prepared for F.T.i.r measurements the same as for CFS measurements. After mixing for 6 minutes, the reacting mixture was placed between KBR plates and then placed in the i.r. beam to react at ambient conditions of the F.T.i.r. sample compartment. More sophisticated measuring techniques should be used if measurements need to be conducted at a precise temperature (Soltero and Gonzalez-Romero, 1988; Venkataraman et al., 1989). However, in this case, F.T.i.r. was used primarily to determine the order of

the hydrosilation reaction. Therefore, the sample was allowed to cure at the ambient conditions of the sample compartment since the order of the reaction should not be dependent on the temperature that the sample is cured. The temperature of the compartment was measured to be $25 \pm 1^\circ\text{C}$. The compartment was constantly purged of H_2O vapor and CO_2 with dry air. The curing kinetics of PBD18 with stoichiometric ratios of 1.0 and 0.5 were measured. F.T.i.r. measurements were made up to 125min. Data was collected and stored in units of absorbance approximately every 3min to 5min for the first hour then every 7min to 10min for the next hour. 32 scans were collected at each time interval. It only required 20 seconds to take 32 scans. Therefore the amount of chemical change that took place during a single F.T.i.r. measurement is negligible and will not cause significant error in the data, i.e. $N_{\text{mu}} \ll 1$. The recorded time of the measurement was taken at the 16th scan. A stopwatch was used to measure the total reaction time (t_r).

Data that was taken early on in the reaction had interference from the absorbance of water vapor since all of the moisture was not completely purged at the time of initial measurements. These interfering peaks were later subtracted out of the spectra using LabCalc before quantitative analysis was performed.

7.2 Effect of Precursor Composition on the Gel Time

7.2.1 Effect of Stoichiometric Ratio on t_c

The gel time was found to be strongly affected by the stoichiometric ratio. Figure 7.1 shows the evolution of the dynamic moduli at 3.16 rad/s for PBD38 at $r=0.5$, 1.0, and 3.0 cured at 28°C . The value of n for all three samples are 0.45, 0.45, and 0.47 respectively. Therefore, the instant of the crossover of G' , G'' occurs very close to t_c . It can be seen that as the silane content is increased from an $r=0.5$ to $r=3.0$, the value of t_c decreases dramatically. Such a trend was observed for all precursor molecular

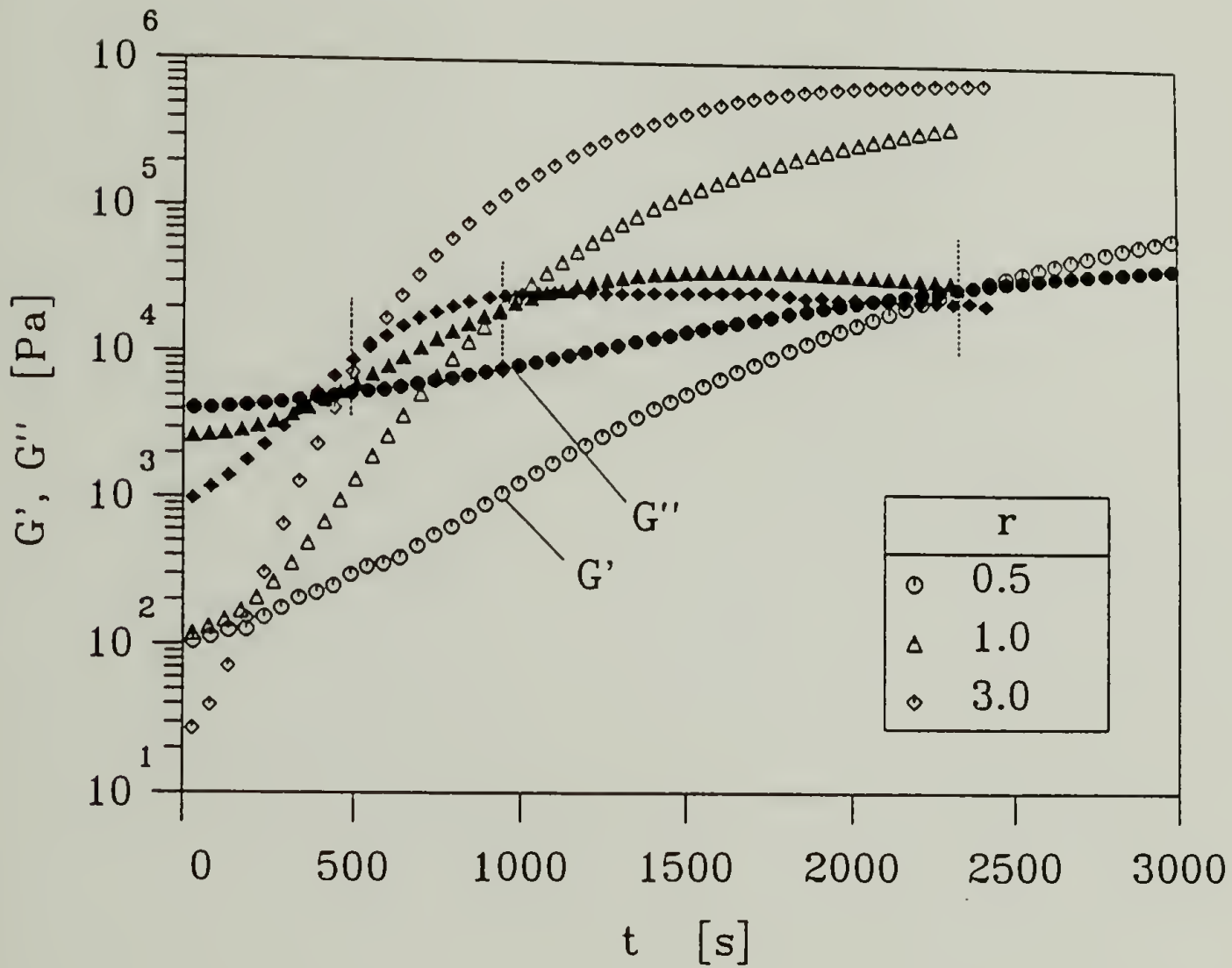


Figure 7.1 Evolution of the dynamic moduli at 3.16 rad/s during gelation for sample PBD38 at 28°C for three values of stoichiometric ratio (r). Filled symbols represent G'' . The approximate gel times (t_g) are indicated by the dotted hash marks.

weights. The cure temperature, catalyst concentration, and time of mixing and loading the sample into the rheometer for a single precursor molecular weight were kept constant.

7.2.2 Effect of Functionality on t_c

The precursor functionality was also found to affect the gel time. Figure 7.2 shows the evolution of the dynamic moduli at 3.16 rad/s for samples PBD18, PBD38, and PBD70 cured at 28°C with balanced stoichiometry. Since the values of n for these samples were found to be 0.49, 0.46 and 0.48 respectively the value of t_c is very close to the crossover point in G' , G'' during the cure cycle. From the data it is evident that as the functionality of the precursor sample is increased, the value of t_c decreases. The catalyst concentration, cure temperature, and mixing and loading time of the reacting sample were kept constant.

7.2.3 Branching Theory Prediction

As shown in figures 7.1 and 7.2 the gel time is significantly influenced by the composition of the precursor materials. One can therefore change the time it takes to reach the gel point simply by changing the stoichiometric ratio, the functionality of the precursor polymer, or if desired, a combination of both parameters. The qualitative trend in the value of t_c with the stoichiometry and the functionality of the precursor can be described by using the branching theory of Flory (1941, 1953) and Stockmayer (1943).

For the crosslinking of two species, the result of the Flory-Stockmayer branching theory predicts the critical extent of reaction of silane needed to reach the gel point as a function of stoichiometry, and functionality of the polybutadiene (f) as

$$P_{c, SiH} = \frac{1}{\sqrt{r(f-1)}} \quad (7.1)$$

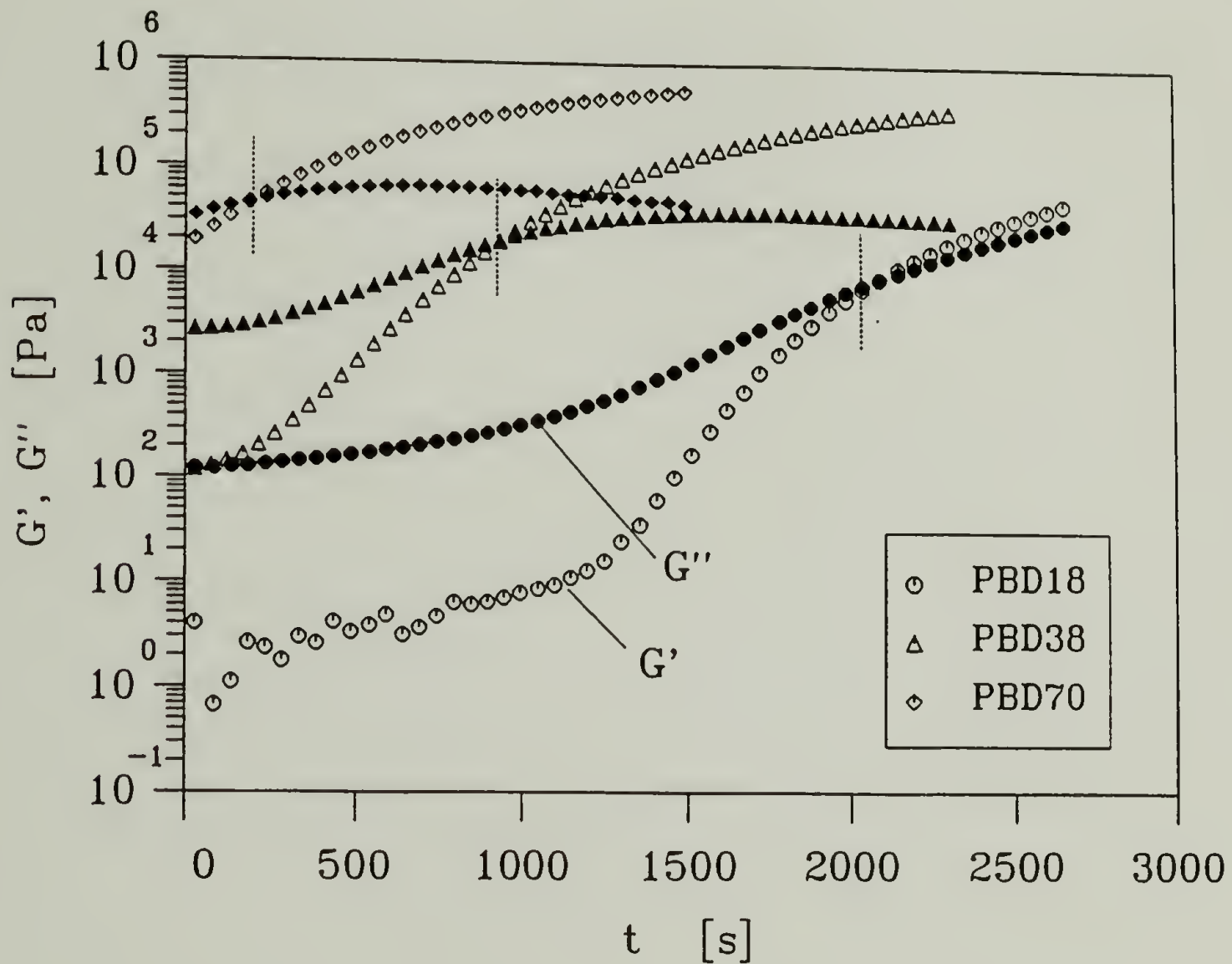


Figure 7.2 Evolution of the dynamic moduli at 3.16 rad/s during gelation at balanced stoichiometry for three precursor molecular weights. Filled symbols represent G'' . The approximate gel times (t_g) are indicated by the dotted hash marks.

For the two cases examined, either constant functionality or constant stoichiometry, equation 7.1 can be used to describe the trend in the gel time that was observed experimentally in the following manner.

Case 1: Variable r , Constant f

For the first case, the functionality is kept constant and the stoichiometric ratio was changed. From equation 7.1, $p_{c,SiH}$ is decreased as r is increased by increasing the amount of crosslinker. Therefore, if the other factors that could influence the rate of gelation are kept constant, such as the amount of catalyst and the cure temperature, t_c should occur at shorter times as r is increases as seen in figure 7.1.

Case 2: Variable f , Constant r

In the second case, the stoichiometric ratio is kept constant and the functionality was increased by increasing the precursor molecular weight. From equation 7.1, $p_{c,SiH}$ is decreased if f is increased and r is kept constant. Therefore, by the same argument made for case 1, t_c would be expected to decrease as f increases as seen in figure 7.2. Arellano et al. (1990) examined the kinetics of a crosslinking epoxy system. They observed similar trends in the gel times as a function of stoichiometry and functionality.

7.3 Simple Kinetic Model to Predict the Gel Time

In the previous section, it was found that branching theory could be used to qualitatively account for the trend observed in the gel time as a function of f and r . Though this finding is quite useful, it currently lacks the ability to quantitatively predict the gel time. In this section, these results will be expanded on by combining branching theory with simple kinetics to derive a model that will be able to predict the gel time quantitatively as a function of f and r .

7.3.2 Derivation of the Kinetic Model to Predict the Gel Time

To derive the kinetic model, the consumption of silane is assumed to be first order and given by

$$-\frac{d[\text{SiH}]}{dt} = k[\text{Pt}][\text{SiH}] \quad (7.6)$$

where $[\text{Pt}]$ is the concentration of platinum and k is the rate constant. The extent of reaction is defined as

$$p = \frac{[\text{SiH}]_0 - [\text{SiH}]}{[\text{SiH}]_0} \quad (7.7)$$

where $[\text{SiH}]_0$ is the initial concentration of silane at time $t=0$ and $[\text{SiH}]$ is the concentration of silane at some time t during the reaction. Substitution of equation 7.7 into equation 7.6 results in an expression for the rate of conversion

$$-\frac{dp}{dt} = \bar{k}(1-p) \quad (7.8)$$

where $\bar{k} = k[\text{Pt}]$. The same result was obtained to describe the kinetics of the hydrosilation cure of polydimethylsiloxane (Macosko and Lee, 1985; Soltero and Gonzalez-Romero, 1988). Equation 7.8 was derived assuming that the hydrosilation is a simple bimolecular reaction at the platinum sites with one rate constant k as illustrated in figure 2.6. The model presented here is expressed in terms of the rate of consumption of silane since the conversion of silane will be directly measured by F.T.i.r.

The equation above can be evaluated for the isothermal experiment after having loaded the sample. The isothermal experiment starts with a sample which already has reached an extent p_i which affects the gel time t_c . The value of p_i will be estimated later.

In the initial stage of the kinetic experiment, the precursor, catalyst, and crosslinker are mixed at ambient conditions before being loaded into the rheometer for CFS kinetic

gel time measurement. During this mixing and loading stage, the sample is reacting. Therefore, the extent of reaction at the beginning of the kinetic CFS measurement is not zero. The CFS measurement on the reacting sample begins at the reaction time $t_r = t_j$ at an initial extent of reaction $p = p_j$. It is noted here that the reaction time (t_r) and CFS time (t_{CFS}) are not the same. t_{CFS} is given by $t_r - t_j$. The time of gelation measured by CFS is given as $t_{gel,CFS} = t_c - t_j$. A schematic representation of the cure cycle of the kinetic experiment is given in figure 7.3

Equation 7.8 can be integrated in the vicinity of the gel point from p to p_c at t to t_c respectively

$$-\int_p^{p_c} \frac{dp}{1-p} = \int_t^{t_c} \bar{k} dt. \quad (7.9)$$

Evaluation of equation 7.9 gives

$$\ln\left(\frac{1-p_c}{1-p}\right) = -\bar{k} (t_c - t). \quad (7.10)$$

Rearrangement of 7.10 gives

$$t_c - t = -\frac{1}{\bar{k}} [\ln(1-p_c) - \ln(1-p)]. \quad (7.11)$$

Substituting 7.1 into 7.11 gives an expression of the gel time in terms of the stoichiometric ratio and functionality of polybutadiene

$$t_c - t = -\frac{1}{\bar{k}} \left[\ln\left(1 - \frac{1}{\sqrt{r(f-1)}}\right) - \ln(1-p) \right]. \quad (7.12)$$

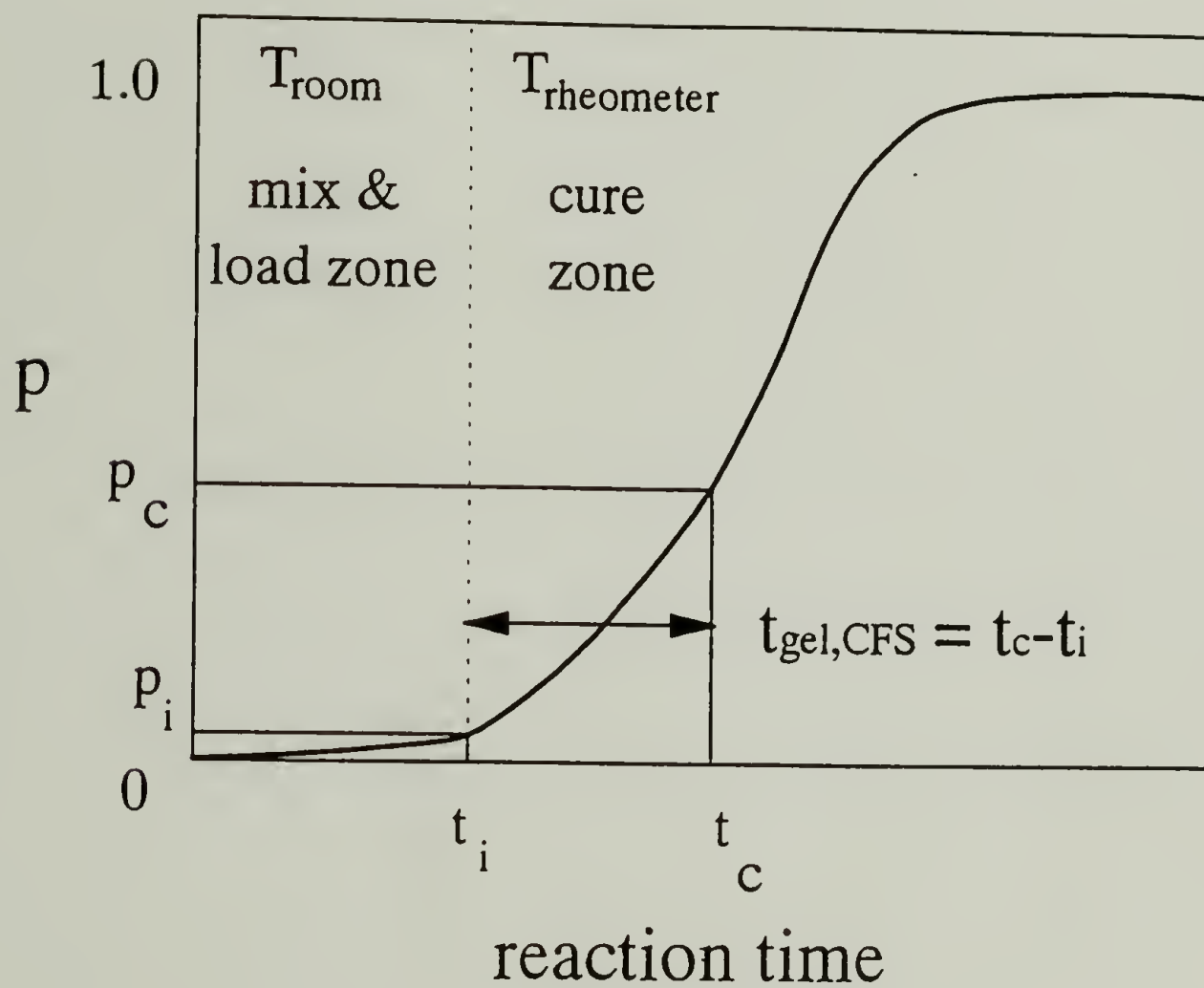


Figure 7.3 Schematic of kinetic experiment showing the extent of reaction (p) versus reaction time (t_r). p and t_r are given initially as p_i and t_i at the beginning of the CFS measurement in the cure zone with temperature of the rheometer ($T_{\text{rheometer}}$).

Since the measured gel time by CFS is $t_c - t_i$, the integration limits of equation 7.9 can be set from t_i to t_c and p_i to p_c to give

$$t_{\text{gel, CFS}} = t_c - t_i = -\frac{1}{\bar{k}} \left[\ln \left(1 - \frac{1}{\sqrt{r(f-1)}} \right) - \ln(1 - p_i) \right]. \quad (7.13)$$

A similar expression can be derived to predict the gel time in which the reaction is not first order in silane. Initially equation 7.6 can be modified for an n^{th} order reaction

$$-\frac{d[\text{SiH}]}{dt} = k_p [\text{Pt}] [\text{SiH}]^n. \quad (7.14)$$

By substituting equation 7.7 into 7.14 the result is

$$-\frac{dp}{dt} = \bar{k} [\text{SiH}]_0^{n-1} (1-p)^n \quad (7.15)$$

where $[\text{SiH}]_0$ is the initial concentration of silane and n is the reaction order. For a first order reaction, 7.15 simplifies to 7.8. 7.15 is integrated over the same limits as in 7.9.

$$\int_p^{p_c} \frac{dp}{(1-p)^n} = \int_t^{t_c} \bar{k} [\text{SiH}]_0^{n-1} dt \quad (7.16)$$

which results in

$$t_c - t = -\frac{1}{\bar{k} [\text{SiH}]_0^{n-1}} \left[\frac{(1-p)^{1-n} - (1-p_c)^{1-n}}{1-n} \right]. \quad (7.17)$$

Substituting 7.2 into 7.17 gives

$$t_c - t = -\frac{1}{\bar{k} [\text{SiH}]_0^{n-1}} \left[\frac{(1-p)^{1-n} - \left(1 - \frac{1}{\sqrt{r(f-1)}} \right)^{1-n}}{1-n} \right]. \quad (7.18)$$

7.3.3 Evaluation of Kinetic Model Parameters

To test the assumption that the rate of reaction of silane was of first order, F.T.i.r. was used to directly measure the conversion of silane during gelation. This can be done relatively easily since the silane appears as a well isolated peak at 2116cm^{-1} and there is no interference by any other absorption bands from either the rest of the crosslinker structure or the polybutadiene. F.T.i.r. has been used by others to monitor the evolution of silane conversion during hydrosilation (Chalk and Harrod, 1965; Miron et al., 1973; Friedmann and Brossas, 1985; Venkataraman et al., 1989). F.T.i.r. data in figure 7.4 shows the decrease in the silane peak during the crosslinking of sample PBD18.

In order to make quantitative measurements with F.T.i.r. a calibration curve had to be made to determine whether Beer's law (Colthup, 1990) was valid for the concentrations of silane used. To do this, four mixtures of silane and PBD18 were made with stoichiometric ratios of $r=1.0, 0.75, 0.5,$ and 0.25 . Peak heights were measured to determine the amount of silane present. The peak height of silane was normalized with an internal reference peak at 1436cm^{-1} . The reference peak for normalization is chosen to account for any change in the sample thickness. Since spacers were not used, the sample thickness varied for each measurement thus causing the absorbance to increase with sample thickness. By using an internal reference peak for normalization, the problem of sample thickness is removed. The peak at 1436cm^{-1} was chosen for an internal standard because it was found to remain at a constant height (i.e. changed by less than 5%) during the reaction. Figure 7.5 shows the plot of normalized silane peak heights versus r . The linear dependence of the normalized silane peak height with r signifies that Beer's law holds and therefore the concentration of silane is directly proportional to the normalized peak heights.

The extent of reaction was calculated with equation 7.7. Some problems were encountered when the initial silane concentration was taken from the calibration curve. It appeared that if $[\text{SiH}]_0$ is not precisely known, then a shift in the p vs. t curve was

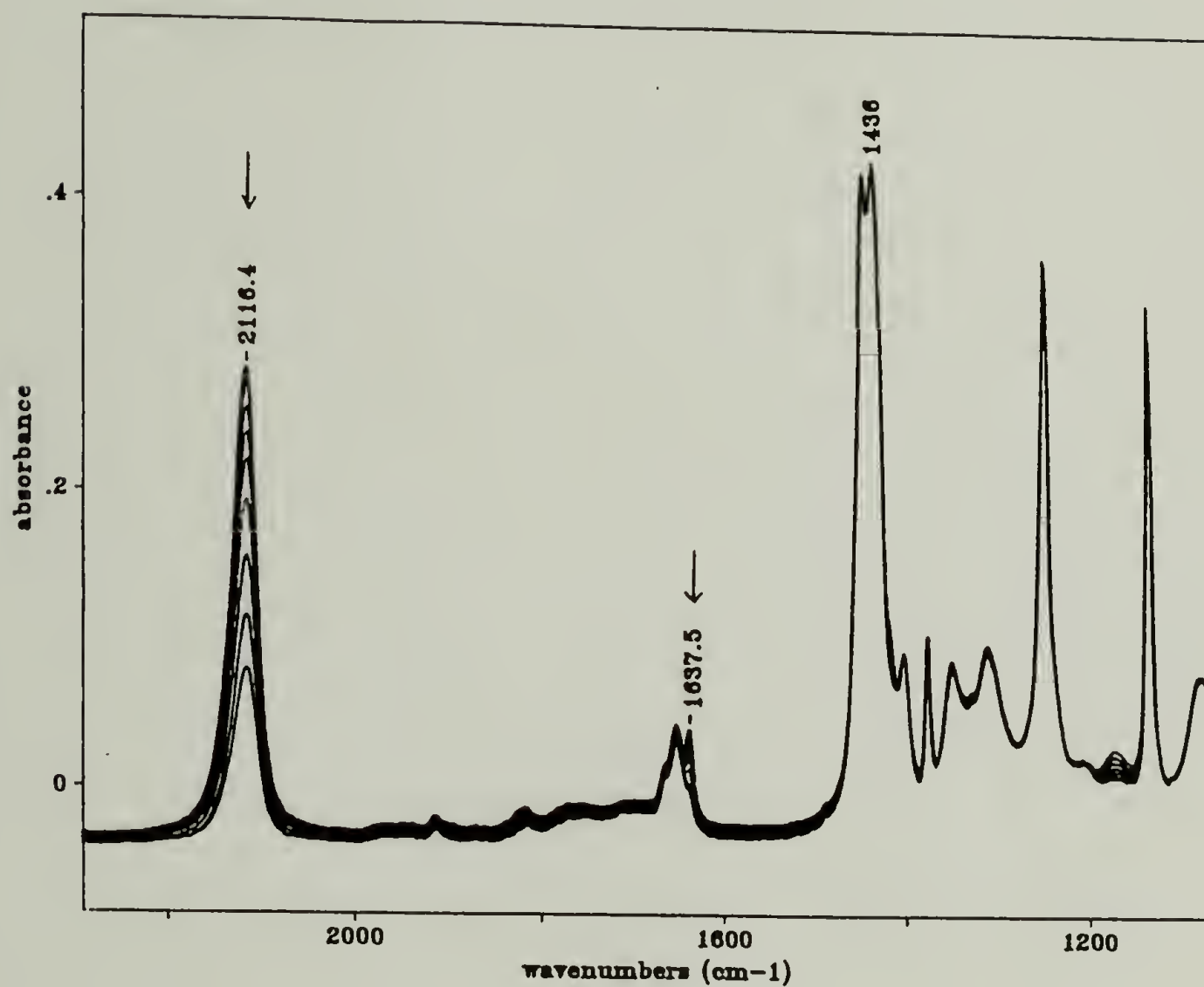


Figure 7.4 F.T.i.r. kinetic data at $25 \pm 1^\circ\text{C}$ showing the conversion of silane at 2116 cm^{-1} of PBD18 with stoichiometric amount of silane. The peak at 1436 cm^{-1} was used as an internal reference peak.

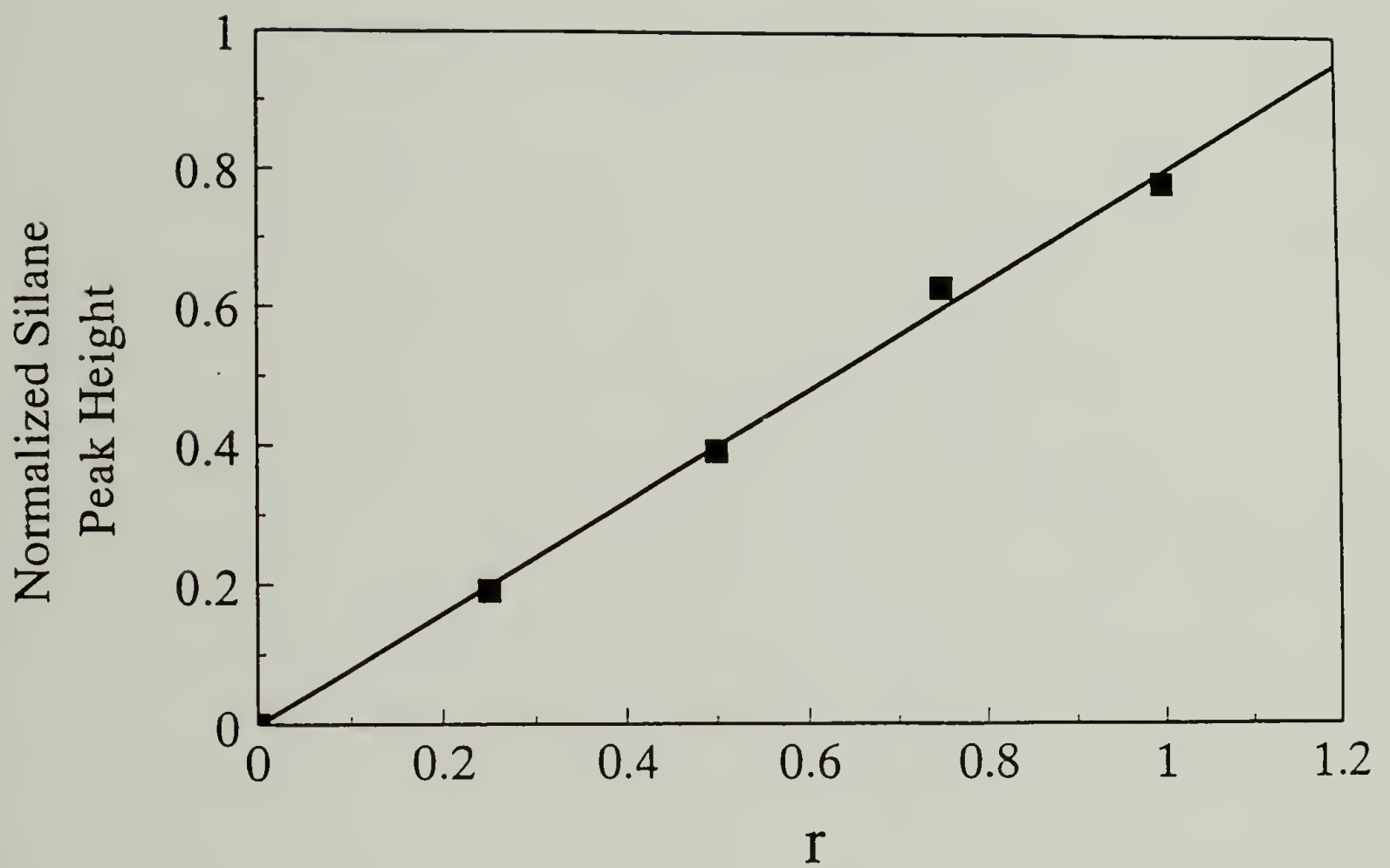


Figure 7.5 F.T.i.r calibration curved showing the linear dependence of the normalized silane peak intensity versus stoichiometric ratio (r).

observed. During the analysis, negative extents of reaction were actually calculated for the earliest measurements due to an inaccurate value of $[\text{SiH}]_0$ used. The error is most likely due to sample inhomogeneity. If the sample is analyzed at a section where the initial amount of crosslinker is higher than the calibration curve, then these negative value of p could be calculated. To determine a more accurate value of $[\text{SiH}]_0$, linear first order plots of $\ln 1/R_0$ vs. time were made and extrapolated to zero time. The analysis of the reaction order is discussed in the next paragraph. The extent of reaction versus time are shown in figure 7.6.

The approach used in determining the order of the reaction is now given. Equation 7.14 is integrated with limits $[\text{SiH}]_0$ to $[\text{SiH}]$ at times from 0 to t respectively for a second, three halves, and first order reaction to give the equations

$$[\text{SiH}] = [\text{SiH}]_0 e^{-kt} \quad (7.19)$$

$$\frac{1}{\sqrt{[\text{SiH}]}} = \frac{1}{\sqrt{[\text{SiH}]_0}} + \frac{kt}{2} \quad (7.20)$$

$$\frac{1}{[\text{SiH}]} = \frac{1}{[\text{SiH}]_0} + kt. \quad (7.21)$$

Linear plots of $\ln [\text{SiH}]$ vs. t , $\frac{1}{\sqrt{[\text{SiH}]}}$ vs. t , and $\frac{1}{[\text{SiH}]}$ vs. t will provide evidence whether the reaction is of order 1, 1.5, or 2 respectively (Noggle, 1985). The silane concentrations are plotted in terms of normalized absorbance intensities. Figure 7.7 shows plots of F.T.i.r. kinetic data of curing PBD18 at $r=1.0$ and 0.5 . For $r=0.5$ it appears that the reaction rate could be described as first or 1.5 order. However, for $r=1.0$, the data are still described quite well with either a first or 1.5 order, however, upon close inspection, it was found that the data is best fitted by the first order plot. Due to the closeness of the fit

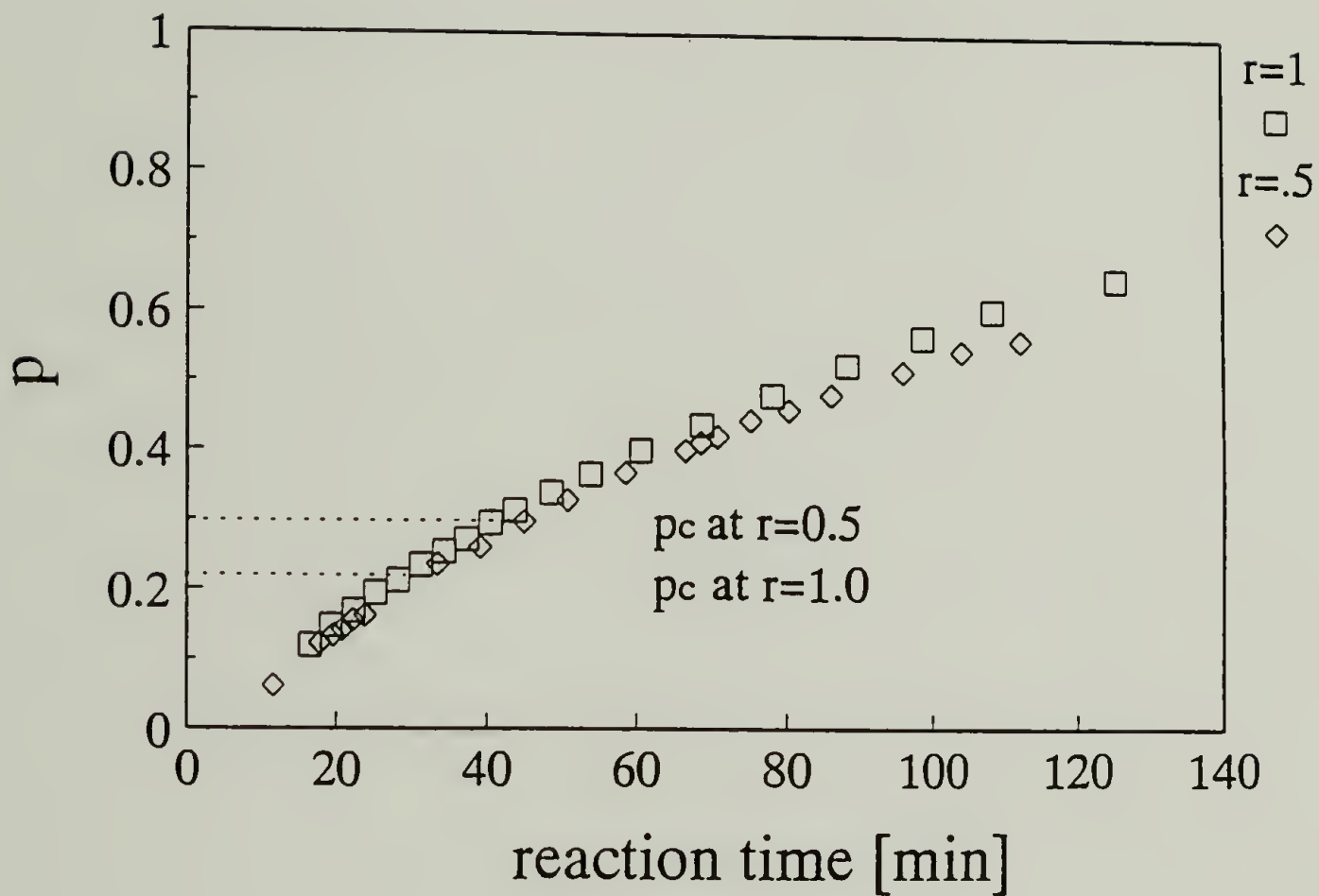


Figure 7.6 F.T.i.r. kinetic data results. Extent of reaction of silane (p) is plotted versus reaction time for two initial compositions of PBD18 and crosslinker ($r=1$, and $r=0.5$). The values of the critical extents of reaction (p_c), calculated by branching theory, are given for the two initial compositions. The temperature is $25 \pm 1^\circ\text{C}$.

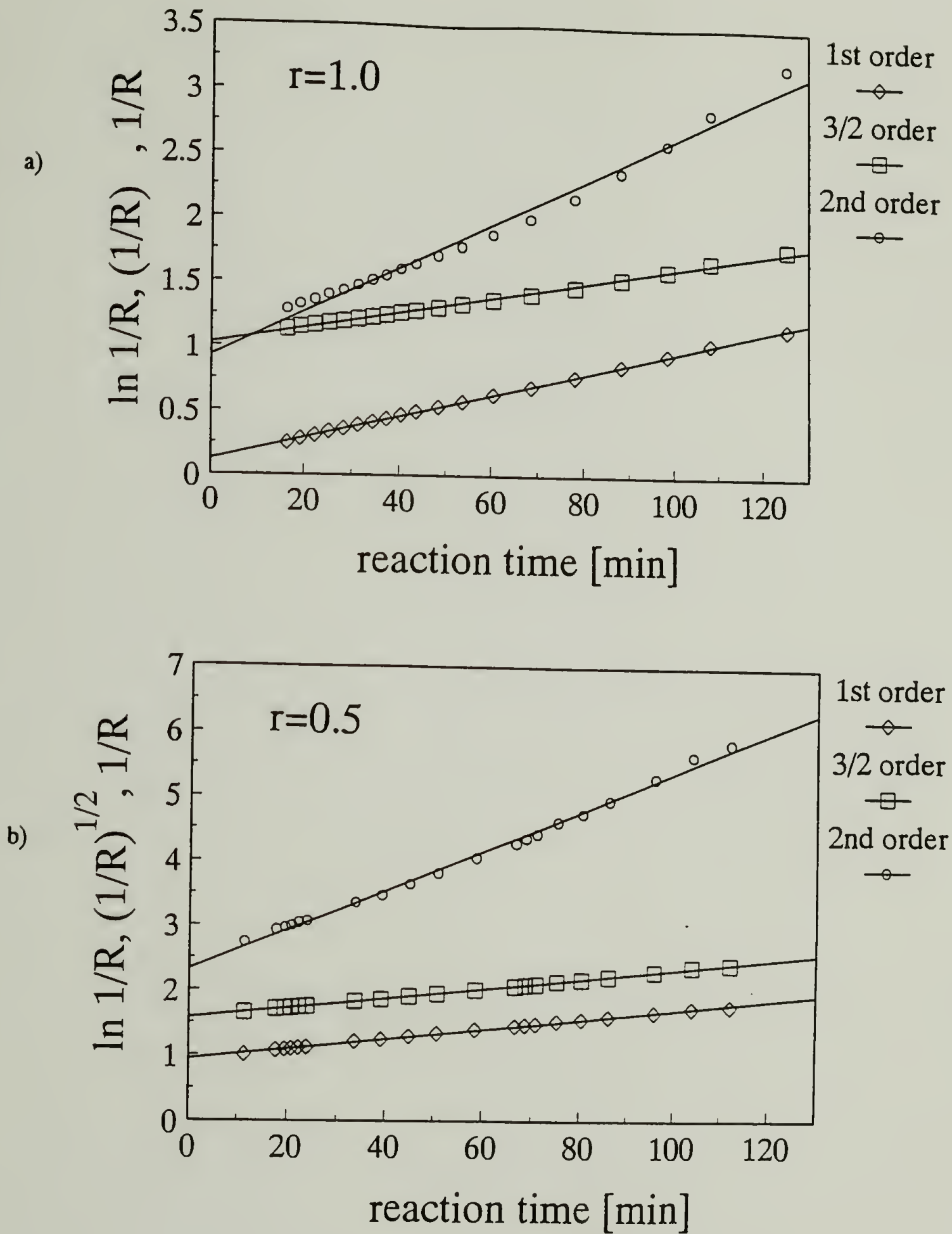


Figure 7.7 F.T.i.r. kinetic data plotted for determination of the reaction order. R is the normalized silane peak ratio which is directly proportional to silane concentration. Data is plotted for initial compositions of (a) $r=1$ and (b) $r=0.5$.

of either the first or 1.5 order plot the reaction actually may be some type of pseudo first order with $1.0 < n < 1.5$. However, since n appears to be close to 1, the first order rate assumption seems to be justified for the kinetic model described by equation 7.13. Soltero and Gonzalez-Romero (1988) also found that a first order kinetic scheme fit reasonably well for the hydrosilation reaction of polydimethylsiloxane.

In the model, the assumption of first order only needs to hold up to and just past the gel point. It is speculated that well beyond the gel point the reaction may not behave in a first order manner due to a decrease in the reaction rate. This decrease would most likely be caused by some type molecular diffusion limitation where the reactive sites attached to the infinite cluster are much more restricted in their motion. This makes it much more difficult for these species to move into a vicinity where the hydrosilation reaction can take place to create an effect elastic crosslink.

This effect is somewhat evident in the F.T.i.r. data in figure 7.6. By using Flory-Stockmayer theory, the gel points would be expected to occur approximately at 30 and 45 minutes for $r=1.0$ and 0.5 respectively. Up to these times the p vs. reaction time curves are almost identical. This is also an indication that the reaction is of first order. The slight discrepancies of the curves could be accounted for by the fact that precise temperature control was not used, thus causing one data set to be shifted to a small degree. The other possibility is that the reaction order is only pseudo first order and thus dp/dt is slightly affected by the initial concentration of silane used. At around 100 minutes, well past the expected gel points, the curves appear to be diverging slightly. This may indicate that the first order rate assumption breaks down at these higher extents of reaction. Measurements to much longer reaction times are needed to confirm this. Deviations from first order kinetic was observed by Soltero and Gonzalez-Romero (1988) at higher extents of reaction for hydrosilation of PDMS.

The parameters of the kinetic model of equation 7.13 were evaluated by analyzing the results of three sets of CFS kinetic data taken at three temperatures. CFS gel time,

$t_{\text{gel,CFS}}$, vs. $\ln\left(1 - \frac{1}{\sqrt{r(f-1)}}\right)$ yield linear plots. The slope gives the rate constant $\frac{1}{\bar{k}}$. The intercept gives the extent of reaction at the end of the mixing and loading time p_i as $\frac{1}{\bar{k}} \ln(1-p_i)$. An average value of p_i is reported from the data sets at 34°C and 40°C since they were done at the same room temperatures. The gel time results are given in table 7.1, 7.2, 7.3 and plotted in figure 7.8.

The dependence of the rate constant on the cure temperature is given by an Arrhenius relationship (Noggle, 1985)

$$\bar{k} = A e^{-E_a/RT} \quad (7.22)$$

where E_a is the activation energy of the reaction and A is the preexponential or frequency factor. Values of \bar{k} are given in table 7.4. A plot of $\ln \bar{k}$ vs. $1000/T$ gives a slope of $-E_a/R$ from which the activation energy of 75 kJ/mole is calculated (see figure 7.9). Once the activation energy is known, the gel time for any precursor composition at any temperature can be calculated. The parameters of the kinetic model are given in table 7.5.

7.3.4 Comparison of Predicted Gel Time to Experimental Results

To test if the proposed model can successfully predict the gel time at different cure temperatures, three compositions of PBD18 samples were prepared for crosslinking. The room temperature for all three samples or the mixing and loading stage were at $25.5 \pm 1.0^\circ\text{C}$. The predicted gel times and experimental gel times are given in table 7.6.

7.3.5 Discussion

The proposed model agrees well with the measured experimental gel time within 10% to 13%. The model is rather sensitive to the input parameters. The greatest source

Table 7.1 Gel times measured by CFS ($t_{gel,CFS}$) for samples cured at 28°C.

Sample	functionality (f)	r	$t_{gel,CFS}$
PBD38	51.5	0.25	2560
		1.0	958
		2.0	580
		3.0	513
PBD44	63.7	0.25	2140
		0.50	1240
PBD70	93.0	0.5	845
PBD97	135.0	0.5	820

Table 7.2 Gel times measured by CFS ($t_{gel,CFS}$) for samples cured at 34 °C.

Sample	functionality (f)	r	$t_{gel,CFS}$
PBD38	51.5	0.10	5090
		0.15	3200
		0.25	2300
		1.39	670
PBD44	63.7	0.25	1140
		0.50	750
		0.80	450

Table 7.3 Gel times measured by CFS ($t_{\text{gel,CFS}}$) for samples cured at 40 °C.

Sample	functionality (f)	r	$t_{\text{gel,CFS}}$
PBD18	23.8	0.09	3070
		0.122	2140
		0.175	1750
		0.404	876
PBD38	51.5	0.124	1170

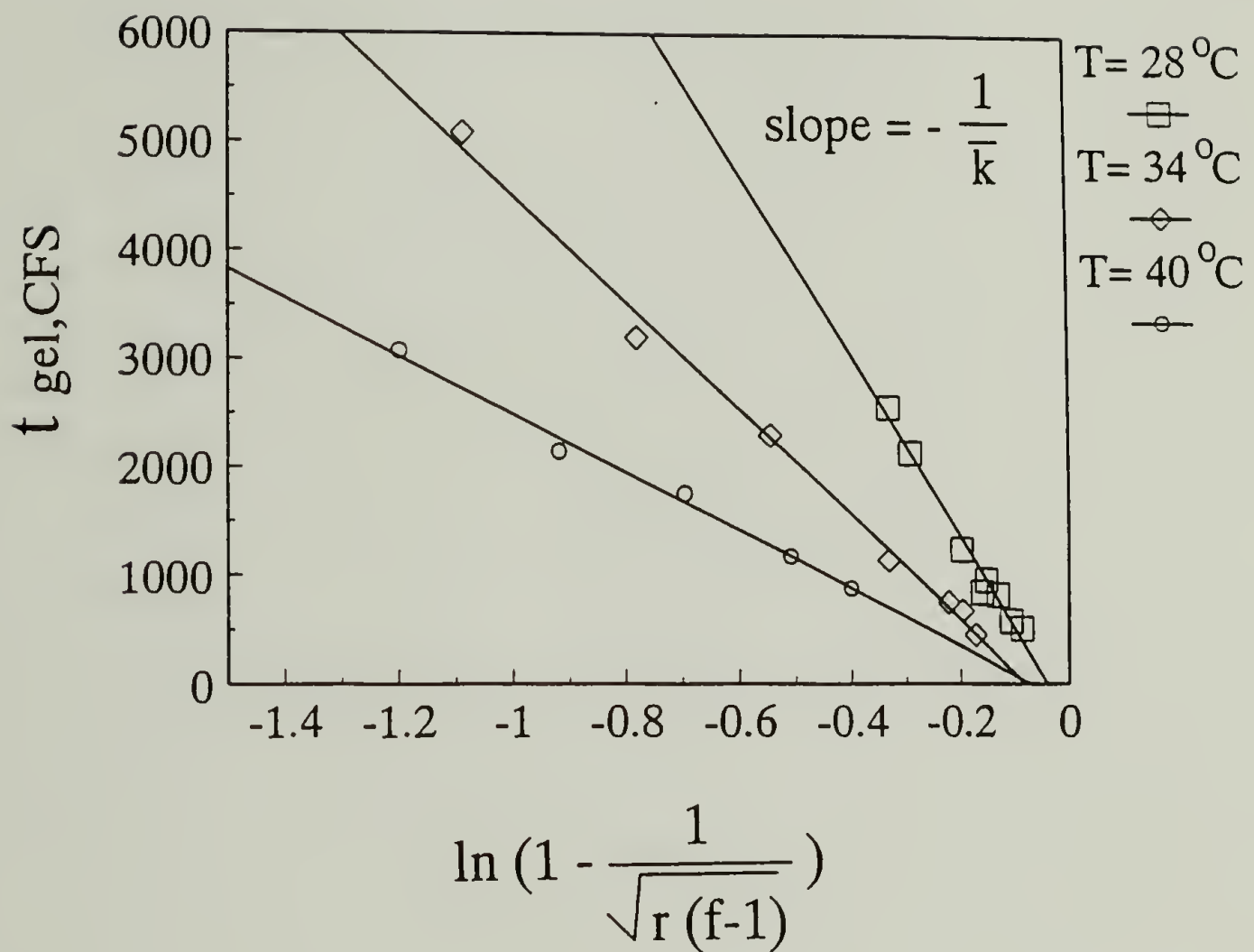


Figure 7.8 Experimental gel times measure by CFS ($t_{gel, CFS}$) plotted vs. a function of p_c from equation 7.13. p_c is calculated from equation 7.1. Data is plotted for three temperature. The slope of the plot gives the rate constant $-1/\bar{k}$.

Table 7.4 Rate constants evaluated from kinetic data.

T(°C)	\bar{k} (s ⁻¹)
28.0	1.18 E-4
34.0	2.04 E-4
40.0	3.74 E-4

Table 7.5 Parameters of the gel time kinetic model.

E_a/R [°K]	8.856
E_a [kJ/mole]	74
A (s ⁻¹)	6.95 E +8
Pi	0.0748

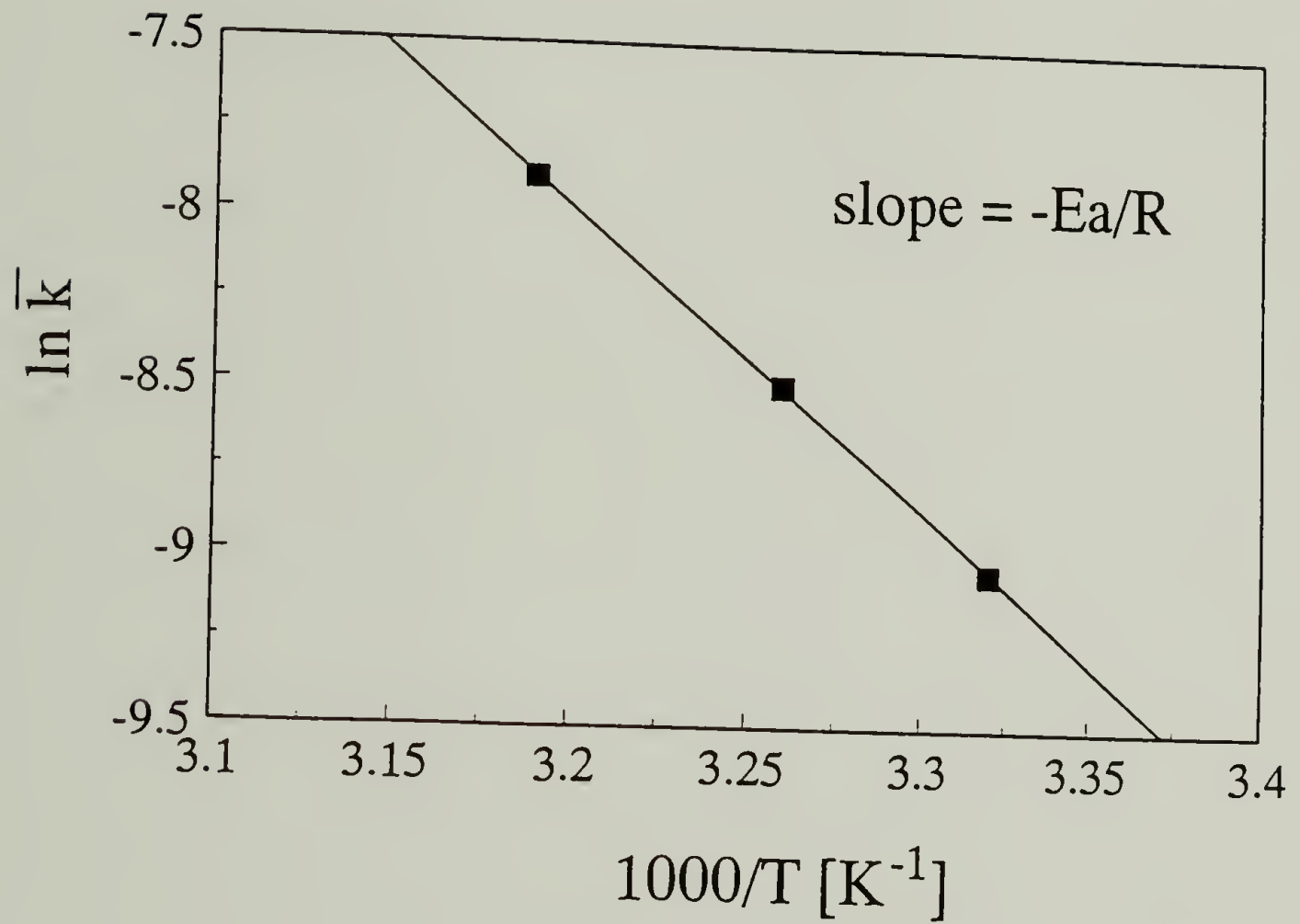


Figure 7.9 Plot of the rate constant vs the cure temperature. The slope gives the activation energy $-E_a / R$.

Table 7.6 Experimental CFS gel times compared to predicted gel times at three temperatures using the kinetic model with parameters in table 7.5.

T(°C)	r	Predicted gel time (s)	Experimental gel time (s)	% Difference
26.0	0.50	2870	3210±30	+12
31.0	0.24	3100	3510±30	+13
37.5	0.11	3230	3530±50	+10

of error comes from the parameters p_i and E_a/R . Since only two values of p_i were used to calculate an average p_i , there is significant uncertainty introduced. Only three temperatures were used to evaluate E_a/R . Usually more than three temperatures are needed to obtain a more accurate value. More precise agreement between the model and experiment can be achieved by performing experiments at more temperatures.

An abundance of work has been produced in studying the kinetic evolution of network formation of many systems (Mussatti and Macosko, 1973; Barraall and Flandera, 1974; Feger et al., 1984; Gonzalez-Romero and Macosko, 1985; Macosko, 1985; Arellano et al., 1988; Soltero and Gonzalez-Romero, 1988; Bidstrup and Macosko, 1990; Ishida and Smith, 1991). Models have been proposed to predict the gel times of peroxide cured methacrylate (Gonzalez-Romero and Macosko, 1985) and for the hydrosilation cure of PDMS (Macosko and Lee, 1985; Batch et al., 1990). For the hydrosilation of PDMS, the same approach was taken as in this work to derive a model to predict the gel time in that simple kinetics were combined with the prediction of the extent of reaction at the gel point, given by equation 7.1. Essentially the same expression to predict the gel time was obtained (Macosko and Lee, 1985). Reformulation of the model was later made to account for the presence of chemical inhibitor and the details of the reaction mechanism (Batch et al., 1990). The primary difference between their model and the one presented here is that in this study the gel times are measured directly by rheological techniques. The data is then analyzed to obtain the thermodynamic parameter of \bar{k} and E_a . Macosko and coworkers first obtained thermodynamic parameters by DSC measurements and then predicted the gel times with good agreement with experimental data.

The effects of temperature gradients were not taken into account. Temperature gradients across the thickness of the sample from the plate walls to the center of the sample produce gradients in the extent of reaction, and consequently the mechanical properties as a function of sample thickness. Temperature gradients across the sample thickness were reduced by using cure temperatures that were at most only 15K higher

than ambient condition. Also the samples were only ~0.5 mm thick. Use of higher cure temperatures with greater sample thicknesses increases the potential for gradients and inhomogeneity in samples. Models have been developed to predict temperature gradient effects and their relation to gradients in extent of reaction and mechanical properties as a function of sample thickness (Macosko and Lee, 1985; Batch et al., 1990)

7.4 Frequency Dependence of the Complex Modulus During Cure

Scanlan and Winter (1991) observed that the rate of change of the complex modulus during the reaction time, $\frac{\partial \log G^*}{\partial t_r}$, decreases with increasing frequency at (see figure 7.10). They proposed that the independent variable of extent of reaction, p , could be substituted for the reaction time, t_r , as long as the derivative is evaluated in a small enough region where

$$\Delta p \sim \Delta t_r. \quad (7.23)$$

Therefore the extent of reaction was not needed to relate the rate of change of G^* with respect to p . For small Δp it is assumed that

$$\left(\frac{\partial \log G^*}{\partial p} \right)_{\omega, p} \sim \left(\frac{\partial \log G^*}{\partial t_r} \right)_{\omega, t} \quad (7.24)$$

Though the proportionality of 7.24 holds, it must be noted that the rate of increase of G^* with reaction time, t_r , is not identical to the rate of change in G^* with extent of reaction, p . In analyzing the mechanism of hydrosilation in equations 7.2 through 7.5, it is seen that an increase in G^* is only observed when both sides of the crosslinker are

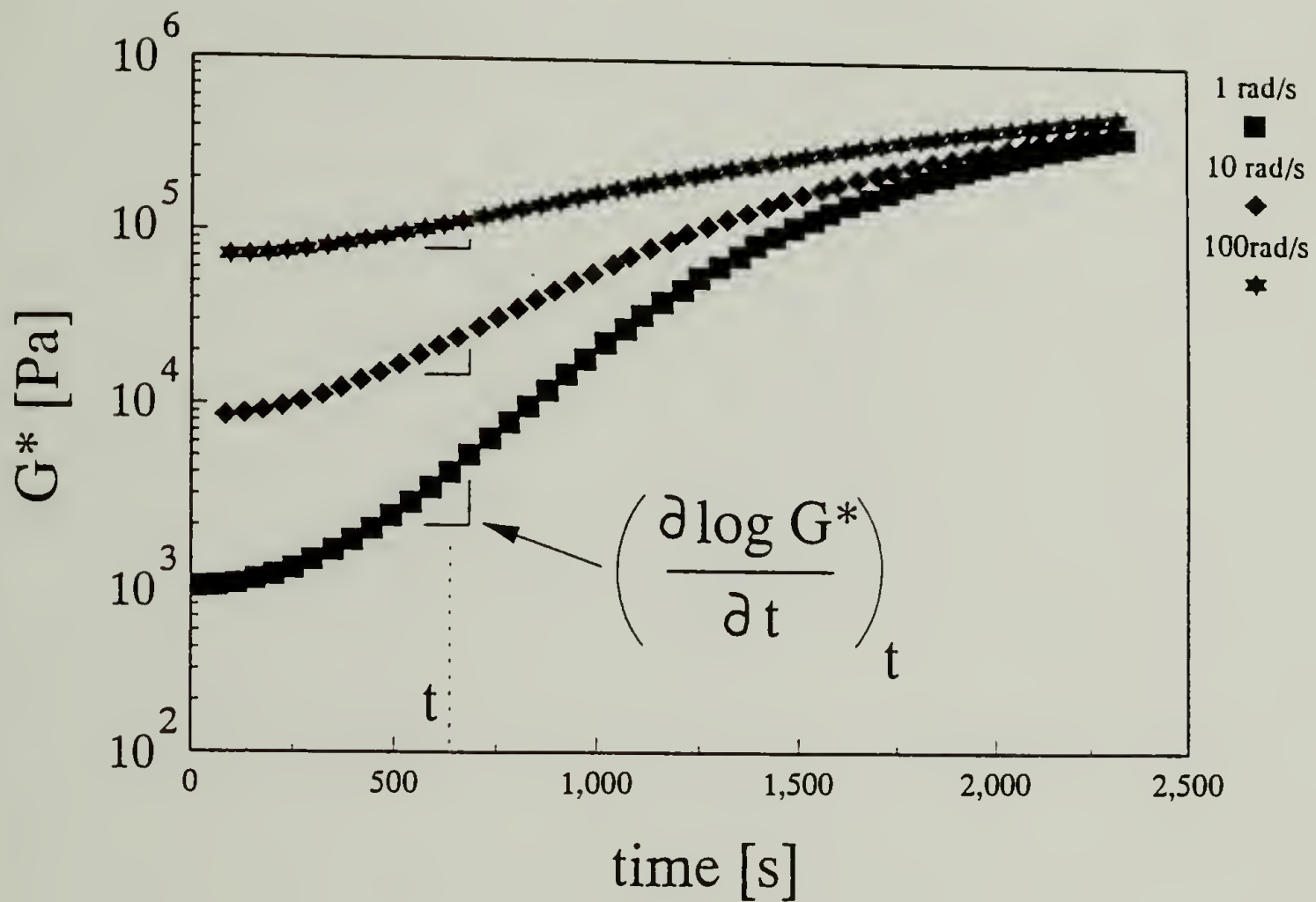


Figure 7.10 G^* vs. reaction time for PBD18 at $r=1$ at 28°C for three frequencies. The slope at time t gives the rate of gelation.

converted to make an effective crosslink. Reaction of one side of the crosslinker only adds one molecule to the polybutadiene chain which will essentially not increase the viscosity at all. The viscosity will still not increase detectably even if several crosslinker molecules become attached to the chain. However when both sides of the crosslinker react between two chains, the molecular weight is immediately doubled thus increasing the viscosity and G^* significantly. Therefore, 7.24 can be rewritten to account for this effect

$$\left(\frac{\partial p}{\partial t}\right)_t \left(\frac{\partial \log G^*}{\partial p}\right)_{\omega, p} = \left(\frac{\partial \log G^*}{\partial t_r}\right)_{\omega, t} \quad (7.25)$$

At the gel point they found that the rate of change of G^* with respect to t_r at t_c scaled with the frequency, ω , as

$$\left(\frac{\partial \log G^*}{\partial p}\right)_{\omega, p_c} \sim \left(\frac{\partial \log G^*}{\partial t_r}\right)_{\omega, t_c} \sim \omega^{-\kappa} \quad (7.26)$$

In the time domain the scaling behaves as

$$\left(\frac{d \log G(t)}{dp}\right)_{t, p_c} \sim t^\kappa \quad (7.27)$$

To evaluate κ , the slope, $\frac{\partial \log G^*}{\partial t_r}$ at $t_r = t_c$, is plotted versus frequency. A power law is fit through the data and the slope of this power law is κ . Therefore, κ simply the relationship of $\frac{\partial \log G^*}{\partial t_r}$ at t_c with respect to frequency (see figure 7.11).

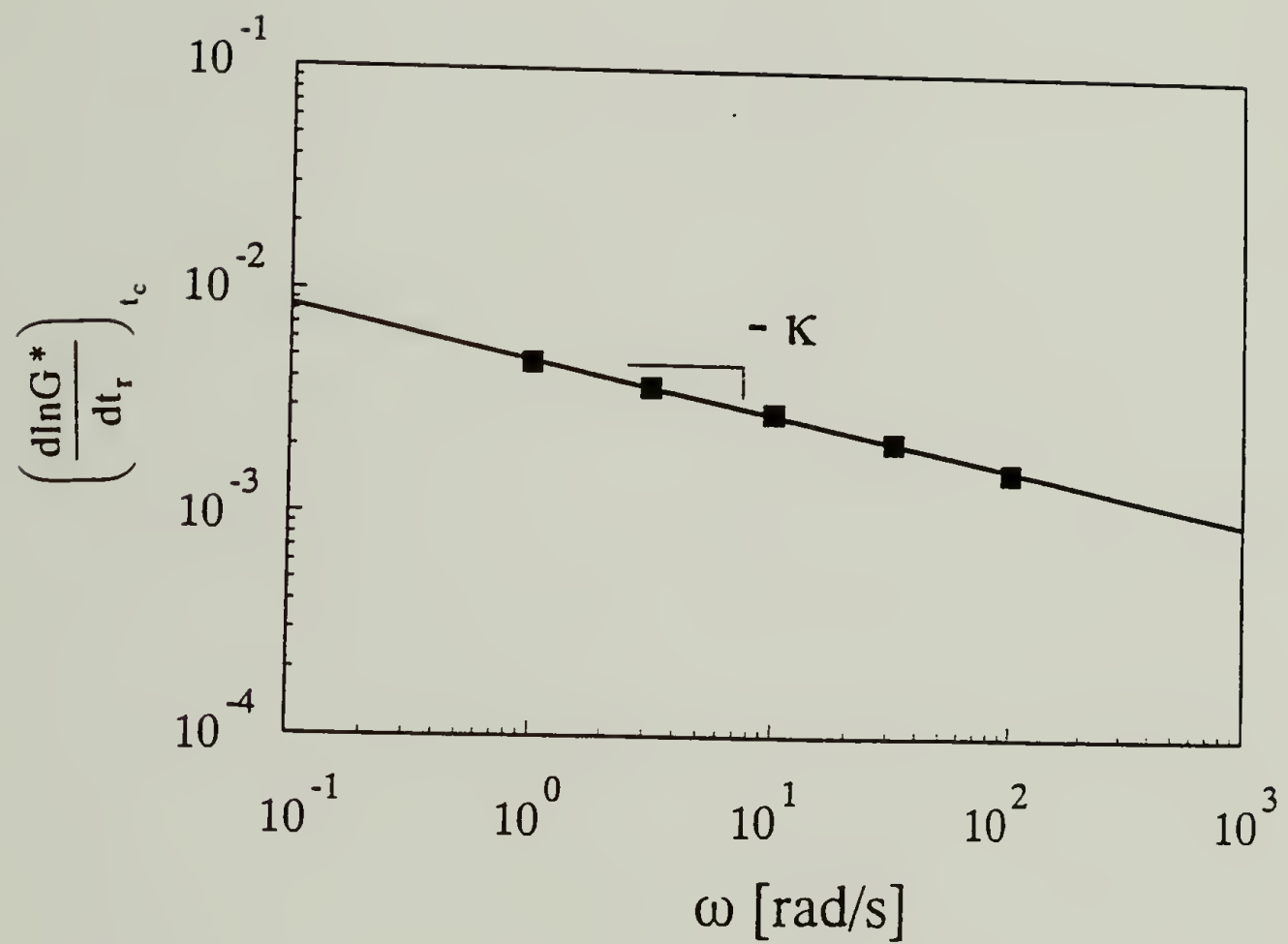


Figure 7.11 Plot of the rate of gelation at t_c time versus frequency for PBD18 at $r=1$ at 28°C . The slope gives the critical exponent $-\kappa$.

Scanlan and Winter, (1991) found a value of $\kappa = 0.21$ and propose it to be a universal value. κ was found to be independent of stoichiometric ratio or precursor molecular weight.

The critical exponents, s and z , describe the equilibrium properties in the vicinity of the gel point

$$\eta_0 \sim (p_c - p)^{-s} \quad (\text{for } p < p_c) \quad (7.28)$$

$$G_e \sim (p - p_c)^z \quad (\text{for } p > p_c). \quad (7.29)$$

κ has been found to be related to the exponents, s and z , by (Winter, 1987)

$$s = \frac{1 - n}{\kappa} \quad (7.30)$$

$$z = \frac{n}{\kappa} \quad (7.31)$$

where n is the same exponent described in equations 1.3 through 1.7.

In this study κ was evaluated for five different precursor molecular weights over many values of stoichiometry. The results are given in table 7.7. κ was found to be independent of stoichiometric ratio but somewhat influenced by the precursor molecular weight. An average value was calculated for the three lowest molecular weights for all the stoichiometric ratios examined and found to be $\kappa = 0.24$. This value is close to the value found by Scanlan and Winter even though the system is different and the mechanism of crosslinking is vulcanization as opposed to endlinking. Such results may suggest a universal value of κ . However, at this time, this can not be certain and more work with other systems needs to be done.

Table 7.7 Values of the critical exponent κ for PBD samples cured at 28°C at various stoichiometric ratios (r).

Sample	r	κ
PBD18	0.25	0.25
	0.5	0.25
	0.8	0.24
	1.0	0.24
	1.1	0.24
	1.5	0.24
	2.0	0.25
	3.0	0.24
PBD20	1.0	0.27
PBD38	0.25	0.27
	0.5	0.26
	1.0	0.29
	1.5	0.29
	2.0	0.27
	3.0	0.29
PBD44	0.25	0.26
	0.5	0.28
	1.0	0.27
PBD70	0.5	0.37
	1.0	0.30

7.4.1 Effect of Precursor Molecular Weight on the Value of κ

The influence of molecular weight on κ was most probably due to the interference of the entanglement region being so close to the upper limit of the CFS frequency window. As discussed in chapter 5, the highest frequencies in the CFS window come closer to probing the entanglement zone as the molecular weight is increased. At these high frequencies, the evolution of the dynamic modulus with reaction time was found to be slowed down drastically. In the entanglement zone, the value of $\frac{\partial \log G^*}{\partial t_r}$ would approach zero since the entanglement region was found to be hardly affected by the introduction of chemical crosslinks. Therefore, when calculating κ , the values of $\frac{\partial \log G^*}{\partial t_r}$ at the highest frequencies deviate from the power law behavior of the lower frequencies (see figure 7.12). These lower values tend to bring the fit of the power law down at the high frequency end thus raising the slope and consequently the value of κ . This phenomenon was not as pronounced for the lower molecular weight precursors. The results of Scanlan and Winter did not show this effect because the molecular weight of their precursors were low enough to not have interference from entanglement effects.

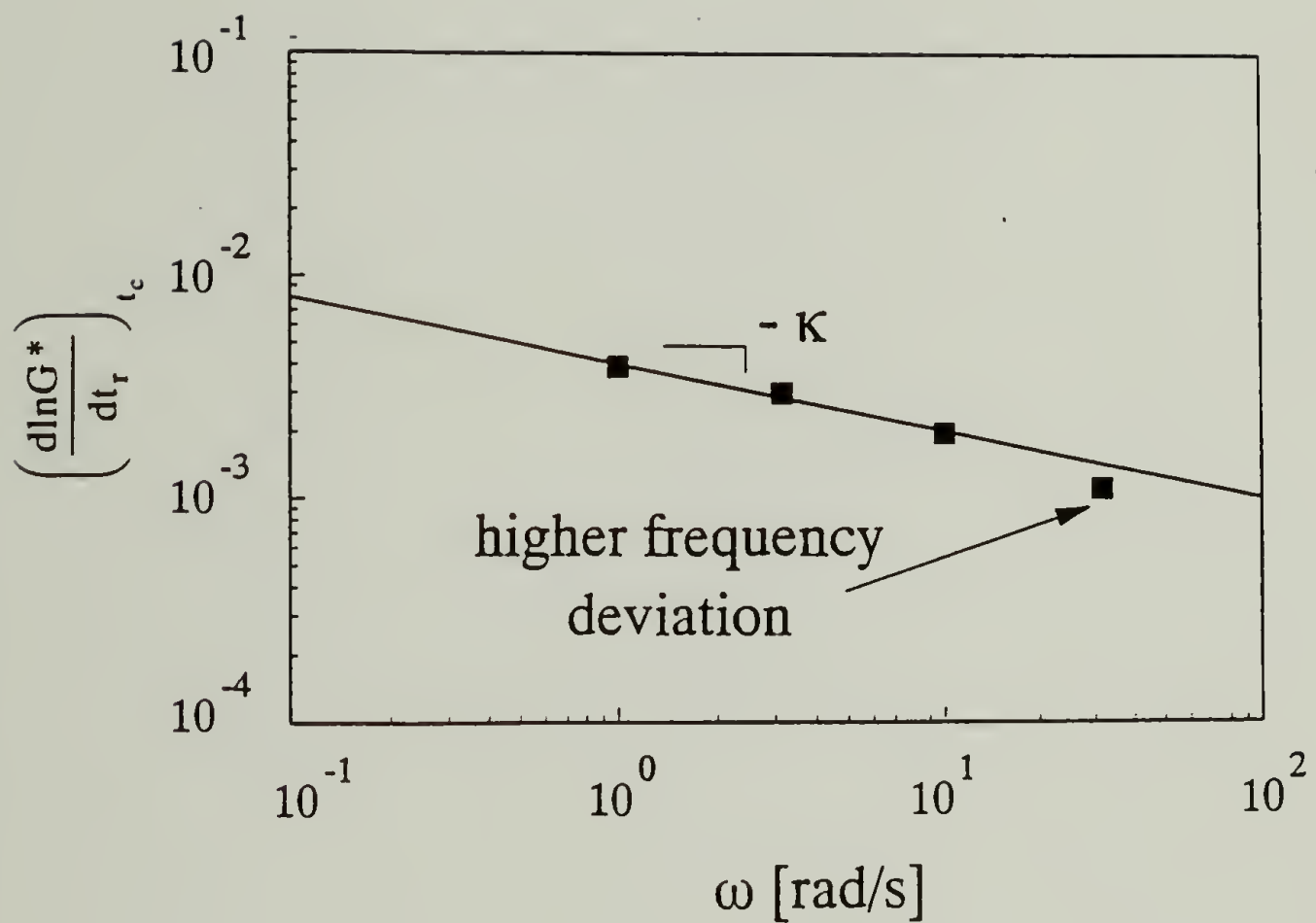


Figure 7.12 Rate of gelation versus frequency at t_c for PBD44 at $r=1$ at 28°C . Deviation from the power law at higher frequencies is seen for higher molecular weights.

CHAPTER 8

CONCLUSIONS AND SUGGESTIONS FOR FUTURE RESEARCH

8.1 Conclusions

The results of this study provide new insight toward understanding the relaxation behavior of critical gels by examining the effect that physical entanglements have on the mechanical properties of materials at the liquid-solid transition. It is found that the presence of physical entanglements primarily affects the mechanical behavior of critical gels by setting an upper frequency or short time limit to the observed power law relaxation in the mechanical shear properties. At times shorter than this limit, the material appears to behave very much like the uncrosslinked initial state. Such behavior is most likely limited to vulcanized systems and not endlinking ones in that the high functionality only requires a small amount of chemical crosslinks to be added to reach the gel point. This small amount of chemical crosslinks is enough to severely affect the long time relaxation mechanisms but insignificant to have any affect on intermediate or short time scale relaxation.

By collecting data over three viscoelastic time regimes, it was possible to empirically formulate a function of the relaxation time spectrum for the critical gel with entanglements. Initially the uncrosslinked state is represented by the BSW-spectrum. It was found that the BSW-spectrum could be modified to account for the presence of diluent and therefore can be used to describe concentrated solutions of linear polymers of low polydispersity. Superposition of the BSW-spectrum and the CW-spectrum with minor modifications gives the final form of $H(\lambda)$ for the entangled critical gel represented by equation 6.9. The relative simplicity of this finding can be appreciated in that it combines the results of studies on the relaxation behavior of two completely different types of materials: high molecular weight linear chains of low polydispersity and low molecular weight precursors crosslinked to the gel point. Only one new parameter (A) is

introduced to account for the discrepancy in the slope of the entanglement regime. At this time the parameter has no physical significance.

The critical gel of vulcanized highly entangled polymers exhibits some quite interesting properties that have not been reported. Quite surprisingly it was found that the relaxation exponent, n , was independent of stoichiometry and precursor molecular weight with a value near 0.5. The gel strength, S , was also found to be independent of stoichiometry but dependent upon the precursor molecular weight. With these findings combined with the expression for the critical spectrum given in equation 6.9 it was possible to derive a new simple scaling relationship that relates the gel strength to the precursor molecular weight given by equation 6.21. Such a unique result is only possible when n is independent of precursor molecular weight and therefore might only be applicable to systems where the crosslinking mechanism is vulcanization.

Physical entanglements affects the ability to detect the liquid-solid transition by *in-situ* rheological methods. As the molecular weight of the precursor is increased, the terminal zone is pushed down to lower frequencies until the entanglement zone enters the frequency window of observation making gel point detection more difficult. Power law behavior in dynamic mechanical measurements during gelation can be observed without the effect of entanglements. This is possible only if the entire terminal zone of the precursor before crosslinking is in the frequency window of observation. The upper limit of the power law behavior is governed by a characteristic modulus, G_0 , occurring at the characteristic time λ_0 . G_0 is related to the plateau modulus of the precursor by equation 6.13 and λ_0 is given by λ_{\max} of the precursor molecule.

With well defined chemistry it was possible gain information about the molecular structure and consequently the gel time. It was found from spectroscopic measurements that the classical theory of gelation could be used to predict the extent of reaction needed to reach the gel point even though the precursors were of very high functionality. By using classical gelation theory in combination with simple kinetics it was possible to derive

a model to predict the gel time as a function of the stoichiometric ratio, r , and functionality of the polybutadiene chain, f , given by equation 7.13. The model agrees well with experimental data. The critical exponent κ , which characterizes the rate of change of modulus at the gel point as a function of frequency, was found to be 0.24.

8.2 Suggestions for Future Research

The simple superposition of the BSW and CW spectrum of equation 6.8 was found to be inadequate to describe the relaxation behavior of entangled critical gels. A slight modification had to be made to account for the change in slope of the spectrum in the entanglement region resulting in equation 6.9. A complete understanding of this phenomenon is not available at this time.

It was speculated that the change in slope is due to some type of polydispersity effect introduced by the crosslinking process. However, this speculation was made based on results from polydispersity effects seen in linear chains. In crosslinking systems, polydispersity arises from the increase of the molecular weight distribution due to branching and therefore the relaxation mechanisms in the two cases are probably not the same. More work needs to be done in this area in order to gain a better understanding of how polydispersity due to chain length and branching affect the spectrum.

A more complex situation would arise from the combination of both types of polydispersity. This could possibly be studied by preparing well defined binary blends of molecular weights with narrow molecular weight distribution and then crosslinking them. Analysis of rheological data of such hybrid materials may help in furthering this understanding of polydispersity effects. Such a material may also possibly give rise to a very unique types of materials such as gels with two gel strengths. Gel properties could also possibly be enhanced by blending in small weight fraction of high molecular weight precursor with a lower molecular weight precursor.

The general form of the spectrum proposed for entangled critical gels here could also possibly be used for branched structures before they reach the gel point. In the case of the gel, the CW-spectrum is used to describe long time behavior. The longest relaxation time of this power law is essentially infinite at the gel point. By using a third power law with different slopes and longest cut-off times, it may be possible to describe branched structures. The slope of the power law will decrease as the degree of branching increases. This slope used in this type of analysis would be strictly used empirically to model the data and could not be compared to the slope used to describe the critical phenomenon of gelation. A rough correlation could then be made between the slope and degree of branching, or extent of reaction.

Rheological measurements in this study were conducted with small strain oscillatory deformations. Little is known about how the kinetics would be effected by large strain steady shear measurements. It is assumed that the gel point would be delayed by such deformations. This could possibly be tested by using the kinetic model given in equation 7.13. Comparisons of measured gel times by steady shear could be compared to predicted gel times to test if such an assumption is true. However, at this moment, more work needs to be done to make the model agree more precisely with dynamic measurements before using it for steady shear experiments. Particularly, development of better temperature control during the mixing and loading stage is needed. Perhaps a new system that could be started to crosslink when desired, such as a U.V. system, would be better for such a study.

Finally, a great deal of potential exists for combining Raman spectroscopy with rheological measurements. By incorporating fiber optics with state of the art Raman technology, it is conceivable that an *in-situ* device could be developed to measure chemical structure changes simultaneously with rheological measurements. Such a device could make a significant contribution to the current field of rheo-optics.

REFERENCES

- Adolf, D., and Martin, J.E., "Time-Cure Superposition During Cross-Linking ", *Macromolecules*, **23**, 3700-3704, 1990.
- Aklonis, J.J., and MacKnight, W.J., *Introduction of Polymer Viscoelasticity*, 2nd ed., John Wiley and Sons, New York, 1983.
- Andrews, R.D., and Tobolsky, A.V., "Elastoviscous Properties of Polyisobutylene. IV. Relaxation Time Spectrum and Calculation of Bulk Viscosity", *J. Polym. Sci.*, **7**, 221-242, (1951).
- Aranguren, M.I., and Macosko, C.W., " Modulus of Polybutadiene Networks Made by Hydrosilation Cross-Linking", *Macromolecules*, **21**, 2484-2491, 1988.
- Arellano, M., Casillas, N., Gonzalez-Romero, V. "Curing of Epoxy Resins with Aliphatic Amines: Effect of Functionality and Stoichiometric Imbalance", *ANTEC Conf. Proc.*, 1069-1074, 1988.
- Barrall, E.M., and Flandera, M.A., "Thermal Analysis of the Crosslinking Reaction in Silicone Rubber", *J. Elastomers and Plastics*, **6**, 16-25, 1974.
- Batch, G.L., Macosko, C.W., Kemp, D.N., "Reaction Kinetics and Injection Molding of Liquid Silicone Rubber", *Rubber Chem. and Tech.*, **64**, 218-233, 1991.
- Baumgaertel, M., and Winter, H.H., "Determination of Discrete Relaxation and Retardation Time Spectra from Dynamic Mechanical Data", *Rheol. Acta*, **28**, 511-519, 1989.
- Baumgaertel, M., "The Relaxation of Linear Flexible Polymers: Correlation Between Molar Mass Distribution and Rheological Data of Polymer Melts", Ph. D. Thesis, University of Massachusetts, Amherst, MA, 1991.
- Baumgaertel, M., De Rosa, M.E., Winter, H.H., Machado, J., Masse, M., "The Relaxation Time Spectrum of Nearly Monodisperse Polybutadiene Melts", *Rheol. Acta*, **31**, 75-82, 1992.
- Baumgaertel, M., Schausberger, A., Winter, H.H., "The Relaxation of Polymers With Linear Flexible Chains of Uniform Length", *Rheol. Acta*, **29**, 400-408, 1990.
- Berry, G.C., Fox, T.G., " The Viscosity of Polymers and their Concentrated Solutions", *Adv. Polym. Sci.*, **5**, 261-357, 1968.

- Bidstrup, S.A., and Macosko, C.W., "Chemorheology Relations for Epoxy-Amine Crosslinking", *J. Polym. Sci., B, Polym. Phys.*, 691-709, 1990.
- Brotzman, R.W., and Flory, P.J., "Elastic Behavior of *cis*-1,4-Polybutadiene", *Macromolecules*, **20**, 351-356, 1987.
- Chalk, A.J., and Harrod, J.F., "Homogeneous Catalysis. II. The Mechanism of the Hydrosilation of Olefins Catalyzed by Group VIII Metal Complexes", *J. Am. Chem. Soc.*, **87**, 16-21, 1965.
- Chambon, F., and Winter, H.H., "Stopping of Crosslinking Reaction in a PDMS Polymer at the Gel Point", *Polym. Bull.*, **13**, 499-503, 1985.
- Chambon, F., "Linear Viscoelasticity of Crosslinking Polymers at the Gel Point", Ph. D. Thesis, University of Massachusetts, Amherst, MA, 1986.
- Chambon, F., Petrovic, Z.S., MacKnight, W.J., Winter, H.H., "Rheology of Model Polyurethanes at the Gel Point", *Macromolecules*, **19**, 2146-2149, 1988.
- Chambon, F., and Winter, H.H., "Linear Viscoelasticity at the Gel Point of a Crosslinking PDMS with Imbalanced Stoichiometry", *J. Rheol.*, **31**, 683-697, 1987.
- Clark, A.H., Ross-Murphy, S.B., "Structural and Mechanical Properties of Biopolymer Gels", *Adv. Polym. Sci.*, **83**, 57-204, 1987.
- Colby, R.H., Fetters, L.J., Funk, W.G., Graessley, W.M., "Effects of Concentration and Thermodynamic Interaction on the Viscoelastic Properties of Polymer Solutions", *Macromolecules*, **24**, 3873-3882, 1991.
- Colthup, N.B., Daly, L.H., Wilberley, S.E., Introduction to Infrared and Raman Spectroscopy, 3rd. ed., Academic Press Inc., Boston, 1990.
- Cornell, S.W., and Koenig, J.L., "The Raman Spectra of Polybutadiene Rubbers", *Macromolecules*, **2**, 540-545, 1969.
- Cutler, D.J., "The Development of Fourier Transform Raman Spectroscopy", *Spectrochim. Acta*, **46A**, (2), 123-129, 1990.
- De Gennes, P.G., "Dynamics of Entangled Polymer Solutions. I. The Rouse Model", *Macrom.*, **9**, 587-593, 1976.
- De Gennes, P.G., "Dynamics of Entangled Polymer Solutions. II. Inclusion of Hydrodynamic Interactions", *Macrom.*, **9**, 594-598, 1976.

- de Gennes, P.G., "Scaling Concepts in Polymer Physics", Cornell University Press, Ithaca, 1979.
- De Rosa, M., and Winter, H.H., "Determination of the Gel Point of Highly Entangled Polymers of High Molecular Weight", ANTEC Conf. Proc. volIII, 2620-2626, 1993.
- des Cloizeaux, J., "Relaxation and Viscosity Anomaly of Long Entangled Polymers: Time Dependent Reptation", *Macrom.*, **23**, 4678-4687.
- Dickie, R.A., and Ferry, J.D., "Dynamic Mechanical Properties of Cross-Linked Rubbers. III. Dicumyl Peroxide of Natural Rubber", *J. Phys. Chem.*, **70**, 2594-2600.
- Doi, M., "Molecular Theory of the Viscoelastic Properties of Concentrated Polymer Solutions", *Chem. Phys. Lett.*, **26**, 269-272, 1974.
- Doi, M., and Edwards, S., The Theory of Polymer Dynamics, Clarendon Press, Oxford, 1986.
- Dossin, L.M., and Graessley, W.W., "Rubber Elasticity of Well-Characterized Polybutadiene Networks", *Macrom.*, **12**, 123-130, 1979.
- Durand, D., Delsanti, M., Adam, M., Luck, J.M., "Frequency Dependence of Viscoelastic Properties of Branched Polymers Near the Gelation Threshold", *Europhys. Lett.*, **3**, 297-301, 1987.
- Ferry, J.D., Viscoelastic Properties of Polymers, 3rd. ed., John Wiley and Sons Inc., New York, 1980.
- Ferry, J.D., Mancke, R.G., Maekawa, E., Oyanagi, Y., Dickie, R.A., "Dynamic Mechanical Properties of Cross-Linked Rubbers. I. Effects of Cross-Link Spacing in Natural Rubber", *J. Phys. Chem.*, **68**, 3414-3418, 1964.
- Fischer, A., Gottlieb, M., "Side Reactions in the Endlinking of PDMS Networks", *Proc. of Networks 86*, Elsinor Denmark, Aug., 1986.
- Flory, P.J., "Molecular Size Distribution in Three Dimensional Polymers. I. Gelation", *J. Am. Chem. Soc.*, **63**, 3083-3090, 1941.
- Flory, P.J., Principles of Polymer Chemistry, Cornell University Press, Ithaca, New York, 1953.
- Friedmann, G., Herz, J., Brossas, J., "Synthesis of Statistical Polydiene Networks by Reaction of Liquid Polyenes with Telechelic Siloxanes", *Polymer Bull.*, **6**, 251-257, 1982.

- Friedmann, G., and Brossas, J., "Synthesis of Statistical Networks From Liquid Polybutadiene-IV", *Eur. Polym. J.*, **20**, 1151-1153, 1984.
- Friedmann, G., and Brossas, J., "Synthesis of Statistical Networks With Liquid Polybutadiene and Telechelic Bishydrogenosilyl Coupling Agents", *Polym. Prepr.*, **26**, 268-269, 1985.
- Gonzalez-Romero, V.M., and Macosko, C.W., "Viscosity Rise During Free Radical Crosslinking Polymerization with Inhibition", *J. Rheol.*, **29**, 259-272, 1985.
- Graessley, W.W., "The Entanglement Concept in Polymer Rheology", *Adv. in Polym. Sci.*, **16**, 1974.
- Grasselli, J.G., Hazle, M.A.S., Mooney, J.R., Mehicic, M. (1979) "Raman Spectroscopy: An Update on Industrial Applications", *Proc. 21st Colloq. Spectrosc. Int. and 6th Int. Conf. Atomic Spectrosc.*, Heyden, London, Ch. 7, 86-105, 1979.
- Grasselli, J.G., Snavely, M.K., Bulkin, B.J., Chemical Applications of Raman Spectroscopy, Wiley-Interscience, New York, 1981.
- Gustavson, W.A., Epstein, P.S., Curtis, M.D., "Metal Complex-Catalyzed Redistribution Reactions of Organsilanes IV. Redistribution Reactions of Methylsiloxanes Catalyzed by Transition Metal Complexes", *J. Organometallic Chem.*, **238**, 87-97, 1982.
- Hendra, P.J., and Jones, C.H., "F.T. Raman Spectroscopy: Its Value in the Study of Polymers", *Makromol. Chem. Macromol. Symp.*, **52**, 41-56, 1991.
- Hess, W., Vilgis, T.A., Winter, H.H., "Dynamic Critical Behavior During Chemical Gelation and Vulcanization", *Macromolecules*, **21**, 2536-2542, 1988.
- Holly, E.E., Venkataraman, S.K., Chambon, F., Winter, H.H., "Fourier Transform Mechanical Spectroscopy of Viscoelastic Materials With Transient Structure", *J. Non-Newt. Fluid Mech.*, **27**, 17-26, 1988.
- Ishida, H., and Smith, M.E., "Evolution of the Rheological Properties During the Reactive Processing of Thermoplastic/Thermoset Epoxy", *Rheol. Acta*, **30**, 184-196, 1991.
- Isono, Y., Fujimoto, T., Takeno, N., Kijirua, H., Nagasawa, M., "Viscoelastic Properties of Linear Polymers with High Molecular Weight and Sharp Molecular Weight Distributions", *Macrom.*, **11**, 888-893, 1978.

- Izuka, A., Winter, H.H., Hashimoto, T., "Molecular Weight Dependence of Viscoelasticity of Polycaprolactone Critical Gels", *Macromolecules*, **25**, 2422-2428, 1992.
- Jackson, J.K., DeRosa, M.E., Winter, H.H., "Molecular Weight Dependence of Relaxation Time Spectra for the Entanglement and Flow Behavior of Monodisperse Linear Flexible Polymers", Submitted to *Macrom.*, 1993.
- Jackson, K.D.O., Loadman, M.J.R., Jones, C.H., Ellis, G., "Fourier Transform Raman Spectroscopy of Elastomers: An Overview", *Spectrochim. Acta*, **46A**, (2), 217-226, 1990.
- Jawahari, T., Hendra, P.J., Willis, H.A., Judkins, M., "Quantitative Analysis Using Raman Methods", *Spectrochim. Acta*, **46A**, (2), 161-170, 1990.
- Kauffman G.B. and Cowan D.O. (1960) "*cis* and *trans*-Dichlorobis(diethyl sulfide) platinum (II)", in *Inorganic Syntheses*, E.G. Rochow ed.
- Lairez, D., Adam, M., Emery, J.R., Durand, D., "Rheological Behavior of an Epoxy/Amine System Near the Gel Point", *Macromolecules*, **25**, 286-289, 1992.
- Lantman, C., W., MacKnight, W., J., Lundberg, R., D., "Structural Properties of Ionomers", *Annu. Rev. Mater. Sci.*, **19**, 295-317, 1989.
- Leung, Y.K., Eichinger, B.E., "Computer Simulation of End-Linked Elastomers. I. Trifunctional Networks Cured in the Bulk", *J. Chem. Phys.*, **80**, 3877-3884, 1984.
- Leung, Y.K., Eichinger, B.E., "Computer Simulation of End-Linked Elastomers. II. Bulk Cured Tetrafunctional Networks", *J. Chem. Phys.*, **80**, 3885-3891, 1984.
- Lin-Vien, D., Colthup, N.B., Fateley, W.G., Grasselli, J.G., *The Handbook of Infrared and Raman Characteristic Frequencies of Organic Molecules*, Academic Press, Inc., Boston, 1991
- Macosko, C.W., and Benjamin, G.S., "Modulus of Three and Four Functional Poly(dimethylsiloxane) Networks", *Pure and Appl. Chem.*, **53**, 1505-1518, 1981.
- Macosko, C.W., and Lee, L.J., "Heat Transfer and Property Development in Liquid Silicone Rubber Molding", *Rubber Chem. and Tech.*, **58**, 436-448, 1985.
- Macosko, C.W., and Miller, D.R., "A New Derivation of Average Molecular Weights of Nonlinear Polymers", *Macrom.*, **9**, 199-206, 1976.
- Macosko, C.W., and Saam, J.C., "The Hydrosilation Cure of Polyisobutene", *Polym. Bull.*, **18**, 463-471, 1987.

- Macosko, C.W., "Rheological Changes During Crosslinking", *British Polym. Journal*, **17**, 239-245, 1985.
- Maekawa, E., Mancke, R.G., Ferry, J.D., "Dynamic Mechanical Properties of Cross-Linked Rubbers. II. Effects of Cross-Link Spacing and Initial Molecular Weight in Polybutadiene", *J. Phys. Chem.*, **69**, 2811-2817, 1965.
- Martin, J.E., Adolf, D., Wilcoxon, J.P., "Viscoelasticity Near the Sol-Gel Transition", *Phys. Rev. Lett.* 2620, 1988.
- Masuda, T., Toda, N., Aoto, Y., Onogi, S., "Viscoelastic Properties of Concentrated Solutions of Poly(methyl methacrylate) in Diethyl Phthalate", *Polymer J.*, **3**, 315-321, 1972.
- McLeish, T.C.B., "Molecular Rheology of H-Polymers", *Macrom.*, **21**, 1062-1070, 1988.
- Miron, J., Bhatt, P., Skeist, I., "Silane-Modified Polybutadienes", In Recent Advances in Adhesion, Gordon and Breach Science, London, 309-315, 1973.
- Muller, R., Gerard, E., Dugand, P., Rempp, P., Gnanou, Y., "Rheological Characterization of the Gel Point: A New Interpretation", *Macromolecules*, **24**, 1321-1326, 1991.
- Mussatti, F.G., and Macosko, C.W., "Rheology of Network Forming Systems", *Polym. Eng. and Sci.*, **13**, 236-240, 1973.
- Nakagasu, H., Fox, T.G., Abstracts 137th Meeting Am. Chem. Soc. p.11-I, 1960.
- Nemoto, N., Ogawa, T., Odani, H., Kurata, M., "Shear Creep Studies of Narrow-Distribution Poly (cis-isoprene) III. Concentrated Solutions", *Macrom.*, **5**, 641-644, 1972.
- Noggle, J.H., Physical Chemistry, Little, Brown and Co., Boston, 1985.
- Orbey, N., Dealy, J.M., "Determination of the Relaxation Spectrum from Oscillatory Shear Data", *J. Rheol.*, **35**, 1035-1049, 1991.
- Odian, G., Principles of Polymerization, 2nd ed., John Wiley and Sons, New York, 1981.
- Pasco, I.K., and Waters, D.N., "Determining Monomer Content in PMMA Elements", *British Patent 1,528,418*, 1976.

- Raju, V.R., Menezes, E.V., Marin, G., Graessley, W.W., Fetters, L.J., "Concentration and Molecular Weight Dependence of Viscoelastic Properties in Linear and Star Polymers", *Macrom.*, **14**, 1688-1676, 1981.
- Rennar, N., and Opperman, W., "Swelling Behavior and Mechanical Properties of Endlinked Poly(dimethylsiloxane) Networks and Randomly Crosslinked Polyisoprene Networks", *Coll. Polym. Sci.*, **270**, 527-536, 1992.
- Riande, E., Markovitz, H., Plazek, D.J., Raghupathi, N., "Viscoelastic Behavior of Polystyrene-tricresyl Phosphate Solutions", *J. Polym. Sci., Polym. Symp.*, **50**, 405-430, 1975.
- Richtering, H., W., Gagnon, K., D., Lenz, R., W., Fuller, R., C., Winter, H., H., "Physical Gelation of a Bacterial Thermoplastic Elastomer", *Macrom.*, **25**, 2429-2433, 1992.
- Roovers, J., "Melt Rheology of H-Shaped Polystyrenes", *Macrom.*, **17**, 1196-1200, 1984.
- Roovers, J., Graessley, W.W., "Melt Rheology of Some Model Comb Polystyrenes", *Macrom.*, **14**, 766-773, 1981.
- Ross-Murphy, S.B., "Incipient Behaviour of Gelatin Gels", *Rheol. Acta*, **30**, 401-411, 1991.
- Rouse, P.E., "A Theory of Linear Viscoelastic Properties of Dilute Solutions of Coiling Polymers", *J. Chem. Phys.*, **21**, 1272-1280, 1953.
- Rubenstein, M., Zurek, S., McLeish, T.C.B., Ball, R.C., "Relaxation of Entangled Polymers at the Classical Gel Point", *J. Phys. France*, **51**, 757-775, 1990.
- Saam, J., Speier, J., "The Addition of Silicon Hydrides to Olefinic Double Bonds, Part VI. Addition to Branched Olefins", *J. Am. Chem. Soc.*, **83**, 1351-1355, 1961.
- Scanlan, J.C., "The Linear Viscoelasticity of Polydimethylsiloxane Polymers Near the Gel Point", Ph. D. Thesis, University of Massachusetts, Amherst, MA, 1990.
- Scanlan, J.C., and Hicks, M.J., "The Evolution of Linear Viscoelasticity During the Vulcanization of Polyethylene", *Rheol. Acta*, **30**, 412-418, 1991.
- Scanlan, J.C., and Winter, H.H., "The Evolution of Viscoelasticity Near the Gel Point of End-Linking Poly(Dimethylsiloxane)s", *Makromol. Chem., Macromol. Symp.*, **45**, 11-21, 1991.

- Scanlan, J.C., and Winter, H.H., "Composition Dependence of the Viscoelasticity of End-Linked Poly(dimethylsiloxane) at the Gel Point", *Macromolecules*, **24**, 47-53, 1991.
- Schrader, B., Hoffmann, A., Simon, A., Sawatzki, J., "Can a Raman Renaissance Be Expected Via the Near-Infrared Fourier Transform Technique?", *Vibr. Spectr.*, **1**, 239-250, 1991.
- Silas, R.S., Yates, J., Thornton, V., "Determination of Unsaturation Distribution in Polybutadienes by Infrared Spectrometry", *Anal. Chem.*, **31**, 529-532, 1959.
- Soltero, J., and Gonzalez-Romero, V., "Kinetic Study of the Curing of Poly(Dimethylsiloxane) with Polyfunctional Silanes Using Temperature Programmed IR", *ANTEC*, 1057-1061, 1988.
- Stauffer, D., Coniglio, A., Adam, A., "Gelation and Critical Phenomena", *Adv. Polym. Sci.*, **44**, 103, 1982.
- Stauffer, D., Introduction to Percolation Theory, Taylor and Francis Inc., Philadelphia, PA., 1985.
- Stockmayer, W.H., "Theory of Molecular Size Distribution and Gel Formation in Branched-Chain Polymers", *J. Chem. Phys.*, **11**, 45, 1943.
- Tant, M., R., and Wilkes, G., L., "An Overview of the Viscous and Viscoelastic Behavior of Ionomers in Bulk and Solution", *JMS-Rev. Macromol. Chem. Phys.*, C28(1), 1-63, 1988.
- te Nijenhuis, K., and Winter, H., H., "Mechanical Properties at the Gel Point of a Crystallizing Poly(vinyl chloride) Solution", *Macrom.*, **22**, 411-414, 1989.
- Tobolsky, A.V., Properties and Structure of Polymers, John Wiley and Sons, Inc., New York, 1960.
- Valentine, R.H., Ferry, J.P., Homma T., Ninomiya, K., "Viscoelastic Properties of Polybutadienes - Linear and Lightly Crosslinked Near the Gel Point", *J. Polym. Sci., A-2*, **6**, 479-492, 1968.
- Valles, E.M., and Macosko, C.W., "Structure and Viscosity of Polydimethylsiloxane With Random Branches", *Macromolecules*, **12**, 521-526, 1979.
- Venkataraman, S.K., "Rheology of a Polydimethylsiloxane Model Polymer Network Near its Gel Point", Ph. D. Thesis, University of Massachusetts, Amherst, MA, 1990.

- Venkataraman, S.K., Coyne, L., Chambon, F., Gottlieb, M., Winter, H.H., "Critical Extent of Reaction of a Polydimethylsiloxane Network", *Polymer*, **30**, 2222-2226, 1989.
- Venkataraman, S.K., and Winter, H.H., "Finite Shear Strain Behavior of a Crosslinking Polydimethylsiloxane Near its Gel Point", *Rheol. Acta*, **29**, 423-432.
- Walton, J.R., and Williams, K.P.J., "In-situ Fourier Transform Raman Studies of Thermally and Photochemically Induced Curing Reactions", *Vibr. Spectr.*, **1**, 339-345, 1991.
- Watanabe, H., and Kotaka, T., "Viscoelastic Properties and Relaxation Mechanisms of Binary Blends of Narrow Molecular Weight Distribution Polystyrenes", *Macrom.*, **17**, 2316-2325, 1984.
- Williams, K.P.J., and Mason, S., "Future Directions for Fourier Transform Raman Spectroscopy in Industrial Analysis", *Spectrochim. Acta*, **46A**, (2), 187-196, 1990.
- Winter, H.H., and Chambon, F., "Analysis of Linear Viscoelasticity of a Crosslinking Polymer at the Gel Point", *J. Rheol.*, **30**, 367-382, 1986.
- Winter, H.H., "Evolution of Rheology During Chemical Gelation", *Progr. Colloid and Polym. Sci.*, **75**, 104-110, 1987.
- Winter, H.H., "Gel Point", In the Encyclopedia of Polymer Science and Engineering, Supplemental Volume, 2nd. ed., 343-351, 1989.
- Winter, H.H., "Can the Gel Point of a Cross-linking Polymer Be Detected by the G' - G'' Crossover?", *Polym. Eng. and Sci.*, **27**, (22), 1698-1702, 1987.
- Winter, H.H., Morganelli, P., Chambon, F., "Stoichiometry Effects on Rheology of Model Polyurethanes at the Gel Point", *Macromolecules*, **21**, 532-535, 1988.
- Zallen, R., Physics of Amorphous Solids, Wiley-Interscience Pub., New York, 1983.

